THE UNIVERSITY
of EDINBURGH

Clean Water from Clean Energy: Removal of Dissolved Contaminants from Brackish Groundwater Using Wind Energy Powered Electrodialysis

Payam Malek

Submitted for the degree of Doctor of Philosophy

The University of Edinburgh

School of Engineering

2014

Declaration

I confirm that this thesis has been composed by myself and the work submitted is my own, except where work which has formed part of jointly-authored publications has been included. The contribution of the candidate and the other authors to this work has been explicitly indicated below. The candidate confirms that appropriate credit has been given within the thesis where reference has been made to the work of others. Further, this work has not been submitted for any other degree or professional qualification.

Materials included in Chapter 4 of this thesis has been already published in a journal article: P. Malek, J.M. Ortiz, B.S. Richards, A.I. Schäfer, *Electrodialytic removal of NaCl from water: Impacts of using pulsed electric potential on ion transport and water dissociation phenomena*, Journal of Membrane Science, 435 (2013) 99-109. DOI: 10.1016/j.memsci.2013.01.060

Payam Malek's contribution to this paper was to design the experimental work, to setup the experimental equipment, to conduct the experiments, to compile and analyse the data and finally to write the paper. The contribution of the other co-authors to the work was more focused on the supervising the research and helping with reporting the analysed data in a coherent manner.

Payam Malek

December 2014

Thesis Supervisors

Dr Helfrid Schulte-Herbruggen, University of Edinburgh, School of Engineering, Edinburgh, United Kingdom

Dr Juan M. Ortiz, University of Alicante, Institute of Electrochemistry, Alicante, Spain

Professor Asif Usmani, University of Edinburgh, School of Engineering, Edinburgh, United Kingdom

Lay Summary

"*As the world charts a more sustainable future, the crucial interplay among water, food and energy is one of the most formidable challenges we face. Without water there is no dignity and no escape from poverty.*" *-UN Secretary-General Ban Ki-moon on his message for World Water Day 2011*.

According to World Health Organisation (WHO), around 768 million people still lack access to improved drinking water, of which 83% live in remote areas of developing countries with limited access to reliable electricity. Development and implementation of off-grid water purification systems, such as desalination technologies powered by renewable energy could be an effective solution for the water scarcity issue in remote arid regions.

Electrodialysis (ED), a membrane technology, is an energy efficient and robust technique for brackish groundwater desalination, but requires a reliable power supply. Wind is particularly abundant on islands, coastal areas and mountain regions, and hence a suitable source of energy in such off-grid locations.

In this PhD, a directly coupled wind energy powered ED system (Wind-ED) without energy storage was developed for the first time to improve water quality and enable use of brackish groundwater sources for human consumption. The impact of a highly variable energy supply on desalination performance was investigated in experiments using both controlled conditions and simulations based on real wind data. Moreover, the impact of varying ED stack resistance, caused by changes in the flow rate and feed salt concentration, on the power production of the wind turbine was explained.

The results showed that although the rate of desalination reduced when operating under extreme wind speed fluctuations and intermittencies, the quality of the drinking water produced was always within the WHO guidelines. The energy required for desalination also remained relatively unaffected by the fluctuations inherent to the wind resource. In conclusion, the wind-ED system was proven to be an energetically robust and reliable desalination technique with the ability to produce safe drinking water from brackish waters in water stressed remote locations.

Abstract

Around 770 million people lack access to improved drinking water sources (WHO 2013), urgently necessitating implementation of contaminant removal by *e.g.* desalination systems on a large scale. To improve water quality and enable use of brackish water sources for human consumption in remote arid areas, a directly coupled wind – electrodialysis system (Wind-ED) was developed. Modularity, sustainability and above all suitability for the practical use in off-grid locations were the main motivations and design objectives. The direct coupling of wind energy with membranes reduces the system costs as well as technical drawbacks associated with using intermediate energy storage systems. During this research, systematic experiments were performed using the Wind-ED system in order to determine desalination performance and clean water production, specific energy consumption (SEC) and current efficiency (η_c) under relevant conditions, such as varying: i) wind speed, ii) wind turbulence intensity, iii) oscillation periods, iv) varying NaCl concentrations and v) flow rates. Moreover, the competitive removal of four commonly available inorganic contaminants in brackish groundwater sources, nitrate (NO_3^-), fluoride (F^-), sulphate (SO_4^{2-}) and chloride (Cl^-), were investigated.

Firstly, to establish a systematic understanding of how and to what extent energy fluctuations influence the transport of the salt (*i.e.* NaCl) ions across the membranes, experiments were conducted using pulsed electric field assisted electrodialysis (pulsed-ED) over a wide range of frequencies (0.001 – 10 Hz) and duty cycles (20 – 80). The results showed that pulsation applied in the sub-limiting regime resulted in reduced water production, explained by the delays caused by the off-periods during the pulsed desalination process. At higher current densities, pulsation led to considerable improvements in current (*e.g.* up to 95%, for a feed solution of 500 mg/L and a pulse regime of 1 Hz at 50 V peak voltage) and significant reduction in water dissociation, explained by a reduction of concentration polarisation. Importantly, the pulsation had no significant effect on energy consumption or current efficiency suggesting that ED could be suitable for direct coupling to fluctuating energy sources such as wind energy.

ED was consequently coupled to a wind turbine system and a series of desalination tests were performed over a wide range of wind speeds (2-10 m/s), turbulence intensities (TI of 0-0.6) and oscillation periods (0-180 s). Results showed that water production and SEC increased with wind speed. However, both the water production and SEC stopped increasing as the power output from the turbine levelled off at wind speeds above the rated value (v_{rated}: 7.9 – 8.4 m/s). The impact of wind speed fluctuations on the system performance were insignificant up to a TI of 0.4. The desalination performance declined under high turbulence intensity fluctuations (TIs ≥ 0.5) and long periods of oscillation (> 40 s), as the wind-ED system periodically cycled off in response to operation below the cut-in wind speed of the wind turbine ($v_{cut\text{-}in}$: ~ 2 m/s). The off-cycling of the system caused significant delays in the desalination process, and thus resulted in reduced water production. Further reduction in the water production resulted as the wind-ED system operated under intermittent wind speed conditions with off-wind periods longer than 10 s. It was concluded that the main challenge in direct coupling of ED to a wind resource was not the magnitude of the fluctuations but the impact of the power cycling off during long periods of oscillation and lengthy periods of no wind. Interestingly, the SEC of the process remained relatively unaffected by the fluctuations and intermittencies in the wind resource.

The effect of energy fluctuations on the competitive transport of F^-, Cl^-, NO_3^- and SO_4^{2-} from artificial brackish water (TDS ~4350 mg/L) was investigated using different sets of real wind data. The ion removal, independent of the wind regime tested, followed the order: $NO_3^- \geq Cl^- > F^- > SO_4^{2-}$. The competitive removal of the ions was linked to differences in physicochemical properties (*i.e.* hydration energy, ionic mobility and valence). The specific selectivity (*e.g.* preferential transport of NO_3^- over SO_4^{2-} ions) was found to increase with concentration polarisation being either minimised (by lowering the mean wind speed) or disrupted (by fluctuations in the wind resource).

The results from flow rate and feed concentration experiments, showed that power production of the wind turbine depended on not only the available wind energy but also the resistance of the load (*i.e.* the ED stack). Thus, increasing the feed

concentration and the flow rate resulted in reduced resistance in the ED stack (R_{stack}), which inversely influenced the current induction counter torque force applied on the shaft of the wind turbine and caused the rotor to spin at a lower angular velocity. This led to increased sensitivity of the wind-ED system to wind speed fluctuations (*e.g.* system cycled off due to extreme fluctuations and intermittencies with low TDS feed concentration of 2400 mg/L) and hence a reduction of desalination performance. Impact of flow rate on the SEC was found to be negligible; this was attributed to the automatic voltage to current adjustments done by the wind turbine, in order to minimise the impacts of R_{stack} on the power production by the turbine at a given wind speed.

Increased flow rate and resulting shrinkage of the boundary layer's thickness, caused the concentration profiles at the solution-membrane interface to become steeper. This favoured the transport of ions with the highest diffusion coefficients in the mixture (*i.e.* Cl^- and NO_3^-). Decreased flow rate favoured the transport of ions with larger valence numbers and higher electric mobility inside the electrolyte (*i.e.* SO_4^{2-}); as the former property governed the faster migration of SO_4^{2-} ions through the thick boundary layer and the latter property assisted with the improved affinity of the ion-exchange membrane to SO_4^{2-} ions compared to the monovalent anions in the mixture. Increasing the feed concentration of Cl^- from 500 to 2,550 mg/L led to reduced transport numbers for the other anions in the mixture and significantly reducing their removal rate.

The results obtained from both the pulsed-ED and wind-ED experiments showed that, despite direct coupling to the fluctuating energy source the SEC of the process remained relatively unaffected by the energy fluctuations. Although the desalination process might require more time to be completed when operating under extreme wind speed fluctuations and intermittencies, the quality of the drinking water produced was always within the WHO standards. In conclusion, the findings from this research prove the wind-ED system to be an energetically robust and a reliable off-grid desalination technique suitable for the treatment of brackish groundwater in water stressed remote regions.

Acknowledgements

As with most people, this PhD has been a challenging while rewarding experience for me, from both the personal and intellectual perspectives; a great journey which could have never been completed successfully without the scientific and moral support of those who believed in me and this project.

Firstly, I would like to thank Prof Andrea Schäfer and Prof Bryce Richards for giving me the opportunity to embark on this research experience, for supervising me during the first half of my PhD studies and for their scientific contribution to parts of this research, which resulted in a paper publication. I am particularly thankful to Prof Richards who made me realize that often the questions worth answering are the ones starting with "WHY"!

Many thanks to Dr Juan M. Ortiz for his invaluable friendship and supervision along this journey. Juan, your enthusiasm for the research and knowledge of the field were instrumental to the progress of this project. A massive thank goes to Dr Helfrid Schulte-Herbrüggen for supervising me during the second half of my PhD studies. Helfrid, your positive attitude, constant support and scientific knowledge helped me to bring this project into the completion in form of a coherent PhD thesis; it was a pleasure working with you. Also I would like to thank Prof Asif Usmani for taking me on board as his student and for providing me with critical advice and support during the second half of my PhD studies.

Vincent Esparros, Molly Patrick and Pasidu Pallewela are all thanked for their contribution to the setup of the electrodialysis system. Sean Reid, Gavin Park and Morgan Letellier are thanked for their contribution to the design, modification and setup of the wind turbine simulator. My special thanks to Pasidu Pallawela for his technical advice and scientific discussions, helping me with better understanding of the wind turbine behaviours. Heriot-Watt University is thanked for providing a lab space and laboratory facilities (*i.e.* wind turbine simulator) for carrying out a part of this research. I also wish to acknowledge the technical, academic and administrative employees of both the University of Edinburgh and Heriot-Watt University for their

massive help and support during this project. My special thanks to Katherine Moore for her support throughout my PhD studies.

This PhD project was supported by the University of Edinburgh Diversity in Engineering studentship. Scottish Enterprise PoC REEDR and Leverhulme Royal Society Africa Award (SADWAT-Tanzania) are acknowledged for providing project equipment and materials funding, respectively. European Membrane Society (EMS), Royal Society of Chemistry (RSC) and IChemE – the Water Special Interest Group are acknowledged for allocating travel grants for attending the international conferences ICOM 2011 and MELPRO 2014.

I am very grateful to all my colleagues from the Membrane Technology Research Group, Dr Andrea Semião, Dr Annalisa De-Munari, Dr. Laura Richards, Dr İme Akanyeti and Mr Than Hieu for their insights, friendship and support. I am also very thankful to my office mates in room G.1, John Muir Building, Juan Hidalgo Medina, Liming Jiang, Zafiris Triantafyllidis, Martyn McLaggan, Shaun Devaney and Brian Miller for the joy, friendship and enthusiasm that they brought to our office every day. A massive thank you to my dear friend, Maryma Babaei, for her positive attitude and great support during the early stages of my PhD. Maryam Babaei is also thanked for proof reading my thesis. Thanks to my dear friends Dr Helen Ramsden, Madeleine Berg, Andrew Buddery, David Abelman, Laura Underwood, Helen Cope, James Lee, Dr Peyman Moghadam, Dr Emad Noorizadeh, Dr Enzo Mangano, Dr Maria Chiara Ferrari and Dr Ali Eslami for their support, the amazing times that I had with them and for all the great conversations we had on science or social aspects over these years.

I am beyond grateful to my beloved family; my father Bahram, my mother Firouzeh, my uncle Nasser and my caring brother Pooya. Your love and continuous support made this journey so pleasant and successful. Also a great thanks to Prof Mohammadali Bigdeli for his encouragement at the beginning of this road. At the end, my heartfelt thanks go to a special person, Martyna Haponska for the relentless support, constant encouragement and immensely positive energy that she has given me over these years; your presence in my life is invaluable.

Table of Contents

List of Figures

List of Tables

Glossary of Terms

Acronyms

AEM	Anion exchange membrane
CEM	Cation exchange membrane
CP	Concentration polarisation
DAQ	Data acquisition system
DBL	Diffusion boundary layer
DSE	Dimensionally stable electrode
EC	Electric conductivity (μS/cm, mS/cm)
ECT	Electric charge transferred (C/m^3)
ED	Electrodialysis
ER	Electric rinse
IC	Ion chromatography system
LCD	Limiting current density
MED	Multi-effect distillation
MSF	Multi stage flash
PMG	Permanent magnet generator
Pulsed-ED	Voltage pulse assisted electrodialysis system
PV	photovoltaic
RE	Renewable energy
RO	Reverse osmosis
R_{stack}	ED stack resistance
SEC	Specific energy consumption (kWh/m^3)
TDS	Total dissolved solids (mg/L)
TI	Turbulence intensity
TVC	Thermal vapour compression
WHO	World health organisation
Wind-ED	Wind energy powered electrodialysis system
WP	Water production (m^3/m^2day)

Nomenclature

Symbols

A_a	cross-sectional area of the air bundle under investigation (m^2)
A_m	Effective membrane surface area (m^2)
A_s	Swept area of the wind turbine blades (m^2)
c	Molar concentration (mol/m^3)
C_{aer}	Aerodynamic efficiency of the wind turbine
C_p	Practical efficiency of the wind turbine
D	Diffusion coefficient (m^2/s)
E	Energy consumption (kWh)
F	Faraday constant (96,485 As/mol)
h	Width of channel (m)
I	Current (Amp)
j	Current density (Amp/m^2)
J	Ionic flux (mol/m^2s)
j_{lim}	Limiting current density (Amp/m^2)
k	Specific resistance (Ωm)
k_m	Mass transfer coefficient
l	Membrane thickness (m^3)
N	Number of membrane cell pairs
P	Power (W)
P_e	Electric power output from the wind turbine generator (W)
P_m	Mechanical power output from the wind turbine rotor (W)
P_t	Transmitted power by a device such as gear box (W)
P_w	Wind power
Q	Volumetric flow rate (m^3/s)
Q_t	Volume of treated water (m^3)
R	Resistance (Ω)
R_g	Gas constant (8.314 J/mol K)
R^i	Ion removal from diluate stream

S_j^i	Specific selectivity of ion *i* relative to ion *j*
t	Time (s)
T	Temperature (K)
t_d	Total time of desalination (s)
t_i^b	Transport number of ion inside the solution
t_i^m	Transport number of ion inside the membrane matrix
T_o	period of oscillation (s)
t_{OFF}	Off period of the pulse
t_{off}	Off-wind period
t_{ON}	On period of the pulse
t_{on}	On-wind period
t_{twd}	Transition wind speed decrease time
t_{twi}	Transition wind speed increase time
U	Voltage (V)
u	Fluid velocity (m/s)
v	Wind speed (m/s)
v_{mean}	Average wind speed (m/s)
x	Distance from the membrane surface (m)
x	Mole fraction
y	Ion mobility in the global electrolyte-membrane system
z	Valence number
z	Hub height
ΔP	Pressure gradient along the channel (Pa)
Λ	Molar conductivity (Sm^2/mol)
α	Amplitude of fluctuations (m/s)
δ	Boundary layer thickness
ε	Roughness index
η_c	Current efficiency (%)
η_g	Generator efficiency
η_t	Power transmission efficiency
φ	Electric potential (V)

λ	Tip speed ratio
ρ	Air density (kg/m^3)
τ_c	Total counter torque force
τ_i	Inertial generated counter torque force
τ_I	Current induced counter torque force
τ_{net}	Net torque force
τ_W	Wind speed generated productive torque force
υ	Stoichiometric coefficient
ξ	Current utilization

Subscripts

AEM	Anion-exchange membrane
BL	Boundary layer
C	Concentrate stream
cell	Membrane cell pair
CEM	Cation-exchange membrane
D	Diluate stream
des	Desalination process
ED	Electrodialysis process
ER	Electrode – electrode rinse reaction
i	Ion *i*
j	Ion *j*
p	Solution pumping process
ref	Reference
s	Salt
z	Hub height condition

Superscripts

B	Bulk solution
conv	conversion
diff	Diffusion
f	feed

in	Inlet of the channel in the ED stack
mig	migration
out	Outlet of the channel in the ED stack
S	Solution-membrane interface
s	Product

List of publications

Journals

P. Malek, J.M. Ortiz, B.S. Richards, A.I. Schäfer, *Electrodialytic removal of NaCl from water: Impacts of using pulsed electric potential on ion transport and water dissociation phenomena*, Journal of Membrane Science, 435 (2013) 99-109. (**Chapter 4**)

P. Malek *et al.*, *Wind energy powered electrodialysis: the impact of wind speed and energy fluctuations on NaCl removal from artificial brackish groundwater*, 2014 (in preparation to be submitted in Energy and Environmental Science) (**Chapter 5**)

P. Malek *et al.*, *Wind energy powered electrodialysis: the impact of intermittency in the renewable energy on NaCl removal from artificial brackish groundwater*, 2014 (in preparation) (**Chapter 6**)

P. Malek *et al.*, *Brackish groundwater desalination using a directly coupled wind energy powered electrodialysis system*, 2014 (in preparation) (**Chapter 7**)

P. Malek *et al.*, *Wind energy powered electrodialysis: the effects of flow rate and feed concentration on the removal of fluoride, chloride, nitrate and sulphate from artificial brackish groundwater*, 2014 (in preparation) (**Chapter 8**)

Conferences

P. Malek, J.M. Ortiz, H. Schulte-Herbrüggen, B.S. Richards, A.I. Schäfer, *Directly Powered Wind-Electrodialysis System: a Solution to the Drinking Water Scarcity in Remote Arid Areas*, International conference MELPRO - membrane and electromembrane processes, 18-21 May 2014, Prague, Check Republic (oral presentation)

P. Malek, J.M. Ortiz, B.S. Richards, A.I. Schäfer, *Enhanced Electrodialysis Process: Using a Pulsed Electric Field for Desalinating from Brackish Water*, the

International Euromembrane Conference, 23-27 September 2012, London, UK (poster presentation)

P. Malek, M. Patrick, P. Pallawela, B.S. Richards, A.I. Schäfer, The Effects of Competing Ions on Electrodialytic Removal of Monovalent Anions from Brackish Water, International Congress on Membranes and Membrane Processes – ICOM, 23-29 July 2011, Amsterdam, the Netherlands (poster presentation)

Chapter 1

Introduction

Energy and freshwater are undoubtedly the two inseparable and key resources for sustaining human life on earth. Supply of potable water requires energy and unfortunately most of the countries with minimal access to safe drinking water are also poor in terms of access to reliable energy grids. A worldwide map created by Vorosmarty *et al.* (Figure 1.1 A) suggests high levels of exposure to water security risks for more than 80% of the world's population [1]. The term "incident" used in this map refers to exposure to a complex array of stress factors, sourced from both anthropogenic and natural sources, at a given location. Vorosmarty *et al.* argued that developing countries, and in particular the inhabitants of remote locations, suffer more severely from exposure to water security risks because they don't have the resources necessary to mitigate pressures on water supplies. However, in contrast the developed countries often have the investment required to offset high stressor levels experienced by the human population, even though the actual pressure on water resources may be worse in these countries compared to the developing countries. Vorosmarty *et al.* backed up their arguments by publishing a second map, showing shifts in spatial patterns of threat to drinking water scarcity after accounting for water technology benefits (Figure 1.1 B). According to the recent report by World Health Organisation [2, 3], around 768 million people lack access to freshwater sources, 83% of whom live in remote areas of developing countries. The problem of fresh water scarcity in remote regions is exacerbated by the fact that more than 84% of 1.3 billion people who have limited access to electricity, also live in these locations [4].

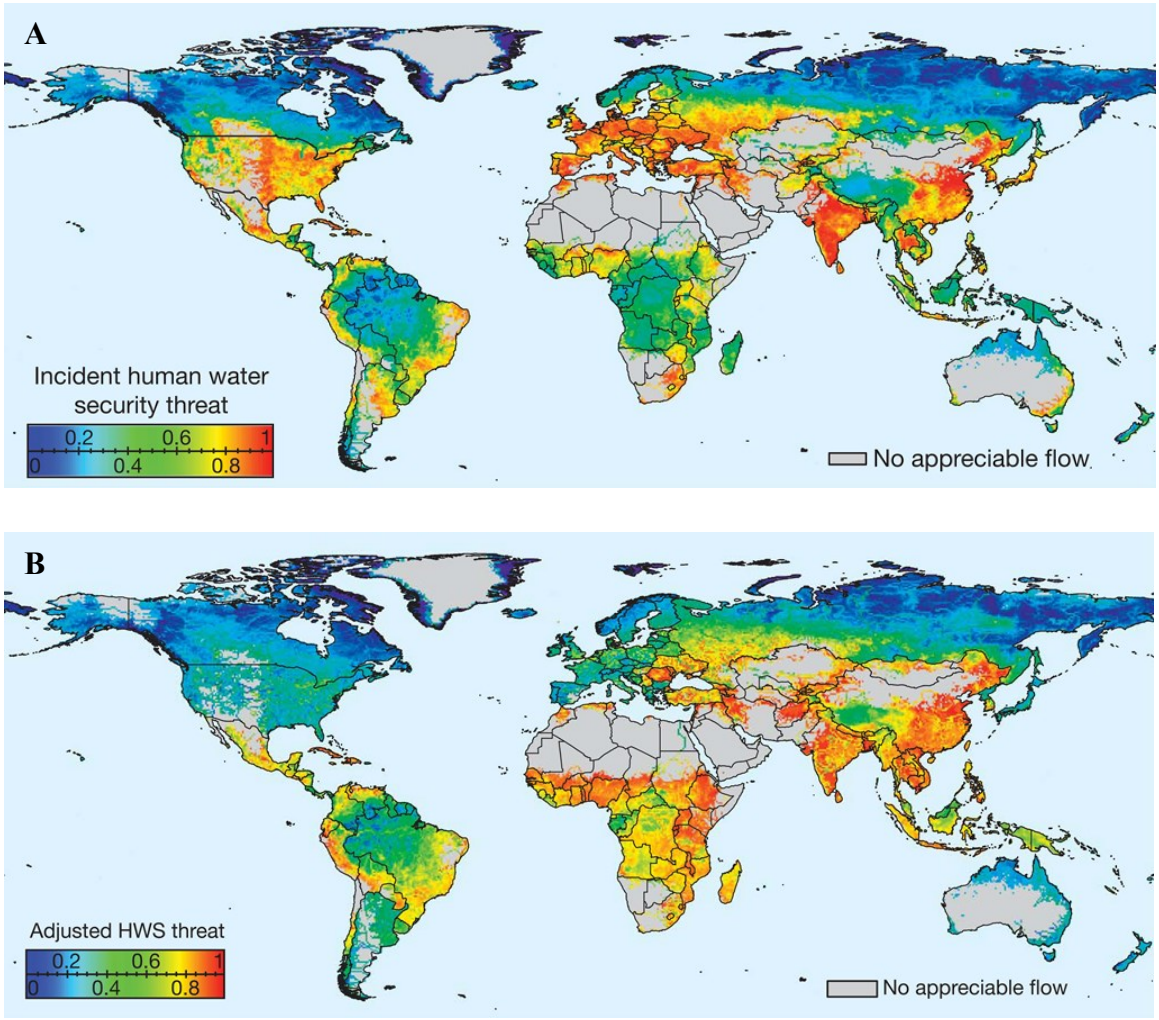

Figure 1.1 Worldwide incident threat to water security (A) before and (B) after, accounting for water technology benefits (adapted from [1]).

While the lack access to improved water supply is significantly acute in remote locations, many of such regions have access to other sources of water (such as brackish and groundwater) that can be treated for producing drinking water if correct treatment systems are put in place [5-9]. Moreover, many of the electrically remote areas are rich in terms of renewable energy (RE) resources (such as wind and solar) which can be potentially employed as the main source of energy for powering water purification systems [10-16]. Therefore, development and implementation of off-grid RE powered contaminant removal systems, for producing fresh water from available resources (such as brackish and groundwater), can be considered as an effective and potentially sustainable solution for overcoming the drinking water scarcity issue in remote regions of developing countries.

Trace inorganic ions are among the main sources of contamination in groundwater. The levels at which these contaminants exist in groundwater depends on the geological (*e.g.* leaching from surrounding rocks) or anthropogenic (*e.g.* industrial or domestic effluents) sources that these contaminants are discharged from [6, 17, 18]. Consumption of water containing trace inorganic contaminants, such as fluoride (F^-) and nitrate (NO_3^-), at concentrations above their recommended levels by drinking water guidelines may result in severe short and long-term physical and nervous disorders [19-24]. There are some other common inorganic ions in brackish and groundwater which are of no significant health concern, but their excess concentrations in a water resource can make the water resource undrinkable (*e.g.* due to high salt content, taste issue or colour problem). Chloride (Cl^-) and sulphate (SO_4^{2-}) are in this category, for which only drinking water guideline limits for taste have been proposed [21]. Concerns over the toxicity and chemistry of inorganic contaminants in brackish and groundwater have resulted in increased interest in development of cost effective desalination techniques in the recent years.

Renewable energy (RE) powered-membrane systems are promising technologies for brackish water desalination in remote regions due to their flexibility to be designed according to the number of inhabitants, available water supply and energy resources [10, 16, 25-28]. Moreover, the application of membrane technologies for brackish water desalination was shown to be energetically less expensive (reverse osmosis (RO): 1.5-3.0 kWh/m^3 and electrodialysis (ED): 0.7-2.5 kWh/m^3) compared to other alternative technologies such as multi-stage flash distillation (MSF: 19.5-27.3 kWh/m^3), vapour-compression evaporation (VC: 7.0-16.2 kWh/m^3) and multi-effect distillation (MED: 14.5-21.6 kWh/m^3) methods [10, 12, 13]. Among several membrane systems, electrodialysis (ED) has been established as a feasible desalination technique due to its simple ion recuperation, high ion selectivity and efficient ionic separation [29-32]. High water recovery of 85-94%, small maintenance required, long lifetime of ion-exchange membranes due to their strong mechanical and chemical stability plus their tolerance for operation at high temperatures (up to 50 ^{o}C) and extreme pH-levels are the features that make ED a particularly suitable desalination system for the use in remote regions with limited water resources. Moreover, the easy start up and shut down of ED makes this system

suitable for direct coupling to fluctuating and intermittent sources of energy, such as renewable energies [31, 33, 34].

ED is an electrically driven ion separation technique with a well-established use in many industrial applications such as brackish water desalination [35-37], wastewater treatment [29, 38-40], desalting of amino acids and organic solutions [41-44] and salt production [45-47]. An ED system consists of a number of alternatingly positioned cation and anion exchange membranes that are stacked together between two electrodes and are separated from each other by flow spacers [29, 31, 35, 48, 49]. The ion removal principle in an ED system is illustrated in Figure 1.2.

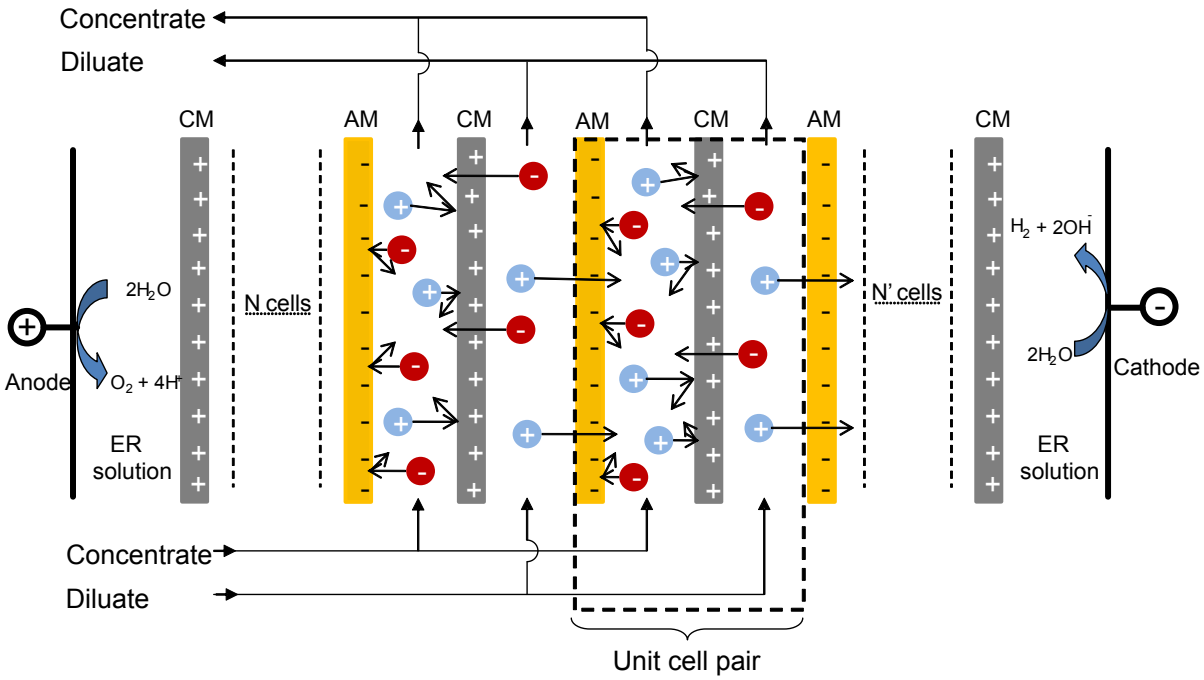

Figure 1.2 Schematic illustrating the ion transport principle across the ion-exchange membranes in an ED system (AM: anion exchange membrane. CM: cation exchange membrane, ER: electrode rinse).

The salt solution is fed into the ED stack in a direction parallel to the ion-exchange membranes. Once a potential difference is applied across the electrodes, each ion in the solution starts to travel toward an oppositely charged electrode. While the passage of the ions is permitted through the oppositely charged ion-exchange membranes, their travel is terminated once they reach a similarly charged ion-exchange membrane. This results in the formation of a series of alternatingly positioned concentrate and diluate channels within the ED stack, through which the

ion separation process takes place. This process continues in a batch circulating mode until the target salt concentration, which is often application dependent, is obtained in the diluate stream.

Most of the studies carried out on ED over the last 40 years focused on the conventional mode of operation where a constant voltage or current source is used for operating the membrane system [29, 31, 49-52]. The available studies on renewable energy powered ED technologies are very limited. Lundstrom (1979) [53] was the first to present the application of a renewable energy powered ED system for water purification purposes. He demonstrated the use of an off grid photovoltaic (PV) powered-ED system for brackish water desalination in remote regions in the south-western states of the USA where access to reliable electricity grid is minimal but the solar radiation is abundant. Later, Ishimaru [54] presented a study in which a series of PV cells were applied to charge a set of battery banks, which were subsequently used for powering an ED system to desalinate brackish water (TDS ≤ 1,500 mg/L). The system showed reliable performance, producing freshwater in the range of 150 – 400 m^3/day, depending on the season and the solar irradiation, during the two year period of testing. Although using deep cycle lead-acid batteries governs uninterrupted operation in indirect configuration of RE-membrane system coupling, they result in reduced robustness, lower efficiency, associated with continuous DC-AC-DC conversions and charging-discharging losses, plus increased capital and running costs [55-57]. The impacts of applying pulsed electric fields on minimising concentration polarisation [33, 58-61] and fouling mitigations [34, 62-66] in ED processes were investigated in a number of studies. The satisfactory operation of ED, despite having fluctuations in the energy source in these studies, suggests the possibility of coupling ED directly to fluctuating energy sources such as renewable energies (REs). Direct coupling of ED to an RE source can eliminate the need for having energy storage facilities (*e.g.* lead-acid batteries and flywheels); hence to minimise the aforementioned adverse behaviours linked with using such systems [55, 67]. More importantly the fact that ED operates with direct current (DC) [29, 31] makes this system particularly favourable for direct coupling to RE sources, as in such configuration no need for DC-AC conversion systems exists. AlMadani [68] was among the first who developed a directly coupled PV-ED system consisting of

four hydraulic and two electric stages and demonstrated the impacts of process parameters, *i.e.* flow rate and temperature on removal of salt from groundwater. Ortiz *et al.* [69, 70], Uche *et al.* [71] and Cirez *et al.* [72] developed mathematical models describing the behaviour of different directly connected PV-ED systems. The models employed to predict the quality of the water product, the rate of desalination and specific energy consumption under given meteorological conditions and PV cell configurations. The results from these models showed very good corroboration with the experimental findings obtained in desalinating of real brackish water using the PV-ED systems.

Wind energy is particularly abundant on islands, coastal areas and mountain stations [73-77], and thus it is a favourable source of energy for desalination in such environments. Opposite to solar energy where availability is limited to the availability of sunlight during daytime, wind energy is readily available to be harvested over both day and night, assuming the wind system is well sited [78]. This makes wind energy a superior alternative, in locations which are rich in terms of wind resources, compared to solar power for continuous powering of different processes, with less need for long term energy storage. The use of wind energy for powering membrane based desalination technologies was investigated by a number of researchers [14, 28, 79-85] and was proven to be economically feasible for some technologies including ultrafiltration (UF) and reverse osmosis (RO) [14, 25, 86]. Comparisons made between the solar powered and wind powered membrane techniques show slightly lower specific energy consumption (SEC) for the wind powered membrane systems (*e.g.* 3.4 kWh/m^3 for a wind-RO system versus 4 kWh/m^3 for a PV-RO system, using the same RO module in both of the setups and desalinating from similar seawater feeds (32,800 – 34,300 mg/L TDS)) [81, 87-89]. The overall cost of desalination was also suggested to be lower when using wind energy as opposed to solar energy for powering the membrane systems [90]. In a review by El-Ghonemy [91] the cost of water production from brackish water desalination at the rate of 250 m^3/day using PV-RO and wind-RO systems, were reported to be 6.7 and 2.7 US$/m3, respectively. Despite the advantages that wind energy has over solar energy, the number of wind-membrane systems developed and commercialised so far are very limited compared to the solar powered membrane

techniques. This can be partially attributed to the extreme fluctuations and intermittencies inherent to wind, making the harvesting of wind energy and coupling the wind turbines to the membrane systems technically very difficult. The latter is expected to be particularly challenging for pressure driven membrane systems (*e.g.* RO) that require constant power supply to perform satisfactory desalination [92, 93]. However, the extreme variations in the energy supply are expected to be less problematic for electrical driven techniques (*e.g.* ED) as their desalination performance has shown to be relatively robust despite energy fluctuations [34, 60-63, 66].

To the best knowledge of the author, to date no work on directly coupling ED with wind energy has been done. Veza *et al.* and Carta *et al*. [84, 94] studied a large scale wind energy powered electrodialysis reversal (EDR) system, where a flywheel was employed as an intermediate temporary energy storage/energy buffering device between the wind turbines and the EDR stack (*i.e.* an indirect coupling of the renewable energy source with the membrane system). The aim was to develop automatic control electronics to allow the system to operate optimally, producing maximum volume of freshwater with minimum energy consumption. Although good quality drinking water was obtained using the wind energy powered membrane system, the field pilot nature of these tests did not allow drawing systematic and comprehensive understanding on how ion transport is influenced by wind speed fluctuations. Moreover, the fact that intermediate devices such as maximum power tracking and energy buffering systems (*i.e.* flywheel) were involved, it was difficult to specify the direct impacts of actual wind speed fluctuations on the ED performance.

The power produced from a permanent magnet generator based wind turbine is principally dependent not only on the available wind condition but also on the resistance of the load directly connected to the wind system [95, 96]. Therefore, when connecting a wind turbine directly to an ED system the power performance of the wind turbine is expected to vary with the change in the resistance of the ED stack during the desalination process. The latter is expected to happen due to the change in the feed concentration or the flow rate of the diluate and concentrate streams. The

change in the power performance of the wind turbine can result in further variations in the desalination characteristics of the membrane system and influence the energy expense of the desalination process. The potential behaviours to be seen from the membrane system in direct connection with a wind resource operating at steady wind speed conditions are yet unknown, hence they require systematic studies to be fully understood.

As mentioned earlier, the main challenge in using a wind turbine for direct coupling with the membrane system, with no form of energy storage or energy regulator, is associated with the fluctuations and intermittencies inherent to the wind resource. These fluctuations are a result of movements of large bulks of air over long periods (tens to hundreds of hours) and turbulence and gusts over short periods (seconds to a few minutes) [97-99]. The direct coupling of the wind system to the ED stack can inevitably result in fluctuations in the voltage and the current, ranging from mild fluctuations at low turbulence intensities to cycling on/off incidences occurring at extreme fluctuations. In order to establish solid understandings on how and in what extent the wind fluctuations affect the process of the ED system, it is necessary to carry out desalination studies using the membrane system over a range of wind speed fluctuations and intermittencies.

The magnitude and the mode of power supplied to the membrane system can also influence the competitive transport of ions through the system when desalinating from a complex salt solution. Zang *et al.* and Nikonenko *et al.* carried out extensive work on the impacts of current density on transport of ions through ion-exchange membranes and showed that increasing current density can result in poor ion selectivity when desalinating from solutions containing multi ion mixtures [100-102]. These studies were all focused on the conventional mode of operation where only constant power was utilized for operating the ED system. Therefore, the results obtained from these investigations cannot be extended to the operations where unconventional/fluctuating modes of power is employed (*e.g.* coupling the ED system to a RE resource). Mishchuk *et al.* [61] studied the impacts of applying short electric pulses on the transport of ions through the membranes in an ED process. Although applying voltage pulses resulted in a significant increase of the current

density within the ED stack, it did not cause any deterioration in the ion selectivity. In fact, the disruption of the concentration polarized boundary layer by means of applying high frequency voltage pulses to the ED stack (≥ 1 Hz), caused the specific selectivity of the ion-exchange membranes to increase for divalent Ca^{2+} ions over the relatively less conductive monovalent Na^{+} ions. The contrasting results regarding ion selectivity in conventional and unconventional modes of operation necessitates systematic investigations in order to determine the impacts of energy levels and fluctuations on the competitive removal of monovalent and divalent ions from complex solutions through the ion-exchange membranes.

1.1 Aims

The overall aim of this research is to determine an operating window of wind speeds and fluctuations over which a newly developed directly powered wind-membrane system can perform satisfactory desalination of brackish groundwater. To achieve this aim the following objectives were set:

1- To determine the impacts of power fluctuations, in a uniform and well controlled form of short voltage pulses applied across the membrane system, on the ion transport, concentration polarisation (CP) dissipation, water production and energy consumption (Chapter 4).

2- To determine the water production and energy consumption of the wind-membrane system under controlled i) steady state, ii) fluctuating and iii) intermittent wind speed conditions (Chapters 5 & 6).

3- To determine the impacts of wind speed and fluctuations on the competitive removal of inorganic contaminants (fluoride, chloride, nitrate and sulphate) from artificial brackish water (Chapter 7).

4- To determine the impacts of random fluctuations and intermittencies, inherent to the wind resource, on the desalination performance when the wind-ED system is operated under real wind speed conditions and with different ED stack resistances (*i.e.* different initial feed concentrations and different flow rates) (Chapter 8).

1.2 Thesis outline

An outlined structure of this PhD research is shown in Figure 1.3. Chapter 2 contains a survey of ion transport mechanisms taking place in ED, an overview of ED processes conducted with unconventional (fluctuating) modes of electric power, an introduction to wind energy and power production from small scale wind turbines and finally a highlight of existing challenges in direct coupling and operation of the membrane system with a wind turbine. Moreover in this chapter, the occurrence and fate of inorganic contaminants in brackish water, their environmental and health concerns and the impacts of operating parameters (*e.g.* power input, flow rate and feed concentration) on competitive transport of monovalent and divalent ions through ion-exchange membranes are reviewed. Chapter 3 (Materials and Methods) provides a full description of the ED system and the ion-exchange membranes employed for the experiments, the pulsed voltage system, the wind turbine simulator and its power characteristics plus the analytical techniques used for water samples analysis. As the starting point to this research, Chapter 4 contains a systematic investigation of the impacts of power fluctuations, in form of well uniform and controlled voltage pulses applied across the membrane system, on ion transport, CP dissipation, water production and energy consumption of the ED system. In Chapters 5 and 6 the membrane system is directly coupled to a wind turbine simulator to investigate the impacts of controlled i) steady state, ii) fluctuating and iii) intermittent wind speed conditions on the water production and the energy consumption of the membrane system. Chapters 5 and 6 also present the results of tests conducted under real wind conditions to determine the impacts of random fluctuations inherent to the wind energy resource on the desalination performance of the wind-membrane system. In Chapter 7 the impacts of real wind speed fluctuations on competitive removal of selected inorganic contaminants (fluoride, chloride, sulphate and nitrate) from artificial brackish water was investigated. In Chapter 8 the impacts of feed concentration and flow rate, as the two main operating parameters that influence the resistance of the directly connected load (*i.e.* the ED stack) to the wind system, on the competitive removal of ions under different real wind speed conditions are investigated. The main conclusions obtained from this research and suggestions for future work will be outlined in Chapter 9.

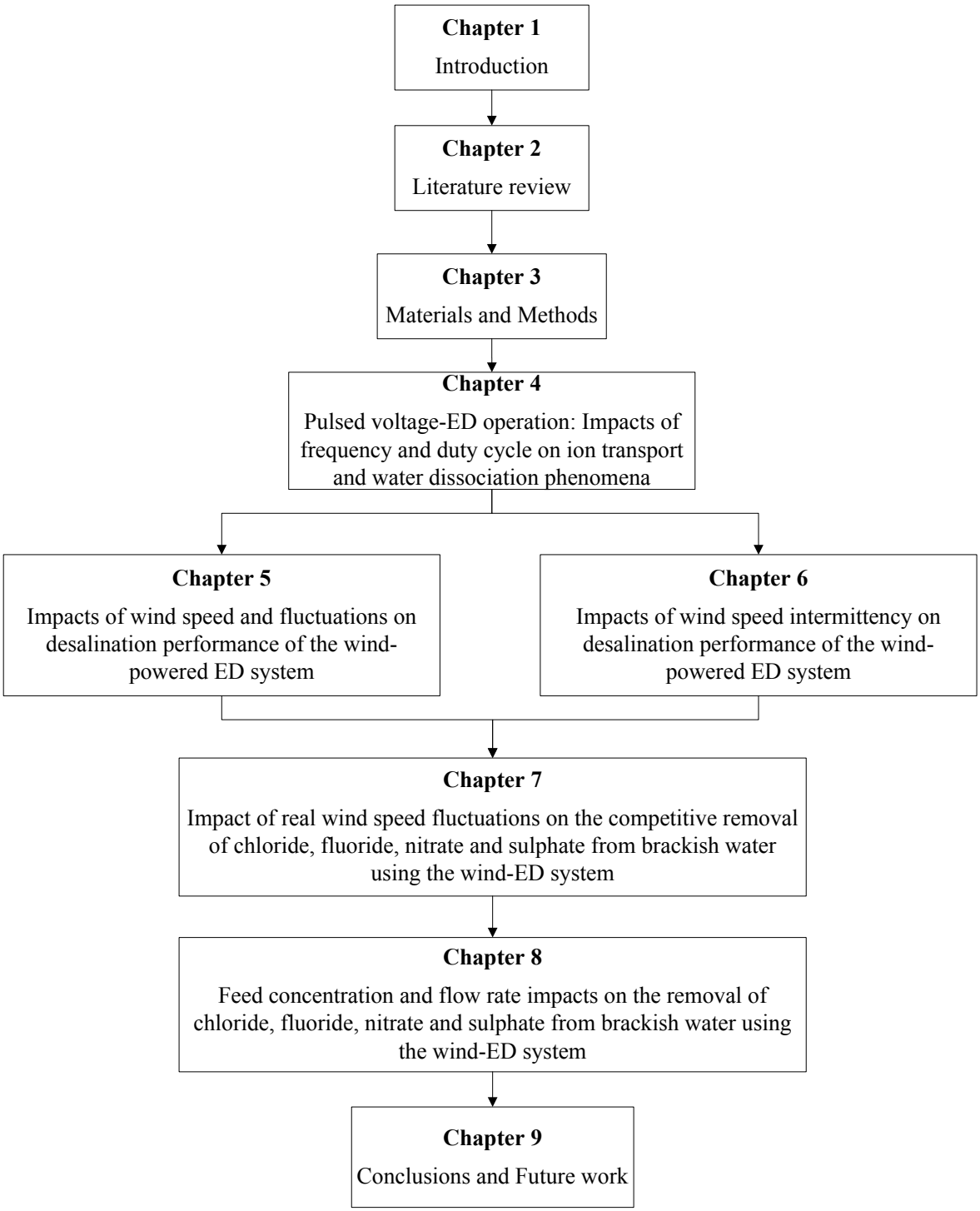

Figure 1.3 Overview of thesis structure

Chapter 2

Literature Review

2.1 Introduction

The synergic issue of water scarcity and energy crisis was highlighted in Chapter 1, and renewable energy powered membrane systems were suggested as suitable technologies to be part of a solution addressing the urgent water demands in remote areas of developing countries. Electrodialysis (ED) was introduced as an energetically efficient system, compared to other membrane techniques, for the particular purpose of brackish water desalination. The high water recovery of 85-94%, low maintenance required, long lifetime of ion-exchange membranes due to their strong mechanical and chemical stability plus their tolerance for operation at high temperatures (up to 50^{o}C) and extreme pH-levels were the other added values of ED when considering the use of this system in remote regions with limited water resources [29-32]. The easy start up and shut down of ED in operation with intermittent sources of energy [31, 33, 34], suggests that this membrane technique can be a suitable match for direct coupling to extremely fluctuating power sources such as wind energy. Development of directly coupled wind-ED systems can potentially open new horizons toward simpler and more feasible ways of drinking water production in remote regions in both developing and developed countries where the access to brackish groundwater and wind energy are particularly abundant.

In this chapter first the fate and occurrence of common inorganic contaminants (fluoride, nitrate, sulphate and chloride) in brackish water are described, in order to highlight the importance of conducting desalination processes. Secondly, a thorough description of the ion removal principles in ED as well as an introduction to the power performance of small scale wind turbine systems is given, in order to determine the synergies between the two systems. Based on the existing literature the coupling of ED with wind energy systems and other relevant fluctuating forms of energy are discussed. The objective is to determine the gaps and limitations in the literature regarding the development and operation of directly coupled wind-ED systems and to determine the main research questions that are to be addressed by this research.

2.2 Inorganic contaminants in brackish groundwater

Groundwater is the water beneath the surface of the earth, trapped in the fractures of rock formations and in the soil pore spaces [103]. Groundwater makes up 30% of global fresh water, about 0.8% of the entire world's water including the oceans and the glaciers [104]. For many rural regions in both developing and developed countries, groundwater is the only reliable source of water supply, which is normally exploited by installing boreholes and wells [105]. The main advantages in using groundwater in remote regions are as follows [9, 99, 103, 106]:

i. Due to multiple filtrations through different layers of sand and soil under the earth's surface, groundwater is often remained protected from microbial pollutants which are the main sources of waterborne illnesses in developing countries;

ii. Groundwater is available in many environments, and compared to rain and surface water it is less affected by drought and seasonal variations;

iii. Groundwater is relatively easy to locate near the point of use, making its uptake and management easier for the local community, if surface water is unavailable or inappropriate;

iv. Particularly with regards to rural areas of developing countries, groundwater is a more economically feasible option compared to piped water from central water supplies;

Figure 2.1 provides a qualitative demonstration of groundwater availability and distribution in the world.

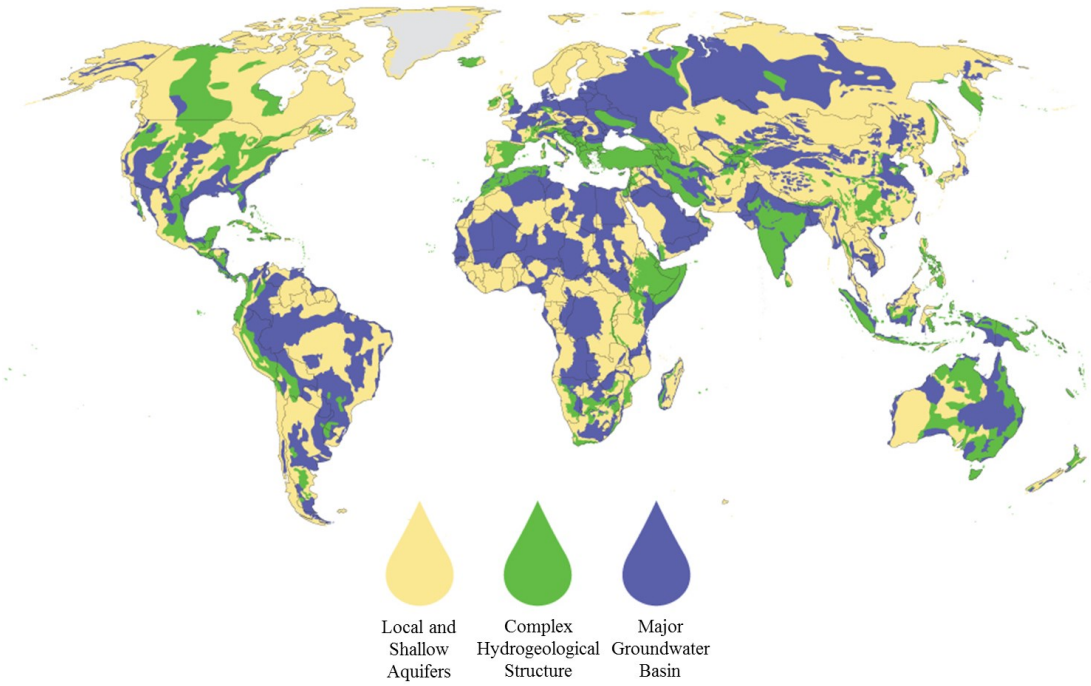

Figure 2.1 Availability and distribution of groundwater in the world (map created by Peder Engstrom and Kate Brauman of the Institute on the Environment's Global Landscape Initiative. Data provided by BGR & UNESCO (2008)) [107].

Despite all these advantages, using groundwater is still of some major concern such as i) waterlogging and salinization due to insufficient re-charge, ii) depletion due to overdraft [108] and iii) contamination by micro-pollutants, mainly inorganic compounds, sourced from both natural and anthropogenic activities [9, 103]. Inorganic contaminants are mineral based compounds, such as carbon-free nutrients and metals that are released into the environment due to anthropogenic activities [109, 110] or geological weathering [17]. Although some inorganics are nutritionally vital for health (*i.e.* calcium, potassium, chloride, sodium, magnesium, sulphur,

phosphorous, etc.), consuming excessive amounts of them may lead to serious physical and nervous disorders. For example, while a consumption of 1 mg/L fluoride (F^-) helps to prevent dental and skeletal problems, the excess consumption of this element (≥ 10 mg/L) leads to skeletal and dental fluorosis and lesions of the endocrine glands, thyroid and liver [19, 22, 111]. The maximum acceptable fluoride concentration in drinking water, as recommended by World Health Organisation (WHO) is 1.5 mg/L [21]. Fluoride constitutes 0.06 – 0.09% of the earth's crust [112]. Volcanic activities and fumarolic phenomena are the main pathways for the fluoride to reach the earth's surface and be released into the environment. Granitic and gneissic rocks, volcanic minerals and sediments of oceanic origin in mountainous regions are the main natural sources of fluoride discharge into natural water bodies [113]. Coal combustion, treatment of water and waste from various industrial processes, including phosphate fertilizer production, phosphate ore processing, aluminium, copper and nickel production, glue and adhesive production and ceramic, brick and glass manufacturing are the other sources releasing fluoride into the aqueous environment [21, 110, 114]. The concentration of fluoride is often very low in surface waters (< 0.1-1.5 mg/L) [21, 24], but, depending on geology, it can occasionally reach concentrations as high as 20 mg/L in some ground and surface waters [114]. A detailed survey of fluoride concentration in brackish water in Kenya was compiled by Nair *et al.* [115]. From 1,000 samples taken nationally for this survey, 61% exceeded 1 mg/L, approximately 20% exceeded 5 mg/L and 12% exceeded 8 mg/L.

Nitrate (NO_3^-) is another increasingly important inorganic contaminant in groundwater [116, 117]. The health issues related to consumption of NO_3^- include cancer risks for adults and infantile methemoglobinaemia (known as 'blue-baby' syndrome) for babies and young children [23]. Blue-baby syndrome occurs due to competition of nitrates with oxygen molecules in binding with haemoglobin which eventually leads to reduction of oxygen carrying sites in blood. The maximum concentration of nitrate in drinking water accepted by WHO is 50 mg/L [21]. The nitrate concentration in groundwater is often low (0 – 18 mg/L), but can reach high levels due to contamination by human and animal excreta, overflow of waste dumps

and agricultural runoff. The mass utilization of artificial fertilizers is the main source for abundant NO_3^- discharge to groundwater [23]. According to DEFRA agricultural activities are responsible for approximately 70-80% of nitrate release into ground and surface waters in UK [118]. In Germany, UK and Spain, respectively 36%, 50% and 80% of groundwater have average nitrate concentration of above 25 mg/L [119]. The situation is often worse in the developing countries. Studies carried out by Rossiter *et al.* on the quality of more than 190 boreholes and wells in Ghana determined the mean NO_3^- concentration of approximately 34 mg/L in these water bodies [6]. The study by Rossiter *et al.* showed that the nitrate level in some groundwater in Ghanaian agricultural suburbs reached as high as 507 mg/L.

Other inorganic contaminants in groundwater sources pose no significant health concern, but their presence at high concentrations leads to aesthetic problems such as taste and smell that make the water less desirable for consumption. The poor aesthetic quality of the water resource can lead to more severe issues if it causes people to resort to drinking water contaminated by other things (*e.g.* surface water contaminated by disease causing pathogens). Chloride (Cl^-) is in this category of inorganic contaminants, for which only a drinking water guideline limit due to taste has been proposed (250 mg/L) [21]. Although chloride concentrations do not exceed 10 to 50 mg/L in most of groundwater sources [6, 120, 121], occasionally depending on geological or anthropogenic activities the level of chloride in water resources can go significantly beyond the recommended maximum level set by WHO. For example, in a case of 1329 wells examined over 19 states in the United States of America (USA) between the years 1990 and 2004, 2.5% of the wells was found to have chloride contents above 250 mg/L [121]. Rossiter *et al.* also showed that in some Ghanaian water sources (*i.e.* boreholes and groundwater) the level of chloride reaches as high as 597 mg/L [6]. The main natural and anthropogenic sources of chloride discharge into groundwater include irrigation drainage, industrial effluents, animal feeds, septic tank waste, landfill leachates, and run-off containing road de-icing salts [122]. Seawater intrusion was also introduced as a major source of chloride contamination in groundwater and aquifers in coastal areas (*e.g.* chloride

concentrations as high as 5,460 mg/L were detected in brackish groundwater of Greek coastal regions) [123, 124].

Sulphate (SO_4^{2-}) is another common inorganic contaminant in groundwater; mainly a result of sulphur emissions produced from the fossil fuel combustion processes [110, 125]. So far no significant health impact was associated with the presence of SO_4^{2-} in low concentrations in drinking water. However, long term exposure to SO_4^{2-} concentrations above 500 mg/L (maximum recommended level by WHO) can lead to laxative problems [21]. The large amounts of SO_4^{2-} in water (*i.e.* 400–600 mg/L for magnesium sulphate, 250–1,000 mg/L for calcium sulphate and 250–500 mg/L for sodium sulphate) can impart bitter taste and odours, hence making the water less desirable for drinking [126, 127]. In terms of aesthetic consequences SO_4^{2-} can be more troublesome than chloride since it generally occurs in greater concentrations. According to the literature, the SO_4^{2-} concentration in groundwater is often in the range of 0 – 270 mg/L [128], however, higher levels of this compound have also been reported; for example up to 931 mg/L in Ghanaian wells and boreholes [6] and up to 3040 mg/L in rivers in western Canada [129].

The widespread presence of contaminants such as fluoride, nitrate, chloride and sulphate necessitates their removal to concentrations below the WHO guideline. Moreover, making available sources that would be less salty (brackish) to drink could be invaluable for communities without access to good quality drinking water. Therefore, ion removal mechanisms using the selected membrane desalination technique (*i.e.* electrodialysis) are reviewed in the next section.

2.3 Electrodialysis (ED) process

2.3.1 Mass transport and mass balance in ED

The principles for salt removal in electrodialysis (ED) were briefly described in the introduction (Chapter 1). As shown in Figure 1.1, an ED system is constructed of several unit cell pairs that are stacked together in series between two electrodes. Every unit cell pair consists of an anion-exchange and a cation-exchange membrane,

separated from each other via a flow spacer. During the process the salt solution flows in a laminar velocity between the ion-exchange membranes. By applying an electric potential across the system, the salt ions start to travel toward the oppositely charged electrode. During their migration the ions pass the oppositely charged membranes, but are restricted from further migration once they approach the membranes having similar charge to them. The charge selective transport of ions through the ion-exchange membrane results in the construction of alternatively positioned diluate and concentrate channels within the ED stack. Every two neighbouring channels, formed of a diluate and a concentrate compartment, make a so called "unit cell pair" as shown schematically in Figure 2.2.

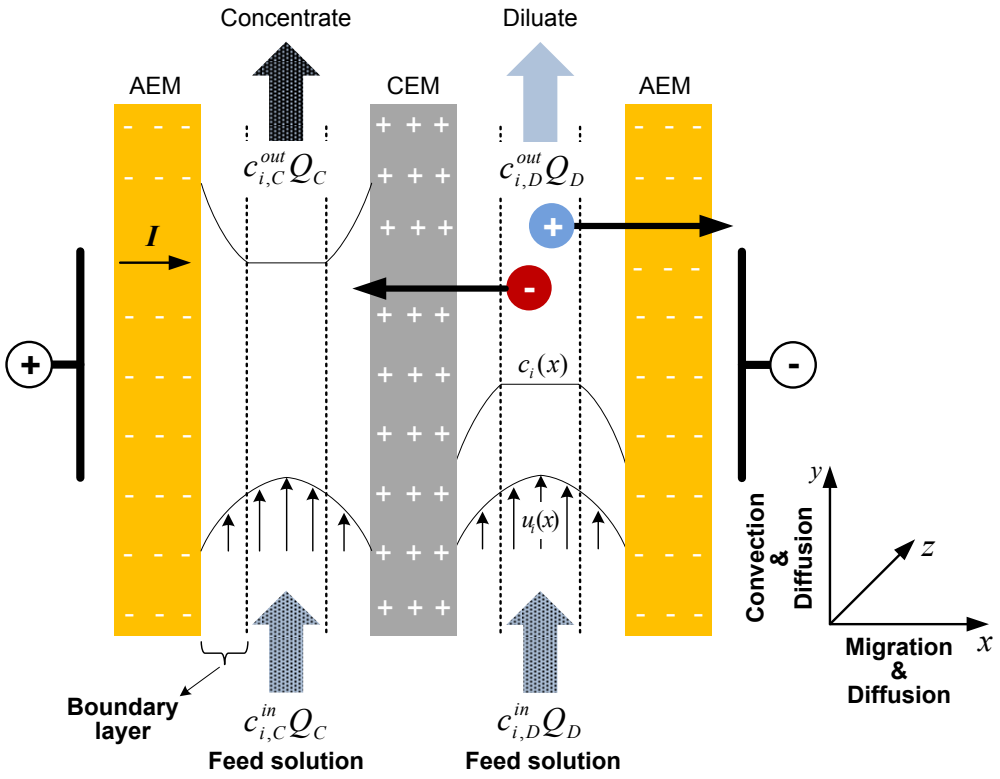

Figure 2.2 Schematic of an ED unit cell pair consisting of a diluate compartment and a concentrate compartment, positioned next to each other and separated via anion-exchange (AEM) and cation-exchange (CEM) membranes (adapted from Strathmann (2004) [31] and Nikonenko (2010) [130]).

In Figure 2.2, c represents the ion (i) concentration (mol/m^3), Q, the volumetric flow rate of the solution (m^3/s), and I, the total current passing through the membrane-

electrolyte system (Amp). Subscripts *D* and *C*, represent the diluate and concentrate streams, respectively, and superscripts *in* and *out* show the inlet and outlet conditions, respectively. The fluid velocity in the direction parallel to the membrane surface and with *x* distance (m) from the membrane is represented by $u_i(x)$. The ion concentration at *x* distance from the membrane surface is represented by $c_i(x)$.

The transport of ions across the membranes is principally governed by the migration of the ions in the *x* direction, as a result of applying an electrical potential gradient across the solution-membrane system. This process is usually accompanied by a less significant diffusive flux of ions from the bulk solution to the solution-membrane interface, resulting from the formation of a thin concentration polarisation boundary layer near the membrane surface. The mechanisms for development of such concentration profiles and their contribution to the total salt flux across the membranes will be described in detail in section 2.3.2.

Salt transport in the *y* direction is mainly governed by the convection of dissolved ions, resulting from the formation of a hydrostatic pressure gradient by the flow of the solution inside the compartment and along the membrane surface. There is also a diffusion process occurring in the *y* direction, resulting from the formation of an ion concentration gradient between the inlet and the outlet of the compartment. The diffusion process in the y direction is relatively small and its contribution to the total salt flux across the membranes is often deemed negligible.

It is important to note that in all the theoretical studies concerning the ion transport phenomena in an ED system, the hydrodynamic conditions and the cell geometry is assumed to be identical for both the diluate and concentrate compartments. This is a realistic and crucial requirement for an ED system, so as to obtain similar pressure drops in all the channels and thus to avoid osmotic pressure gradient across the ion-exchange membranes [31].

A mass balance, that takes into account the volumetric flow rates as well as the current passing the ED stack, to describe the global transport of salt ions from the diluate stream into the concentrate channel is expressed as follows [31],

$$(c_{i,D}^{in} - c_{i,D}^{out})Q_D = (c_{i,C}^{out} - c_{i,C}^{in})Q_C = \frac{\xi I}{\sum_i z_i \upsilon_i F} \tag{2.1}$$

where, c is the ion concentration (mol/m^3), Q is the volumetric flow rate (m^3/s), ξ is the current utilization, I is the total current passing the ED stack (Amp), z is the valence, υ is the stoichiometric coefficient and F is the Faraday constant (96485 A s/mol). The subscript i represents the particular ion of interest. The subscripts D and C represent the diluate and concentrate compartments, respectively and the superscripts *in* and *out* refer to the compartment's inlet and outlet conditions, respectively.

The current utilisation (ξ) is a fair representation for the current efficiency in a unit cell pair, showing the portion of the total current (I) utilized to transfer ($c_{i,in}^{D} - c_{i,out}^{D}$) mass of an ion ($i$) from the diluate stream into the concentrate channel [31]. The current utilisation is often smaller than unity ($\xi < 1$), which is due to small current leakages occurring across the membranes and the flow channels, incomplete selectivity of the ion-exchange membranes as well as the partial transport of H^+ and OH^- ions instead of the salt ions [50, 131]. The latter is mostly the case occurring at high current densities. This will be discussed in detail in section 2.3.3.

2.3.2 Ion transport mechanisms in ED

Under idealised steady state conditions the mass transport of ions through both the solution and the ion-exchange membrane can be described by the extended Nernst-Plank equation with a convection term [130]:

$$J_i = \underbrace{-D_i \nabla c_i}_{J_i^{diff}} \underbrace{- D_i z_i c_i \frac{F}{R_g T} \nabla \varphi}_{J_i^{mig}} + \underbrace{c_i u}_{J_i^{conv}}, \tag{2.2}$$

where J_i is the net ionic flux perpendicular to the flow direction (mol/m^{2}s) , c_i, D_i and z_i are the concentration (mol/m^3), diffusion coefficient (m^2/s) and the valence of the ions, respectively; F is the Faraday constant (96485 A s/mol); φ, R_g and T are the electric potential (V), the gas constant (8.314 J/mol K) and the temperature (K), respectively and u is the mean velocity of the fluid inside the compartment and in direction parallel to the membrane surface. The subscript i represents either the positively or the negatively charged salt ion or H^+ and OH^-. The first term in the right hand side of the Eq.2.2 represents diffusion, the second one, migration and the third one, convection.

Assuming that the global electroneutrality is conserved at all time during the process, the sum of concentrations for all the ions, taking into account their charges, is equal to zero.

$$\sum_i c_i z_i = 0 \tag{2.3}$$

The current density (j , Amp/m^2) is directly related to the total fluxes of all charged species in a system as shown in Eq. 2.4.

$$j = F\sum_i J_i z_i \tag{2.4}$$

Considering the ideal case where no dissolved charged component apart from the salt ions is present in the solution-membrane system, it is possible to substitute the flux terms for the ions as described in the Eq.2.2 into Eq.2.4 and apply Eq.2.3, so to exclude the electric potential from the flux relationships and rearrange the Nernst-Plank equation (Eq. 2.2) as follows;

$$J_i = -D\nabla c_i + \frac{jt_i}{z_i F} + c_i u \tag{2.5}$$

where, D is the electrolyte diffusivity (m^2/s) and t_i is the transport number of the ion. Ion transport number is a function of electro-physical properties of both the ion

and its surrounding environment, this being either the membrane or the solution. Both t_i and D can be expressed by the local ionic concentrations (c_i, mol/m^3) and diffusion coefficients (D_i, m^2/s).

$$t_i = \frac{D_i z_i^2 c_i}{\sum D_i z_i^2 c_i} \tag{2.6}$$

$$D = \frac{D_1 D_2 (z_1^2 c_1 + z_2^2 c_2)}{\sum D_i z_i^2 c_i} \tag{2.7}$$

The subscripts 1 and 2 in these relationships (Eqs. 2.6 and 2.7) refer to the salt counter-ions (*i.e.* ions with opposite charge to that of the reference ion-exchange membrane) and co-ions (*i.e.* ions with similar charge to that of the reference ion-exchange membrane), respectively.

Detailed explanation of the mass transport inside solution and ion-exchange membrane will be supported by theoretical description of the ionic flux using Eq. 2.5 in sections 2.3.2.1 and 2.3.2.2, respectively.

2.3.2.1 Ion transport inside the solution

The flux terms contributing to the transport of a cation from the diluate to the concentrate compartment via a cation-exchange membrane (CEM) are shown in Figure 2.3. The conceptual representation of all the transport phenomena shown in this model would be analogous for the transport of an anion through an anion-exchange membrane (AEM).

Once an electric potential is applied across an equilibrium membrane-electrolyte system, ions inside the electrolyte solution start to migrate (J^{mig}, mol/m^{2}s) in the direction of the current (I, Amp) and perpendicular to the membranes. The difference between the ion transport numbers in the solution and the membrane structure causes the concentration of the ions to decrease at the vicinity of the membrane in one compartment (diluate) and to increase near the membrane in the neighbouring compartment (concentrate) (Figure 2.3). This process takes place between t_0,

representing the time at the beginning of the process when yet no concentration profile is formed within the boundary layer, and $t_{st.st}$, representing the steady state condition when the concentration profiles are fully developed within the boundary layer. Development of such concentration profiles within thin boundary layers near the membrane surface triggers the diffusion of the ions (J^{diff}, mol/m^{2}s) from the bulk solution to the membrane surface in the diluate channel (and from the membrane surface to the bulk solution in the concentrate channel). In Figure 2.3, concentration of ions in the solution is represented by c (mol/m^3). The subscripts "+" and "-" represent the charge of the ion. The subscripts D and C link the concentration and the flux elements to their corresponding compartments, D for diluate and C concentrate. The superscripts b and m, represent the boundary layer and the membrane environments, respectively.

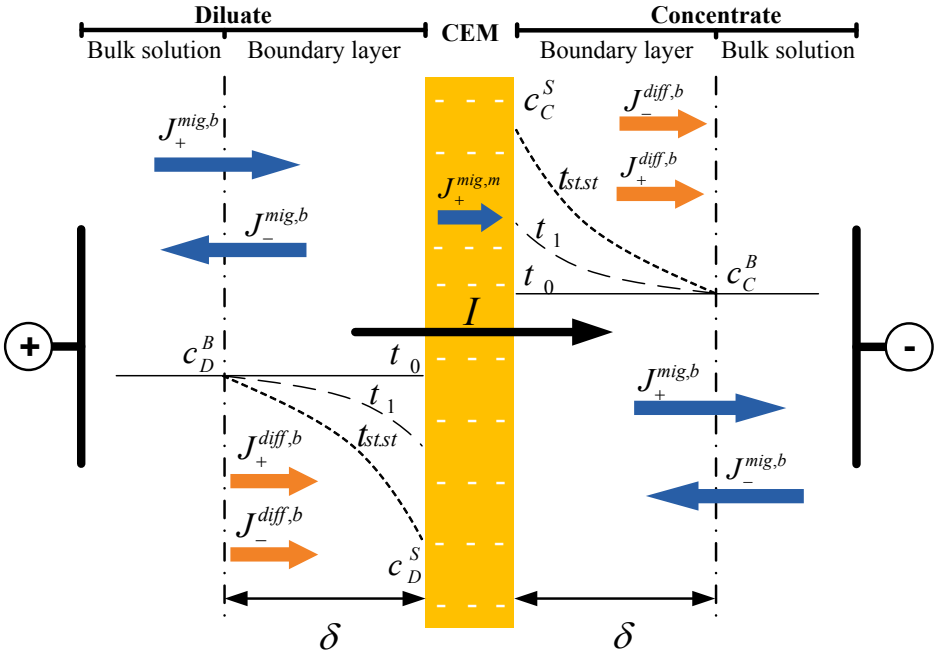

Figure 2.3 Conceptual model showing the main ion transport phenomena occurring in a membrane-electrolyte system (CEM: cation exchange membrane, *t*: time from the beginning of the process).

As mentioned earlier, apart from the migration and diffusion processes that take place in a perpendicular direction toward the surface of the membranes, there is also a convection flux that occurs in the direction of the flow and parallel to the

membranes, which is primarily governed by the velocity of the fluid at the solution-membrane interface (Eq. 2.5). Considering that the fluid has laminar characteristics when is flowing between the membranes, the contribution of the convective flux terms to the total salt flux through the bulk solution can be considered negligible.

Taking all the aforementioned conditions into consideration, the ion transport mechanisms taking place at the membrane interface of the solution under idealized steady state conditions can be described by the following modified version of the extended Nernst-Plank equation ;

$$J_i = -D\left(\frac{\partial c_i}{\partial x}\right)_{x=\delta} + \frac{jt_i^b}{z_i F} \tag{2.9}$$

Where, t_i^b refers to the ion transport number in the solution. Also considering 0 of the x-axis being on the solution-membrane interface, δ refers to the thickness of the diffusion boundary layer (m).

2.3.2.2 Ion transport inside the ion-exchange membrane

In a membrane, where the fixed ions are well distributed through the polymeric matrix, the gradients of the concentration profiles for both the co and counter-ions are assumed to be close to zero. The latter is conserved by the Donnan exclusion principles, governing the charge balance and thus the electroneutrality in both the solution and the ion-exchange membrane under idealised steady state conditions. The diffusion coefficient (D, m^2/s) for an ion inside membranes is believed to be 10 to 10^3 times smaller than that of an ion in solution [130]; hence the contribution of the diffusive flux terms (J_i^{diff}, mol/m^2s) to the ion transport through the ion-exchange membrane is considered to be negligible [31]. Moreover, the flow of the solution inside the membrane is presumed to be zero, hence the contribution of the convection terms (J_i^{conv}, mol/m^2s) to the transport of ions inside the polymer structure is also assumed to be negligible. Taking all these into consideration, the transport of ions inside the membrane can be only expressed by the migration flux terms (J_i^{mig}, mol/m^2s);

$$J_i^m = \frac{jt_i^m}{z_i F} \tag{2.10}$$

where the subscript *m* refers to the ion-exchange membrane. It is important to note that ion transport numbers in ion-exchange membranes that are highly permselective to counter ions are much higher than those in the bulk solution. This number for commercial membranes is often bigger than 0.95 [132].

In normal steady state conditions and in absence of any chemical reaction, a mass balance is maintained between the ingoing (Eq. 2.9) and outgoing (Eq. 2.10) flux terms, which can be described as follows;

$$D\left(\frac{c_i^B - c_i^S}{\delta}\right) + \frac{jt_i^b}{z_i F} = \frac{jt_i^m}{z_i F} \tag{2.11}$$

where c_i^B and c_i^S refer to the concentration of the counter-ion (mol/m^3) in the bulk solution and on the membrane surface, respectively. It is important to note that Eq. 2.11 takes into account an idealised steady state condition where the concentration profile within the boundary layer has a linear gradient:

$$\frac{\partial c_i}{\partial x} = \frac{\Delta c_i}{\Delta x} \tag{2.12}$$

Considering the fact that diffusivity (*D*) of an ion is principally dependent on the physicochemical properties of the ion inside a given solution and that the boundary layer's thickness (δ) is a parameter solely dependent on the hydrodynamic characteristics of the process (*e.g.* flow rate and the geometries of the ED stack, membranes and the spacers) a mass transfer coefficient (k_m) that would describe the global transport behaviours of an ion in the membrane system can be given as follows [31];

$$k_m = \frac{D}{\delta} \tag{2.13}$$

The mass transfer coefficient, (k_m), is a function of Sherwood number which itself depends on a series of parameters including: the length of the cell (*l*), the hydraulic diameter of the cell (*de*), α and β, which are respectively representing the angle between the spacer filaments and the flow attack angle, Reynolds number (*Re*), which is a function of the fluid flow properties, and Schmidt number (Sc), which is a function of the transport characteristics of the electrolyte [133].

The relationships introduced in this section will be later used to analyse the boundary layer conditions and limiting current density in Chapter 4 and in Appendix C.

2.3.3 Concentration polarisation and limiting current density

As mentioned in the previous section, immediately after applying an external electric field across an equilibrium electrolyte-membrane system, a concentration profile starts to develop within a thin diffusion boundary layer near the membrane. This phenomena that principally occurs due to the difference between the ion transport number in the solution and the ion-exchange membrane is termed, following IUPAC suggestions, concentration polarisation (CP) [134]. CP is a non-favourable but common phenomenon in many membrane processes, hindering the ionic flux through the membrane [31, 135]. Influence of CP on ED performance is negligible at low current densities, but becomes particularly significant when the limiting current density (j_{lim}, Amp/m^2) is exceeded and thus the concentration of ions at the solution-membrane interface approaches zero [136, 137]. By applying the latter condition ($i.e.\, c_i^s \approx 0$) into Eq. 2.11, a theoretical relationship for calculating the limiting current density (LCD) can be obtained (Eq. 2.14).

$$j_{\lim} = \frac{Dc_i^B F}{\delta(t_i^m - t_i^b)} \tag{2.14}$$

Exceeding j_{lim} leads to formation of an excessive electric potential across the boundary layer that results in water dissociation at the solution-membrane interface [137-140]. The emergence of H^+ and OH^- ions due to water splitting not only reduces the current efficiency of the process, but also causes a reduction in local pH close to

the membrane surface in the diluate channel and, vice-versa, a local pH increase in the concentrate channel. These unfavourable pH variations can be extended into the bulk solutions and reduce the quality of the water product. Extreme pH variations also reduces the lifetime of membranes that have low acidic/basic resistance [141]. Moreover, the variation of acidity close to the membrane surface may enhance membrane fouling and scaling [131] and contribute to a further reduction in the system performance. Therefore, in conventional ED processes the current density is often kept well below j_{lim} in order to minimise the loss in current efficiency and to avoid damage to the membranes and the desalination products.

Limiting current density can be determined using different methods. One of these methods is based on measuring the current density against a wide range of voltages applied across an ED stack for a given feed concentration and a fixed flow rate [31, 142]. A schematic representation of a current-voltage curve obtained from such a test is shown in Figure 2.4A. As seen in this figure, in a so-called "sub-limiting current density regime" the system exhibits an Ohmic behaviour, meaning that the current density increases linearly with an increase in the applied voltage. The sub-limiting current density regime extends up to a voltage at which the concentration of the ions at the surface of the membrane reaches zero due to the evolvement of a significant concentration polarisation. In the absence of charge carrying ions at the surface of the membrane the resistance of the ED stack increases immediately to high levels, causing the slope of the current-voltage curve to decrease drastically and thus the system enters into a so-called "limiting current density regime". The current density corresponding to the voltage at which the current-voltage curve starts deviating from linearity is referred to as the limiting current density, j_{lim}. At a voltage somewhat higher than that of the limiting current density the current again starts to increase linearly with voltage. This is the beginning of the so-called "over-limiting current density regime", where the majority of salt ions are believed to be transported across the boundary layer by a phenomena different from diffusion [138, 143]. Based on the literature this additional phenomenon that contributes significantly to the transport of the ions from the bulk solution to the membrane surface at the over-limiting current density regime is based on electro-convection [50, 144].

Since the exact point at which the current-voltage curve begins to deviate from linearity is often not easily detectible experimentally, Cowan and Brown suggested a new representation of the current-voltage measurements for determining the limiting current density [145]. Based on their suggestion, the overall resistance of the ED stack (R_{stack}) is plotted against the reciprocal of the current density (schematically shown in Figure 2.4B) and j_{lim} is determined as the current density at which a sudden increase in R_{stack} is appeared.

Another indication of exceeding the limiting current density would be the observation of a sudden decrease of the pH in the diluate stream, as shown schematically in Figure 2.4C. The reason for this pH drop was suggested to be the more significant water dissociation occurring at the surface of the aion-exchange membrane compared to cation-exchange membrane at current densities above j_{lim}, causing the number of H^+ ions to increase much faster than OH^- in the diluate stream [31, 140].

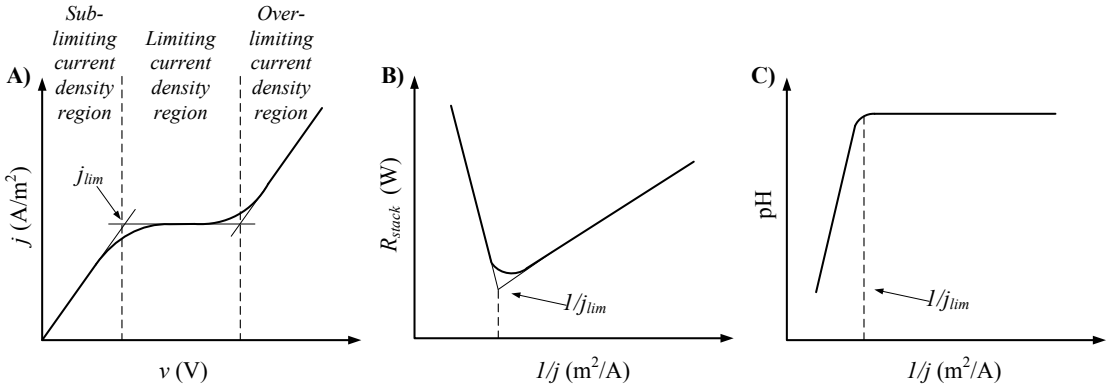

Figure 2.4 Experimental determination of limiting current density (j_{lim}) using A) current density-voltage measurements, B) R_{stack} measurements and C) pH measurements.

Detailed investigations regarding the impacts of concentration polarisation on ion transport in an ED system at different current regimes (below and above j_{lim}) will be carried out in Chapter 4. The possibility of disrupting CP by means of applying a fluctuating source of power (pulsed-voltage) to ED stack and thus operating at high current densities with no significant water dissociation will be also studied in the same chapter.

2.3.4 The impacts of physicochemical properties of inorganic contaminants on their removal in ED process

Ion transport in ED strongly depends on the physicochemical properties of the ions, as well as the way they interact with each other and with the ion-exchange membrane polymer.

The dependence of electrodialytic removal of inorganic contaminants on their valence has been studied by many researchers [146-148]. Sadrzadeh *et al.* showed that in a competing environment the selective monovalent, divalent and trivalent ions were separated in the following order: Na^{+} > Cu^{2+}, Zn^{2+}, Pb^{2+} > Cr^{3+} [149]. In a similar experiment carried out on a mixture of anions by El Midaoui *et al.* the order of ion removal observed was as follow: NO_3^{-} > Cl^{-} > HCO_3^{-} > SO_4^{2-}. It was hypothesised that the ions with smaller valence number occupy more active sites in the membrane's structure; hence they limit transport of ions with a greater valence number through the membrane. Since the number of active sites in an ion-selective membrane is constant, the ionic separation through the membrane was assumed to increase with decreasing the ionic valence.

The mechanism of separation for ions with similar charge and valence in ED is governed by a combination of other physicochemical properties, among which Gibbs free energy of hydration is assumed to be the most crucial [150, 151]. Gibbs free energy of hydration is the energy required for an ion to be stripped from its surrounding water molecules when entering from the solution to the membrane structure. The smaller the size of an ion, the greater is its charge density; hence the ion forms stronger and tighter bonds with the water molecules in its surrounding. The latter causes the Gibbs free energy of hydration of the ion to be higher and thus the transport of the ion through the membrane takes place at a slower rate and to be energetically more expensive. Banasiak *et al.* [152] showed that in competition with fluoride ions, nitrate ions were removed more efficiently from an organic matter containing solution due to the weaker hydration shell of nitrate compared to fluoride. Similar explanations were given in the work of other researchers to explain the competitive removal of ions in different membrane systems (*e.g.* Nanofiltration (NF)

and ion-exchange membranes) [23, 100, 101, 151-161]. Although molar conductivity and ion mobility are determining factors for the transport of ions in electrolyte solution, they often fail to completely explain the transport of ions at the solution-membrane interface and also that inside the polymer structure [23, 154, 157].

In a study carried out by Van der Bruggen et al. [162] on separation of mono- and multivalent ions (NO_3^-, Cl^-, Na^+, SO_4^{2-}, Mg^{2+}) from single model salt solutions ($NaNO_3$, NaCl, Na_2SO_4, $MgSO_4$ and $MgCl_2$) using ACS anion-exchange and CMS cation-exchange membranes, NaCl showed the fastest removal compared to the other compounds. The salt containing both divalent cation and anion, $MgSO_4$, showed the slowest separation from the brine. The differences observed in removal characteristics of different ions were explained to be due to the membrane selectivity and also the differences in the sizes of the ions.

Sata et al., [163, 164] investigated the permselectivity of particular ions (F^-, Cl^-, Br^-, I^-, NO_3^-, SO_4^{2-}) through methylene groups of diamines cross-linked AEMs. They showed that the ionic separation and transport number of ions was primarily governed by a balance of the hydrophilicity of the membranes with the Gibbs hydration energy of the anions, and partially by the hydrated ionic radii of the ions. The anions with higher transport number (*e.g.* SO_4^{2-}) showed more reduction in permeation through the membrane compared to those with smaller transport number (*e.g.* I^-). Permeation of an ion through an ion-selective membrane was shown to be dependent on both the ionic mobility and the affinity between the membrane and the specific ion.

2.3.5 The impacts of operating conditions on the ED process

Not only the physicochemical properties of the salt ions but also the operating conditions in a process, such as voltage, flow rate and feed concentration can significantly influence the removal of ions from electrolyte solutions. As is clear from the Nernst-Plank relationship (Eq. 2.2), an increase in the electric potential applied across the membranes (φ, V) results in a faster migration of the ions through the solution-membrane system; hence it enhances the desalination rate. This is a

well-established behaviour, observed in the work of many researchers [149, 165, 166]. It is important to note that the increase in the voltage is only advantageous when operating in the sub-limiting current density regime. Increasing voltage at regions above the limiting current density (j_{lim}) is not desirable, since it leads to the loss in power efficiency. It can also results in dissociation of water molecules into H^+ and OH^- ions and thus causes severe pH variations in the diluate and concentrate streams that is detrimental to both the membranes and the desalination product quality (detailed in section 2.3.3).

The relationship between membrane selectivity and current density was also studied by some researchers. Based on the theory of competitive ion transport in electrodialysis, proposed by Nikonenko *et al.* [102, 167] and Zabolotsky *et al.* [168] specific selectivity can be obtained at currents below the liming current density. Based on this theory, the selectivity of ions decreases with increasing the applied electric filed and approaches zero once the limiting current density is reached.

Increasing the feed concentration is equal to increasing the number of charge carrying ions in the bulk solution. Therefore, the higher the feed concentration at a given voltage, the larger is the current passing through the ED system and, correspondingly with that the higher is the flux of ions through both the solution and the membranes. This behaviour is clearly seen in all ED batch processes, where the desalination rate is the highest at the beginning of the process, but it diminishes as the salt concentration decreases in the diluate channel throughout the process.

The findings obtained so far about the impacts of flow rate on the ion removal in ED processes have been somewhat conflicting. Mishchuk *et al.* [61] and El Midaoui *et al.* [23] showed improvement in the desalination rate due to increasing the flow rate. They discussed that increasing the flow rate can result in thinning of the convective diffusion boundary layer that ultimately enhances the diffusion of the ions from the bulk solution to the membrane-solution interface. In some contrary results obtained by Sadrzadeh *et al.* [149], Yang *et al.* [165] and Sik Ali *et al.* [51] the increase in the flow rate was shown to have an adverse impact on the ED process and resulted in the lowering of the desalination rate. In these studies increase in the flow rate was

assumed to lead to the decrease in the residence time for the ions passing the ED stack, hence reducing the number of ions available in any time increment to be transported across the membranes. In a study carried out on removal of nitrate from groundwater by using electrodilysis, Bi *et al.* [159] showed that the possibility of the either of the above mentioned behaviours to happen strongly depends on the flow regime at which the operation is carried out. Bi observed a critical flow rate (*i.e.* 7 L/min) below which an increase in the flow rate resulted in an improved current transfer through the membranes and thus higher desalination rates; while oppositely any increase in the flow rate above 7 L/min resulted in prolonging the desalination process. The contradictory results obtained in these studies with regards to the impacts of flow rate on the performance of the membrane system necessitates more in-depth research to determine the actual influence of flow rate on the salt flux in ED. Such studies are particularly crucial as they can further elucidate the impact of flow rate on the water production capacity of the desalination system.

The impacts of feed salt concentration and flow rate will be investigated systematically using the wind-ED system and the obtaining results will be discussed in detail in Chapter 8.

2.3.6 Energy requirement in electrodialysis

The energy required for an ED process (E_{ED}, kWh) is a combination of two energy components; i) the energy required to pump the salt and electrode rinse solutions into the ED stack (E_p, kWh), and ii) the energy required to transfer the salt ions from the diuate channel, and through the ion-exchange membranes, into the concentrate channel (E_{des}, kWh) [31]. Depending on the efficiency of the pumps and the flow rate required for circulating diluate, concentrate and electrode rinse solutions into the ED stack, E_p can be expressed as follows,

$$E_p = \eta_p \frac{\left(Q_D \Delta P_D + Q_C \Delta P_C + Q_{ER} \Delta P_{ER}\right)}{Q_D} \tag{2.15}$$

where η_p is an efficiency term for the pump, Q is the volumetric flow rate (m^3/s) and ΔP is the pressure gradient (Pa) between the inlet and the outlet of the channel.

Subscripts *D*, *C* and *ER* represent the diluate, concentrate and electrode rinse solutions, respectively.

For a batch recirculation process, where the resistance of the cell pairs and the current vary with time throughout the process, the energy required for desalination (E_{des}) can be expressed by the integration given in Eq. 2.16.

$$E_{des} = \int (N\ R_{cell} + R_{ER}) I^2 dt \tag{2.16}$$

Here, N is the number of cell pairs in the ED stack, R_{cell} is the net resistance in a cell pair (Ω), R_{ER} is the resistance generated by the reaction of electrode rinse solution with the electrodes (Ω) and I is the current (Amp). Normally R_{ER} is negligible and thus it is not taken into account when calculating the global energy consumption of the process. In desalination applications for the production of potable water from medium to high salinity salt solutions (*e.g.* brackish groundwater: 1,000 – 10,000 mg/L TDS and sea water: ≥ 30,000 mg/L), E_{des} is often much larger than E_p, and therefore it is considered as the main contributor to the total energy cost of the process.

By rearranging Eq. 2.11 for a single salt solution, the current (I) passing through the membrane cell pairs of the ED stack can be expressed as follows,

$$I = A_m j = \frac{z\ A_m F}{\delta} \frac{\left(c_D^B - c_D^S\right)}{\left(t^m - t^b\right)} \tag{2.17}$$

where j is the current density (Amp/m^2), A_m is the effective surface area of the membrane (m^2), F is the Faraday constant (96485 A s/mol), δ is the thickness of the boundary layer (m), c and z are the molar concentration (mol/m^3) and the valence number of the ion i and, t^m and t^b refer to the ion transport numbers in the membrane matrix and in the solution, respectively; superscripts B and S represent the bulk solution and the solution-membrane interface environments, respectively.

The electric resistance of a membrane cell pair (R_{cell}) is the sum of the resistances of the ion-exchange membranes (R_{AEM} and R_{CEM}), the diluate and concentrate streams

(R_D and R_C) and the boundary layers forming at the solution-membrane interfaces ($R_{BL,D}$ and $R_{BL,C}$) (Eq. 2.18).

$$R_{cell} = R_{AEM} + R_D + 2R_{BL,D} + R_{CEM} + R_C + 2R_{BL,C} \quad (2.18)$$

Here the subscripts *AEM*, *CEM*, *C*, *D* and *BL* represent the anion-exchange membrane, the cation-exchange membrane, the diluate and concentrate streams and the boundary layer, respectively.

The electric resistance of the anion- and cation-exchange membranes can be calculated using Eqs. 2.19 and 2.20, respectively.

$$R_{AEM} = k_{AEM} \frac{l_{AEM}}{A_m} \quad (2.19)$$

$$R_{CEM} = k_{CEM} \frac{l_{CEM}}{A_m} \quad (2.20)$$

where l is the membrane thickness (m) and k is the membrane area resistance (Ωm). The latter parameter, k, is a complex term which depends on the electrochemical properties of the membrane, type of the fixed charged groups inside the membrane matrix, the ion exchange capacity of the membrane and its swelling capacity [169]. Parameters such as ion mobility inside the membrane, which itself depends on the temperature, molecular weight and size of the ions as well as their interactions with each other and with the fixed charged groups inside the membrane are also influential on the membrane area resistance, k. An overview of the impacts of physicochemical properties of the ions on their removal in ED was given in section 2.3.4; this topic will be discussed in more detail in the Chapter 7.

Assuming that i) the concentration is homogenous in both the diluate and concentrate channels, ii) the thickness of the Nernst diffusion boundary layer, δ, is negligible against the channel width, h, and iii) the water conductivity is negligible, the resistance off the diluate (R_D) and concentrate (R_C) streams can be calculated using Eqs. 21 and 22, respectively [169].

$$R_D = k_D \frac{h-2\delta}{A_m} \cong \frac{1}{c_D \Lambda_D} \frac{h}{A_m} \tag{2.21}$$

$$R_C = k_C \frac{h-2\delta}{A_m} \cong \frac{1}{c_C \Lambda_C} \frac{h}{A_m} \tag{2.22}$$

Here, h is the width of the channel, defined as the distance between two neighbouring membranes in a membrane cell pair, and k_D and k_C are the specific resistances of the diluate and concentrate streams, respectively. The specific resistance of each stream of solution is inversely proportional to the molar conductivity (Λ, Sm^2/mol) and average salt concentration (c, mol/m3) in that solution, as shown in Eqs. 21 and 22 [31].

Assuming that the operation is in a steady state condition (*i.e.* Eq. 14 is valid) and also that the conductivity of water is negligible, the resistance of the boundary layers in the diluate and concentrate channels can be expressed by Eqs. 2.23 and 2.24.

$$R_{BL,D} = \frac{2}{(c_D^B + c_D^S)\Lambda_{BL,D}} \frac{\delta}{A_m} \tag{2.23}$$

$$R_{BL,C} = \frac{2}{(c_C^B + c_C^S)\Lambda_{BL,D}} \frac{\delta}{A_m} \tag{2.24}$$

where c^B is the concentration in the bulk solution and c^S is the concentration at the solution-membrane interface and Λ_{BL} is the molar conductivity of the solution within the Nernst diffusion boundary layer (Sm^2/mol). It is important to note that the thickness of the boundary layer, δ, is independent from both the feed concentration and the electric potential applied across the membranes and is principally a function of hydrodynamic properties of the process, such as flow rate and the cell geometry [31, 50]. For instance, the higher the flow rate the less laminar is the flow of the streams inside the channels of the ED stack, hence the smaller is the thickness of the boundary layer through which the ions need to diffuse to reach the solution-membrane interface. The result of the shrinkage of the boundary layer thus is a reduction in the overall electric resistance of the ED stack (R_{stack}), and

correspondingly with that a reduction in the energetic cost of the salt transport across the membrane (E_{des}). However, the studies carried out so far on the parameters influencing the overall energy consumption of ED process has not claimed a significant difference in the energy consumption due to the change in the flow rate [36, 170, 171]. An electric circuit representation of an electrodialysis system, showing the regional resistances within a membrane cell pair and their resulting local potential gradients, is given in Figure 2.5.

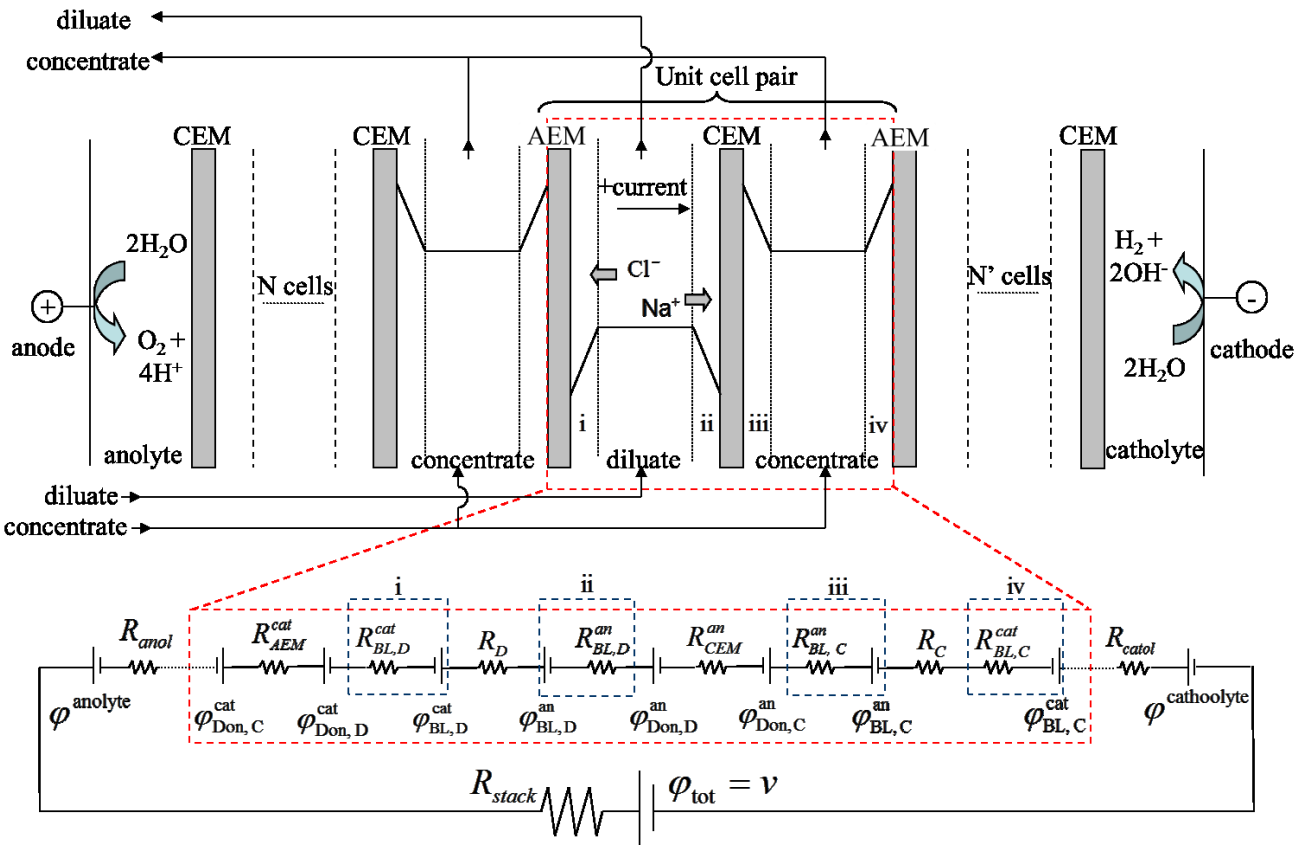

Figure 2.5 Electric circuit representation of electrodialysis stack; *j* and *R* represent the electric potential (V) and resistance (W), respectively; subscripts *D* and *C* represent the diluate and concentrate streams, respectively; subscripts *BL*, *AEM* and *CEM* represent the boundary layer, anion-exchange membrane and cation-exchange membrane, respectively; Subscript *Don* refers to Donnan potential; superscripts *an* and *cat* represent the anion and the cation, respectively (adapted from [172]).

By substituting current, I, and cell resistance, R_{cell}, in Eq. 2.16 with their expressions, as given in Eqs. 2.17 – 2.24, the energy required for desalination in absence of a significant electrode reaction resistance (R_{ER}), can be expressed as follows:

$$E_{des} = \int (NR_{cell})I^2 dt = \frac{NA_m F^2 z^2}{(t^m - t^b)^2 \delta^2} \int \left(\begin{array}{l} k_{AEM} l_{AEM} + \dfrac{h}{c_D \Lambda_D} + \dfrac{4}{(c_D^B + c_D^S)\Lambda_{BL,D}} \\ + k_{CEM} l_{CEM} + \dfrac{h}{c_C \Lambda_C} + \dfrac{4}{(c_C^B + c_C^S)\Lambda_{BL,C}} \end{array} \right) \left(c_D^B - c_D^S\right)^2 dt \tag{2.25}$$

The energy dissipation due to the resistances in the ED stack has a square relationship with the current (Eq. 2.25), whereas the relationship of the salt flux with the current is of a linear nature (Eq.2.5). Therefore, one can expect any variation of current to have a greater influence on the energy consumption of the process than the rate of desalination. Taking into account the direct relationship that exists between the current and the salt concentration in the diluate stream (Eq. 2.11), the influence of concentration variation is also expected to be more pronounced on the energy cost of the process (Eq.2.25) than the rate of desalination. The diagrams given in Figure 2.6 are schematic representations of the cost of electrodialysis process as a function of current density and feed salt concentration.

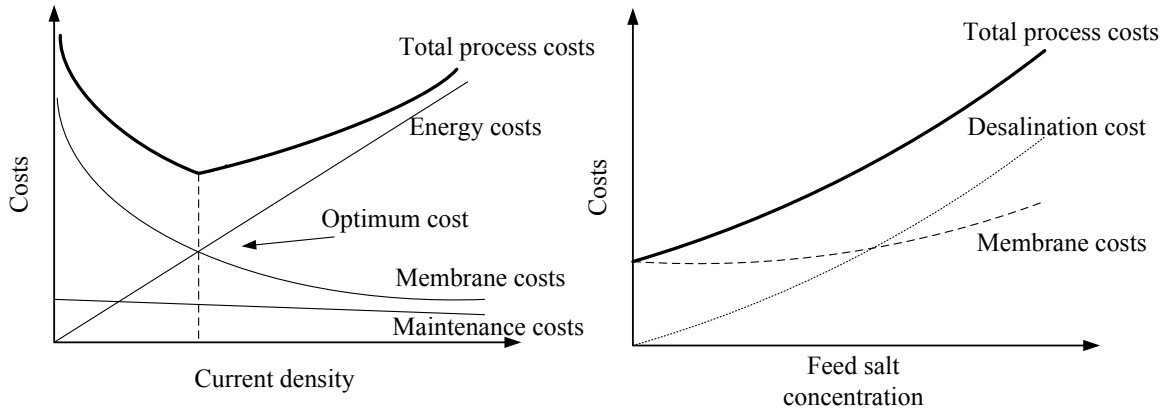

Figure 2.6 Schematics demonstrating the cost of ED process as functions of current density and feed salt concentration (adapted from [31]).

It is important to note that higher the current density the smaller is the required membrane surface area to maintain a certain level of water production for a

desalination plant. However, to keep the energy consumption and thus the costs of the process to a minimum level, always a balance should be maintained between the available membrane surface area and the current density.

2.4 Wind energy

2.4.1 Formation, availability and inherent fluctuations

Approximately 1-2% of the energy received from the sun is converted into wind energy [98, 173]. Differential heating between the poles and the equator together with the rotation of the earth create atmospheric pressure gradients, leading to the formation of jet streams in 10-12 km altitudes. The jet streams transfer the energy from the upper atmosphere to the ground where the wind characteristics are determined by the geographical location, latitude, seasonal period and roughness of the earth's surface [174]. These parameters are all critical to the variability and magnitude of the available wind energy that can be exploited by a wind turbine [97, 99]. The wind energy available in one location is strongly dependent on the level and variations of the wind speed in that site, as it can be clearly seen from Eq. 2.26 [98].

$$P_w = 0.5\rho A_a v^3 \tag{2.26}$$

In Eq. 2.26 P_w is the kinetic power preserved in the wind resource (W), v is the wind speed (m/s), ρ is the air density (kg/m^3) and A_a is the cross-sectional area of the bundle of air under investigation (m^2). Based on a wind speed classification proposed by International Electrotechnical Commission (IEC) standards for small scale wind turbines (minimal hub height of 25 m), wind speeds below 7.5 m/s are classified as low, between 7.5 and 10 m/s as medium and above 10 m/s as high wind speeds [175]. To make this classification more applicable for a micro wind turbine system installed at a hub height of 8 m (like the one used in this research) the log law relationship (Eq. 2.27) can be used [98].

$$v_z = v_{ref} \times \left(\frac{\ln\left(z/\varepsilon\right)}{\ln\left(z_{ref}/\varepsilon\right)} \right) \qquad 2.27$$

In the log law relationship v_z is the wind speed (m/s) at the hub height z (8 m) and v_{ref} is the originally measured wind speed (m/s) at the reference hub height of z_{ref} (minimum 25 m). The chosen value for the roughness index (ε) in this research is 0.1; this is to take into account the terrain condition in countryside with trees and hedges [98, 99]. The modified wind speed classification for the micro wind turbine system, resulted from the log law method, will then be proposed as follows;

Low wind speed: $v < 6$ m/s

Medium wind speed: 6 m/s $\leq v \leq$8 m/s

High wind speed: $v > 8$ m/s

Figure 2.7 gives a global map of wind speed availability, measured at the height of 80 m, over both the land and the water.

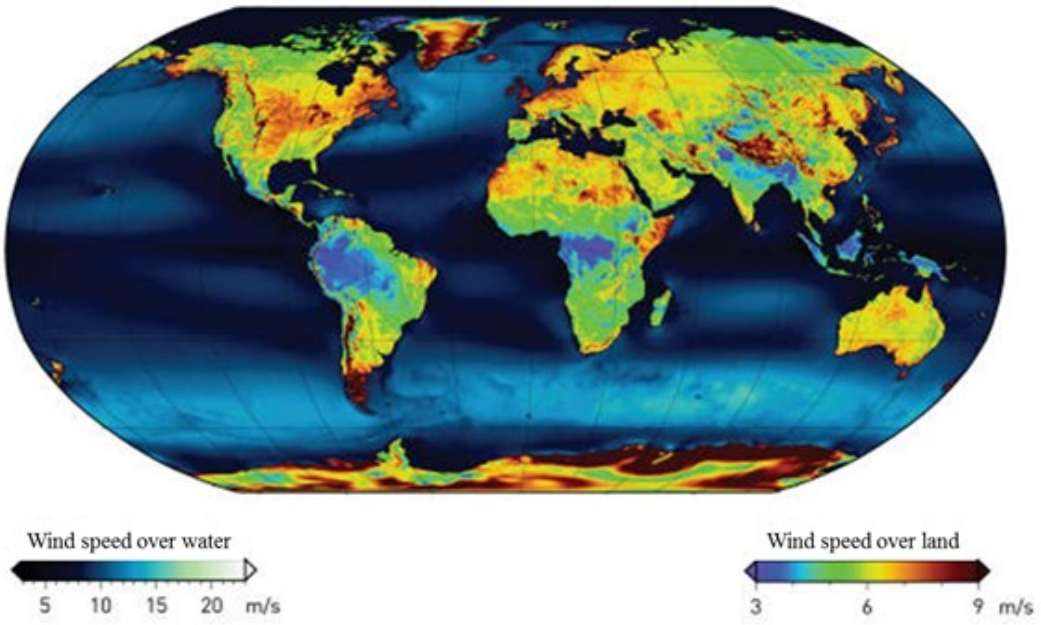

Figure 2.7 Worldwide average wind speed map, created based on wind speed measurements at the height of 80 m [176].

In the literature wind speeds between 5 and 6 m/s were reported as the ones with the highest frequency of occurrence [177] and suitable for satisfactory operation of small scale wind systems with hub heights between 8 and 10 m [74, 75, 98].

The distribution of the wind speed fluctuations over a mean wind speed is described by the Van der Hoven spectral model (Figure 2.8) [178]. This model was developed based on a series of wind speed measurements taken place in Brookhaven, New York, USA. In Figure 2.8, the x-axis shows the log frequency of the wind speed oscillations and the y-axis shows the wind speed spectrum, which is proportional to the variance of the wind speed fluctuations over a mean wind speed. Two distinct regions of short-term and long-term fluctuations are seen in this model. Short term fluctuations are majorly linked with the turbulence and fast occurring intermittent wind speed variations, while the long-term fluctuations are associated with the synoptic (caused by the passage of weather systems) and diurnal (dependent on the time of the day) variations of the wind speed [179].

As seen in Figure 2.8, there is a so-called deep "spectral gap" in the frequency range of 0.5 – 10 cycles/hour separating the short term and long term fluctuations from each other [178, 179]. The lack of strong physical processes, capable of creating fluctuations to support eddy energy in the atmosphere in this frequency range is believed to be the main reason for such a gap to appear.

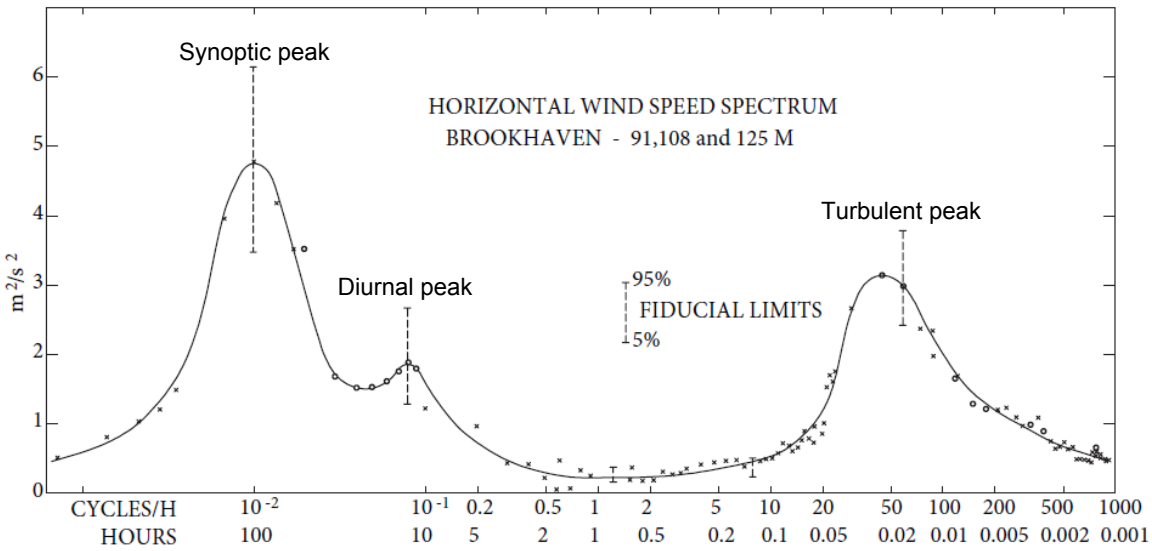

Figure 2.8 Spectral model of wind speed by (adapted from [178])

Short-term fluctuations, caused by rapid variations of the wind speed over the time period of 10 s to 10 min, have negative impacts on the power performance of the wind turbines [78, 97]. These fluctuations, which are generally caused by the gust and turbulence in the wind resource, were shown to be particularly challenging and significantly more detrimental compared to that of synoptic and diurnal fluctuations for the implementation of the wind turbine systems [99]. Short-term fluctuations are often demonstrated by turbulence intensity (TI), which is a dimensionless parameter used to measure the wind speed fluctuations imposed on a mean wind speed [98].

$$TI = \frac{\sigma v}{v_{mean}} \tag{2.28}$$

In Eq. 2.28 σv is the standard deviation of the wind speed (m/s) and v_{mean} is the mean wind speed (m/s) obtained from averaging the stochastic variations in the wind over a period of ten minutes. TI often has a value between 0.1 and 0.4 [76, 98, 178], but the possibility of having more extreme fluctuations (*e.g.* in case of intermittent wind) and TIs up to 0.6 were also reported [14, 99, 180]. To simplify the theoretical and practical analysis carried out on the variability of the wind resource, the wind speed fluctuations are often approximated by sinusoidal functions [181]. A generic form of such sinusoidal function is as follows;

$$v(t) = v_{mean} + \alpha \sin\left(2\pi \frac{t}{T_o}\right) \tag{2.29}$$

where, $v(t)$ is the wind speed (m/s) at a given time (t, s), α is the amplitude of fluctuations (m/s) and T_o is the period of oscillations (s) [98].

2.4.2 Power generation in small scale wind turbines

Upon approaching a tube of moving air (wind), the kinetic energy of the wind in contact with the airfoils of the wind turbine's blades create a combination of drag forces (in the direction of the wind) and lift forces (perpendicular to the direction of the wind) [98, 173]. The resultant of these force vectors on the oppositely positioned blades of the rotor creates a productive torque force that tends to spin the rotor. The

rotor either directly (in case of direct drive permanent magnet generators (PMGs)) or indirectly (via gearbox for larger fixed gear generators) is connected to a generator [95, 174, 182-185]. The generator is responsible to transmit the mechanical energy received from the rotor to an electrical output, which is often in the form of voltage. The schematic below simply shows the sequences taken for producing electricity in a wind turbine.

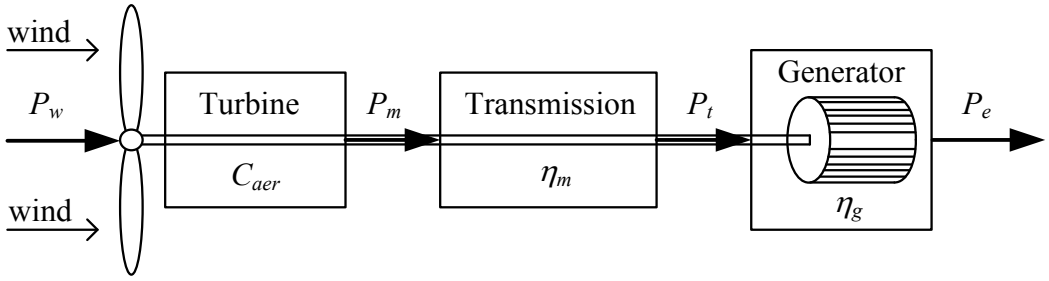

Figure 2.9 Schematic of a wind turbine in power production from wind (adapted from [173]).

In Figure 2.9, P_w is the wind power, P_m is the mechanical power output from the turbine, P_t is the transmitted power to the generator and P_e is the electric power produced by the wind turbine's generator. η_m is the transmitter's (*e.g.* the gear box) efficiency, η_g is the power conversion efficiency of the generator and C_{aer} is the aerodynamic efficiency of the wind turbine [173]. The maximum theoretical value found for C_{aer} is 0.593, known as Betz coefficient. This coefficient indicates that an actual wind turbine is not able to extract more than 59.3% of the available energy in the bundle of air that passes through the swept area of its blades [97, 98, 173]. Taking into account the efficiency terms demonstrated in Figure 2.9, the electric energy generated by a wind turbine (P_e, W) can be calculated as follows,

$$P_e = C_{aer}\eta_t\eta_g P_w \qquad 2.30$$

By inserting Eq. 2.26 in Eq. 2.30, the electric energy produced by a wind turbine can be demonstrated by the following simplified relationship,

$$P_e = 0.5C_p\rho A_s v^3 \qquad 2.31$$

where, A_s is the swept area of the wind turbine blades and C_p is the product of the efficiency terms C_{aer}, η_g and η_g, referred to as the practical efficiency of the wind turbine [97, 98, 173]. C_p is significantly influenced by the number of the blades (wind turbine's solidity), as shown in Figure 2.10.

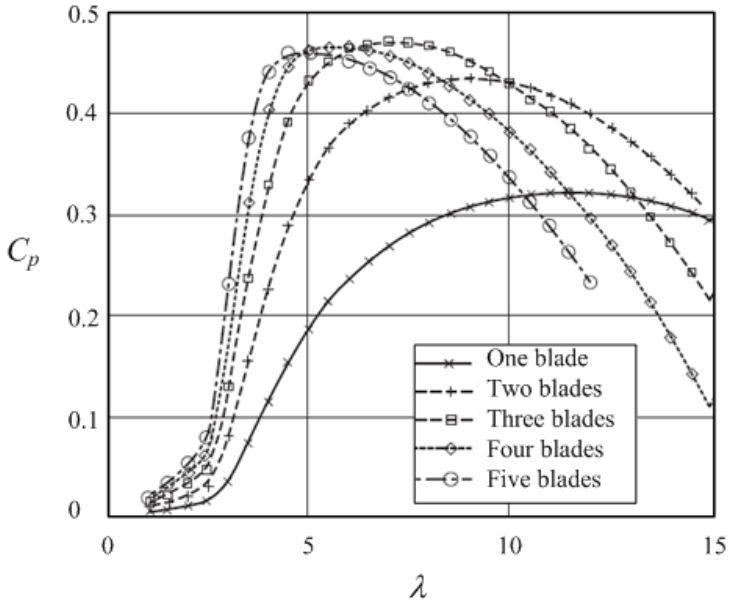

Figure 2.10 Impacts of solidity on the practical efficiency (C_p) of a wind turbine (adapted from [97]).

Commercialised large scale wind turbines often utilise 3 blades as this number of the blades govern obtaining larger aerodynamic efficiencies over a relatively wide range of tip speed ratios (λ: the ratio between the rotational speed of the blade and the mean velocity of the wind) [97]. Using rotors with more blades (*e.g.* 5 blades or more in the small scale wind turbines) results in higher torques to be obtained at low tip speed ratios and thus more energy to be extracted from the wind resource at low wind speeds. The maximum C_p obtained for large wind turbines is about 45% [97] and for small scale design is close to 30% [186]. The lower C_p obtained in small scale wind turbines is mainly linked to i) the poor aerodynamic design of the blades, enforced by manufacturing cost limitations and ii) the absence of equipment necessary to adjust the pitch angle of the blades to available wind speed in these systems [99].

Small scale wind turbines with power outputs smaller than 6 kW and the swept area of the blades smaller than 25 m^2 are technically classified as "micro-wind turbines". These turbines often work based on the high speed rotation of a PMG which is directly driven by the rotor with no gearbox or other mechanical/electrical intermediate system involved [99, 183]. The direct rotor-generator configuration employed in micro-wind turbines makes these systems particularly reliable and maintenance free compared to the large scale designs. Advantages such as high power to weight ratio, small repair requirements and the elimination of DC excitation have resulted in the rapidly increasing popularity of PMG based wind turbine systems in the recent decade [96, 187].

The amount of electrical energy produced by a PMG micro-wind turbine is linked to the rotational speed of the generator [95, 98, 184]. During the process the shaft of the turbine is subjected to various co and counter torque forces, among which the only co torque force, that tends to spin the rotor, is the one received from the wind. However, the counter torque force is a combination of i) the current induction torque force, and ii) the inertial forces of the rotating objects (particularly the rotor as it has the largest bulk in the system). The resultant of these co and counter torque force vectors is a net torque force, which is ultimately determining the angular velocity at which the rotor and the generator spin [95, 187, 188]. It should be noted that in such wind turbine systems the voltage output from the generator varies proportionally with the angular velocity of the rotor.

The inertial forces, which are mainly linked with the size of the turbine, are normally fixed and thus do not contribute to the variation of the rotor's angular velocity in a process. Moreover, the energy dissipation due to frictional and heat losses are very small and their impact on the variation of the angular velocity of the rotor is expected to be negligible. Therefore, the only two forces that can vary during a process and control the variation of the rotor's angular velocity are i) the productive torque force which is directly linked to the available wind speed (v), and ii) the current induction counter torque force, which is inversely proportional to the resistance of the load connected to the wind turbine. The latter is of significant importance to this research,

as it suggests that for a wind turbine directly coupled to a batch ED system, even at a constant wind speed the voltage output from the generator can be adversely influenced by the inevitable increase of the resistance in the ED stack (R_{stack}). An increase in the R_{stack} occurs in all batch recirculating processes due to the continuous ion removal from the dilaute (see section 2.3.1 for more information). Apart from the feed concentration, variation of flow rate, membrane resistance and the degree of concentration polarisation can influence the R_{stack}, and thus impact the energy performance and the desalination behaviour of the wind-ED system. The occurrence and fate of such behaviours and the extent to which changing principle operating parameters, such as initial feed concentration and flow rate, would influence the energy consumption and desalination performance of the wind-membrane system will be studied systematically in Chapters 5-8.

To date the majority of the literature that investigated the behaviour of PMG wind turbines was focused on the operation of such systems in direct connection to relatively fixed resistance loads, such as electricity grids or energy storage systems [95, 98, 187]. Therefore, coupling the wind turbine system to an ED stack in this research can be considered as a novel attempt to investigate power production by a PMG wind turbine as a function of not only the wind speed but also the resistance of the load directly connected to the wind turbine.

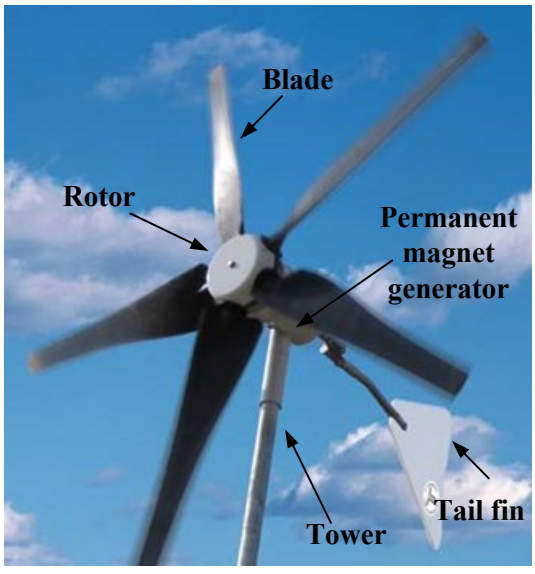

Figure 2.11 Main components of a small scale 1kW Future Energy wind turbine (adapted from [189]).

The main components in a small scale wind turbine are shown in Figure 2.11. The fin installed at the back of the wind turbine is to help with the stability as well as the aerodynamics of the wind system [99]. At high wind speed conditions, when the cut-off limit of the wind turbine ($v_{cut\text{-}off}$) is exceeded, the tail helps with moving the rotor away from the wind direction. This self-protecting mechanism, which is known as "furling mechanism", causes the swept area of the blades to decrease rapidly during the occurrence of high wind condition, hence it prevents from the overloading of the wind turbine and possible damage to the rotor and the generator.

Having the fundamentals of ED system and micro wind turbine operations reviewed in the previous sections, the next section aims to give an overview of the studies carried out on coupling ED with wind energy systems to date.

2.5 Transient operation of the wind-membrane system

The work carried out so far on using wind energy for powering ED systems is limited to few investigations, all of which only considered the indirect coupling between the membrane system and the wind turbine. Employing complicated energy storage and power regulating devices in all these studies has left gaps in understanding the direct impacts of wind speed fluctuations on the operation of the membrane system; knowledge which is of great importance when designing a directly coupled wind energy powered ED system.

Corbus *et al.* [190] were the first who studied the operation of an electrodialysis reversal (EDR) system powered by a small wind turbine. This research was part of a larger scale project aiming at characterising small wind turbines and introducing new applications for such systems. The specific goals of the study were to determine the energy consumption, water production and maintenance required during the operation of the wind-EDR system. A schematic of the wind-battery-EDR system investigated in the study is shown in Figure 2.12.

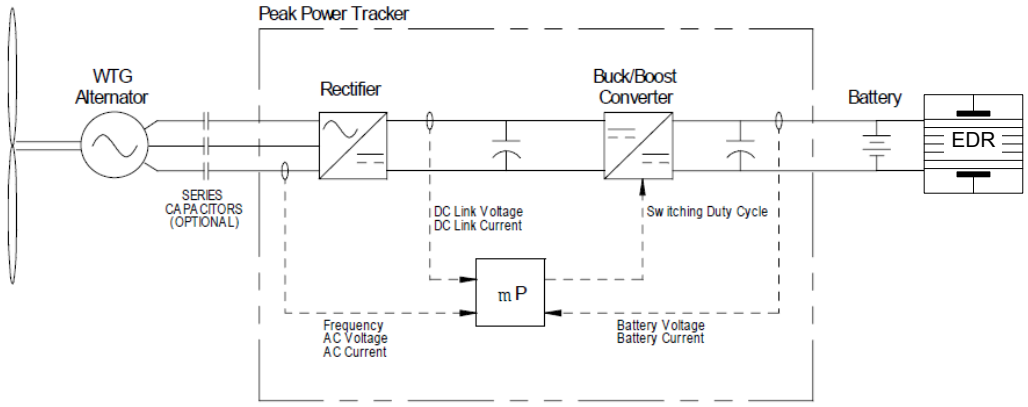

Figure 2.12 Schematic of the wind-battery-EDR system investigated by [190].

The wind energy system consisted of a 850 W turbine that was used to charge a single string of 8 L-16 batteries (Figure 2.12). The power output from the battery bank was used as the input to the EDR system. A peak power point tracking system was utilized to optimise the energy supply from the wind turbine to the batteries.

A natural brackish water feed of 900-1,000 mg/L total dissolved solid (TDS) was used for the desalination experiments. After the water was desalinated in the EDR system, it was fed into an ultraviolet (UV) system to be disinfected from viruses and bacteria. The UV system was directly powered by a DC-to-AC converter from the EDR controller. The desalination process was continued in a batch process until the desired TDS level of 250-300 mg/L was achieved in the product water.

The wind-EDR system was tested for over 1,400 hours (*i.e.* 59 days) at the fixed feed flow rate of 1.1 L/min. During this period 97 m^3 of fresh water was produced. The average wind speed experienced during the operation was 4 m/s, which is considered low for the operation of small scale wind turbines [77, 183]. After the completion of the process only the brushes on the DC motors had to be replaced. The relatively maintenance-free nature of the operation suggested the wind-membrane system as a suitable option to be used for desalination purposes in remote areas. The SEC of the process was 1.76 kWh/m^3, considered as competitive compared to reverse osmosis (RO: 1.5 – 5 kWh/m^3) and significantly more efficient compared to multi stage flash (MSF: 19.58–27.25 kWh/m^3) for desalination of brackish water (≤ 5,000 mg/L TDS) [10, 11, 191, 192]. The authors suggested that EDR would perform optimally if

connected to a larger wind turbine or operated under higher and more constant wind speeds, with less system on/off (due to intermittency in the wind resource) being experienced during the desalination process.

Although the off-grid test conducted in this work exhibited a successful operation in terms of drinking water production and SEC, the impacts of wind speed fluctuations on the process parameters such as voltage, current and salt flux across the membranes were not systematically investigated; hence it resulted in minimal engineering understanding of the wind-ED system operation. Moreover, only the average wind speed of the operation (*i.e.* 4 m/s) was reported but no data on the magnitude and frequency of the wind speed fluctuations was given; this thereby limited the applicability of the data reported by Corbus *et al.* for drawing solid conclusions on the feasibility of the wind-ED system for practical use under various wind speeds and fluctuations. Therefore, more detailed research and with different wind speed conditions is necessary in order to obtain comprehensive results, enabling the determination of a realistic operating window for wind-ED systems.

In another study a wind-EDR system was developed and studied as part of a wider scope project named SDAWES (Seawater Desalination with Autonomous Wind Energy Systems). SDAWES was initially designed to examine the suitability of different desalination systems when operated with a wind farm on the Grand Canaria Islands, Spain [28, 84, 85]. At first a set of on-grid tests were carried out to determine the optimal performance of the system regarding the water product quality and quantity, minimum SEC and the feed flow rate as well as to establish the operating intervals for different parameters (*e.g.* power, conductivity, flow rate, etc.) [85]. The results of the on-grid tests were stored in a database to predict the outcomes of the off-grid wind powered tests as well as to develop a control system to be used in the subsequent stages of the project.

The configuration used for the experimental setup was decided based on the results obtained from a series of non-stationary simulations carried out in the preliminary stages of the project [94]. The desalination system consisted of two EDR units, each housing 340 membrane cell pairs and operating with two electrical and four

hydraulic stages. The following modifications were applied to the system in order to overcome the power fluctuations in the subsequent off-grid tests;

i. DC drivers with embedded signal control devices were used to convert the AC output from the wind turbines to DC voltage, required for operating the EDR units.

ii. Variable frequency drivers (VFDs) were fitted to the hydraulic facilities to enable varying the feed flow rate according to the control signals.

iii. A control system was developed to store the plant data (water quality, voltage and current, power required and flow rates) and set the drivers to their optimal power consumption according to the available power at every instant of the process.

Artificial brackish water with a relatively constant conductivity of 4,500 μs/cm was used in all the experiments. The tests were carried out over a range of product flow rates: 3 – 8 m^3/h. The ratio between the voltages applied to the first and the second electrical stages (E) of the EDR units were set fixed in all the tests (E_2/E_1=0.6). The plant was equipped with an off-specification product conductivity (OSP) control system, enabling the system to automatically discharge water products having conductivities in the range of 750 – 1,000 μs/cm, depending on the pre-set parameters.

All the parameters were found to be in their optimum range when the system was operated at E1: 80-100 V and E2: 48-60 V and with the OSP was set to discharge water products having conductivities above 1,000 μs/cm. Under these optimal conditions acceptable water quality in the range of 300 to 750 μs/cm was obtained and the plant maintained its fresh water production capacity of between 92 and 192 m^3/day. The SEC increased only slightly from 1.48 to 2.32 kWh/m^3 with the increase in the voltage (80 to 100 V for E1), but remained relatively constant over the product flow rate of 3 to 8 m^3/h. This suggested EDR as an energetically robust system when operating under various flow rates and voltages.

In 2004 the wind-EDR system underwent a series of off-grid tests, where the desalination plant was powered by a portion of the energy generated from a 2×230 kW wind turbine power station. Each wind turbine had a three-bladed rotor with adjustable pitch angle and variable angular velocity. A synchronous-type electrical generator was used in these turbines. A series of power inverters and rectifiers were employed to convert the power output from the generators to an electrical energy that can be supplied to the grid. The wind farm was also equipped with a 100 kW synchronous machine coupled to a flywheel. The flywheel i) acted as a temporary energy storage system, ii) stabilised the load against disturbances and fluctuations in the wind resource and iii) match the frequency of the power output from the wind turbine to that of the grid. The energy output from the wind power station was regulated by the DC drivers, before being supplied to the EDR unit. A small portion of the energy output from the wind turbine was fed to an uninterrupted power system unit (UPS), supplying the energy required for running the wind-EDR control system. A schematic of the wind-EDR plant is shown in Figure 2.13.

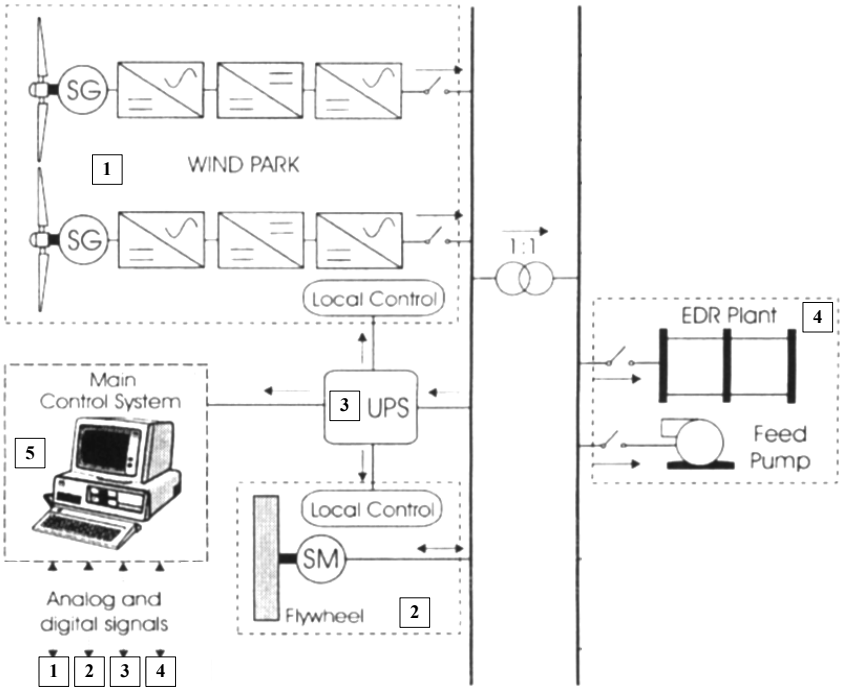

Figure 2.13 Schematic of the wind-EDR system used in the off-grid tests (modified schematic from [94]).

The conductivity of the feed water was 5,000 μs/cm, which was slightly higher than that used in the on-grid experiments (4,500 μs/cm). The off-grid tests showed that to maintain the product flow rate and conductivity in the range similar to those obtained in the on-grid tests (3-8.5 m^3/h for the product flow rate and 200-500 μs/cm for the treated water conductivity), the power driven from the wind turbines must be in the range of 4 – 19 kW (Figure 2.14).

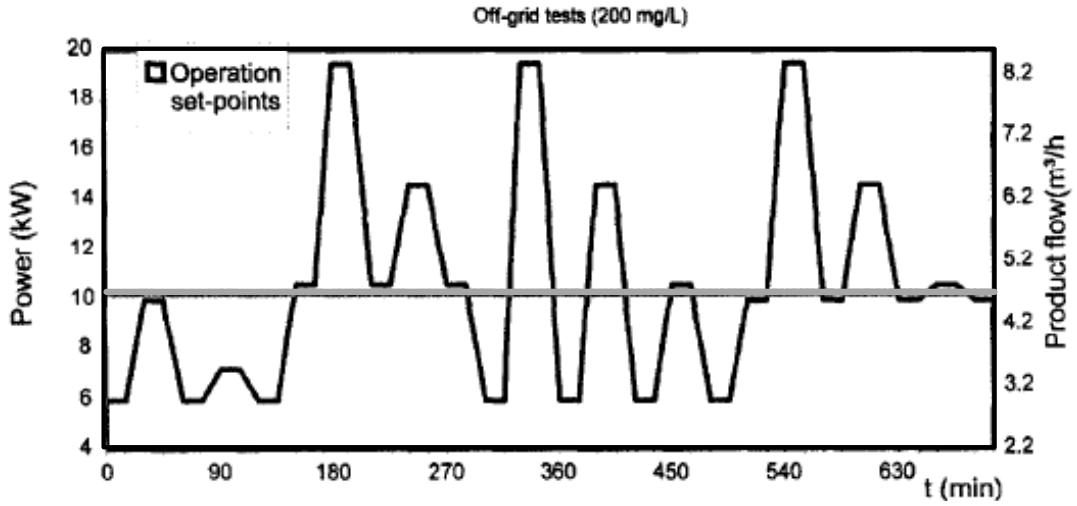

Figure 2.14 variations in the product flow rate, corresponding to the power output from the wind turbine during a complete set of off-grid desalination tests; the product water quality was set at 200 mg/L (TDS) (modified schematic from [94]).

The grey line in Figure 2.14 defined the wind power above which the second EDR unit was automatically brought in line in order to maintain the flow rate and conductivity of the water product at their required levels. In these tests the EDR unit was shown to be capable of rapidly and smoothly adapting to the wind power variations. The time required for adapting the operating parameters to the new power condition was found to be approximately 20 s, when no shifting from one to two EDR units (or vice versa) was required, and about 40 to 45 s when the power conditions necessitated the change in the number of the EDR units in line. Despite having large variations in both the power output from the wind turbine and the product flow rate, the SEC of the process oscillated in a narrow range of 1.22 – 2.32 kWh/m^3 for all the experiments.

It is important to note that the smooth adaptation of the EDR unit to the wind power variations was mainly due to having various power regulating and energy storage systems (*i.e.* the flywheel and the DC drivers for the EDR system, and the variable frequency drivers (VFDs) for the flow pumps). Although Veza *et al.* [84, 85] proved the feasibility of a wind energy powered ED system for the use in water purification applications under certain operating conditions, they did not provide systematic and comprehensive understanding of how and to what extent each and every operating parameter is influenced by random variations in a wind resource. This again highlights the lack of systematic studies on directly coupling wind with ED and subsequent effects on key operating parameters. The severe knowledge gap in the scientific literature necessitates in-depth research to obtain comprehensive data to assist with developing, determining safe operating windows and optimising the operation of directly powered wind-ED systems.

On the other hand, a beneficial side-effect of using a fluctuating power supply in direct connection to the membrane system is the potential disruption of concentration polarisation (CP), which limits effective ion transport and has negative impact on current density, as described in detail in section 2.3.3. Karlin and Kropotov were the first who examined the use of fluctuating power supply, in form of short voltage/current pulses applied across the ED stack, to enhance the current transfer through the membranes [33]. Following the study by Karlin and Kropotov, applying pulse electric field has been introduced as an effective method for minimising concentration polarisation (CP) [59-61] and fouling mitigation [34, 62, 63, 65, 66, 193] in different studies.

The idea behind the pulsed electric field ED process is as follows: immediately after applying the external power to the ED system, concentration profiles start to develop within thin diffusion boundary layers close to the membrane surface. This phenomenon, which is known as concentration polarisation (CP), causes the rate of migration to decrease significantly and thus the ions to travel slower through the membranes (explained in detail in the section 2.3.3). If the external power supply is terminated before the complete development of CP at the solution-membrane

interface, the system goes into an off-period, also known as the relaxation lapse. During the off-period, and in absence of any migration process, the concentration of the ions at the solution-membrane interface is restored by the salt ions diffusing from the bulk solution to the membrane surface. As a result of this the concentration profiles are significantly dissipated and the resistance against the salt flux through the membrane is reduced. Subsequently in the next pulse the ion transfer is enhanced and the current density will be higher than that in a conventional process with a constant power supply.

CP is generally found to be the most severe when the system is operated above the limiting current density regimes and under constant power conditions [130, 131, 194]. Consequently, applying a pulsed electric field during over-limiting regimes is expected to have a pronounced effect on ion transfer compared to sub-limiting regimes. Mishchuk *et al.* showed improvement in current density and thus enhancement in desalination time by applying pulsed electric field in extreme over-limiting regimes (using 5-50 V per membrane cell and low feed concentration of 580 mg/L NaCl) [60]. The increased current transfer in the study by Mishchuk *et al.* was attributed to a significant contribution of electro-convective processes to rapid dissipation of CP at the solution-membrane interface during the pause periods.

Although the impacts of electric field pulsations is expected to be more pronounced in the over-limiting regimes, yet no systematic studies have been carried out to prove whether or not energy fluctuations (*e.g.* pulsation) are also influential on CP dissipation and ion flux when operating in sub-limiting regimes. Studying the latter is of significant importance when considering the application of ED in a direct connection to a fluctuating energy source for the purpose of drinking water production, since these processes normally take place in sub-limiting regimes (*e.g.* high feed concentrations and/or low applied voltages). The salinity of feeds requiring desalination for drinking water purposes range from 1,000 mg/L NaCl in reused wastewater or mild brackish water to about 35,000 mg/L NaCl in seawater [31]. The voltage used in conventional ED processes is about 0.5 - 1.5 V per cell, which again

is much lower than the voltage range used in the study by Mishchuk *et al.* [60] and thus defines the conditions normally applied to sub-limiting current density regimes.

Concentration polarisation at high current densities normally occurs with the concentration of salt ions at the vicinity of the membrane surface decreasing to levels as low as zero. Disappearance of the salt ions leads to development of a current induced space charge at the solution-membrane interface, ultimately enforcing the water molecules at the vicinity of the membrane to dissociate to their atomic components, H^+ and OH^- [131, 195]. The water splitting phenomenon and its adverse impacts on ED operation were explained in more detail in section 2.3.3. Some studies of water dissociation under different pulse regimes have been reported in the literature. Mishchuk *et al.* (using 1,400 - 2,900 mg/L NaCl-$CaCl_2$ mixture in the voltage range of 10 – 30 V/cell) and Casademont *et al.* (using 2,700 mg/L TDS and 32,600 mg/L WIP with fixed current densities of 10 - 30 mA/cm^2) showed greater pH drop in the diluate channel, attributed to severe water dissociation, using pulsed electric field compared to constant power [61, 64]. In these studies pulsation stimulated some fluid instabilities, due to electro-convective processes, on layers adjacent to the membrane where the concentration was lowest; hence leading to supressed levels of water dissociation. Contrary to these findings, Cifuentes-Araya *et al.* (using 2,052 mg/L Mg-Ca-K salt mixture in the diluate (initial pH=6.5) and 2,000 g/L KCl in an alkaline concentrate (pH=12) at the fixed current density of 40 mA/cm^2) showed significant increase in diluate pH using pulsed-power; which was attributed to leakage of OH^- ions via CEM into the diluate channel [65]. The latter was explained to be due to high concentration of OH^- ions in the concentrate channel, reduced permselctivity of CEM due to fouling plus splitting of water molecules at high current densities. Ruiz *et al.* (using 2,600 mg/L TDS and 32,000 mg/L casein based protein at the fixed current density of 15 mA/cm^2) demonstrated a lower rate of water dissociation when using short current pulses compared to constant power mode ED process [34]. The reason for this lower rate of water splitting due to power fluctuations in the pulsed process is not fully understood. Conflicting results between these studies indicate the requirement for systematic investigations on pulsation and its impacts on water dissociation to determine mechanisms involved.

Ruiz *et al.* showed that energy consumption by using pulsed current was lower compared to when constant power was used, when small amount of charge (approximately 1.09×10^6 C/m^3) was transferred. The feed contained 2,600 mg/L total dissolved solids (TDS) and 32,000 g/L casein based protein while current densities of 10 and 20 mA/cm^2 were used [34]. Reduction in the fouling gel layer due to applying intermittent power was explained as the main reason for lower energy consumption in the pulsed mode compared to the constant potential mode. However, in a similar study Casademont *et al.* showed that when transferring a larger amount of electric charge (about 2.72×10^6 C/m^3), the energy consumption difference between the pulsed and constant power modes were negligible [64]. The feed used contained 2,700 mg/L TDS and 32,600 mg/L BiPROWhey Protein Isolate (WIP) and experiments were conducted at a current density of 15 mA/cm^2. The contradictory results between these studies, which can partly be explained with different materials and experimental conditions used shows that a systematic study on the impacts of energy fluctuations (*e.g.* pulsed voltage or current operation) on energy performance of ED is needed.

2.6 Conclusion

The scarcity of drinking water is a severe problem in remote regions of developed and developing countries, necessitating a sustainable solution such as the implementation of off-grid renewable energy powered desalination and contaminant removal technologies.

Compared to other desalination techniques, electrodialysis (ED) has been shown to be an energy efficient method for brackish water desalination. The high water recovery (85-90%) and low maintenance required in operating ED as well as the long lifetime and strong chemical and mechanical stability of the ion-exchange membranes make this system particularly favourable for the use in water stressed remote areas. Taking into account the promising desalination and energy performance observed when operating ED under fluctuating power conditions (*i.e.* pulsed-ED and PV-ED operations), this membrane technique could potentially

provide an energetically robust desalination system for direct coupling to extremely fluctuating renewable energy systems, such as wind turbines.

Scientific investigations to date on wind-ED system operations were either focused on the design of prototype wind-membrane installations or the initial feasibility of such systems. Moreover, all these studies employed complex energy storage and power regulating devices (*e.g.* flywheels, lead-acid battery banks and synchronous electrical machines) to overcome the severity and unpredictability of fluctuations and intermittencies inherent to the wind resource. Although employing such electrical/mechanical intermediate devices between the wind turbine and the membrane system helped to maintain the water production to its desired levels during long periods of low wind speed or when the fluctuations are the most extreme, using such systems resulted in significantly high maintenance and operating costs as well as serious drawbacks associated with using energy storage devices.

A more feasible and less complex approach would be to employ the direct coupling configuration between the membrane system and the wind turbine, where the RE-membrane system is allowed to operate based on the available energy in the RE resource. In such conditions the extra potable water produced in the high wind speed conditions can be stored and used when needed (*i.e.* during the low wind speed conditions) to ensure that water demand is met.

However, development of directly powered wind-ED systems is technically challenging, since it requires having thorough understanding of the fluctuations and intermittencies in the wind resource and their impacts on the desalination performance of the membrane system. Finding the correct match between the wind turbine and the ED module and developing the RE-membrane system as a whole and not a combination of separately developed components is another technical challenge in this process. Systematically tackling each of these challenges in detail is the main objective of this research. Furthermore, the effects of fluctuating and intermittent energy source on key operating parameters such as specific energy consumption (SEC), quality and quantity of water produced, CP dissipation, current efficiency and competitive transport of some common inorganic contaminants in brackish

groundwater (*i.e.* Cl^-, F^-, NO_3^- and SO_4^{2-}) through the membranes have been systematically investigated for a directly coupled wind-ED system.

Chapter 3

Materials and Methods

3.1 Introduction

This chapter provides detailed information of the materials used and the methods employed for carrying out the experimental work in this research. Reference to these materials and methods will be made throughout the thesis.

The electrodialysis (ED) system and the ion-exchange membranes used in the desalination tests are described. Details of the voltage pulse amplifier designed for the use in the pulsed-ED experiments (Chapter 4) is presented. A full description of the wind turbine simulator employed in the wind-ED experiments (Chapters 5 – 8) is provided.

This chapter also provides the following information: i) the chemicals used to prepare the artificial brackish water solutions ii) a description of the analytical equipment and data monitoring facilities, iii) the main process parameters and relevant calculations, and finally iv) the general quality control and quality assurance protocols employed for this research.

3.2 Experimental equipment

3.2.1 Electrodialysis stack

All the desalination experiments were carried out using a FT-ED-100 ED stack (Fumatech, Germany) with integrated dimensionally stable electrodes (DSEs) and flow channels for distributing process solutions. DSEs were made of titanium/iridium plasma coated stainless-steel and were housed in polypropylene made endplates. Figure 3.1 shows the ED stack on its own (A) and inserted in the operation line, connected to the feed tanks, pipelines, power supplies and the sensors (B).

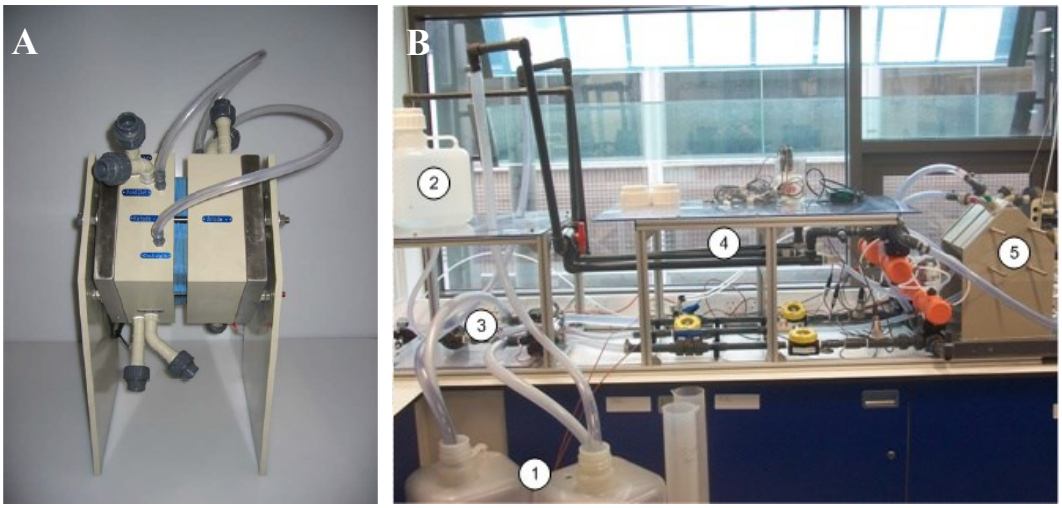

Figure 3.1 A) FT-ED 100 module configuration and B) the ED stack (5) connected with the diluate and concentrate feed tanks (1) the electrode rinse tank (2), the diaphragm pumps (3) and the conductivity, pH, pressure and flow sensors (4).

Diluate and concentrate solutions are fed into the stack from two separate 10 L tanks, using two diaphragm pumps (Jabsco 31801-0094, UK). The flow rates provided by these pumps are controlled by a DC power supply (Xantrex XHR 120 V 10 A, USA). The electrode rinse solution is fed through the ED system at a fixed flow rate of 3 L/min from a 5 L tank, using a diaphragm pump (Jabsco CW495-1, UK). Figure 3.2 shows the flow paths for the diluate, concentrate and electrode rinse solutions through the endplates of the ED stack.

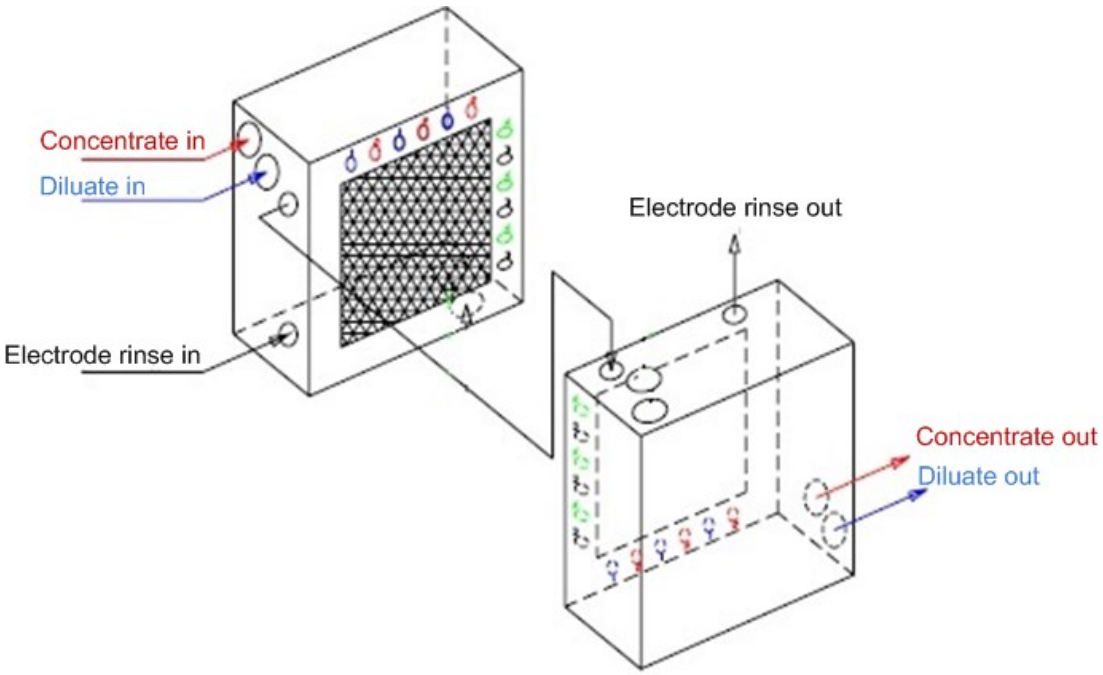

Figure 3.2 Diluate, concentrate and electrode rinse solutions pathway through the endplates of the ED stack.

3.2.2 Membranes and spacers

Two types of commercially available membranes were used in this study: Neosepta® AMX-SB (anion exchange membrane, AEM) and Neosepta® CMX-SB (cation exchange membrane, CEM) (manufactured by ASTOM Corporation, Japan; supplied by Eurodia, Germany). The ED stack housed 21 CEM and 20 AEM membranes, positioned parallel to the flow direction and separated from each other by flow spacers. The membranes had an effective surface area of 0.01 m^2 (0.1 m height and 0.1 m width). AEMs contain alkylammonium groups ($N(CH_3)_3$) and CEMs have sulfonic acid (SO_3H) groups attached to the aromatic rings of a PS-DVB matrix on a micro-porous PVC gel supported by a plasticised PVC cloth [50, 196, 197]. A polymer mesh additionally reinforces the membranes. The detailed characteristics of both AEM and CEM membranes are listed in Table 3.1. The chemical structures of both of these membranes are shown in Figure 3.3.

Table 3.1 Properties and Characteristics of AEM and CEM membranes as specified by the membrane manufacturer ([196, 198])

Properties	**CMX-SB (CEM)**	**AMX-SB (AEM)**
Type	Strongly acidic, Cation permeable	Strongly basic, Anion permeable
Polymer material	Polystyrene divinylbenzene	Polystyrene divinylbenzene
Functional group	SO_3H	$N(CH_3)_3$
Electric resistance[a] (Ω cm^2)	1.8 - 3.8	2.0 - 3.5
Transport number	0.98< (for Na^+)	0.98< (for Cl^-)
Water content[a] (g H_2O/g dry membrane)	0.25 - 0.30	0.25 - 0.30
Thickness (mm)	0.17	0.14
Burst strength (Mpa)[b]	$\geq$ 0.4	0.3
Mechanical strength	High	High
Chemical resistance, significantly against:	Strong oxidising agent	Strong oxidising agent
Chemical resistance, slightly against:	Acetone, dioxane, phenol	Caustic soda, Ammonia, dioxane
Contact angle (Θ)	61.8 ± 5.1	69.9 ± 3.4
Exchange capacity (meq/g dry membrane)	1.5 - 1.8	1.4 - 1.7
Volume during the process (cm^3)	6.9	4.9

[a] Equilibrated with 0.5 M-NaCl solution at 25°C; [b] Burst strength measured by a Mullen Burst Strength device

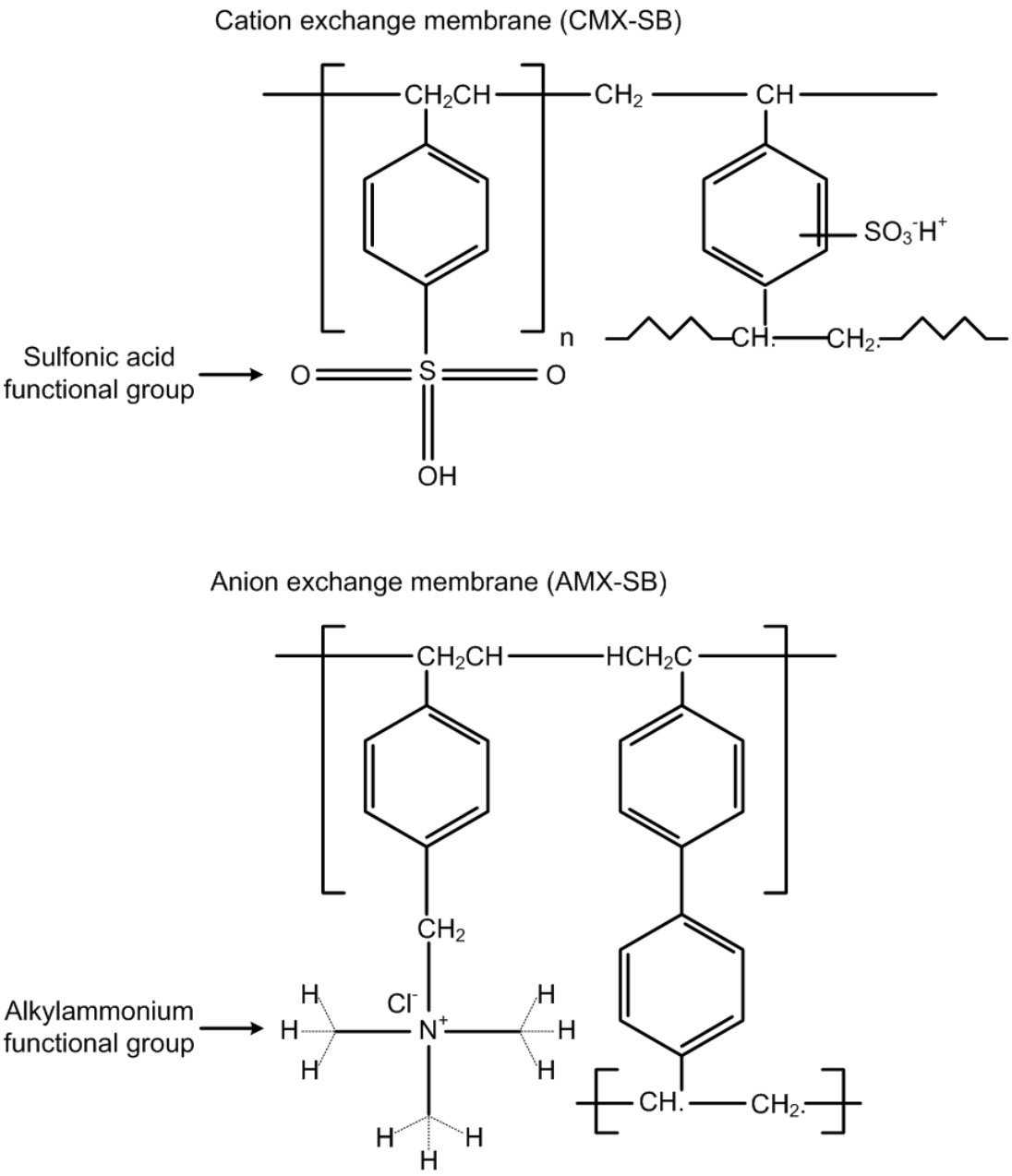

Figure 3.3 Chemical structures of the Neosepta® CMX-SB and AMX-SB membranes (re-drawn from [197]).

Flow spacers are used to provide pathways for the feed solutions to run between the membranes. They promote turbulence and help the flow velocity to stay even everywhere within the channel and thus help to reduce concentration polarisation at the membrane vicinity. The spacers used in this ED module are of PVC type, with their net mesh made of polyester. Figure 3.4 shows the cross section of the ED stack

with a membrane and a spacer (in blue) on top of it, both positioned on one of the ED stack's endplates.

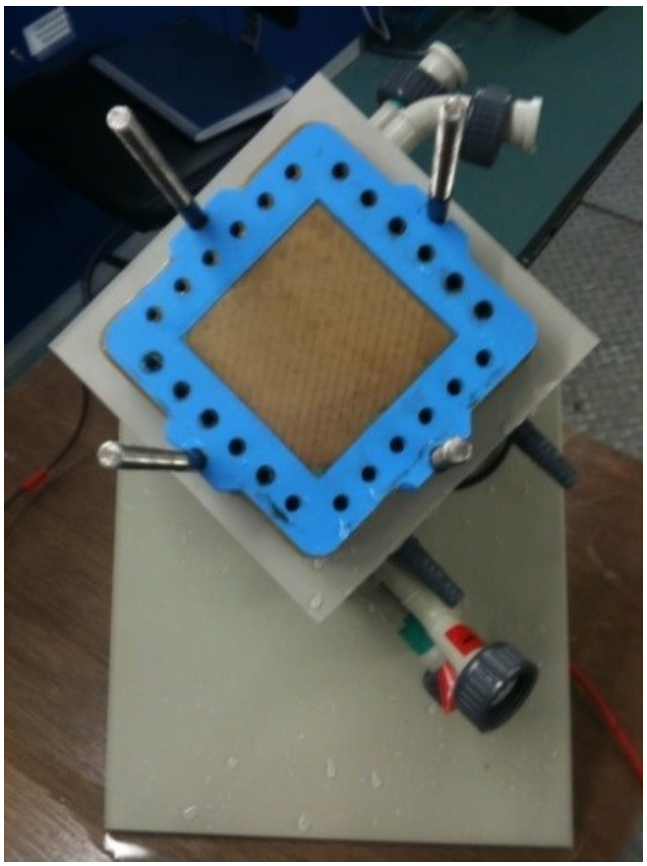

Figure 3.4 the cross section of the ED stack; the blue flow spacer and a CEM membrane below that are placed on top of an endplate of the ED stack.

3.2.3 Operating modes of the membrane system

Schematics of the ED system in both the continuous (A) and batch (B) operation modes are shown in Figure 3.5. In the continuous mode (Figure 3.5A) the feed solutions are fed into both the diluate and the concentrate channels via a shared tank. This mode of operation was used when measuring the limiting current density (j_{lim}) and investigating concentration polarization (CP) (Chapter 4) as well as for characterising the intermittent behaviour of the wind-ED system (Chapter 6).

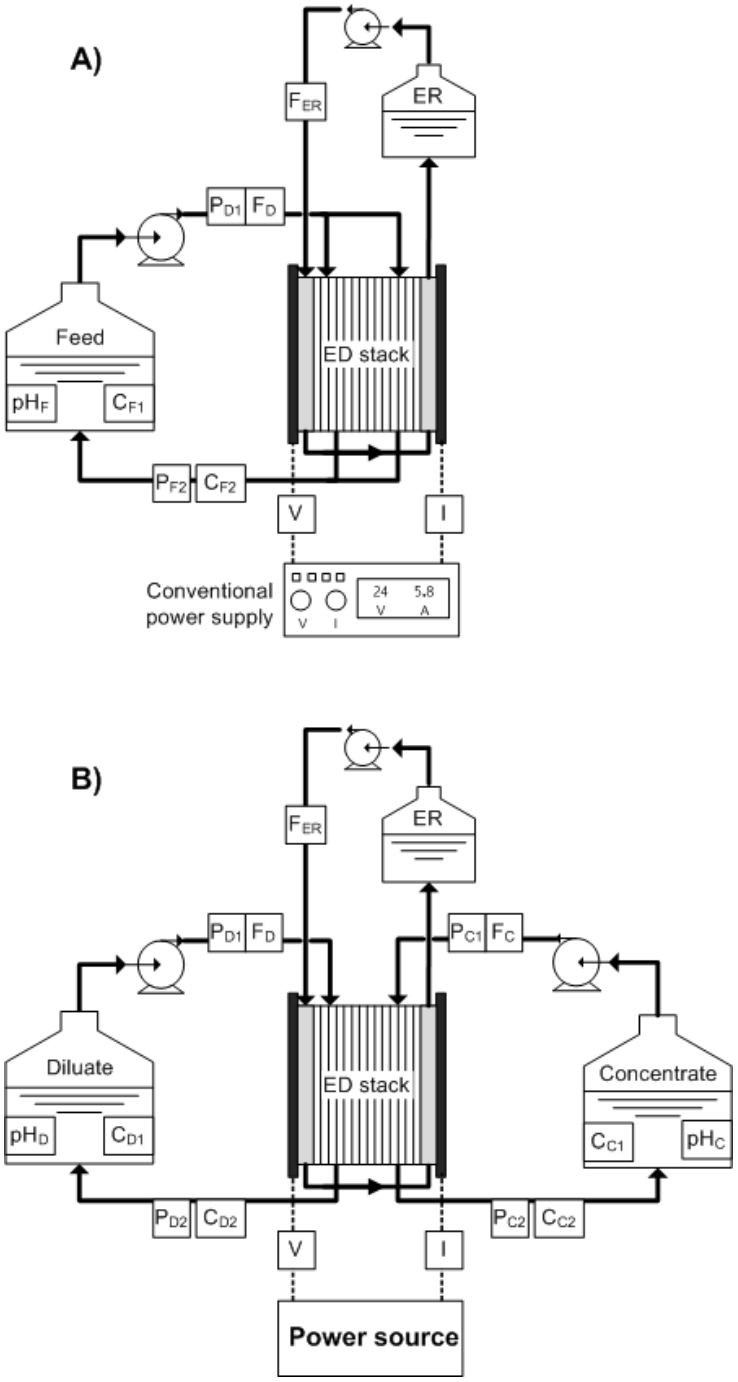

Figure 3.5 schematics of the ED setup in two different modes of continuous recirculation (A) and batch (B) configurations.

The batch configuration (Figure 3.5B) was the main mode of operation for all the desalination experiments. In this mode of operation the diluate and concentrate solutions are circulated via separate tanks and channels through the ED stack. The power source used with this mode of operation was selected from the following

options, depending on the nature of the experiment: a fixed voltage conventional power supply (3.2.1), a pulsed assisted power supply (3.2.4) and a wind turbine simulator (3.2.5). During the desalination process, together with the continuous requisition of data from the online sensors, samples were taken from both the diluate and concentrate tanks in specific time intervals for further analysis.

3.2.4 Voltage pulsed system

In the pulsed electric field assisted experiments (Chapter 4), the voltage pulses over a range of frequencies and duty cycles were applied across the ED stack using a function generator (HP-Agilent 33120A, UK), coupled with a DC power supply (Xantrex XHR 150 V 7 A, USA). The coupling between the function generator and the DC power supply was made by a custom-designed pulse amplifier. The pulse amplitudes, frequencies and duty cycles were all monitored using a digital oscilloscope (Tektronix TD1020, USA) during the experiments. The block diagram of the voltage pulse amplifier, designed in the electronics workshop at Heriot-Watt University (UK), is shown in Appendix A.

3.2.5 Wind turbine simulator

A wind turbine simulator was used for all the wind-ED experiments in this research. This system was a lab designed module, developed by Park *et al.* based on the data obtained from testing a 1kW Future Energy wind turbine under controlled conditions in a wind tunnel [99]. The tested wind turbine was equipped with a 5 bladed rotor (1.8 m diameter), installed at the hub height of 8 m. The choice of having 5 bladed rotor, as opposed to the commonly used 3 bladed ones, was to have higher torques at low tip speed ratios and thus to obtain improved power performance at low wind speeds [97] (more explanations were given in section 2.4.2).

The wind turbine simulator was developed using a geared induction motor (Nord, SK51E-160M/4) with a 10:1 speed reduction (range 300-1000 rpm) which is controlled by a vector frequency inverter (Nord, SK700E-112-340-A). By varying the speed output of the frequency inverter and taking into account the inertias of the various components, the torque that would have been applied by the wind rotor is given to the wind turbine generator and it is allowed to rotate accordingly. A

LabVIEW interface is used to control the operation of the simulator and supply wind speed data to the frequency inverter. The output from the wind turbine generator, which is already in form of DC voltage, is applied across the ED electrodes. In the wind-ED experiments, only the ED stack is connected to the wind system, while the pumps are still controlled by the conventional Xantrex power supplies (section 3.2.1). The wind turbine simulator and its block diagram are shown in Figure 3.6 and Figure 3.7, respectively.

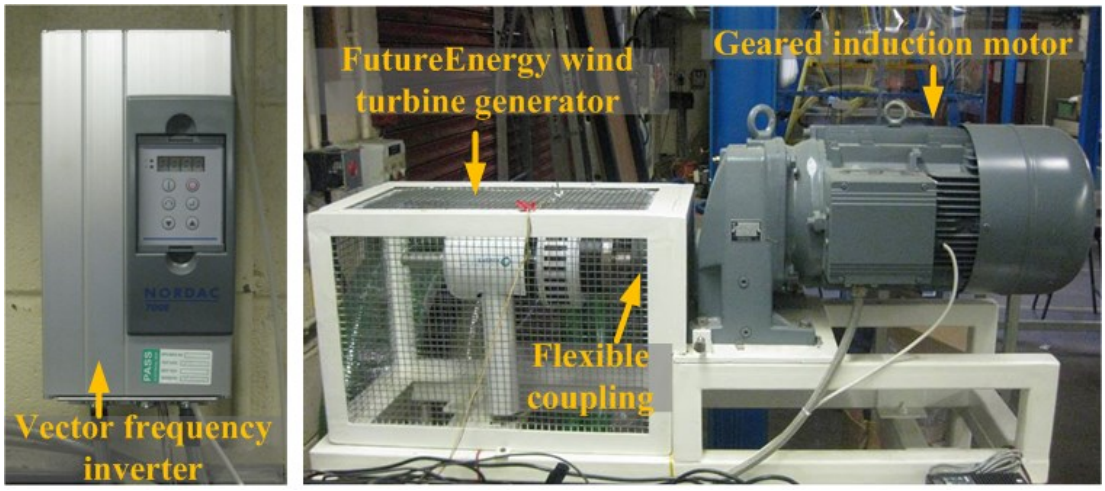

Figure 3.6 Wind turbine simulator: vector frequency inverter (left), FuturEnergy wind turbine generator inside the safety cage (middle) and the geared induction motor (right).

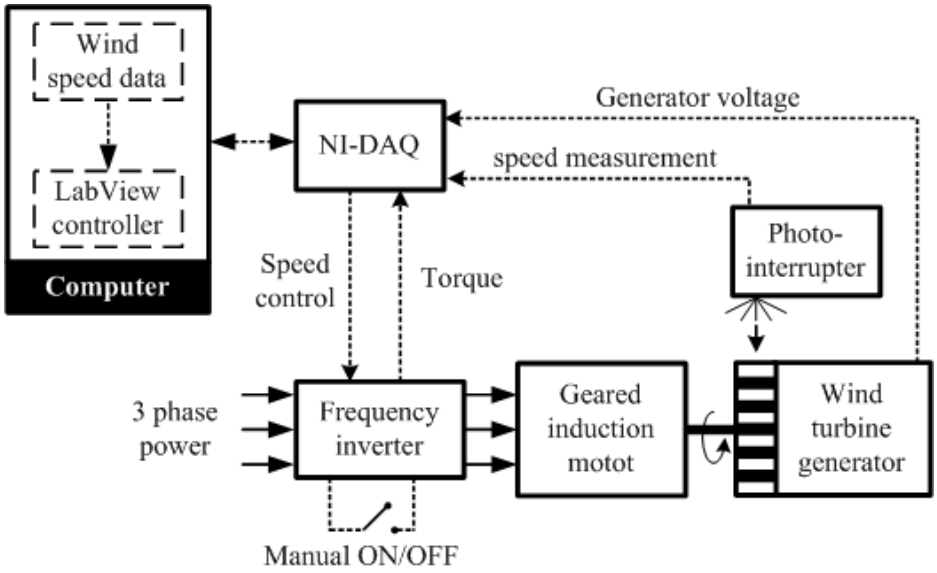

Figure 3.7 Block diagram of the wind turbine simulator (re-drawn from [99]).

To provide an energetically suitable match between the wind turbine simulator and the ED system, the originally installed generator on the simulator was replaced by a generator from the same kind but with lower energy output (Future Energy with the rated output of 600 W at 12.5 m/s wind speed). This was to make sure that the voltage output from the wind turbine does not exceed the recommended value (2.5 V/cell pair) by the ED stack manufacturer at any time during the process. Meanwhile, the generator was required to be still powerful enough to produce good level of power for carrying out satisfactory desalination tests with the feed water solutions of 5,000 – 10,000 mg/L NaCl. The power curves obtained from this modified wind turbine simulator over a range of wind speeds and resistances are discussed in detail in the following section.

3.2.6 Wind turbine simulator power performance

To understand the behaviour of the directly coupled wind-membrane system, it is initially important to determine the full range of power that the wind turbine simulator is able to produce over a wide range of wind speeds and at different resistances. For this reason a series of power characterisation tests were carried out using the wind turbine simulator directly connected to a controllable resistance bank (Figure 3.8). The resistances used for these tests (5 – 31.1 Ω) were selected carefully to cover the complete range of resistance that the ED stack experiences (R_{stack}) during the subsequent desalination tests. As will be shown later, depending on the initial feed concentration used in the process the R_{stack} at the beginning of the test is around 7 - 8 Ω for a feed of 5,000 mg/L NaCl and 5-6 Ω for a feed of 10,000 mg/L NaCl. This resistance increases throughout the desalination process until it reaches 28 – 30 Ω toward the end, when approaching the target concentration of 600 mg/L NaCl [21]. The results obtained from this section are later used to describe the power performance of the wind-membrane system and further explain the Ohmic behaviour of the ED stack in the wind-membrane desalination tests (Chapters 5-8).

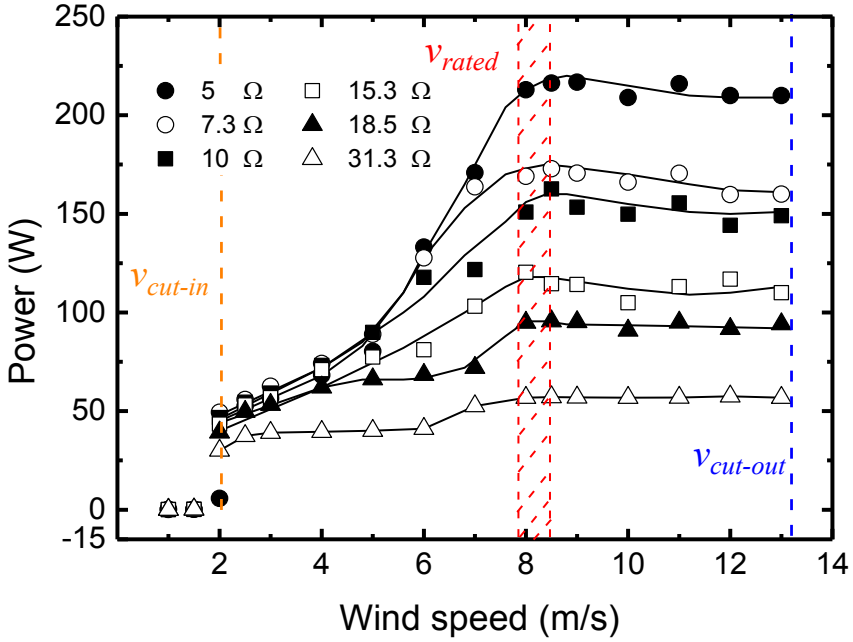

Figure 3.8 Wind turbine simulator power curve over a resistance range of 5-31.3 Ω and wind speeds of 0.5 – 13.5 m/s.

The wind turbine started to generate good level of power (30 - 50 W), sufficient for conducting desalination, at the cut-in wind speed ($v_{cut\text{-}in}$) of approximately 2 m/s and resistances above 5 Ω (Figure 3.8). Beyond the $v_{cut\text{-}in}$, the power output increased with wind speed until it reached its maximum value at the rated wind speed (v_{rated}). The rated wind speed varies according to the design features of the rotor and the generator coupled to it as well as the size of the resistance connected to the wind turbine [98, 183]. As shown in Figure 3.8 the rated wind speed for this wind turbine was in the range of 7.9 - 8.4 m/s, with v_{rated} was the smallest at the highest resistance (31.1 Ω) applied.

The maximum power efficiency for a wind turbine (C_p) is achieved at its rated wind speed (v_{rated}), beyond which the power output from the turbine levels off and becomes constant [98, 182]. This mechanism and the point *(i.e.* v_{rated}) at which it happens strongly depends on the aerodynamic design of the wind turbine [174, 199]. In large scale pitch controlled wind turbines these adjustments are done by automatically changing the pitch angle of the rotor based on the existing wind speed, hence fixing the power output at its rated value between v_{rated} and $v_{cut\text{-}out}$ [98, 182].

However, the power control mechanisms are different in permanent magnet generator based wind turbines, in which the blades are solid and have fixed angles (similar to the system used in this research). In such small scale wind turbines the power output from the generator is controlled by a frequency inverter that restricts the angular velocity of the rotor from exceeding a certain level and thus avoid the power output from the generator to go beyond its rated value at v_{rated} [98, 183]. As observed in Figure 3.8, the rated power increased significantly as a smaller resistance was applied.

The wind turbine was shut down at the cut-off wind speed ($v_{cut\text{-}out}$) of 13.3 m/s due to occurrence of furling. Furling is a self-protection mechanism in wind turbines, using the tail of the wind turbine to turn the blades away from the wind direction at high winds to avoid excess mechanical and electrical loading and prevent from possible damage to the turbine [98, 182].

As seen in the Figure 3.8, the impact of wind speed on the wind turbine power performance was more evident when the system was connected to lower resistances. From this it can be expected that the impacts of varying wind speed on the desalination performance of the ED system to be more pronounced when desalinating from higher feed concentrations (lower stack resistances (R_{stack})[31]).

3.3 Background solution and chemicals

Chemicals used for the experiments were all of high purity and purchased from Acros Organics, Sigma-Aldrich (UK) or Fisher Scientific (UK). A list of all the chemicals along with their supplier, grade/purity and general purpose of their use is shown in Table 3.2. Concentrations of target inorganic contaminants varied depending on the type of the experiment and are specified where relevant. The electrode rinse solution was prepared using 0.5 M Na_2SO_4.

Table 3.2 Chemicals and their grades, suppliers and applications

Chemical	Purity (%)	Supplier	Purpose*
Acetone (C_3H_6O)	99	Fisher Scientific	IC analysis
Oxalic acid ($H_2C_2O_4$)	99.8	BDH Chemicals	IC analysis
Sodium carbonate (Na_2CO_3)	99.9	Fisher Scientific	IC analysis
Sodium chloride (NaCl)	99.9	Fisher Scientific	Desalination experiments
Sodium fluoride (NaF)	99.9	Fisher Scientific	Desalination experiments
Sodium hydrogen carbonate ($NaHCO_3$)	99+	Fisher Scientific	IC analysis
Sodium nitrate ($NaNO_3$)	>98	Fisher Scientific	Desalination experiments
Sodium sulphate (Na_2SO_4)	>99	Sigma-Aldrich	Desalination experiments & ER solution
Sulphuric acid (98%) (H_2SO_4)	--	Fisher Scientific	IC analysis

* IC: Ion chromatography, ER: Electrode rinse

The quality of the water used for preparing the feed solutions was site specific: i) deionised water (EC ~10 μS/cm, pH 6.4) for the conventional and pulsed voltage ED experiments, carried out at the University of Edinburgh, and ii) Filtered water (EC ~56 μS/cm, pH 6.7 – 7.4) for the wind powered-ED experiments, carried out at Heriot Watt University. In the latter case, to make sure that the ions of interest has been effectively removed from the background water after filtration, the filtered water was analysed in an ion chromatography (IC) instrument. Examples of results obtained from chromatography analysis of the background water were given in Table 3.3. As seen in this table the concentrations of the ions of interest (F^-, Cl^-, NO_3^- and SO_4^{2-}) are negligible (*i.e.* < 2% of the salt concentration in the feed solution) in the background water prior to mixing with the salt (see sections 7.2 and 7.8).

Table 3.3 Ionic composition of background water after filtration (Heriot Watt University)

Backgroundwater	F^-	Cl^-	NO_3^-	SO_4^{2-}
	mg/L			
measured no.1	0.02	7.97	1.64	0.03
measured no.2	0.03	7.45	1.54	0.01
measured no.3	0.05	8.48	1.79	no detection
measured no.4	0.03	8.64	1.84	no detection

3.4 Data analysis and monitoring

3.4.1 Online data acquisition systems

The data acquisition (DAQ) system consisted of a set of pressure (Burkert 8314, Germany) and flow sensors (Omega FPR204P-PC, UK), which were all connected to a data logger (DataTaker DT 500, Australia). A Labview interface enabled recording data with 1 Hz frequency and monitoring of operational parameters during the period of an experiment. Voltage and current were recorded with higher frequencies (up to 65 Hz) via a second data logger (Omega OMB-DAQ-55, UK).

3.4.2 Conductivity, pH and temperature

A pH/conductivity meter (WTW 340i, Germany), equipped with a probe (TetraCon 325, Germany), was used to measure pH. For conductivity readings, both diluate and concentrate solutions were sampled and analysed throughout the experiments using conductivity probes (WTW-325, Germany). Carrying out a set of conductivity calibration tests at 19.9 ± 0.4 ^oC, a conversion factor of $\kappa = 0.55$ was determined for converting electrical conductivity (EC, µS/cm) into NaCl concentration (mg/L) (Appendix B).

3.4.3 Ion chromatography

Samples containing inorganic contaminants were collected and stored in plastic vials and refrigerated at 4^{o}C for maximum 48 hours (according to Standard Methods for Examining Water and Wastewater [200]), prior to analysis. Concentrations of inorganic ions (chloride, fluoride, nitrate and sulphate) were analysed using an ion

chromatography instrument (IC 883, Basic IC Plus, MetrOhm UK). The chromatography procedure was conducted in three main steps;

1- a sample was injected via an i-pump into a high capacity column (METROSEP A SUPP 5 – 150) at 0.7 ml/min.

2- while passing through the column the dissolved anions were separated from each other according to their increasing charge to mass ratio.

3- the concentration of each ion was determined by a conductivity detector once a spike appeared on the screen at the ion-specific retention time.

The eluent used was a carbonate/bicarbonate buffer (3.2 mM Na_2CO_3 and 1.0 mM $NaHCO_3$). The eluent was prepared fresh on the day of analysis and kept in use for no longer than one week. The chemicals used for preparing the eluent solution were all of analytical grade, as detailed in the Table 3.1.

Calibration curves were constructed for F^-, Cl^-, NO_3^- and SO_4^{2-} ions, using concentrations of calibration standards bracketing the range of concentrations for the ions in the samples. The range of concentrations used for the calibration standards are shown in Table 3.4. The calibration curves for the four ions are reported in Appendix B.

Table 3.4 Calibration standards

Calibration standards	F^-	Cl^-	NO_3^-	SO_4^{2-}
	mg/L			
S1	0.20	38.20	2.77	17.05
S2	0.40	77.25	5.51	34.11
S3	0.80	157.49	11.15	68.81
S4	1.62	314.82	22.27	138.34
S5	3.18	621.89	44.30	276.25

The precision of the analysis was determined by analysing the calibration standard solutions against the calibration curves during the sample analysis. As seen in Table 3.5 no significant decline in the system analysis performance was observed and the precision factor remained below 4% for all the ions at all times.

Table 3.5 Standard solutions analysis and precision factor for F^-, Cl^-, NO_3^- and SO_4^{2-} ions

Average values obtained from standard solutions analysis	F^-	Cl^-	NO_3^-	SO_4^{2-}
	mg/L			
Calibration standard solutions				
S1	0.20	38.20	2.77	17.05
S2	0.40	76.29	5.52	34.06
S3	0.80	153.33	11.10	68.46
S4	1.61	306.06	22.16	136.65
S5	3.19	607.25	43.97	271.13
Precision factor (%)	1.8	3.6	0.6	1.8

To determine the accuracy of the analysis a certified standard solution was analysed in multiple occasions during the sample analysis. The certified solution used in this research was Multielement Ion Chromatography Anion Standard Solution from Sigma-Aldrich, containing 10.0 mg/L ± 0.2% of F^-, Cl^-, Br^-, NO^{3-}, PO_4^{3-} and SO_4^{2-} ions. The average values obtained from analysing the certified solution together with the standard deviation of the analysis are reported in Table 3.6. The less accurate detection obtained for Cl^- was associated to the concentration of this ion in the certified solution being lower than this ion's lowest concentration in the calibration standard solutions (Table 3.4).

Table 3.6 Certified solution analysis

Certified Sigma Aldrich standard solution	F^-	Cl^-	NO_3^-	SO_4^{2-}
	mg/L			
Expected concentration	10	10	10	10
Average value obtained from concentration measurements (n = 3)	10.18 ± 0.30	7.33 ± 0.74	9.56 ± 0.42	9.02 ± 0.07

Samples were often diluted 2 to 5 times in order to bring the samples into the detection range of the instrument. The degree of dilution was chosen based on the expected concentration of the ions of interest in the sample. Blanks (*i.e.* ultrapure water samples) were analysed at specific intervals (*i.e.* after every 10 sample) to assess the quality of the background solution as well as to determine the instrument contamination. The results obtained from analysing the blanks were also used for determining the detection limit of the analytical system. A series of example blank

analysis plus the calculations carried out for determining the detection limit of the system are reported in Appendix B. The detection limits calculated in this way were 0.1, 0.5, 0.1 and 0.2 mg/L for F^-, Cl^-, NO_3^- and SO_4^{2-} ions, respectively.

3.4.4 Process parameters

Current density (j, Amp/m^2), resistance across the ED stack (R_{stack}, Ω) and power (P, W) in all the ED experiments were calculated using Eqs. 3.1, 3.2 and 3.3, respectively.

$$j = \frac{I}{A_m} \tag{3.1}$$

$$R_{stack} = \frac{U}{I} \qquad \left(= N\ R_{cell} + R_{ER}\right) \tag{3.2}$$

$$P = U \times I \tag{3.3}$$

where U is the voltage applied across the ED stack (V), I is the operating current (Amp) and A_m is the effective membrane surface area (m^2). Voltage and current data were measured experimentally throughout the process. The relationship given in the bracket for Eq. 3.2 is the theoretical representation of the R_{stack}, driven from Eqs 2.18-2.24; where N is the number of cell pares in the ED stack, R_{cell} is the resistance across a unit cell pair of the membranes and R_{ER} is the resistance generated due to the reaction of the electrode rinse solution with the electrodes.

Specific energy consumption (SEC, kWh/m^3) defines the energy required for producing one cubic meter of fresh drinking water by the membrane system (Eq.3.4).

$$SEC = \frac{1}{3.6 \times 10^6 \times Q_t} \int U(t) I(t) dt \qquad \left(= \frac{E_{des}}{Q_t} \right) \tag{3.4}$$

In Eq.3.4, Q_t is the volume of the treated water (m^3). The relationship given in the bracket for Eq. 3.4 is the theoretical representation of SEC, driven from Eq. 2.25, where E_{des} represents the energy required for the desalination process using the ED stack.

In all the desalination experiments, water production (*WP*, m^3/m^2day), defining the cubic meter of drinking water produced by the membrane system per available membrane surface area per day, was calculated using Eq. 3.5;

$$WP = \frac{86400 \times Q_t}{N \times A_m \times t_d} \tag{3.5}$$

where, t_d is the total time taken for the completion of the desalination process (s) and N is the number of membrane cell pairs in the ED stack.

Current efficiency (η_c, %) defines the ratio of total mass of salt removed from the diluate channel to the amount of electric charge transferred across the membranes (ECT, C/m^3) over a complete process of desalination. η_c and ECT were calculated using Eqs. 3.6 and 3.7, respectively.

$$\eta_c = \frac{\upsilon \times z \times F \times \left(c_s^f - c_s^p\right)}{ECT} \tag{3.6}$$

$$ECT = \frac{N}{Q}\int I(t)dt \tag{3.7}$$

where, υ and z represent the stoichiometric coefficient and the valence of the salt ions, respectively and F is the Faraday constant (96,485 As/mol). c_s^f and c_s^p represent the molar concentrations of salt in the feed and the product solutions (mol/m^3), respectively.

3.5 Quality assurance and quality control

This section describes the safety, quality assurance and quality control procedures employed.

Protective safety equipment (safety goggles, gloves and laboratory coat) was worn at all times when in the laboratory. The work environment was kept tidy and cleaned regularly. Laboratory supplies and glassware in contact with chemicals were washed in a dishwasher. The cleaning solutions used in the dishwasher were selected according to the solutes used in the experiments. Solutions of 30% v/v RBS® (Sigma Aldrich, UK) were employed for general cleaning of the glassware and laboratory

supplies and 8% v/v acetic acid solutions (Fisher Scientific, UK) were used to remove inorganic solutes.

The electrodialysis system was cleaned frequently (once in a week or in every two weeks depending on the nature and quantity of the experiments) in order to prevent biological growth within the stack and scaling of salts on the membranes. The cleaning procedure was consisted of flushing the membrane system for approximately 20 minutes in consecutive steps with the following solutions; 0.1M HCl (Fisher Scientific, UK), ultrapure water, 0.1M NaOH (Fisher Scientific, UK) and again ultrapure water. The last step, flushing with ultrapure water, was repeated three times and each time for up to 60 minutes to make sure that NaOH was completely washed out from the system.

Chemicals used for the experiments were all of analytical grade, as detailed in the Table 3.1. The chemicals were all dated once opened, labelled and kept in cool and dry storage, and discarded when expired. The chemicals were sometimes discarded prior to their expiry data in case some deterioration was detected. The quality of water supply was examined daily, to make sure that the conductivity of the background water was below 70 μs/cm and pH was in the neutral range of 6-8 for all the experiments.

Before starting each experiment, pure water was circulated through the ED system for at least one hour to wash out any remaining solutes from the previous tests. For each experiment the feed solutions were first prepared in form of concentrated stock solutions and were then added to deionised water in the diluate and concentrate tanks. More deionised water was then added until the volume of the solutions reached 10 L in the both tanks. The feed solutions were circulated within the ED system for approximately 3 hours before starting each experiment to reach equilibrium between the solution and the ion-exchange membranes.

Selected experiments were repeated in triplicate to assess reproducibility of the results when using the ED system. The error analysis was carried out for two main parameters: specific energy consumption (SEC) and water production (WP) in all the experiments, using standard deviation technique. The SEC errors varied between 0.1

and 0.3% when using the pulsed-ED setup and ranged from 0.1 to 0.5% when using the wind-ED system. The error in water production of the membrane system was in the range of 2 - 3% when using the pulsed-ED setup and in the range of 5 - 6% when using the wind-ED system. The generally higher errors observed in the wind-ED experiments was associated to the slight variations of the wind turbine simulator's performance due to minor changes in the atmospheric conditions of the laboratory plus heating up of the coils within the generator. In the experiments where changing the operating conditions had little effects on the results, the error bars are presented in the relevant graphs, in order to distinguish between experimental errors and real changes occurring due to the change in the operating parameters.

Desalination from feeds of 2,000 mg/L NaCl at 20 V and flow rate of 7 L/min was repeated regularly (*e.g.* once in a month) during this research. The current efficiency of these experiments was calculated (Eq. 3.6) to determine the performance stability of the ED stack and the ion-exchange membranes. The average current efficiency of 87.45% with standard error of 0.54% was obtained throughout this research, indicating that the performance of the system was maintained and remained within the range reported for similar systems in the literature.

Chapter 4

Pulsed-ED operation: Impacts of frequency and duty cycle on ion transport and water dissociation phenomena

4.1 Introduction

Electric pulse is a uniform and well defined mode of energy fluctuation. Studying the operation of an electrodialysis (ED) system powered by a pulsed electric field can yield key insight into the membrane system behaviour when connected to a fluctuating energy source such as renewable energies. Applying electric field intensification, in the form of short voltage/current pulses, was introduced in the literature as a method for improving current transport through the membranes [33, 62, 63, 201]. These studies in general focused on two features; concentration polarisation (CP) dissipation [58-61] and fouling mitigation [34, 64-66] by means of applying pulsed electric field across the ion-exchange membranes. Despite the greater progress resulted from these works, still a number of uncertainties remain regarding the impacts of applying pulsed electric field on the transport of ions through ion-exchange membranes. Some of the important gaps that question the role of electric field pulsation in intensifying or minimising CP progression at the solution-membrane interface, water dissociation, and power consumption were specified in detail in section 2.5 (Chapter 2).

This chapter aims to systematically investigate the potential of applying pulsed voltage on disrupting CP and, hence, improving the current density in both sub-limiting and limiting current regimes. The specific objectives are to:

i. Determine the impacts of pulsation on the desalination performance and water production by ED;

ii. Determine the optimum pulse regime where no significant water dissociation is experienced when operating above the limiting current density (j_{lim}), so as to operate safely at high current densities and achieve greater water production compared to when operating conventionally below j_{lim};

iii. Study the energy performance of the process under various pulse regimes to determine whether ED is an energetically suitable option for direct coupling with fluctuating energy sources such as renewable energies.

A conceptual model for the pulse-ED process is provided in section 4.2. Also in that section the main criteria for an optimal pulse regime that result in improved CP dissipation at high current densities, are proposed. The protocols employed for the experimental work will be detailed in section 4.3. This will be followed by the detailed discussion of the results obtained from the pulsed voltage assisted ED experiments that will be detailed in section 4.4.

4.2 Concentration polarisation in pulsed-ED process

When operating under a pulsed electric field, the process repeatedly shifts between steady and unsteady states at all times. This shifting is due to CP being repeatedly devolved and again dissipated at the solution-membrane interface as the system goes into consecutive power ON and OFF-periods during the process [58-61]. To study the pulsed potential ED operation it is first important to understand the mechanisms of ion transport during these CP development and dissipation stages, as this will be the key to optimising the pulse regime for operating safely (with no significant water dissociation) at high current densities.

For a further clarification it is important to note that the term “steady state” in this chapter refers to the condition where a balance is maintained between the in-going

and out-going salt fluxes through the boundary layer (*i.e.* CP is fully developed within the diffusion boundary layer following the application of an electric potential across the ED stack).

4.2.1 ON period

Once an electric potential is applied to an equilibrium solution/membrane, the ions start to be dominantly transferred by elevated electro-migration forces through the membranes. Immediately after this, the concentration of ions gradually decreases at the solution-membrane interface in the diluate compartment (and inversely, the ion concentration starts to increase at the solution-membrane interface in the concentrate channel). This results in concentration profiles to develop within thin boundary layers at the both sides of the membrane. The concentration polarisation phenomenon and its adverse impacts on the ED system and desalination process were explained in detail in section 2.3.3.

Though the influence of CP on ED performance is negligible at low current densities, it becomes particularly significant when the limiting current density (j_{lim}) is exceeded and thus the concentration of ions at the solution-membrane interface approaches zero [136, 137]. Loss in power efficiency and the occurrence of water dissociation are the main constraints against working above j_{lim} [202]. Extreme pH variations resulted from water dissociation reduce the lifetime of membranes which have low acidic/basic resistance [141]. Moreover, the variation of acidity close to the membrane surface in the diluate channel may enhance membrane fouling and scaling [131] and contribute to a further reduction in the system performance.

In the pulsation process, CP is either partially or fully developed within the diffusion boundary layer during the ON-period [59, 60]. The time required for the CP to become fully established at the solution-membrane interface (transition time), and thus generating a steady state, depends on the magnitude of the electric potential applied across the membranes [130, 134, 203]. If the ON-period of the selected pulse (t_{ON}) is sufficiently short, the CP evolution is interrupted before reaching a steady state by the elimination of the external power source; hence, the concentration profile at the solution-membrane surface slowly dissipates and results in a lower resistance

across the membranes. This causes the next pulse to start at a lower CP and, thus, the ionic concentration to remain above zero at all times during the process. By the frequent disruption of CP under carefully selected pulse regimes, it is possible to avoid adverse phenomena such as water dissociation from occurring even at high current densities. It is important to note that this requires systematic studies on CP development over a range of current densities before being able to optimise the pulse regime. To this end, detailed studies will be carried out in this Chapter.

The flux terms contributing to ion transport at the vicinity of the ion-exchange membranes over the course of CP variations during both the ON (t_{ON}) and OFF (t_{OFF}) periods of a pulse are shown in a conceptual model given in Figure 4.1. While the diagram shows an anion-exchange membrane (AEM), the conceptual representation of all these phenomena would be analogous for a cation-exchange membrane (CEM).

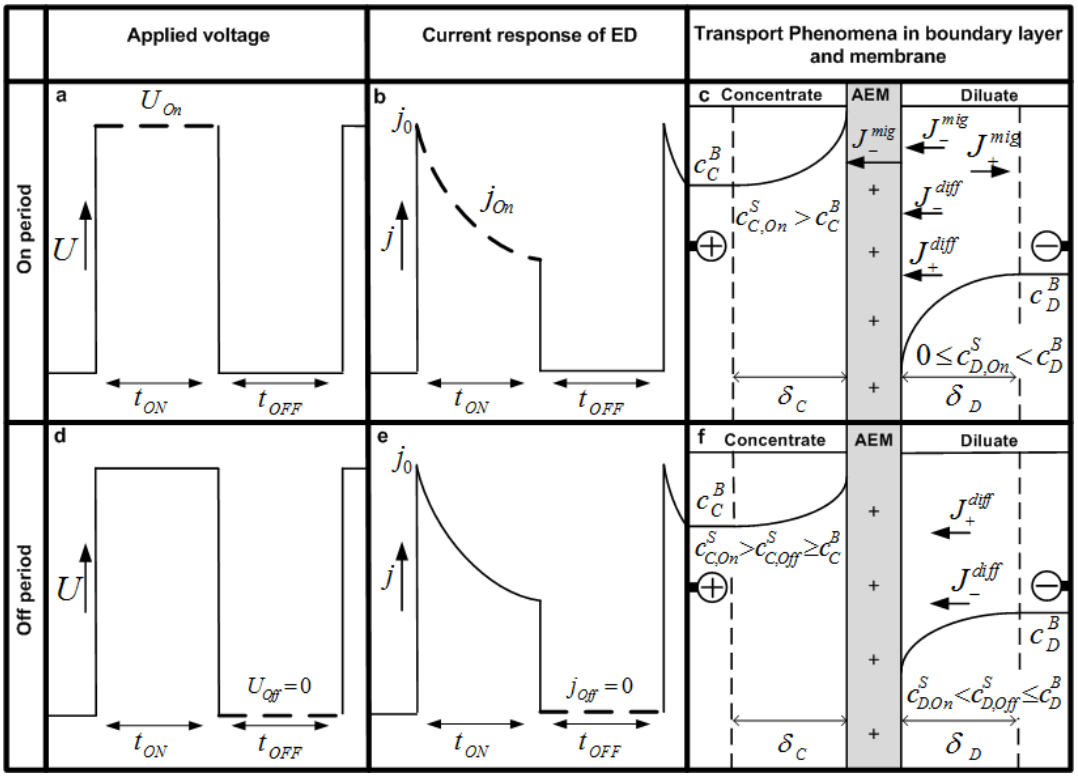

Figure 4.1 Conceptual model showing the voltage input (a,d), current density response of ED (b,e) and the main transport processes (c,f) occurring during the ON-period (a,b,c) and OFF-period (d,e,f) of a complete pulse [204].

In Figure 4.1, U is voltage (V) and j is current density (A/m^2), superscripts B and S represent the bulk and the membrane surface conditions, respectively. Subscripts D and C stand for diluate and concentrate compartments, and subscripts ON and OFF show the on and OFF-periods of the pulse, respectively.

4.2.2 OFF period

During the OFF-period (t_{OFF}), migration processes occurring in both the electrolyte solution and the membrane are negligible [59, 60]. In the absence of an applied electric potential, the only on-going transport process is the diffusion of ions from the bulk solution to the surface of the membrane, governing the restoration of ionic concentration at the solution-membrane interface, as shown in Figure 4.1 f. The degree of concentration restoration is highly dependent on the length of the pause period and the rate of diffusion, which itself is governed by the degree of concentration gradient across the boundary layer. The duty cycle of a pulse, showing the ratio between the ON and OFF-periods, is as follows:

$$Duty\ cycle = \frac{t_{ON}}{t_{ON} + t_{OFF}} \tag{4.1}$$

In the sub-limiting regime, both diffusion and migration fluxes are of comparable orders of magnitude. As a result, both the transition and restoration processes occur with similar speeds and, thus, t_{ON} is relatively in the same range as t_{OFF} [59, 60]. The extensive growth of current density in regions above j_{lim} causes the migration processes to become more substantial, rendering the transition process much faster than the restoration process [58]. Therefore, to avoid water dissociation in this regime, the OFF-period should be longer than the ON-period to ensure restoration to the initial state of the pulse. This requires duty cycles below 50% in the limiting and over-limiting regimes, with further decrease at high voltages.

Systematic studies on CP development at different current densities and subsequently detailed investigations on minimising water dissociation by means of applying carefully selected optimal pulse regimes to the ED system were done, which will be explained in detail in the following sections.

4.3 Experimental protocols

4.3.1 Current – voltage characterisation and concentration polarisation (CP) analysis

A set of experiments were carried out to:

(i) Determine the limiting current density (j_{lim}) at the feed concentrations of 500 and 5,000 mg/L NaCl, at 2 L/min, using Cowan and Brown method [145].

(ii) Establish the significance of CP and its impacts on operating current density reduction over a range of applied voltages (0 - 60 V).

(iii) Evaluate the transition time and the rate of current density drop between the non-polarized state (immediately after applying a voltage across the cell) and steady state (when the concentration profile within the boundary layer is fully developed) in both the sub-limiting and limiting regimes.

The tests were all carried out using the continuous mode of operation (Figure 3.5A). In these experiments, the feed concentration was kept constant and circulating the solutions through the system via a shared tank between the diluate and concentrate solutions. The applied voltage was increased from 0 to 60 V in 2 V increments. After applying voltage, sufficient time (approximately 5 min) was given for the current to reach steady state. Each voltage step increment was followed by another 5 min OFF-period (0 V) to ensure CP was recovered (*i.e.* the concentration restoration process close to the membrane surface was completed).

The feed values of 500 and 5,000 mg/L NaCl, employed in these CP determination tests, correspond to the two extents of concentrations, the start and end points respectively, in the subsequent desalination experiments.

Experiments in this chapter were all carried out at 2 L/min where the limiting current density (j_{lim}) and the mass transfer coefficient (k_m) of the process were found to be the lowest among the flow rates tested (Appendix C), hence the influence of concentration polarisation (CP) on current transfer across the membranes was expected to be most pronounced. The latter was important in enabling us to highlight

the impacts of applying electric potential pulsation on the current transfer in the ED process, as will be detailed below.

4.3.2 Pulsed electric field electrodialysis process (pulsed-ED)

The aim was to determine the impacts applying pulsed voltage on the desalination performance of the ED system when operating in both regimes of sub-limiting and limiting current density. For this goal to be achieved, desalination experiments were conducted over a wide range of constant and pulsed voltage modes:

(i) Constant voltage mode; applying constant DC voltage to the ED stack throughout the process at 15, 30 and 50 V.

(ii) Pulsed DC voltage mode; applying frequency over a range of 0.05 – 10 Hz at a 50% duty cycle at 15 and 50 V.

(iii) Pulsed DC voltage mode; applying 5 Hz over a range of duty cycles, 20-100% using three voltages of 15, 30 and 50 V.

These experiments were all carried out using the batch flow configuration (Figure 3.5B) with the initial feed of 5,000 mg/L NaCl and flow rate of 2 L/min. The desalination tests were considered to be complete when the concentration of the salt ions in the diluate channel reached levels below 600 mg/L NaCl, corresponding to the drinking water guideline for taste for total dissolved solids (TDS) [21]. The power source in the conventional ED tests (part i) was a DC Xantrex power supply (150 V 7 A, USA) and in the pulsed-ED experiments (parts ii & iii) was a pulsed voltage system (detailed in the section 3.2.4). The schematic diagram of the experimental setup used in the pulsed-ED experiments is shown in Figure 4.2.

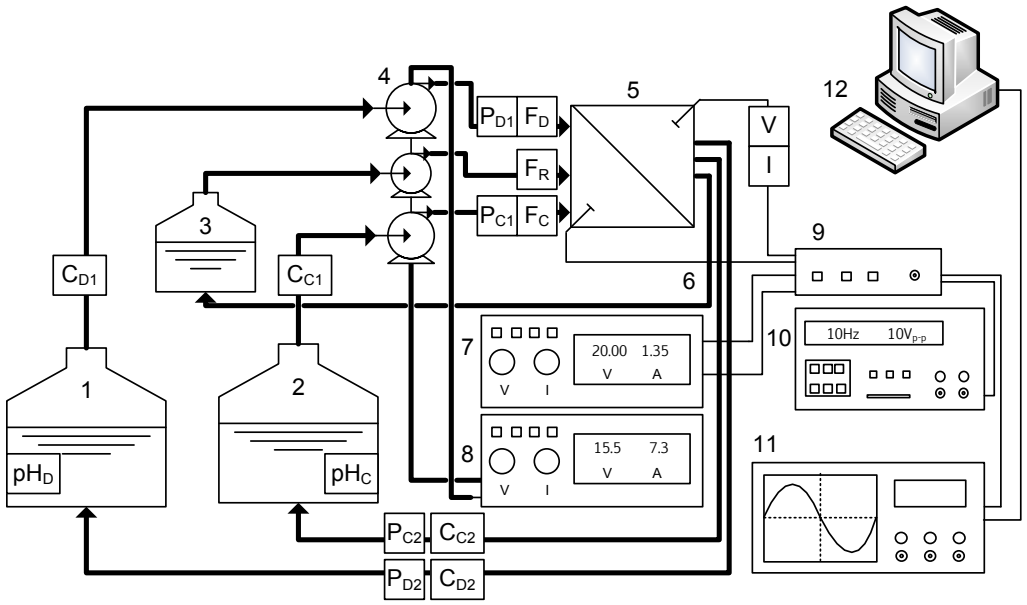

1 Diluate tank (D)
2 Concentrate tank (C)
3 Electrode rinse tank (R)
4 Diaphragm pumps
5 Electrodialysis stack
6 Major pipelines containing conductivity [C], pH [pH], pressure [P] and flow [F] sensors
7 DC power supply for pumps (120 V 10 A)
8 DC power supply for ED stack (150 V 7 A)
9 Pulse input amplifier
10 Pulse generator
11 Oscilloscope
12 Data acquisition and computing systems

Figure 4.2 Schematic diagram of the experimental setup [204].

4.4 Results and discussion

4.4.1 Limiting current density and concentration polarization

In order to analyse the differences of CP in the constant and pulsed power conditions, the relationship between current density and voltage was determined experimentally, using Cowan and Brown method [145]. The limiting current densities for 500 and 5,000 mg/L NaCl, measured at 17 and 30 V, were found to be 42 and 450 A/m^2, respectively (Figure 4.3). Applying these values together with the constants listed in Table C1 (Appendix C) into Eq. 2.14 (Chapter 2), the thickness of the boundary layer (δ) was calculated to be in the range of 5.2 - 5.5×10^{-5} m. It is important to note that the thickness of the boundary layer is independent from both the feed concentration and the electric potential applied across the membranes and is principally a function of hydrodynamic properties of the process, such as flow rate and the cell geometry [31, 50].

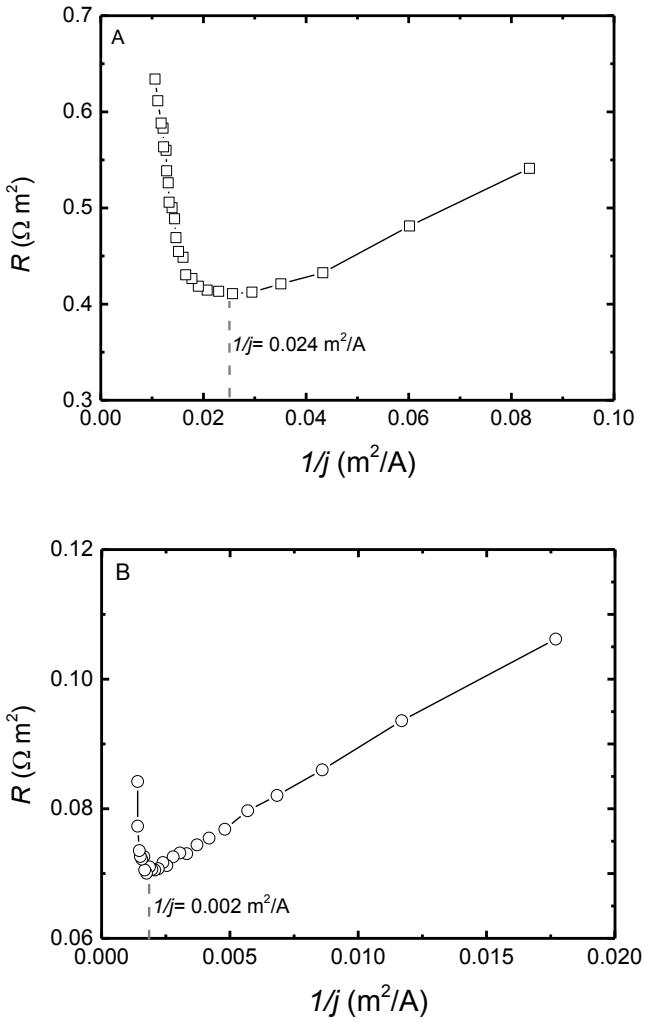

Figure 4.3 Limiting current density for feeds of 500 (a) and 5000 (b) mg/L NaCl at 2 L/min by plotting the electrical resistance of the electrodialysis stack versus the reciprocal current density [204] (mode of operation: continuous recirculation).

Figure 4.4 shows the *j-v* characteristic response of ED over a range of voltages i) upon the initiation of the process, where CP is negligible (solid symbols), and ii) at steady state, where the concentration profile within the boundary layer is well developed and CP is complete (hollow symbols). The grey line defines the voltage at which the *j-v* curve deviates from linearity, rendering the entrance of the system into the limiting current density regime. At steady state, the initial linear region of the *j-v* curve describes the sub-limiting regime. In the sub-limiting regime, where the concentration of ions close to the membrane surface is still greater than zero, the impact of CP on current density is negligible. As seen in Figure 4.4, in this region the

current drop from the non-polarized state to the steady state for the feeds of 500 and 5,000 mg/L NaCl was not more than 8 and 50 A/m^2, respectively.

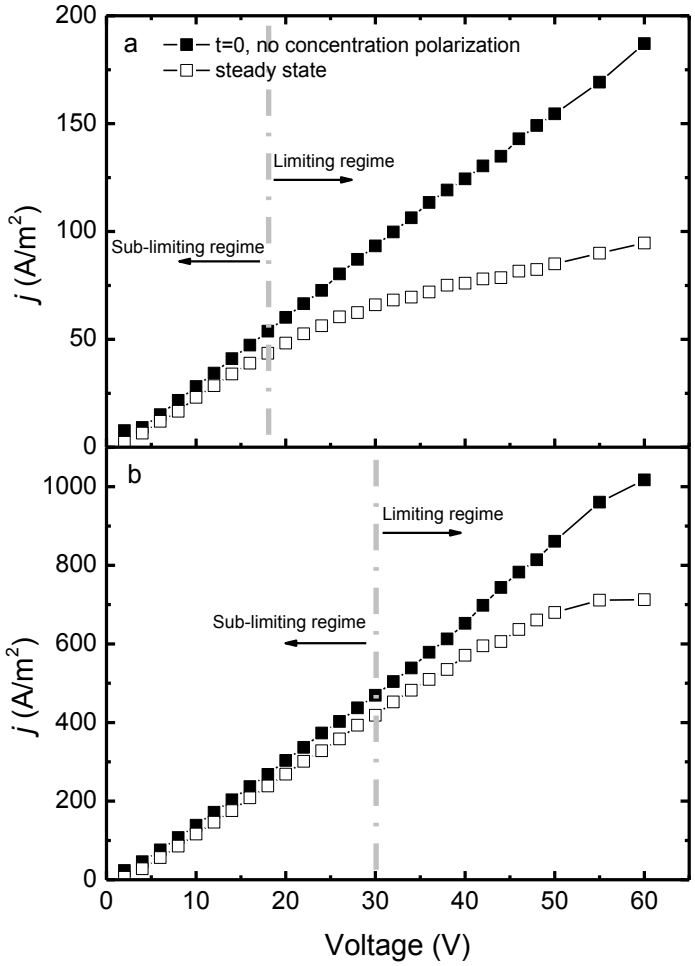

Figure 4.4 *j – V* characteristic response of an ED system at steady state (hollow square) and immediately on starting the process where negligible CP exists (filled square) for a) 500 mg/L NaCl and b) 5,000 mg/L NaCl solutions at 2 L/min and pH 6.4 [204]; (mode of operation: continuous recirculation).

The $j-v$ curve started to deviate from linearity once the applied voltage across the ED stack exceeded 17 V, for the feed of 500 mg/L NaCl, and 30 V, for the feed of 5,000 mg/L NaCl (Figure 4.4). As can be also expected from the limiting current density determination results (Figure 4.3), these are the voltage limits above which the concentration of ions close to the membrane surface drops to zero, and thus the process enters the "limiting current density" region. The impact of CP on the

operating current density increases with voltage and becomes particularly significant above the j_{lim}.

In order to minimise CP by applying pulsed voltage to the system, the degree and rate of CP development in transition from the non-polarized state to the steady state must be determined. This requires knowing the time taken for complete development of concentration profile within the boundary layer. The current density variation at the membrane surface over the transient period are shown in Figure 4.5 for both feed concentrations at two voltages representing the sub-limiting (15 V) and limiting (50 V) regimes. The current density values plotted in Figure 4.5 were all measured experimentally.

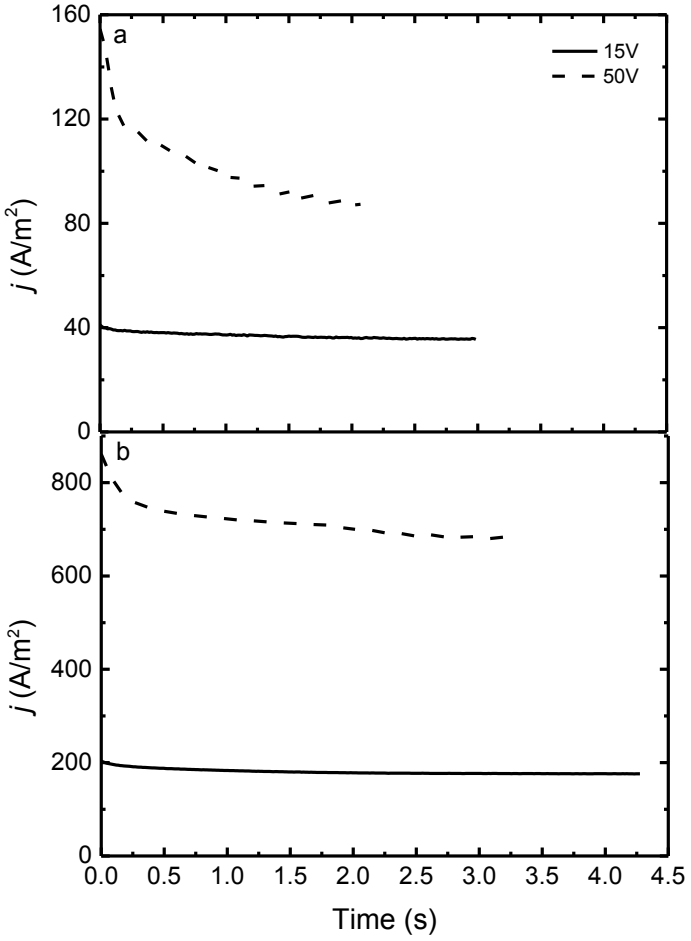

Figure 4.5 current density variations in the transition from the non-polarized state to steady state for feeds of 500 mg/L (a) and 5,000 mg/L (b) NaCl at 15 (solid line) and 50 V (dashed line) at 2 L/min and pH 6.4 [204]; (mode of operation: continuous recirculation).

In the sub-limiting regime the decrease in current density over the course of CP development was negligible (Figure 4.5). In this region, CP develops progressively with time, and the rate of decrease for the current density increases with voltage. The lower current density in the sub-limiting regime results in lower migration fluxes in both the solution and the membrane, slowing down the progression of CP compared to that in the limiting current density regime (Figure 4.5). The extensive growth of current density in regions above j_{lim} causes significant migration, and, hence, the transition process to be completed a lot faster. The complete development of CP and the attainment of steady state for 500 mg/L takes 2.9 s and 2.1 s at 15 and 50 V, respectively, while for 5,000 mg/L NaCl, this takes 4.2 s and 3.3 s at 15 and 50 V, respectively. An increase in concentration gradient across the boundary layer at higher feed concentrations causes the contribution of the diffusion component to increase, and, thus, the transition time for reaching steady state to become longer. Moreover, at higher feed concentrations the drop for the current density is less rapid.

4.4.2 Influence of applied frequency on current density

Figure 4.6 illustrates the current density variation over two seconds at the beginning and two seconds before the end of the pulsed-assisted desalination processes. During each period the concentration is the same, which makes comparison between results more accurate. Experiments were carried out in both the sub-limiting (15V) and limiting (50V) regimes in order to quantify the potential of applying pulsed voltage on current density improvement.

The partial restoration of ionic concentration at the solution-membrane interface, occurring during the OFF-period between two continues pulses, results in the enhancement of the current density. In the sub-limiting regime, where CP effects on ED performance are negligible, applying pulsed voltage had very little impact on current density improvement (Figure 4.6a and c). Consequently, the peak current density at the beginning of the desalination process increased only 8% above the steady state value in this regime. In the limiting regime, the impact of pulsation on CP disruption was more evident (Figure 4.6b); the peak current density at the beginning of the desalination process increased 24% above its steady state level at 0.1 Hz. The lower the feed concentration, the more effective the ion transport is

restricted by CP at the solution-membrane interface. Therefore, the impact of applying pulsed potential on minimising CP, whereby improving current density, becomes more pronounced as the desalination process progresses (the feed concentration decreases). The improvement in peak current density relative to its steady state value reached its maximum value of 33% (in the sub-limiting regime) and 95% (in the limiting regime) when approaching the end of the desalination process (500 mg/L NaCl) using 1 Hz at 50% duty cycle (Figure 4.6d).

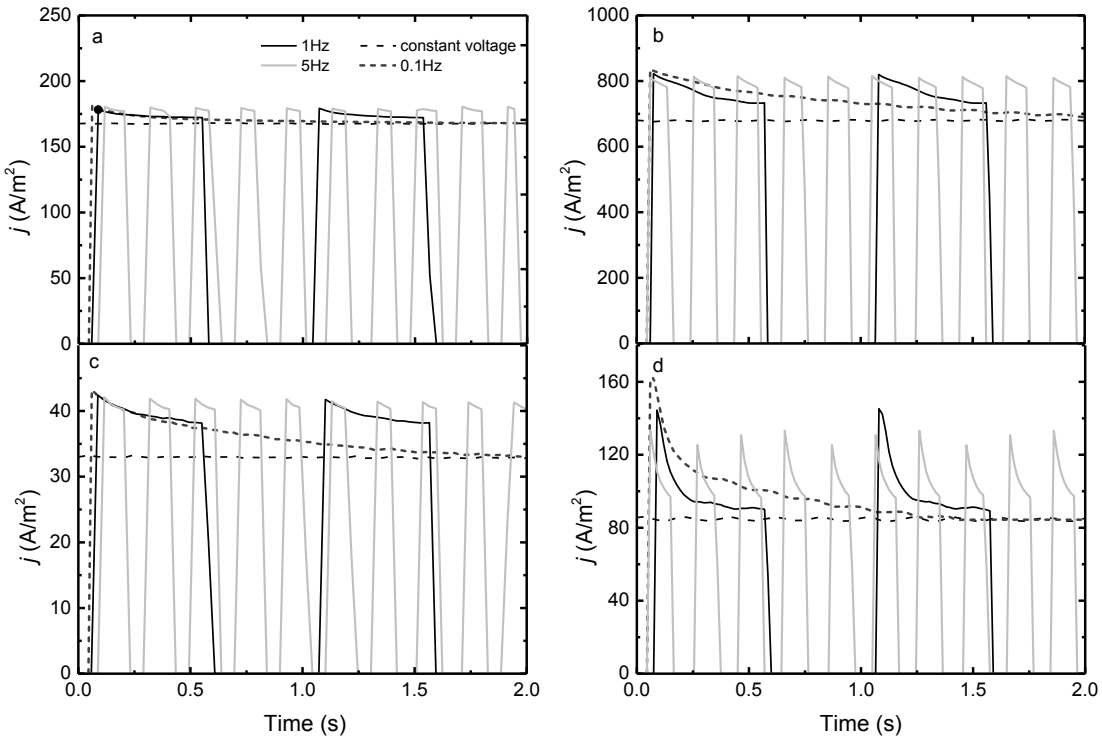

Figure 4.6 Current density variation in desalinating from a feed of 5,000 mg/L at 15 V (a, c) and 50 V (b, d) at constant and pulsed voltages (0.1 - 5Hz, 50% duty cycle, 2 L/min and pH 6.4) over 2 s at the beginning of the process (5,000 mg/L NaCl) (a, b) and 2 s close to the end of the process (500 mg/L NaCl) (c, d) [204]; (mode of operation: continuous recirculation).

The time taken for complete establishment of CP (reaching steady state) was slightly longer than 1.3 s close to the end of the desalination process when operating in the limiting current regime (50 V at 0.1 Hz) (Figure 4.6d). This was lower than the time measured in Figure 4.5 (2.1 s) for complete transition from the non-polarized state to the steady state with 500 mg/L NaCl at 50 V. The difference between these values

was attributed to CP remaining partially intact close to the membrane throughout the process, because the OFF-periods given are not long enough to ensure the complete restoration of the ion concentration at the solution-membrane interface. When CP is only partially dissipated over a pause period, the current density at the beginning of the following pulse will be smaller than that in the complete absence of CP. This results in faster transition to steady state than what was expected from results in Figure 4.5b. The rate of current density drop and the ratio between the peak and steady state current densities were the largest at the end of the desalination process when operating under pulsed mode at 50 V. In this regime, the major drop in current density took place in less than 0.5 s. This suggests that the optimum pulse regime should have an ON-period smaller than 0.5 s (1 Hz at 50% duty cycle) to ensure the steady state is not reached at any point during the process, in order to minimise CP impacts such as water dissociation at the solution-membrane interface.

At a fixed duty cycle, the degree of concentration restoration depends on the OFF-period of the pulse, applied voltage and the feed concentration. As seen in Figure 4.6 the lower the frequency, the longer the relaxation period (off period), and, thus, current density improvement at the beginning of the pulse is more pronounced. This is more evident at higher voltages such as 50V (Figure 4.6b and d). It is important to note that the mean operating current density during the ON-period of the pulse increases with the applied frequency.

4.4.3 Influence of applied frequency on desalination process

Using pulsed electric potential is a way to modify current density, improving mass transport through the ion-exchange membrane during the ON-period [59-63]. Knowing the relationship between applied frequency and desalination rate is essential to optimise the pulsed-ED process. Figure 4.7 demonstrates a comparison between analogues desalination processes using 5,000 mg/L NaCl as feed at constant voltages of 15 V (sub-limiting regime) and 50 V (limiting regime) and pulsed-ED operation at 50 V, using 5 Hz with 50% duty cycle. The grey dashed line in Figure 4.7 shows the drinking water quality guideline for taste for total dissolved solids (TDS < 600 mg/L) [21].

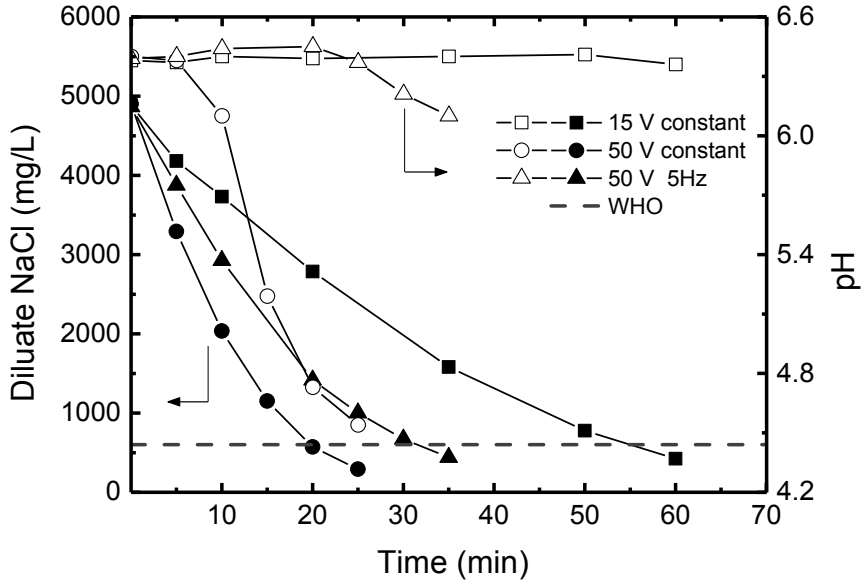

Figure 4.7 NaCl concentration variations (solid symbols) and pH variations (hollow symbols) in the diluate over the complete period of desalination process in desalinating from a feed of 5,000 mg/L NaCl at constant 15 and 50 VDC and pulsed 50 VDC using 5 Hz at 50% duty cycle (2 L/min and initial pH 6.4) [204]; (mode of operation: batch).

As seen in Figure 4.7, pH drop in the pulsed operation is much smaller than that at the constant voltage in the limiting regime (50 V). This indicates that water dissociation can be avoided significantly by applying pulsed potential, governing a safe operation when desalinating in regimes above the liming current density. This is a huge gain when added to the inherent potential of operating at higher voltages, leading to a much faster yet safe desalination process when using pulsed-potential above the j_{lim} (50 V) compared to that of the analogous operation at a constant voltage in the sub-limiting regime (15 V). Figure 4.8 shows the impact of pulsed electric potential on water production and water dissociation (represented by pH) over a range of frequencies. The results obtained at constant voltage mode are shown with arrows, and used as the basis for comparison with the pulsed-ED results, shown with solid symbols.

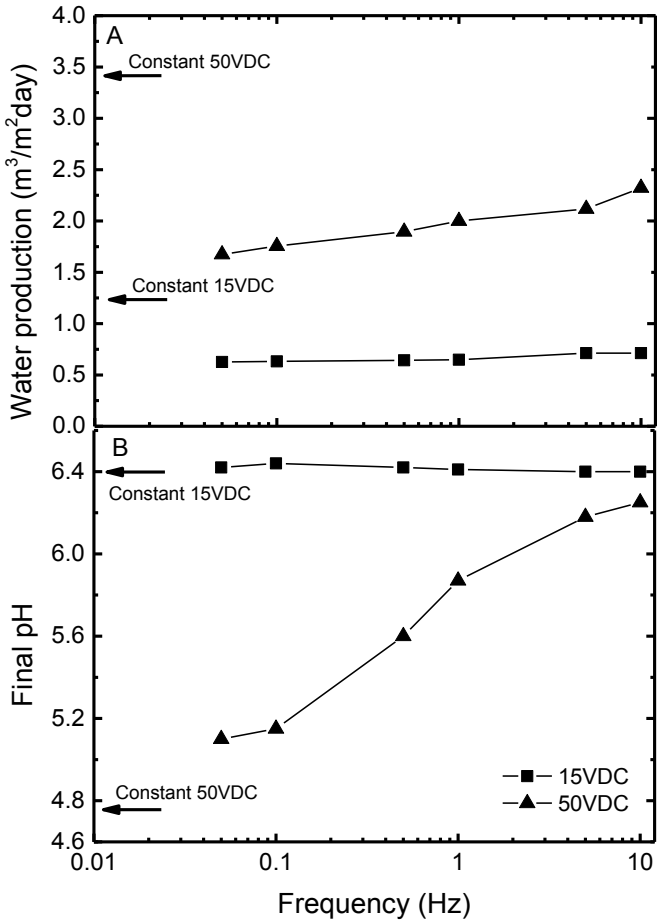

Figure 4.8 Water production (A) and pH at the end of the process (B) using both the pulsed (symbols) and constant (arrows) voltage modes in desalinating from a feed of 5,000 mg/L NaCl at 15 and 50 VDC over a range of frequencies (0.05-10 Hz, 50% duty cycle, 2 L/min and initial pH 6.4) (modified from [204]); (mode of operation: batch).

In the sub-limiting regime (15 V), applying a pulse to the system only leads to longer desalination times, which, in turn, results in lower water production (Figure 4.8a). The water production in the pulsed ED process (over the frequency range of 0.05-10 Hz) is approximately 50-58% of that in the constant voltage mode. This is due to the delay the system experiences during the OFF-periods of pulsed operation. Operating in both the constant and pulsed voltage modes, no pH drop is observed over the course of desalination at these conditions (Figure 4.8b). In the sub-limiting regime,

because the ionic concentration at the solution-membrane interface is above zero at all times, no water dissociation occurs and pH remains constant [137, 140].

By operating in the limiting regime (50V), the water production increases significantly due to increase in the electric potential (Figure 4.8a). In this regime, the effect of electric potential intensification on the process becomes more evident. The water production increases with frequency. This increase becomes relatively gradual at frequencies above 5Hz at the fixed duty cycle of 50% (Figure 4.8a). This can be attributed to the direct relationship between frequency and average current density (Figure 4.6b) leading to a greater NaCl removal at higher frequencies. Similar results were reported by Ruiz *et al.*, when comparing the desalination rate between the constant and pulsed voltage modes, using 0.1M NaCl [205].

It is important to note that the water production never becomes higher than that of the constant voltage mode, since the extent of improvement in current density resulting from applying a pulsed electric field is not sufficient to compensate for the delays caused by regular OFF-periods during the pulsed operation (Figure 4.6b). The highest water production in the pulsed experiments was 2.33 m^3/m^2day at 50V and 10 Hz. This was 68% of the water production obtained at constant 50 VDC (3.41 m^3/m^2day). Mishchuk *et al.* showed that under extreme over-limiting conditions, using very low concentration of 580 mg/L NaCl and a voltage per membrane cell of 50 V, applying pulsed electric potential resulted in a better rate of desalination compared to that of a constant voltage. This was explained as being due to the greater contribution of electro-convective processes to mass transport during the ON-period of the pulse. Moreover, it was argued that strong inertia created by the liquid motion close to the membrane surface led to extended ion transport in the pause period [60]. Similar results were shown by Lee *et al.* who attributed the better rate of desalination in the pulsed mode to both current enhancement and fouling mitigation capability of pulsed-ED operation. They found the best demineralization occurs at optimum frequency of 100 Hz at 50% duty cycle [63].

Since CP can be effectively minimised by applying pulsed-electric potential to ED, the water dissociation resulting from development of a strong concentration profile within boundary layer is expected to be minimised under the pulsed mode as well.

However, there is not yet solid evidence of the occurrence of such behaviour reported in the literature. The experiments carried out in extreme over-limiting regimes by Mishchuk *et al.* [61] and Casademont *et al.* [64] using a voltage per membrane cell of 10-30 and 10-16.5 V, respectively, suggested greater water dissociation in using pulsed electric potential compared to that of constant power. The emergence of significant disrupting effects, such as fluid instabilities caused by electro-convective processes in the layers adjacent to the membrane, was highlighted as the main cause of suppressed water dissociation in the pulsed mode. In contrast with these findings, the current work shows that by operating at a lower voltage per cell (approximately 2.5 V, still above that of j_{lim} that is reached at about 1.5V), using certain pulse regimes leads to lower water dissociation compared to that of constant power mode (see Figure 4.8b). This is attributed to effective disruption of CP by applying optimum frequency in such conditions. Using a properly selected frequency, it is possible to increase water production (2.33 m^3/m^2day at 10 Hz and 50% duty cycle at 50 V) compared to that of the analogous process at constant potential (1.24 m^3/m^2day at a constant 15 V), whilst avoiding significant water dissociation from occurring (Figure 4.8b). When operating in the limiting regime (50 V) water dissociation decreased with the increased frequency and continued with more gradual increase at frequencies above 5 Hz, supporting the results by Ruiz *et al.* showing a smaller rate of water dissociation when operating with a pulsed current compared to constant current mode [34]. In this work, pH drop was significantly minimised from a 27% drop (pH 4.75) at constant potential to 3% (pH 6.2) at 10 Hz and 50% duty cycle (Figure 4.8b).

4.4.4 Influence of applied duty cycle on desalination process

The significance and rate of CP development is highly dependent on the applied potential across the membrane, as well as the ratio between ON and OFF-period in an ideal pulse. The ratio affects the occurrence of water dissociation and hence the choice of duty cycle (Eq. 4.1) is very important when optimising the pulse regime.

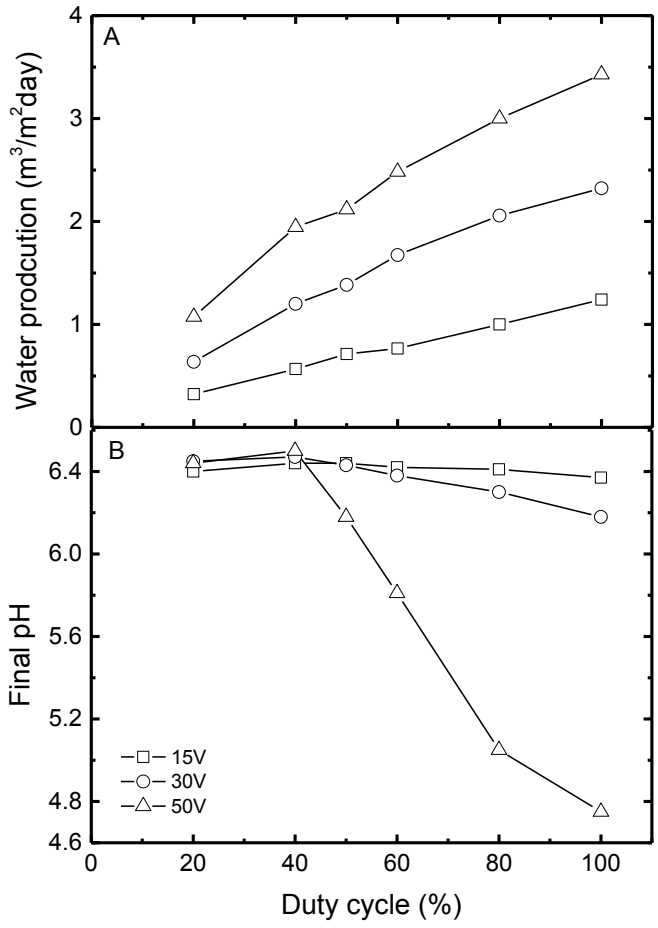

Figure 4.9 Water production (A) and pH at the end of the process (B) in desalinating from a feed of 5,000 mg/L NaCl at 15, 30 and 50 VDC at 5 Hz and over a range of duty cycles: 20-100% (2 L/min and initial pH 6.4) (modified from [204]); (mode of operation: batch).

As shown in Figure 4.9A in both the sub-limiting (15 V) and the limiting (30 and 50V) regimes, the water production of the membrane system increases with duty cycle. The increase was much more pronounced in the limiting current density regime, where pulsation had significant impact on disrupting CP. At the duty cycle of 80% the water production increased to 3.05 m^3/m^2day, which is very close to that with constant voltage (shown as 100% duty cycle in Figure 4.9), 3.41 m^3/m^2day. The experimental work by Mishchuk *et al.,* investigating demineralization from 580 mg/L NaCl, using 10 Hz at 50 V per membrane cell, showed up to three times faster desalination by using duty cycles of 80% compared to operation at constant voltage [60]. It was argued that improvement in desalination was due to continuum of ion

transport during short OFF-periods caused by liquid motion, as well as significant contribution of electro-convectional processes affecting ion transport during this period.

The depletion of ions at the membrane surface (during the ON-period) is caused by rapid migration of ions through the membrane; while ion concentration restoration (during the OFF-period) results from the slow diffusion of ions from the bulk solution to the surface of the membrane. This suggests that to have an ion concentration above zero at the membrane surface, and to minimize water dissociation, the ON-period of the pulse needs to be smaller than 1s (duty cycle <50%). In desalinating from 5,000 mg/L NaCl using 5 Hz at 30 and 50 V, the optimum duty cycles were found to be slightly smaller than 50 and 40%, respectively (Figure 4.9b).

4.4.5 Specific energy consumption and electric charge transfer

ECT and SEC calculations will demonstrate the differences in the energy performance of the ED system when it is operated under constant and pulsed power modes of operation and with different applied voltages. ECT in both the sub-limiting and the limiting regimes, and regardless of the mode of operation (constant or pulsed voltage), was found to be relatively the same for all the experiments ($8.36 \pm 0.14 \times 10^6$ C/m^3). This means that even in the limiting current density regime, the current is still mainly transferred by the salt ions and the contribution of H^+ and OH^- ions, produced from water dissociation, to current transport is negligible. This is in agreement with the studies of Krol *et al.*, suggesting the majority of current (>97%) being transported by the salt ions even when operating above j_{lim} [131].

As shown in Figure 4.10, by using an optimum pulse regime (5 Hz at 40% duty cycle) it is possible to conduct desalination at voltages above the limiting current value (*e.g.* 50 V) with no significant water dissociation (*i.e.* no significant pH drop as previously shown in Figure 4.9); hence to obtain a better desalination rate (40%) compared to the analogous desalination in the sub-limiting regime at constant voltage (15 V). However, it is important to note that increasing the voltage inevitably results

in an increase in the energy consumption of the desalination process, regardless of the operation was conducted under constant or pulsed voltage mode (Figure 4.10).

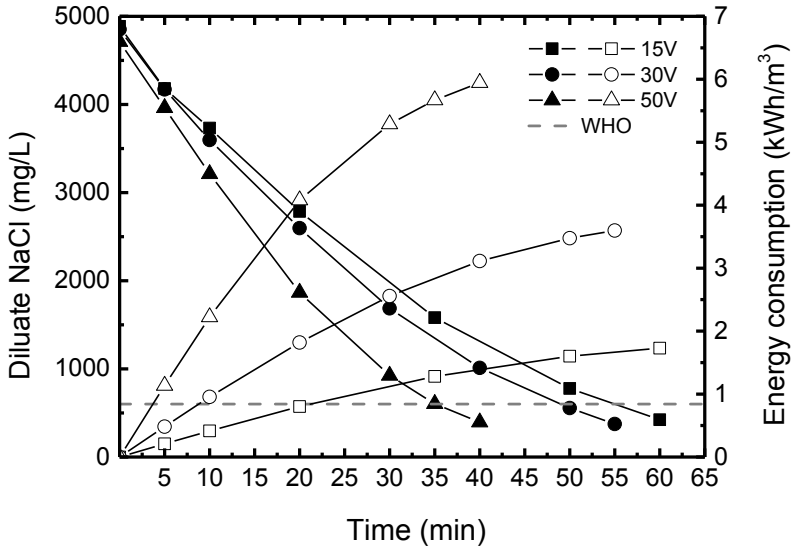

Figure 4.10 NaCl concentration in diluate channel (solid symbols) and energy consumption (hollow symbols) during desalination of 5,000 mg/L NaCl using constant potential of 15 VDC and optimum pulse regimes of 5 Hz with 50 and 40% duty cycles at 30 and 50 VDC, respectively, (2 L/min and pH 6.4) [204]; (mode of operation: batch).

The SEC values calculated using constant voltages of 15, 30 and 50 V were 1.70 ± 0.07, 3.47 ± 0.03 and 5.83 ± 0.05 kWh/m^3, respectively. These findings were in the same order of magnitude as the specific energy consumption measurements reported in the literature for brackish groundwater desalination [12, 206]. The SEC values using the pulsed-electric potential, regardless of the pulse regime applied, were 1.74 ± 0.02, 3.51 ± 0.02 and 5.81 ± 0.08 kWh/m^3 at 15, 30 and 50 V. A comparison between the SEC values for the tests carried out using both constant and pulsed voltage modes suggests that the energy consumption of the process only increases proportionally with the applied voltage across the ED stack; however, the energy consumption is independent of the mode of operation. These results are also in agreement with the study conducted by Casademont *et al.*, showing negligible difference in energy consumption between the experiments conducted under constant voltage and those carried out with pulsed voltage modes [64]. Independency of SEC from the mode of operation, as found in this work, further confirms the findings in

the literature suggesting that ED is an energetically robust desalination technique when directly coupled with fluctuating power inputs such as renewable energy sources [69, 70].

4.5 Conclusion

This Chapter aimed to systematically investigate the impacts of applying pulse voltage, as a uniform and well defined mode of energy fluctuations, on CP disruption, ion transport, and water dissociation phenomena in electrodialytic removal of NaCl from water. For this reason two regimes of sub-limiting and limiting current density were studied. Pulsed ED operation allowed i) operation at higher voltages (above limiting current conditions) while avoiding acidification problems; and ii) increase in the water production level compared to the analogous process at constant potential in the sub-limiting region, but with slightly higher energy consumption. The increase in energy consumption was proven to be solely due to operating at higher electric potentials and independent of the mode of operation.

In the sub-limiting regime, where the impact of CP on charge transfer across the membranes was negligible, no significant improvement in current density was achieved due to electric field intensification. Therefore, applying pulsation only led to consecutive shut down periods during the desalination process, ultimately resulting in reduced water production compared to the operation at constant voltage. In the limiting current density regime where CP was more effectively limiting ionic flux through the membrane, disrupting CP by means of applying pulse voltage led to significantly improved current density over the ON-period. This allowed higher water production (*e.g.* about 40% increase in the water production when operating at 50 VDC with 5 Hz and 50% duty cycle pulse mode) compared to the analogous conventional process at constant voltage in the sub-limiting regime (15 V DC), while the water dissociation still remained negligible throughout the process when employed pulsation, hence the process was considered to occur in a safe zone (only a slight decrease of pH from 6.4 to 6.1 in the diluate stream over the complete course of desalination).

Water dissociation, as the main adverse phenomenon experienced in the over-limiting regime, was minimised by applying pulsed voltage. By optimizing the pulse frequency and duty cycle, the concentration restoration process completed to a sufficient extent during the OFF-period. This ensured that the CP would be dissipated effectively during each pause period, and, thus, water dissociation was minimised. In desalinating from a feed of 5,000 mg/L NaCl at 2 L/min and voltages of 30 and 50 V, experimental findings showed negligible water splitting at 5 Hz and duty cycles below 50 and 40%, respectively.

Pulsation, as a well-defined form of energy fluctuation, had no negative impact on energy consumption and electric charge transference across the membranes. This finding highlighted ED as an electrically robust system with a potential to perform satisfactory desalination if directly coupled to a fluctuating energy source such as renewable energies.

Next chapter systematically investigates the impacts of wind speed and fluctuations inherent to the wind resource on the desalination performance and the energy consumption of the ED system when the membrane system is directly connected to a wind turbine system.

Chapter 5

Impact of wind speed and fluctuations on desalination performance of the wind-ED system

5.1 Introduction

The extremity and unpredictability of wind speed fluctuations [14, 78, 84, 97], and their significant variations from one location and season to another [74, 76, 77, 174, 207], restrict the choices of desalination technologies (*e.g.* RO, thermal or ED) that can handle such extreme energy variations, while exhibiting satisfactory desalination performance, when directly connected to wind turbine systems. The results obtained from Chapter 4 suggested that ED could perform satisfactorily even under fluctuating energy conditions, and, thus, ED may potentially be a suitable option for direct coupling to fluctuating sources of energy such as wind [204]. However, the findings in Chapter 4 did not offer comprehensive conclusions as to what extend the energy and desalination performance of the ED process may be influenced by fluctuations as extreme and random as those often appear in a wind resource (detailed explanations on wind speed availability and variability were given in section 2.4). In a direct connection to a wind turbine, both the voltage and current vary with wind speed fluctuations, expectedly having more uncontrolled impacts on the operation of the ED system compared to that in the pulsed-ED configuration. In this research a

directly coupled wind energy powered-ED system was developed for the first time (Explained in detail in section 3.2) and tested under various wind conditions in order for it to determine a safe operating window of wind speeds and fluctuations.

It is important to note that the direct connection of the wind turbine to a batch recirculating ED system is also a novel attempt (to the best knowledge of the author) in terms of coupling a wind turbine to a varying resistance load; since in all other applications wind turbines are mainly used to power constant resistance loads, these being either electricity grids or in smaller scales battery banks and super capacitors [56, 97, 98, 208].

Firstly, in this chapter a theory describing the performance of the wind-ED system as a function of i) wind speed, and ii) resistance of the ED stack (R_{stack}) is given in detail. Secondly, the results obtained from systematic investigations of the wind-ED system performance under various wind speed conditions is discussed in detail in order to address the following two main objectives:

i) To determine the impacts of low and high wind speeds on the desalination performance of ED by measuring clean water production and specific energy consumption (SEC) under constant wind speed conditions. A range of 2 m/s to 10 m/s was employed in these tests.

ii) To determine the effects of wind speed fluctuations on ED desalination performance and energy consumption by testing the system under a range of turbulence intensities (0-0.6 TI) and oscillation periods (15-180 s).

5.2 Experimental protocols

5.2.1 Impacts of wind speed and fluctuations: simulated wind speed data

First, experiments carried out using simulated wind speed data as inputs to the wind turbine simulator. The reason for using simulated wind speed data was to take into account the fluctuations of the renewable energy source in a controlled manner, thus to avoid complexities inherent to random variations of wind speed in a real wind condition. The wind speed data was chosen carefully to cover a wide range of steady

state and fluctuating wind conditions that are commonly experienced by small wind turbines in remote regions [73-77]. Steady state wind conditions refer to the conditions in which the wind speed is constant. The tests were conducted under two main wind speed conditions: i) steady state and ii) fluctuating wind conditions, as outlined below.

i. Steady state wind conditions

Tests were carried out at constant wind speeds of 2 - 10 m/s (Figure 5.1A). The lower range (2 m/s) was chosen to represent the cut-in speed of the wind turbine, obtained from the power testing of the wind turbine simulator (Figure 3.8). The upper range (10 m/s) represents the region between the rated wind speed (7.9 - 8.4 m/s depending on the load) and the cut-off wind speed (13.3 m/s), where the output from the wind turbine remains relatively constant regardless of the variations in the wind speed. Moreover, the chosen range of 2-10 m/s includes all three distinct wind speed regimes of low, moderate, and high as proposed by the modified wind speed classification for micro wind turbine systems (see section 2.4.1 for more information). Details on the power performance of the wind turbine over a wide range of wind speeds and resistances can be found in section 3.2.6.

Results obtained from the steady state experiments are discussed in two sections:

First; section 5.4.1 provides a systematic understanding of the wind-ED system operation at steady state wind conditions by looking into the impact of selected wind speeds across the 2-10 m/s range (3, 5 and 8 m/s) on the operating parameters of the wind-ED system.

Second; section 5.4.2 discusses the impact of steady state wind conditions on the global desalination and energy performance of the wind-ED system. This is achieved by studying the water production and specific energy consumption (SEC) of the system over a complete range of tested wind speeds (2 – 10 m/s).

ii. Wind speed fluctuations

Simulated wind speed fluctuations, characterised based on turbulence intensity relationships as described in Chapter 2 (Eqs. 2.28 and 2.29), were used as inputs to the wind turbine simulator in these tests. Wind turbulence intensity (TI) and the period of oscillation varied one at a time to cover the full range of operation: (i) TI from 0 (steady state conditions) to 0.6 (extreme fluctuations), and (ii) Period of oscillation from 15 (fast oscillation) to 180 s (slow oscillations) [178] (Figure 5.1B). In these experiments the average wind speed was set at 5 m/s; a wind speed with a high frequency of occurrence [177] and suitable for satisfactory operation of small scale wind systems with hub heights between 8 and 10 m [74, 75].

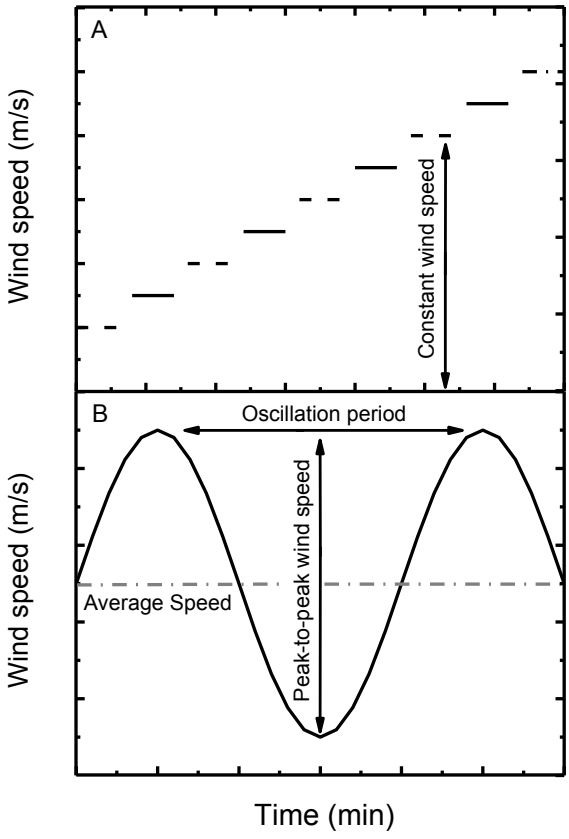

Figure 5.1 Wind speed inputs to the wind turbine simulator in the wind-powered ED experiments; (A) steady state and (B) simulated fluctuating wind speed conditions.

The results obtained from the fluctuating wind speed experiments are also discussed in two sections:

First; section 5.4.3 provides a systematic understanding of the wind-ED system operation under wind speed fluctuations by looking into the impact of extreme turbulence intensity (TI of 0.6) and two extents of oscillation periods (15 and 180 s) on the operating parameters of the wind-ED system.

Second; section 5.4.4 discusses the impact of wind speed fluctuations on the global desalination and energy performance of the wind-ED system. This is achieved by studying the water production and specific energy consumption (SEC) of the system over a complete range of turbulence intensities (0 – 0.6) and oscillation periods (15 – 180 s).

5.2.2 Impacts of wind speed and fluctuations: real wind speed data

At this stage, two sets of real wind speed data were used as inputs to the wind turbine simulator in order to study the desalination performance of the wind-ED system under realistic wind speed conditions. The wind data used for the experiments were obtained from a wind speed measurement taken near the town of Emden at the coast line of the German North Sea in October 1997 [78]. These high quality measurements were carried out at 4 Hz frequency, using an ultrasonic anemometer at the hub height of 20 m. The log law relationship (Eq. 2.27) was used to make this data more applicable for a wind turbine installed at the hub height of 8 m [98].

The wind speed data used in this part was chosen carefully to cover both low and moderate-high wind speed regimes for wind turbine system. The short and long term wind speed fluctuations were selected to provide realistically challenging operating conditions for the wind-ED system. The wind speed data was chopped to reduce the frequency from 4 Hz to 1 Hz in order to make the size of the data set more manageable for the short wind-ED experiments. Further details of the wind speed conditions, including the mean wind speed and the range of turbulence intensity, are given in section 5.4.5.

The desalination experiments in this chapter were all carried out using the batch flow configuration of the ED system (Figure 3.5B) with the initial feed of 5,000 mg/L NaCl and flow rate of 7 L/min. The reason for choosing a higher flow rate compared to that in the previous chapter (*i.e.* 2 L/min) was to make sure that the limiting current density is not exceeded throughout the process. The limiting current density measurements for different feed concentrations and flow rates are given in Appendix C. Some of the experiments were repeated with the higher initial feed concentration of 10,000 mg/L NaCl to investigate the impact of feed concentration on the operation of the wind-ED system. The desalination tests were performed until the target concentration of 600 mg/L NaCl, corresponding to the drinking water guideline for taste for total dissolved solids (TDS), was obtained [21]. The schematic for the complete setup, demonstrating the membrane system in direct contact with the wind turbine system is shown in Figure 5.2.

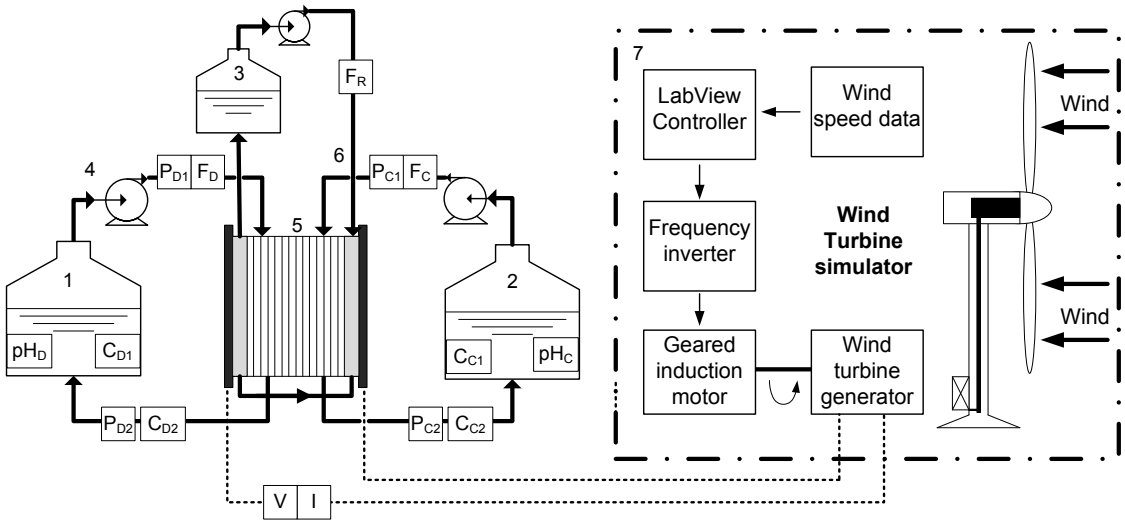

1 Diluate tank (D)

2 Concentrate tank (C)

3 Electrode rinse tank (R)

4 Diaphragm pumps

5 Electrodialysis stack

6 Major pipelines containing conductivity [C], pH [pH], pressure [P] and flow [F] sensors

7 Wind turbine simulator

Figure 5.2 Schematic diagram of the wind-ED experimental setup

5.3 Theory: the wind-ED system performance as a function of wind speed and ED stack resistance

In this section the mechanism of power generation by a small scale direct-drive variable speed PMG based wind turbine when directly connected to an ED system (representing a variable resistance load) is described in detail for the first time (Figure 5.3).

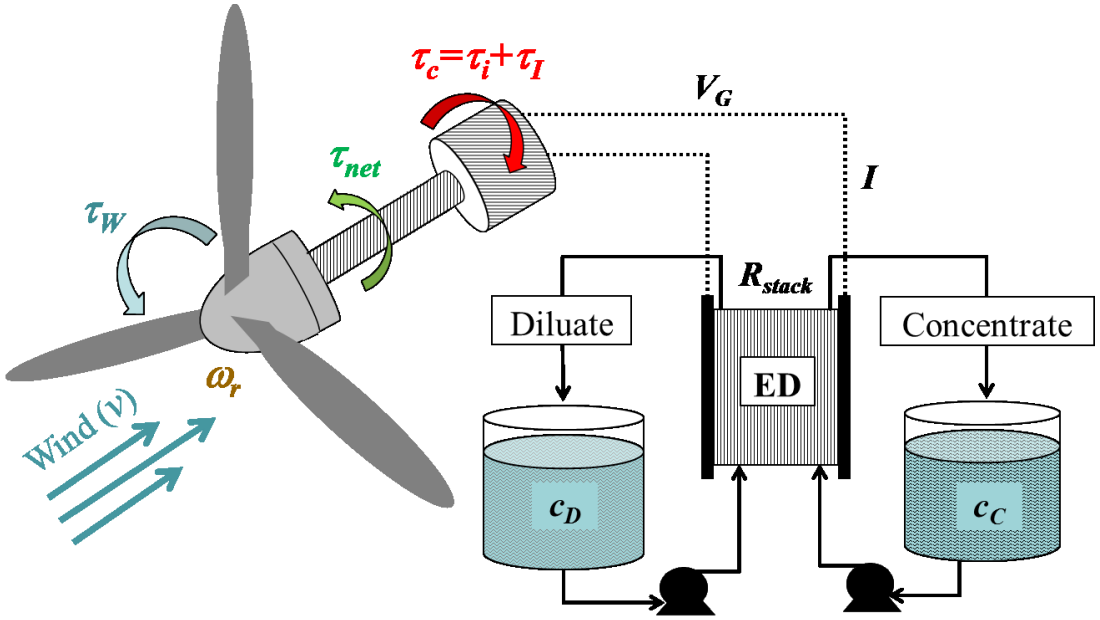

Figure 5.3 Voltage generation by a direct drive PMG wind turbine when directly coupled to an ED system in a batch desalination process. (ED: electrodialyis system, c_D: salt concentration in the diluate stream, c_C: salt concentration in the concentrate stream, R_{stack}: ED stack resistance, I: current, V_G: voltage output from wind turbine, v: wind speed, ω_r: angular velocity of the rotor, τ_c: total counter torque force, τ_i: inertial forces generated counter torque force, τ_I: current induced counter torque force, τ_W: wind speed generated prodctive torque force, τ_{net}: net torque force)

Upon approaching a tube of moving air (wind), the kinetic energy of the wind in contact with the airfoils of the blades of the wind turbine creates a combination of drag forces (in the direction of the wind) and lift forces (perpendicular to the direction of the wind) [98, 173]. The resultant of these force vectors on the oppositely positioned blades of the rotor is a productive torque force that tends to spin the rotor (τ_w) (Figure 5.3). Immediately after the generation of this productive torque force a counter torque force imposes a resistance against the rotation of the

rotor. The counter torque force is predominantly controlled by i) the inertial forces of the rotating components of the turbine (τ_i) and ii) the resistance of the load connected to the wind system (R_{stack}). At wind speeds above the cut-in wind speed of the wind turbine ($v_{cut\text{-}in}$) the productive torque force surpasses the total counter torque force (τ_c) causing the net torque force (τ_{net}) applied to the shaft of the wind turbine to reach the minimum positive level required to make the rotor spin and thereby produce power. In PMG based wind turbines the rotor is directly connected to the generator via a shared shaft [95, 187]. Therefore, with an increase in the net torque force, the angular velocities of both the generator and the rotor (ω_r), and directly proportional with them the voltage output from the generator (V_G), increase.

In common applications, such as supplying energy to a grid or charging a battery bank [56, 97, 98], the resistance of the load connected to the wind turbine is constant and thus its contribution to the net torque force remain relatively unchanged throughout the process. Therefore, in studies of power generation of wind turbines, wind speed is often considered as the only variable that varies and consequently has an effect on voltage output from the turbine generator. However, when the wind supply is directly coupled to ED operating in a batch recirculation configuration, the resistance of the ED stack (R_{stack}) will increase over time since the salt concentration decreases in the diluate channel (c_D) as desalination occurs (Figure 5.3) [31, 169, 209]. As the R_{stack} increases and fewer ions remain available to transfer electric charge across the membranes, the current (I) driven by the ED stack from the wind turbine decreases. The decrease in the current results in the lowering of the current induction counter torque force (τ_I) applied by the load on the shaft of the turbine [95, 187, 188]. Considering the case that the wind speed (v) is constant (*i.e.* the productive torque force (τ_w) excreted on the blades by the wind is fixed), a decrease in the current induction counter torque force causes the net torque force (τ_{net}) to increase and thus the rotor to accelerate to a higher angular velocity (ω_r). By increasing the angular velocity of the rotor, the generator also rotates faster; resulting in more voltage (V_G) to be produced by the wind turbine. Therefore, throughout the desalination process the voltage is expected to increase in inverse proportion to the decrease in current. It is important to note that there is always a balance between

voltage and current, resulting in a relatively steady power output from the wind turbine, unless there is an external control system (*e.g.* a frequency inverter) in line to prevent voltage from increasing further in order to prevent physical damage to the rotor and the generator [95, 98, 210]. These theoretical relationships linking the operating parameters in a wind-ED process and the result of having an active frequency inverter in line were clearly observed in the experiments, described in following sections.

5.4 Results and discussions

5.4.1 Wind-membrane system performance under low and high wind speeds at steady state

Desalination tests were carried out with constant wind speeds in order to determine the operating characteristics of the wind-membrane system at steady wind speed conditions. Figure 5.4 shows the main operating parameters of the wind-ED system while desalinating a 5,000 mg/L NaCl feed solution at three wind speeds of 3, 5, and 8 m/s. These wind speeds were chosen to cover the extent range of $v_{cut\text{-}in}$ to v_{rated} for the wind turbine system (detailed in section 3.2.6). Moreover, these velocities are within the common range of wind speeds measured in several remote locations around the world for small scale wind turbines [73-77].

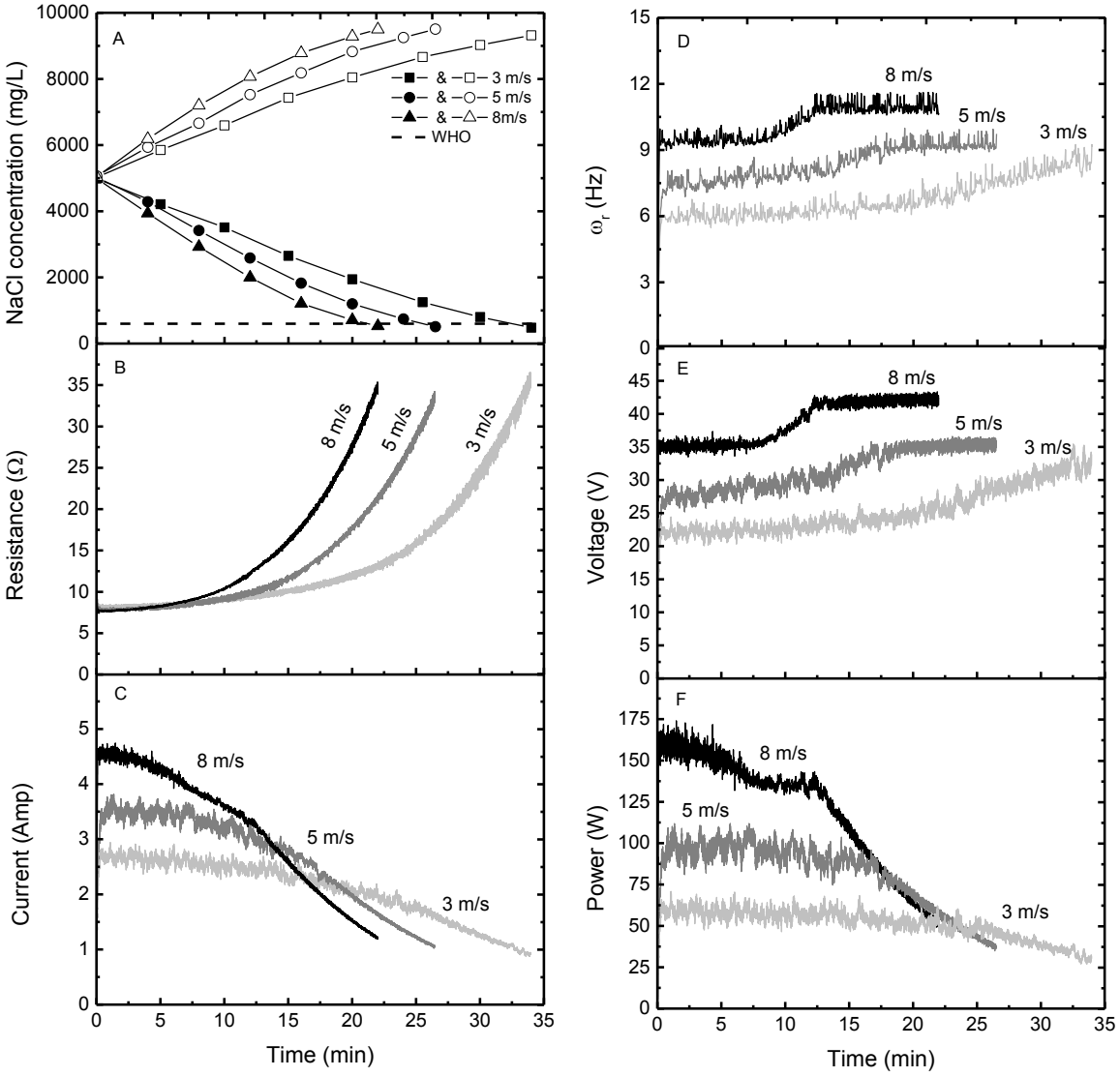

Figure 5.4 Steady state performance of the wind-ED system in desalinating from a feed of 5,000 mg/L NaCl at constant wind speeds of 3, 5, and 8 m/s plotted as (A) NaCl concentration in both the diluate (solid symbols) and concentrate (hollow symbols) streams; (B) ED stack resistance; (C) current driven by the ED stack from the wind turbine; (D) angular velocity of the rotor (ω_r); (E) voltage; (F) wind-ED operating power; (mode of operation: batch).

The resistance of the ED stack (R_{stack}) varies with the feed solution conductivity, membrane resistance and the degree of concentration polarization [31, 169, 204, 209]. Among these, the solution conductivity in the diluate stream has the greatest influence on the stack resistance. Over the course of the desalination process the concentration of NaCl decreased in the diluate stream and proportionally increased in

the concentrate channel (Figure 5.4A). This caused the resistance of the ED stack (R_{stack}) to increase from 8.3 ± 0.2 Ω at the beginning of the experiment to approximately 35 ± 0.8 Ω toward the end of the experiment (Figure 5.4B). As a result of the continuous increase of R_{stack}, the current driven by the membrane system from the wind turbine decreased gradually as the desalination process progressed (Figure 5.4C). According to the mechanism explained in the theory section (section 5.3), the decrease in the current leads to a reduction in the current induction counter torque force, which is ultimately causing the net torque force applied on the shaft of the rotor to increase and thus the rotor to accelerate (angular velocity of the rotor (ω_r) to increase) (Figure 5.4D). Therefore, as the current decreased the rotor spun faster, and hence more voltage was produced (Figure 5.4E). The increase in the voltage, which was the wind turbine's response to the increase in R_{stack}, continued until the angular velocity of the rotor was restricted by the frequency inverter from any further acceleration. This controlled restriction was posed to prevent the turbine from over loading and, thus, to avoid possible damages to the rotor and the generator [95, 98, 173, 184]. This behaviour was particularly evident at higher wind speeds (*i.e.* 5 and 8 m/s) where the frequency inverter began to restrict the acceleration of the rotor at lower resistances (13.4 ± 0.3 Ω at 5 m/s and 12.6 ± 0.3 Ω at 5 m/s) compared to that at the lower wind speeds (15.8 ± 0.3 Ω at 3 m/s). The higher the wind speed, the larger was the power output from the wind turbine (Figure 5.4F) and thus the faster was the rate of desalination (Figure 5.4A).

As it is evident in all these experiments, the wind-ED system exhibited two distinct power behaviours during the desalination process:

i. The preliminary steady power region, appearing before any constraint was posed by the frequency inverter on the increase of the voltage with the stack resistance (R_{stack}). In this region and at lower wind speeds (*i.e.* 3 and 5 m/s) the increase in the voltage was sufficient to effectively compensate for the drop in the current. This caused the electric power output from the wind turbine to stay relatively steady at a certain level in this region (56 ± 5 W at 3 m/s and 94 ± 9 W at 5 m/s) (Figure 5.4F). However, the wind turbine behaviour was slightly different when operating at wind speeds equal or higher than v_{rated} (*i.e.* the

experiment carried out at 8 m/s). In such wind conditions the voltage, which was already close to its rated value, was not permitted to increase effectively to compensate for the fast dropping current throughout the process; hence, the power started to decrease gradually from the beginning of the experiment, although yet no control was posed by the frequency inverter to limit the voltage output from the wind turbine.

ii. Regardless of the wind speed applied, once the rotor's acceleration was restricted by the frequency inverter, the voltage levelled off and the power entered a new region (the second power zone). In this region the power began to lose its dependency on the wind speed and became mainly dependent on the R_{stack}. As a result, the power began to decrease significantly along with the current until approaching the end of the desalination process. The power at the end of the desalination process fell within a narrow range for all the experiments (36 – 43 W); regardless of the wind speed applied (Figure 5.4F). Despite the significant difference at the beginning of the experiments, the current also fell within a narrow range toward the end of the process for all the experiments and regardless of the wind speed applied (0.9 – 1.1 Amp) (Figure 5.4C).

The findings in this section suggest that the desalination performance of the wind-ED system is mainly influenced by the wind speed when operating in the first power region, where no constraints has yet been posed on the voltage increase and, thus, the current transfer across the membranes varies primarily as a result of the wind speed. However, the dependency of the desalination performance on the wind speed diminishes significantly once the torque control system on the frequency inverter is activated to limit the voltage increase, as a result of which the power and correspondingly the desalination performance of the wind-membrane system begin to be principally controlled by the R_{stack} variations. The next section investigates the direct impacts of steady wind speed conditions on the water production and specific energy consumption (SEC) of the wind-membrane system.

5.4.2 Impact of low and high wind speed on water production and specific energy consumption (SEC) under steady wind speed conditions

Figure 5.5 summarises the water production and the SEC results obtained in desalinating from two feeds of 5,000 and 10,000 mg/L NaCl and over a wide range of constant wind speeds: 2-10 m/s. Some of the tests were repeated in triplicate to ensure the reproducibility of the results. The standard deviation gave an average error of 0.1% and 6% for the SEC and water production results, respectively.

Two distinct characteristic regions for both the SEC and water production curves were observed in these experiments (Figure 5.5); regions I and II, as described below.

Region (I), between the cut-in ($v_{cut\text{-}in}$: ~2 m/s) and the rated (v_{rated}: 7.9 - 8.4 m/s) wind speed conditions, where an increase in the wind speed resulted in higher energy consumption and thus larger water production. The increase in the SEC is linked to the increase of the power output from the wind turbine, as it occurs when operating at higher wind speeds [174, 199].

Region (II), the wind speeds above v_{rated} (~ 8 m/s), where plateaus appear in both the SEC and the water production curves. SEC levelling off was a result of operating between the rated and cut-out wind speeds, the range in which the power output from the wind turbine is relatively fixed at its rated level [97, 174, 177, 199]. Thereby, increasing the wind speed in this region does not have significant impact on the desalination performance of the wind-membrane system. The slight lowering of the SEC at 10 m/s was attributed to the occurrence of furling, a self-protecting mechanisms that often occurs at high wind speeds to prevent the wind turbine from overloading and potential damages to the rotor and the generator [98, 173].

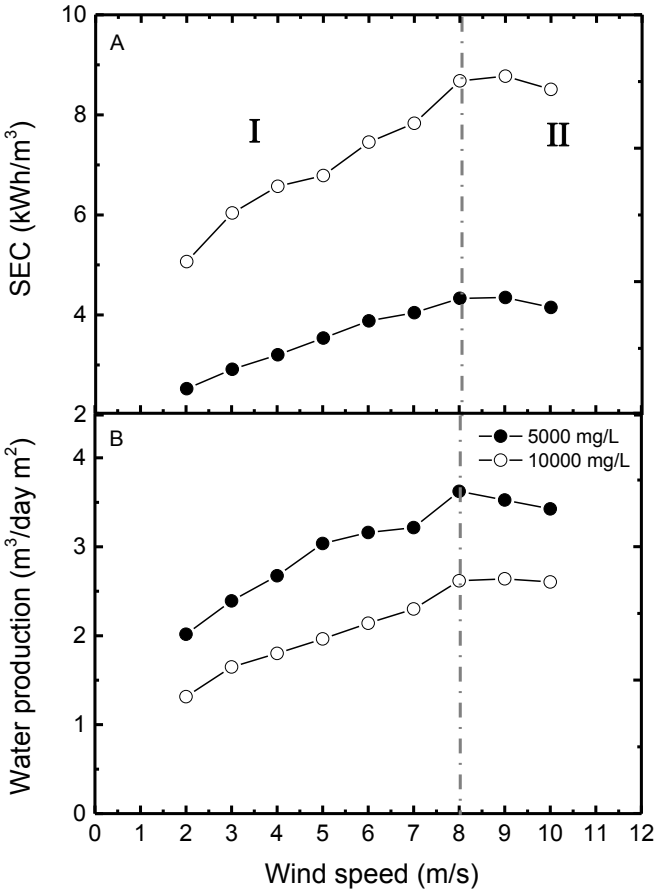

Figure 5.5 SEC (A) and water production (B) from desalinating feed solutions of 5,000 and 10,000 mg/L NaCl over a range of constant wind speeds: 2-10 m/s at the flow rate of 7 L/min. I and II mark the two distinct behavioural regions for operating below and above the rated wind speeds, respectively; (mode of operation: batch).

Over the wind speed range of 2 – 10 m/s, the SEC increased from 2.52 to 4.15 kWh/m^3 when desalinating a feed solution of 5,000 mg/L NaCl. These SEC values were within the range reported in the literature (2.64 and 5.5 kWh/m^3) for ED when desalinating brackish waters containing 2,500 – 5,000 mg/L total dissolved solids (TDS) [10, 211]. These SEC values were promising when compared to the minimum SEC reported by Park *et al.* (2.8 kWh/m^{3}day) for desalination from feed of 2,500 – 5,500 mg/L TDS, using a directly powered wind-reverse osmosis system (wind-RO) [14]. Energy consumption similarities between ED and RO were also shown in the work by Penate *et al.* who reported similar SECs, 0.618 kWh/m^3 for a PV-ED system and 0.613 kWh/m^3 for a PV-RO system, when using these RE-membrane

technologies for desalinating a brackish water feed of 3,500 μS/cm [27]. A comparison between the obtained SEC values in our research and the ones reported for other common desalination techniques, such as reverse osmosis (RO: 1.5-3.0 kWh/m^3), multi stage flash (MSF: 19.5-27.3 kWh/m^3), multi effect distillation (MED: 14.5-21.6 kWh/m^3), and vapour compression based techniques (VC: 7.0-16.2 kWh/m^3), suggests the wind-ED system to be energetically competitive with RO and significantly more efficient than the distillation systems when desalinating solutions containing 5,000 mg/L or lower TDS [10, 11, 191, 192].

SEC values obtained in desalination of 10,000 mg/L NaCl feed solutions were generally higher than those obtained in desalination of 5,000 mg/L NaCl feeds (Figure 5.5 A). This was attributed to the larger mass of salt requiring to be removed from the diluate channel before reaching the target concentration of 600 mg/L NaCl, hence requiring more energy, when starting from a higher initial feed concentration. Having 10,000 mg/L NaCl solution as a feed, the SEC of the process ranged from 5.5 to 8.51 kWh/m^3 over the wind speed of 2-10 m/s (Figure 5.4A). The higher SEC values obtained for desalination of 10,000 mg/L compared to 5,000 mg/L NaCl highlighted the energetic cost sensitivity of ED toward feed salt concentration, compared to other common desalination techniques such as RO [191, 192].

An increase in the concentration of the feed solution also resulted in a longer desalination process, and thus, a lower water production from the ED system (Figure 5.5B). The water production was in the range of 2.02 to 3.62 m^3/m^2day when desalinating from 5,000 mg/L NaCl and 1.31 to 2.61 m^3/m^2day when desalinating from the feed of 10,000 mg/L NaCl, over the wind speed range of 2 – 10 m/s (Figure 5.5B). The water production levels reported in the literature for various ED systems cover a wide range (2 – 145,000 m^3/day) [10, 11, 54, 71, 212]. Due to the differing conditions (*e.g.* flow rate, operating current/voltage, etc.) and the lack of information regarding key parameters, such as available membrane surface area and the number of cell pairs used in many of these studies, a direct comparison between the water production results obtained in our research with the ones reported is the literature is difficult.

The current efficiency of the process was calculated using Eq.3.6, and was shown to be in the narrow range of 86.3 to 88.4% for all the conditions tested. This suggested that the current efficiency of the wind-membrane system was independent of the wind speed applied and the feed concentration used in the desalination experiments. Similar results were obtained in the electric pulsed ED operations in Chapter 4, showing that the ED system is an energetically robust system with no deterioration occurring in its charge transfer behaviour despite variations in the energy resource.

The results obtained from the steady wind condition tests provide a baseline to carry out detailed analysis of the effects of wind speed fluctuations on the performance of the wind-membrane system in the next section.

5.4.3 Operating characteristics under fluctuating wind speed conditions (sine wave oscillations)

The effects of wind speed fluctuations were investigated by performing desalination experiments using an initial feed of 5,000 mg/L NaCl at the mean wind speed of 5 m/s, a peak to peak amplitude of 9.2 m/s (*i.e.* 0.6 TI) and at two different oscillation periods of 15 and 180 s. These oscillation periods correspond to the two extents of the oscillation spectrum proposed by Van der Hoven for short-term wind speed fluctuations [178]. The results obtained from these two experiments were displayed against each other at two different stages of the process; one at the beginning of the desalination when the R_{stack} is in its lower range (7.7 -8.4 Ω) (Figure 5.6) and the other one toward the end of the process when the R_{stack} is in its highest range (32.9 – 33.7 Ω) (Figure 5.7).

Operation under the rated wind speed (~2 m/s) for sufficiently long periods (> 40 s) caused the rotor's angular velocity to drop effectively ($\omega_r \leq 1$ Hz) and thus the turbine to completely shut down. This behaviour was observed during a desalination experiment under the extreme operating condition of 0.6 TI with the oscillating period of 180 s (Figure 5.6A). Simultaneously with the turbine shut down, the voltage output form the turbine was also terminated. The declining voltage, from 2.6 to 1.9 V, shown by the voltage sensors during the off-periods, represented the stack's capacitance and was not a product of the wind turbine. This capacitive voltage was

the product of the potential difference across the ion-exchange membranes, resulting from the concentration difference between the diluate and concentrate channels [31]. The capacitive voltage only appears when no external potential gradient is applied across the stack (*i.e.* when the wind turbine cycles off).

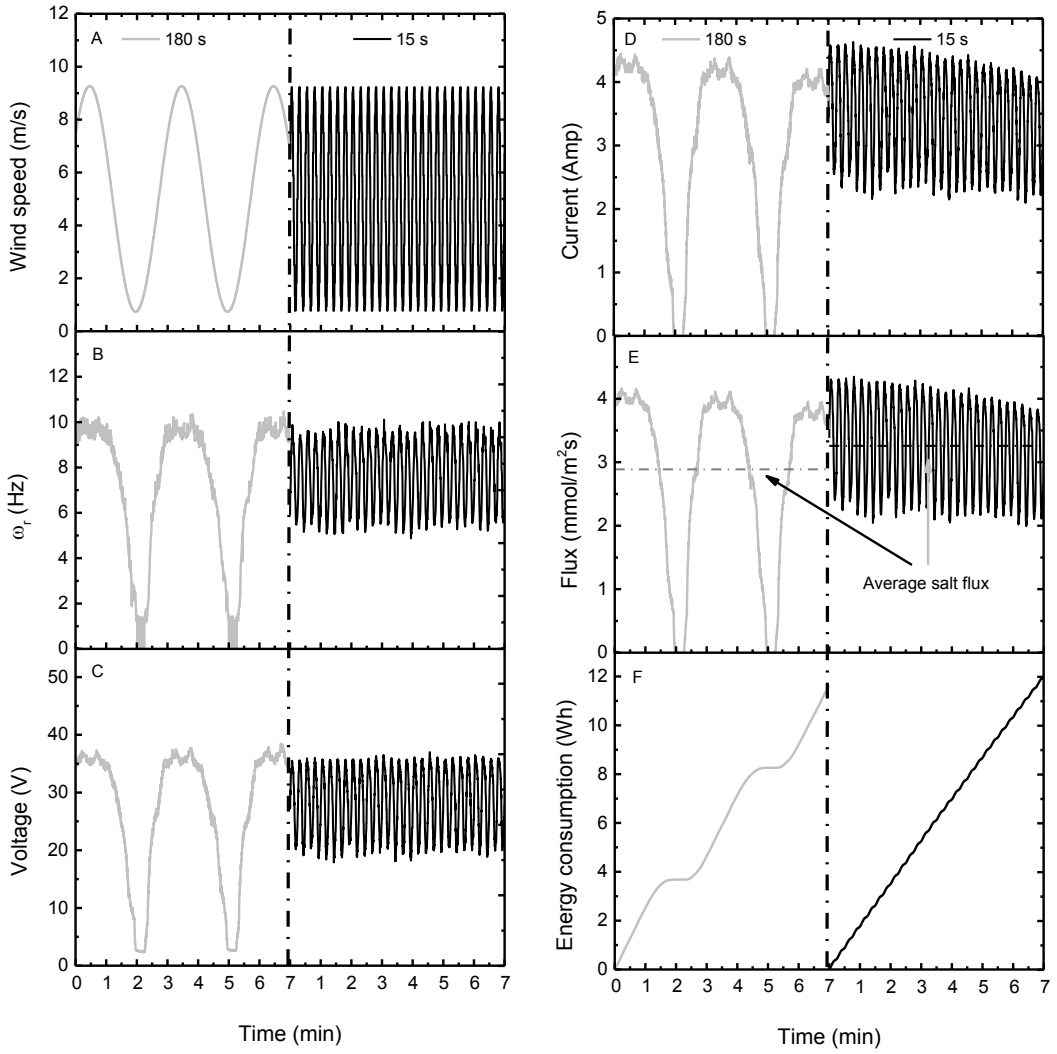

Figure 5.6 Wind-ED system performance during the first 7 minutes of the desalination tests using an average wind speed of 5 m/s at TI of 0.6 and oscillation periods of 180 s and 15 s, the initial feed concentration of 5,000 mg/L NaCl and the flow rate of 7 L/min; (mode of operation: batch).

During the off-period, the diode bridge inside the wind turbine, which is originally responsible for converting the waveforms into DC current, does not allow any current to be drawn in the opposite direction by the capacitive voltage through the ED stack. This significantly reduces the chance of having back diffusion of ions from

the diluate to the concentrate channels during this period. As a result of this, when the wind turbine cycled off the current transfer across the membranes dropped to zero (Figure 5.6D), and, thus, the ionic flux through the membranes during this period became negligible (Figure 5.6E). The cycling off of the turbine caused steady plateaus to appear on the cumulative energy consumption curve of the process (Figure 5.6F).

An increase of the wind speed to values above $v_{cut\text{-}in}$, following a period of low or no wind, caused the rotor to start spinning effectively and produce voltage. As a result of this the current transfer across the membranes increased to values above zero (Figure 5.6A-C). The acceleration of the rotor from a stagnant condition after a sufficiently long off-period required overcoming the moment of inertia of the turbine [98, 173, 174]. Since the turbine was at its lowest angular momentum immediately before the rise in the wind speed, the acceleration process at this stage was more energy consuming and slower than other stages of the process. Regularly occurring off-periods during the process negatively affected the SEC and water production of the wind-membrane system; this will be discussed in detail in section 5.4.4.

In the case of extreme wind speed fluctuations, the upper peak of the wind speed shifted beyond the v_{rated} (*i.e.* 8 m/s), causing the voltage output from the wind turbine to level off and the system to operate at lower average power throughout the process (Figure 5.6C). This also had an adverse impact on the water production and SEC of the wind-membrane system, as they will be shown in section 5.4.4.

When operating under short oscillation periods (*i.e.* 15 s) the rotor did not have sufficient time to adjust its angular velocity to rapid variations in the wind speed. Thus, the turbine's angular velocity only oscillated within a narrow range and did not display the same peak and through phenomena compared to when operating under longer oscillation periods (*i.e.* 180 s) (Figure 5.6 B). This caused the angular velocity of the rotor to be maintained, even when the wind speed fell below the $v_{cut\text{-}in}$, thus no cycling-off occurred during the wind-ED system operation (Figure 5.6 B-E). Moreover, with short oscillation periods, the passage through the peak wind speed conditions also occured fast enough to not enable the system to stabilise in peak conditions. Thus significant levelling off of power was prevented even when the

peak wind speed went beyond the v_{rated} (Figure 5.6 C & D). A combination of these phenomena resulted in the average salt flux over a given time period to be 13% higher when the system was operated at the shorter oscillation period of 15 s compared to that of 180 s oscillation period (Figure 5.6E).

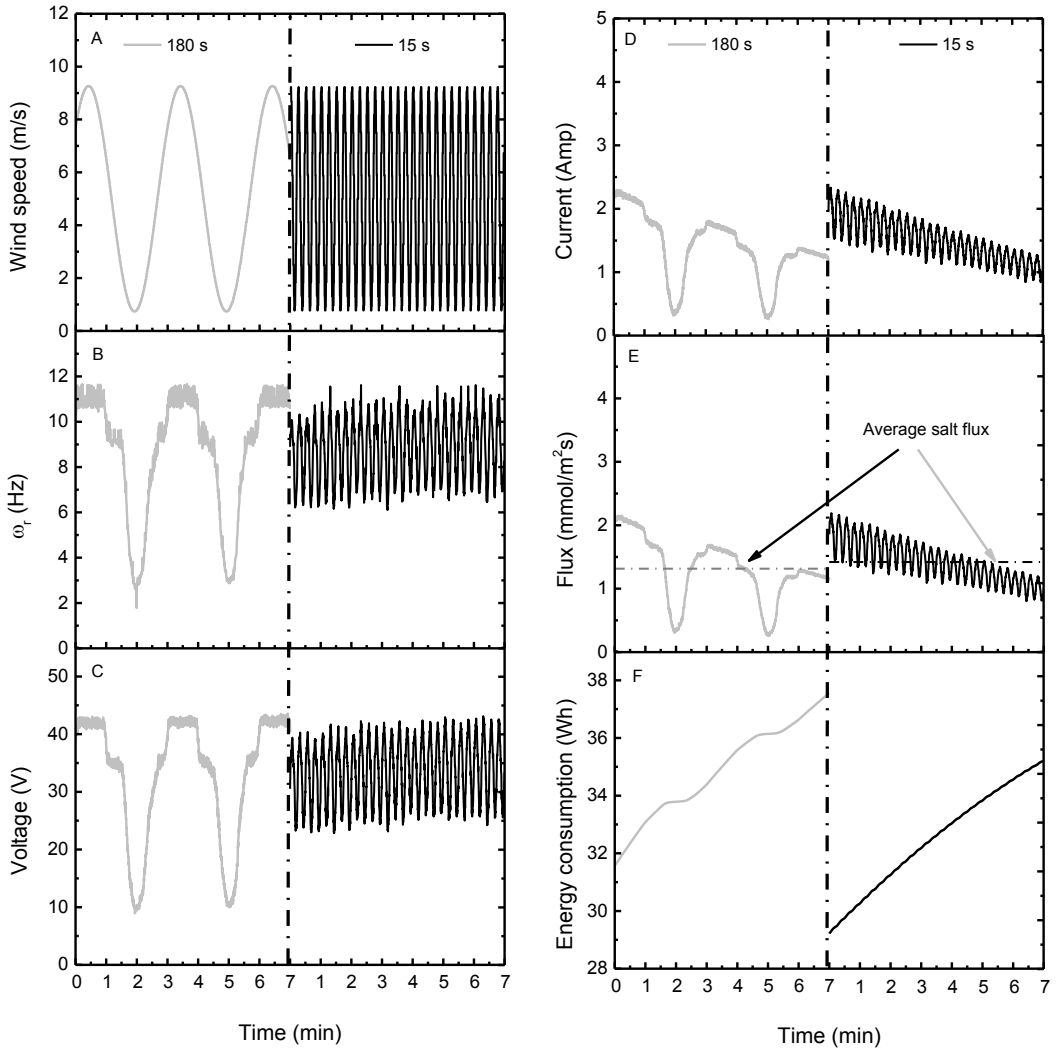

Figure 5.7 Wind-ED system performance during the last 7 minutes of the desalination tests using an average wind speed of 5 m/s at TI of 0.6 and oscillation periods of 180 s and 15 s; the initial feed concentration of 5,000 mg/L NaCl and the flow rate of 7 L/min; (mode of operation: batch).

As explained in the theory section (section 5.4), the angular velocity of the rotor, at every instance of the process, is directly linked to both the available wind speed and the resistance of the directly connected load to the wind turbine (R_{stack} in this

research). During the early stages of the desalination process (Figure 5.6), when the R_{stack} is relatively low (7.7 -8.4 Ω), the rotor spins at a lower angular velocity, but it speeds up together with the increase in R_{stack} as the operation approaches the end of the process (Figure 5.6 B vs. Figure 5.7 B). With an increase in the angular velocity of the rotor the angular momentum of the wind turbine also increases [95, 97]. This causes the turbine's response time to variations in the wind resource to decrease, and, thus, the wind-ED system exhibits less sensitivity to wind speed fluctuations toward the end of the desalination process. For example although extreme fluctuations (*i.e.* 0.6 TI and oscillation period of 180 s) caused regular system shut down at the beginning of the experiment (Figure 5.6 C-F), the effect of similar wind behaviours on the wind-ED performance was not as severe when approached the end of the desalination process (*i.e.* no system shut down was observed) (Figure 5.7 A-C).

The findings discussed in this section revealed that the influence of wind speed fluctuations on the wind-membrane system are more detrimental when operating under slowly oscillating wind speed conditions. The fluctuation impacts were shown to be particularly acute at lower stack resistances (R_{stack}), principally a result of higher feed concentrations of salt at the beginning of the batch process. The extent to which the water production and energy consumption of the membrane system can be influenced by such wind speed fluctuations will be studied in the next section.

5.4.4 The impacts of wind speed fluctuations on the water production and the SEC

To better understand the influence of wind speed fluctuations on performance of the wind-membrane system, the SEC and water production data obtained from the experiments carried out with the initial feed of 5,000 mg/L NaCl and over the TI range of 0 to 0.6 and oscillation periods of 15 to 180 s were presented in Figure 5.8. The error bars in this figure represent the relative error (max error: 2% for SEC and 5% for water production), calculated from the standard deviation of triplicate runs.

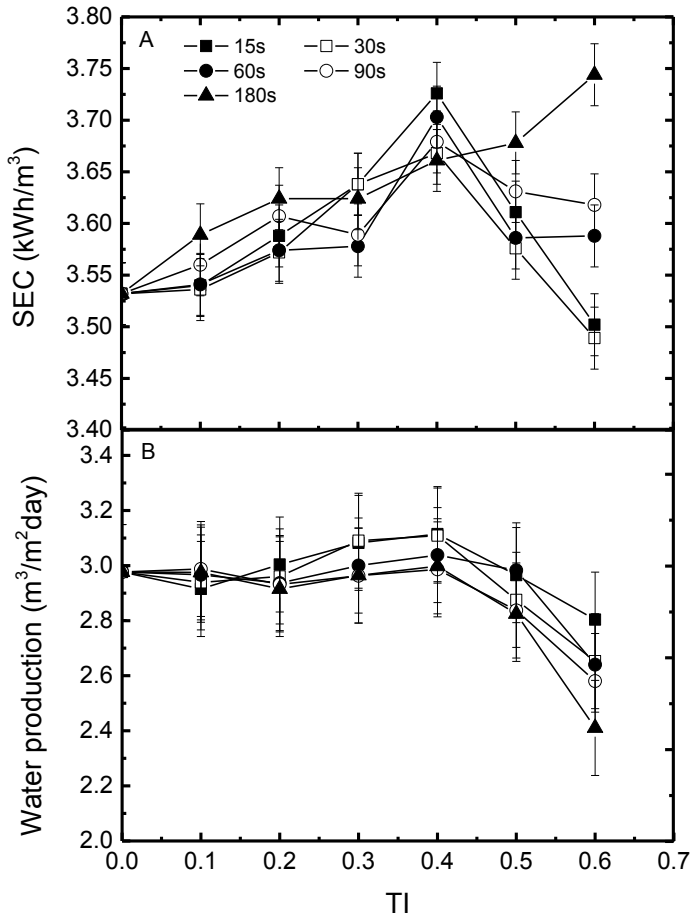

Figure 5.8 SEC (A) and water production (B) over a range of turbulence intensities (TI): 0-0.6 and oscillation periods: 15-180 s when desalinating from a feed of 5,000 mg/L NaCl at average wind speed of 5 m/s and flow rate of 7 L/min; (mode of operation: batch).

The larger angular momentum generated as a result of having turbulence in the wind resource [78, 97] caused the rotor to spin faster, producing more power in comparison to that produced at the steady wind speed conditions. In the TI range of 0 – 0.4, this behaviour caused SEC to increase slightly with the turbulence intensity (Figure 5.8A). The slight increase in the average power also resulted in minor improvements in water production level compared to the steady wind speed conditions (0 TI) (Figure 5.8B & D).

At TIs above 0.4 the water production started to decrease with respect to the amplitude of fluctuations (Figure 5.8B). This behaviour at TI 0.5 (with the oscillation periods equal or shorter than 90 s) and TI 0.6 (with the oscillation periods equal or shorter than 30 s) was attributed to the power levelling off, resulting from frequent

shifting of the peak wind speed above the v_{rated} (7.9 - 8.4 m/s) during consecutive oscillating periods. This behaviour was explained in full in the previous section (Figure 5.6 B & C). The slight decrease in the SEC in the specified wind speed conditions was also linked to the drop in the power output from the wind turbine in these conditions.

When operated at TI 0.5 (with the oscillation period of 180 s) and TI 0.6 (with the oscillation periods equal or longer than 60 s), the power levelling off, resulted from operating in the rated wind speed conditions, was exacerbated by regular cycling off of the wind turbine. The latter resulted from operating below the cut-in value (~ 2 m/s) for a particularly long period (> 40 s), causing an even further decrease in the water production level. The excess energy consumed for overcoming the steady moment of inertia of the rotor following every shut down stage resulted in an increase of the SEC (Figure 5.8A). The adverse impacts of the system regular shut down on the energy consumption was most evident when performing desalination at the TI of 0.6 and the oscillation period of 180 s (Figure 5.8A). The frequent cycling off of the wind turbine posed some delay on the desalination process and eventually resulted in 19% lower water production at TI of 0.6 and long oscillation period of 180 s (Figure 5.8B).

In these experiments the impacts of oscillation period on the wind-membrane performance was shown to be particularly evident when operated at TIs above 0.5. This was attributed to the fact that with slower oscillations of the wind speed, the turbine received more time to adjust itself to the slow changes occurring in the wind resource. Hence the extent to which the membrane system was affected by the wind speed fluctuations was more pronounced. The highest water production, regardless of the oscillating period, was obtained at TI of 0.4 while the lowest water production combined with the largest SEC was obtained at the TI of 0.6 and the oscillating period of 180 s.

5.4.5 Desalination under real wind speed conditions

Desalination tests were carried out with real wind data to i) determine the impacts of wind speed and fluctuations on the desalination performance of the wind-ED system,

and ii) to verify the results obtained from the experiments conducted with simulated wind speed data (Sections 5.4.1 - 5.4.4). The two wind regimes used for these experiments were:

i. Mean wind speed: 3.04 – 4.16 m/s and turbulence intensity (TI): 0.05 – 0.16 (Figure 5.9 A-D).

ii. Mean wind speed 5.99 – 7.16 m/s and turbulence intensity (TI): 0.01 – 0.19 (Figure 5.9 E-H).

The global desalination performance of the wind-ED system was similar to that explained in section 5.3 for the operation under simulated constant wind speeds. Over the course of the desalination process the concentration of charge carrying ions (*i.e.* Na^+ and Cl^-) decreaseed in the diluate channel (Figure 5.9 A and E). This causeed the resistance of the ED stack (R_{stack}) to increase continuously; from 7.63 ± 0.18 Ω at the beginning of the experiment (diluate concentration: 5,000 mg/L NaCl) to 34.75 ± 0.09 Ω toward the end of the process (diluate concentration: 600 mg/L NaCl) (Figure 5.9 B and F). The rate of increase for the R_{stack} was slow during the early stage of the desalination, but it speeded up substantially once the voltage output from the wind turbine reacheed its maximum level.

As the R_{stack} increased (Figure 5.9 B and F), the current driven from the wind turbine by the ED system and, proportionally with that, the load current induction torque force decreased (Figure 5.9 B and F). The decrease in the current induction torque, which was a counter torque force element, caused the net torque force applied on the shaft of the wind turbine to increase and thus the rotor to spin faster (Figure 5.9 C and G). The faster the rotor spun more voltage was produced (Figure 5.9 C and G). This process continued until the rotor was restricted by the frequency inverter from any further acceleration. The latter was to protect the wind turbine from possible damage that may be caused by the overloading of the rotor and the generator at high angular velocities. The maximum voltage output depended on the mean wind speed (*i.e.* 35 ± 1 V in the experiment 1 and 39 ± 4 V in the experiment 2). The higher the wind speed, the lower was the R_{stack} at which the frequency inverter stoped the generator from speeding up. Therefore, when operating at a higher mean wind speed

the voltage reached its maximum level at an earlier stage of the process (Figure 5.9 C and G).

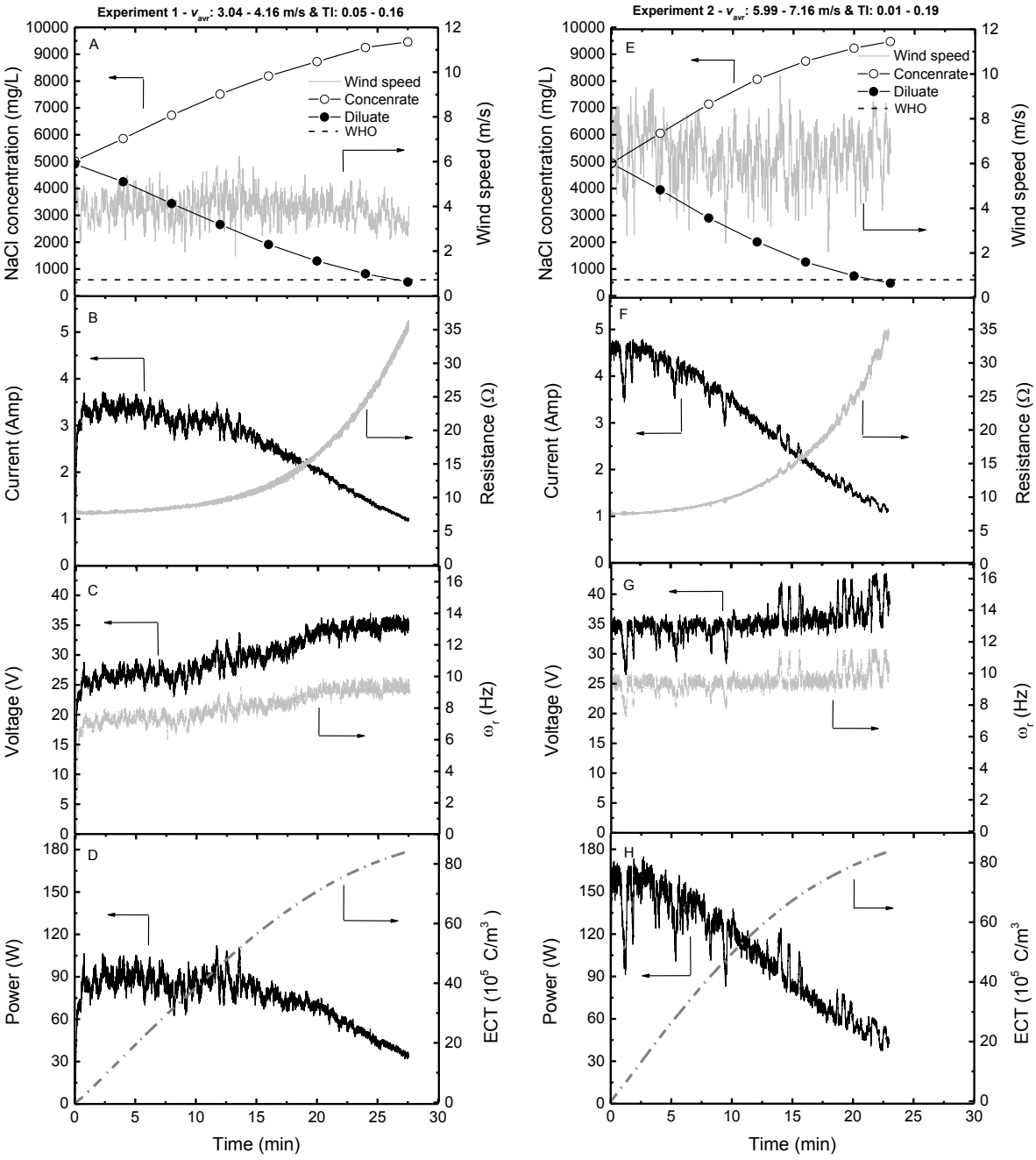

Figure 5.9 Wind-ED performance for desalinating from a synthetic brackish water (5,000 mg/L NaCl) under two different wind regimes. Wind speed and concentration variation in both the diluate and the concentrate channels over time (A & E), operating current and ED stack resistance variations with time (B & F), rotor angular velocity and voltage output from the wind system variations with time (C & G), operating power and electric charge transferred (ECT) across the membranes (D & H); (mode of operation: batch).

During the whole process the wind-ED system exhibited two different patterns of power behaviours:

i. During period before the activation of the frequency inverter the voltage output from the wind turbine increased sufficiently to compensate for the drop in the current passing the ED stack. This caused the power remain relatively constant, maintaining a steady desalination rate (*e.g.* the power remains relatively constant at about 90 ± 10 W until minute 17 in the Experiment 1).

ii. Voltage stopped to increase once the rotor was restrained by the frequency inverter from further acceleration. Therefore, the power began to level off effectively. During this period the power lost its dependency on the wind speed and became solely dependent on the R_{stack}. The power decreased until it reached a certain level at the end of the desalination process (around 32 ± 3 W for both of the experiments), regardless of the wind speed at which the process was conducted (Figure 5.9 D and H).

As seen in Figure 5.9 C and G, the total electric charge transferred across the membranes (ECT) over the complete course of desalination was very similar (approximately 83.7×10^5 C/m^3) for both of the experiments (Figure 5.9 D and H). These values suggested similar current efficiencies for both of the experiments, regardless of the available wind energy. The calculated current efficiencies using Eq. 3.6 were 87.9% and 88.3% for Experiments 1 and 2, respectively. However, due to the fact that Experiment 2 was carried out at a higher mean wind speed, the rate of desalination and thus the energy consumption for the completion of the process were higher compared to those in Experiment 1. The water productions were 2.68 and 3.18 m^3/m^{2}day and the SECs of the processes were 3.36 and 4.04 kWh/m^3 for Experiments 1 and 2, respectively. Both the water production and SEC values were in the range observed for the tests carried out at constant wind speeds of 4 -7 m/s (Section 5.4.1).

For both of the experiments, pH exhibited a gradual decrease from 7.1 to 6.3 until the NaCl concentration in the diluate stream reached levels around 1,000 mg/L. The

value of pH then continued to decline with a faster rate until it reached levels around 5.3-5.5 at the end of the desalination process (NaCl ≤ 600 mg/L). The relatively rapid pH decline toward the end of the process was attributed to possible dissociation of water molecules into H^+ and OH^- ions, a phenomenon occurring due to operating beyond the limiting current density [131, 137, 204]. Using buffers, such as bicarbonate salts, in the post-treatment stages of the water purification process is a common practice for neutralising the pH (*i.e.* achieve a pH of 6.5 -8.5) [213-215].

5.5 Conclusions

In this study the desalination of artificial brackish water (*i.e.* 5,000 and 10,000 mg/L NaCl) using a directly coupled wind-ED system with no form of energy storage was investigated for the first time. In terms of a safe operating window, the wind-membrane system produced good quality drinking water (< 600 mg/L NaCl) over a wide range of wind speeds (2 – 10 m/s), turbulence intensities (0 – 0.6 TI), and periods of oscillation (0- 180 s).

In the experiments carried out under steady wind speed conditions both SEC and water production increased with the wind speed in the region below the v_{rated} (7.8 – 8.4 m/s). At wind speeds above the rated value the power output from the wind turbine levelled off and caused plateaus to appear in both the SEC and water production curves.

In the experiments carried out under controlled wind speed fluctuations, an increase in the turbulence intensity (TI) from 0 to 0.4 resulted in slightly higher SECs compared to that at steady wind conditions. The increase in the TI in this region also resulted in a minor improvement in the water production level. Increasing TI to levels above 0.4 caused regular shifting to the rated wind speed conditions, causing the power output from the wind turbine to level off periodically during the process. This ultimately caused lower water production and lower SEC to be obtained.

The desalination performance declined under high turbulence intensity fluctuations (TIs ≥ 0.5) and long periods of oscillation (> 40 s), as the wind-ED system periodically cycled off in response to operation below the cut-in wind speed of the

wind turbine ($v_{cut\text{-}in}$: ~ 2 m/s). This resulted in significantly lower water production and slightly higher SEC.

The ED system has been demonstrated to be an energetically robust system, performing effectively in the safe operating window when connected to renewable energy sources (wind power has the most extreme fluctuations among renewable energy alternatives). The main challenge in the direct coupling of the membrane system with a RE resource was seen to be not the size of the fluctuations but the impact of the power cycling off during long oscillation periods, which resulted in reduced water production and increased SECs. The next chapter aims to further investigate the impacts of extreme wind speed fluctuations, in form of wind speed intermittency, on the energy and desalination performances of the wind-ED system.

Chapter 6

Impacts of wind speed intermittency on desalination performance of the wind-ED system

6.1 Introduction

Intermittent operation is associated with the wind-ED system cycling off due to sudden variations in the wind speed to levels below the cut-in wind speed ($v_{cut\text{-}in}$) of the turbine. Whilst the fluctuations dealt with in the previous chapter were representing gradual variations in the wind speed (oscillation periods > 15 s), the intermittent conditions represent the wind speeds that vary quickly and significantly, often followed by varying periods of no/low wind speed conditions (from few seconds to several minutes) [78, 177, 178]. Therefore, the impact of such wind regimes on the performance of the wind-ED system is expected to be significantly more detrimental compared to those observed in the previous chapter for the extremely turbulent wind conditions (TIs > 0.5 and oscillation periods > 40 s).

Intermittence is a common characteristic shared among all the renewable energy sources [216-218]. The main characteristic parameters for an intermittent wind condition are i) the frequency of the system cycling on/off, ii) the off-period of the intermittent operation and iii) the amplitude of variation in the wind energy in every cycle. This chapter aims to systematically investigate the impacts of these three key

intermittency characteristics on the desalination performance (desalination rate, SEC, current efficiency and water production) of the wind-ED system. The results obtained from this chapter will be crucial for understanding the effects of the direct coupling of an ED system to an intermittent and highly variable power source, and will facilitate the optimisation of the wind-ED design based on the wind energy availability and variability in any given location.

6.2 Experimental protocols

6.2.1 Transient electric behaviour of the wind-ED system in response to intermittent energy

To study an intermittent operation, it is first important to understand how the wind-ED system reacts to a sudden change in the wind speed. This can be achieved by investigating the transient electric behaviours of the system when it is exposed to a rapid increase or a sudden decrease in the wind speed. The transient electric behaviours of the wind-ED system were investigated by conducting a set of experiments, using simulated intermittent wind speed data in form of square waves as input to the wind turbine simulator. The ON-wind and OFF-wind periods of the intermittent wind regime were selected sufficiently long (> 2 min) to make sure that the system reaches a relatively stabilised condition (referred to as "pseudo- steady state" in this chapter) following every sudden change in the wind speed. It is important not to confuse "pseudo-steady sate" with "steady state", as the latter term refers to the experimental condition where the wind speed is constant. The peak to peak wind speed, as the main parameter influencing the transient behaviour of the wind-ED system, was varied in this set of experiments. For all the tests the trough wind speed was set at zero and the peak wind speed was varied, covering the range between the cut-in ($v_{cut\text{-}in}$) and the rated (v_{rated}) wind speeds: 3, 4, 5, 6, 7 and 8 m/s.

These experiments were carried out using the continuous mode of operation (Figure 3.5A), where a fixed feed concentration of 5,000 mg/L NaCl was circulated at the constant flow rate of 7 L/min through the ED system during the whole process. The main objectives of this section were to systematically investigate;

i. the transient time taken for the wind turbine to adjust to a rapid increase (t_{twi}) or a sudden decrease (t_{twd}) in the wind resource before reaching a pseudo-steady state;

ii. the power performance of the wind turbine during both t_{twi} and t_{twd};

iii. the current transfer through the membranes, which directly determining the salt flux, during both t_{twi} and t_{twd}.

The knowledge gained from these experiments regarding the transient behaviour of the wind-ED system upon the occurrence of a rapid change in the wind speed is the key to understanding the global performance of the wind-ED system (*i.e.* desalination rate, water production and SEC) when conducting desalination experiments under different intermittent wind regimes (Sections 6.3.3 and 6.3.4).

6.2.2 Effect of intermittent energy supply on water production and SEC: desalination under controlled intermittent wind speed conditions

The aim of this section was to systematically study the impacts of continuous intermittent wind speed conditions on the desalination performance of the wind-ED system. The main parameters of interest in these tests were desalination rate, water production and specific energy consumption (SEC) of the wind-ED system. To simulate the intermittent wind speed conditions, the wind speed regimes in the form of repeating square waves were inserted as input to the wind turbine simulator (Figure 6.1).

The desalination experiments were carried out, taking into account the impacts of:

i) The OFF-wind periods; these tests were conducted at three different wind speeds of 4, 6 and 8 m/s (covering the range between $v_{cut\text{-}in}$ and v_{rated}) and with the fixed ON-wind period of 60 s (sufficient for the wind-ED system to reaches a pseudo-steady state following the acceleration from a no-wind condition) and with different periods of OFF-wind: 0, 5, 10, 30, 60 and 90s. These OFF-wind periods corresponded to the range often seen in short term wind speed fluctuations in reality [78, 177, 178].

ii) The frequency (the number of wind ON/OFF cycles in a second); the frequency and duty cycle of the wind ON/OFF cycles are calculated using Eqs. 6.1 and 6.2, respectively:

$$\text{wind ON - OFF frequency} = \frac{1}{((\text{ON - wind period}) + (\text{OFF - wind period}))} \quad \text{(Eq. 6.1)}$$

$$\text{wind ON - OFF duty cycle} = \frac{\text{ON - wind period}}{((\text{ON - wind period}) + (\text{OFF - wind period}))} \quad \text{(Eq. 6.2)}$$

These tests were carried out with three peak wind speeds: 4, 6 and 8 m/s, and with the wind speed ON-OFF cycle frequencies of 0.0027, 0.0055, 0.0083, 0.166, 0.050 and 0.100 Hz. The wind ON-OFF duty cycle in all these experiments were set at 50% (1:1 ratio between the ON-wind and OFF-wind periods). The frequencies of intermittent regimes studied in this chapter were chosen to resemble those of short term wind speed fluctuations, suggested by Van der Hoven wind speed spectral model [178].

iii) The peak to peak wind speed; these tests were carried out with the ON-wind period of 60 s, three OFF-wind periods of 0, 5 and 60 s (selected based on the experiments carried out in the section (i) and with six different peak wind speeds of 3, 4, 5, 6 ,7 and 8 m/s.

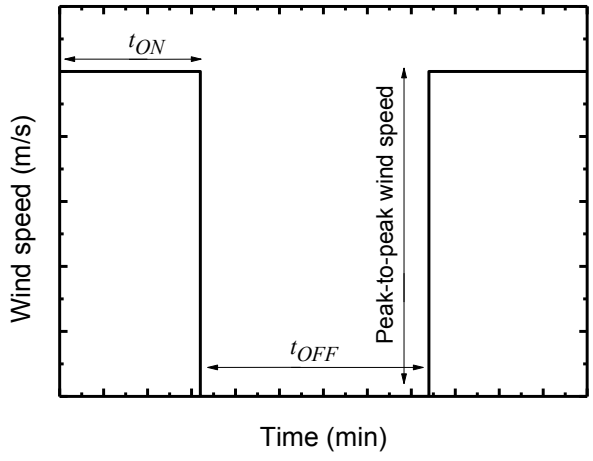

Figure 6.1 Simulated intermittent wind speed regimes used as input to the wind turbine simulator in the wind-powered ED experiments.

The desalination experiments were all carried out using the batch flow configuration of the wind-ED system (Figure 3.5B) with the initial feed of 5,000 mg/L NaCl and the flow rate of 7 L/min. The desalination tests continued until the target concentration of 600 mg/L NaCl, corresponding to the drinking water guideline for taste for total dissolved solids (TDS), was obtained [21].

6.2.3 Effect of intermittent energy supply on water production and SEC: desalination under real wind speed conditions

The aim was to assess the desalination performance of the wind-ED system under real intermittent wind conditions. In this test a real wind data exhibiting highly turbulent and intermittent wind conditions was used as the input to the wind turbine simulator (mean wind speed: 3.11 – 4.56 m/s and turbulence intensity (TI): 0.11 - 0.55). The source and conditions of the real wind speed measurements, as well as the procedure taken for making these data applicable to the wind turbine simulator, was detailed in section 5.2.2. The desalination experiment was carried out with the initial feed of 5,000 mg/L NaCl and the flow rate of 7 L/min. The desalination process was considered complete once the NaCl concentration in the diluate channel reached 600 mg/L.

6.3 Results and discussion

6.3.1 Transient electric behaviour of the wind-ED system in response to intermittent energy supply

To better understand the global behaviour of the wind-membrane system (*e.g.* desalination rate and SEC) under various intermittent wind conditions, it is first important to carry out detailed analysis of the system performance during the two sequential periods of t_{twi} and $t_{twd.}$ Figure 6.2 demonstrates the electric behaviour of the wind-ED system in the event of a rapid increase (Figure 6.2 A-C) or a sudden decrease (Figure 6.2 D-F) in the wind speed. While Figure 6.2 shows the system characteristics for the specific peak to peak wind speed of 4 m/s, the general behaviours observed in this figure would be analogous for any other chosen peak to peak value.

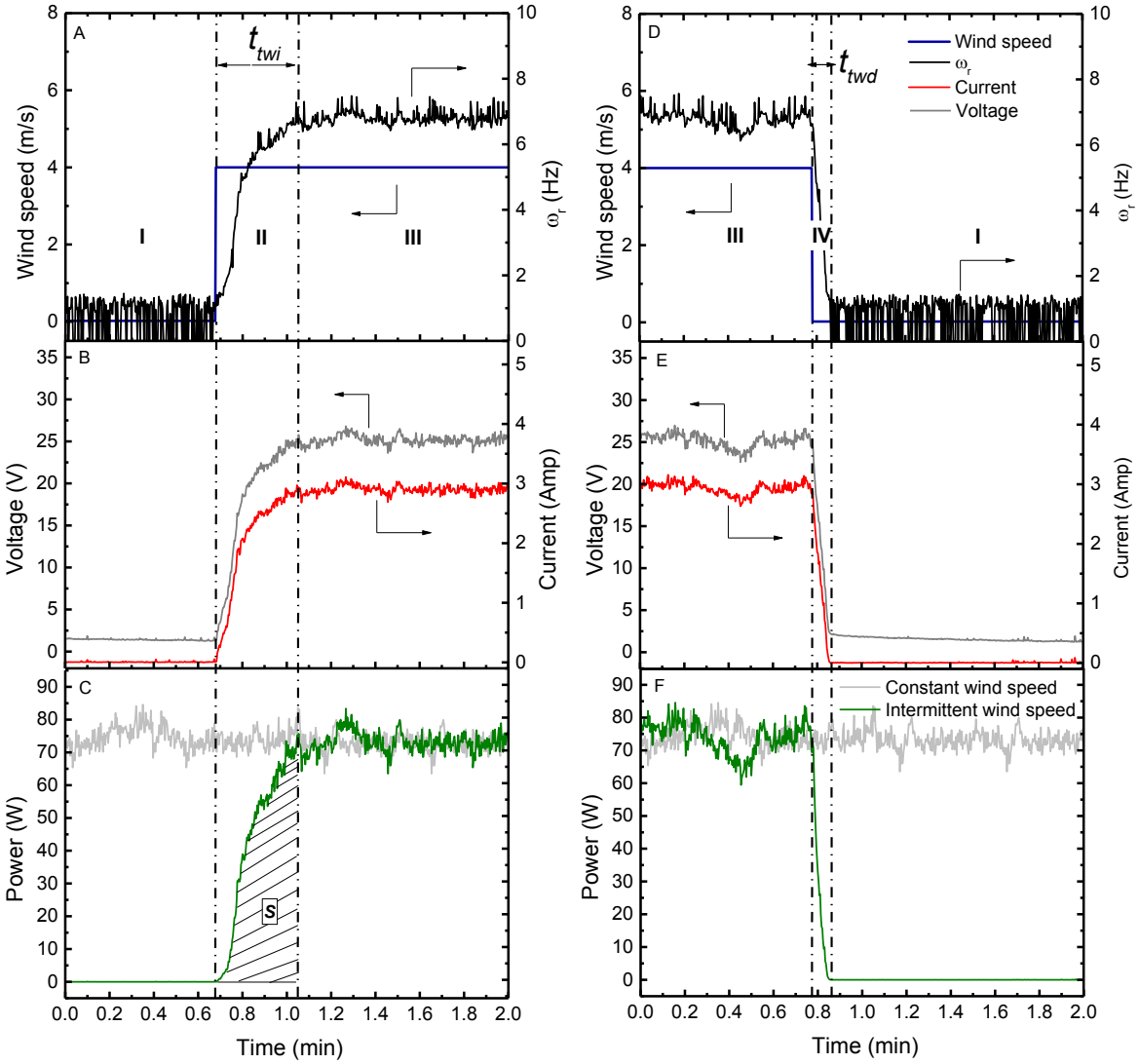

Figure 6.2 the impacts of rapid wind speed increase (A-C) and sudden wind speed decrease (D-F) on the power performance and current transfer of the wind-membrane system using the continuous circulating mode of operation (Figure 3.5A), feed of 5,000 mg/L NaCl, flow rate of 7 L/min and peak to peak wind speed of 4 m/s (trough: 0 m/s and peak: 4m/s); (mode of operation: continuous recirculation). Numbers I – IV mark the different regions of interest during the wind ON/OFF duty cycle.

Normally four distinct regions (numbered as I, II, III, and IV in Figure 6.2) can be distinguished during every complete cycle of intermittent operation. The power consumption by the wind-ED system during each of these four regions (shown in green in Figure 6.2 C and F) can be analysed against the power at the steady state condition, referred to as the "optimal power" in this research, where no interruption

by means of an energy intermittency occurs in the system performance (shown in grey). Below is the detailed analysis of the four distinct behavioural regimes of wind-ED system when operated from an intermittent wind regime:

State (I), the OFF-wind period ($v << v_{cut\text{-}in}$): under these conditions the energy content of the wind resource is below levels exploitable by the wind turbine [97, 98]. Therefore, the rotor does not spin effectively ($\omega_r < 1$ Hz) and no significant voltage is produced by the generator. The voltage detected (~ 2 V) by the sensors during this period (Figure 6.2 B) is the capacitive voltage of the ED stack that is detected only when no external potential is applied across the membranes (explained in detail in section 5.4.3). With no power being produced by the wind turbine during the OFF-wind periods, no electric charge is transferred across the membranes and thus no ions are transported and no desalination takes place.

State (II), when the wind speed suddenly increases to $> v_{cut\text{-}in}$, the wind turbine enters a transient period (t_{twi}) during which the rotor starts spinning effectively ($\omega_r > 1$ Hz). The angular velocity of the rotor continues to increase until it reaches a pseudo-steady state, where the angular momentum of the turbine reaches its maximum level at the given peak wind speed. The rotor's angular velocity at the peak wind speed strongly depends on both the wind speed and the resistance of the membrane system (R_{stack}) (the theory was given in Chapter 5, section 5.3).

During t_{twi}, both the voltage and the current increase with the angular velocity of the rotor (Figure 6.2 B). However, the change in the current, unlike the voltage, is not proportional to the change in the angular velocity of the rotor (ω_r), but is a strong function of the (R_{stack}) (explained in detail in Chapter 5, section 5.3).

During t_{twi} only a portion (shown by *S* in Figure 6.2 C) of the exploitable wind energy is turned into useful power for running the membrane system (compared to the steady state power curve, shown in grey), while the rest is consumed to overcome the steady momentum of the turbine in order to bring

the turbine's angular momentum to that of the peak wind speed. Therefore, it can be concluded that during this period (t_{twi}) the wind-membrane system operates at a reduced power level compared to when the system is uninterrupted at a steady wind speed. The loss in power production efficiency of the wind turbine, due to regular cycling on/off periods, can potentially have adverse impacts on the desalination rate of the ED system. This will be investigated in detail when studying the global desalination performance of the wind-ED system under intermittent wind conditions in the following sections of this chapter (section 6.3.3 and 6.3.4).

State (III), a pseudo-steady state after the sudden increase in the wind speed: During this period the wind turbine produces power equal to that at the steady state condition (grey line), operating optimally. The electric charge transferred across the membranes and thus the desalination rate in this period of time is expected to be at the highest possible level at the given peak wind speed.

State (IV), Once the wind speed drops to < $v_{cut\text{-}in}$, the positive torque force applied on the shaft of the rotor by the wind is quickly dissipated. The net torque force applied on the shaft becomes dominantly controlled by the counter torque forces; namely the current induction torque force controlled by R_{stack} and the gravitational and frictional forces of the rotating components in the wind turbine (*i.e.* the rotor, generator and the coupling shaft). The sudden drop in the energy content of the wind resource and thus the immediate change in the direction and magnitude of the net torque force applied on the rotor push the systems into a transient period (t_{twd}) during which the rotor slows down quickly until its angular velocity becomes less than 1 Hz. In such an occasion the wind-ED system normally cycles off (Figure 6.2 D). Depending on the length and frequency of its occurrence, cycling off can cause significant delays in the process of desalination and lead to considerable drop in the volume of drinking water treated by the wind-ED system. This phenomenon will be discussed in detail in the following sections of this chapter where the global desalination performance of the wind-ED system under different intermittent wind regimes is studied.

6.3.2 Peak wind speed effect on t_{twi} and t_{twd}

Although the nature of the transient electric behaviours exhibited by the wind-ED system in an intermittent operation are independent of the peak wind speed; however, the time taken for these behaviours to be completed and thus the system reaches a pseudo-steady state following a sudden change in the energy source strongly depends on the magnitude of variations in the wind energy (*i.e.* the peak to peak wind speed). Figure 6.3 shows the impact of the peak wind speed in an intermittent wind condition on the two characteristic times of t_{twi} and t_{twd}.

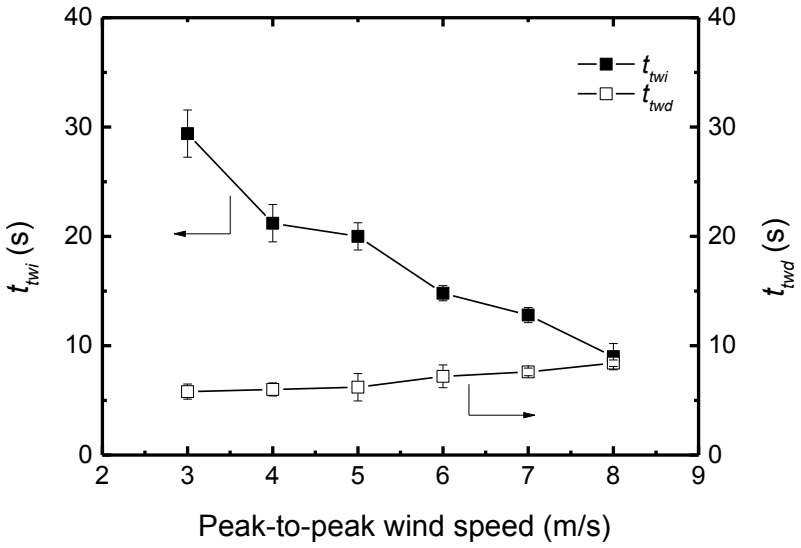

Figure 6.3 The transient time of increase (t_{twi}) and transient time of decrease (t_{twd}) in the rotor's angular velocity before reaching a pseudo-steady state for peak to peak variations in the wind speed of 3 – 8 m/s.

The transient time t_{twi} exhibits an inverse relationship with the peak wind speed (Figure 6.3), as it is decreasing from 30 s at the peak wind speed of 3 m/s to 9 s at the peak wind speed of 8 m/s. The explanation is that the higher the peak wind speed, the lager is the torque created suddenly after a long period of no wind, causing the rotor to overcome its steady momentum and to accelerate faster. Therefore, with a higher peak wind speed, the wind-ED system operates at an averagely higher power state during t_{twi}, and its water production is expected to be closer to that of uninterrupted process at a steady wind speed. This will be discussed later in this chapter (section 6.3.3.3).

In contrast to t_{twi}, the transient time t_{twd} does not exhibit strong dependency on the peak wind speed. As seen in Figure 6.3, t_{twd} increases only slightly from 5.8 s at the peak wind speed of 3 m/s to 8.4 s at the peak wind speed of 8 m/s. The increase in t_{twd} with the peak wind speed is related to the angular momentum of the wind turbine being higher at the higher wind speed [98]. Thus, the turbine's momentum requires more time to be dissipated following a sudden drop in the wind speed before the wind-ED system can cycle-off completely.

So far the main wind-ED system characteristics associated with different transient stages of an intermittent operation have been studied. The next section aims to employ this knowledge to explain the impact of the main intermittency parameters, namely i) OFF-wind period, ii) the frequency of the wind speed cycling on/off, and iii) peak wind speed, on the desalination performance of the ED system.

6.3.3 Desalination under intermittent conditions: simulated wind speed data

6.3.3.1 The impacts of OFF-wind period

To investigate the impacts of off-wind period on the desalination performance (*i.e.* ion removal) of the wind-ED system, a series of desalination experiments with the feed solution of 5,000 mg/L NaCl, ON-wind period of 60 s, and OFF-wind periods of 0, 5, 10, 30, 60 and 90s, were conducted. First, in Figure 6.4 the results obtained during the first 3.5 minutes of desalination experiments carried out at the peak wind speed of 4 m/s and with two OFF-wind periods of 5 and 30 s were displayed against each other to study the impacts of intermittency on the main operating parameters (*i.e.* angular velocity of the rotor, voltage, current, salt flux and NaCl concentration). The information gained in this section will help to explain the water production and SEC results obtained over the complete range of OFF-wind speeds (Figure 6.5).

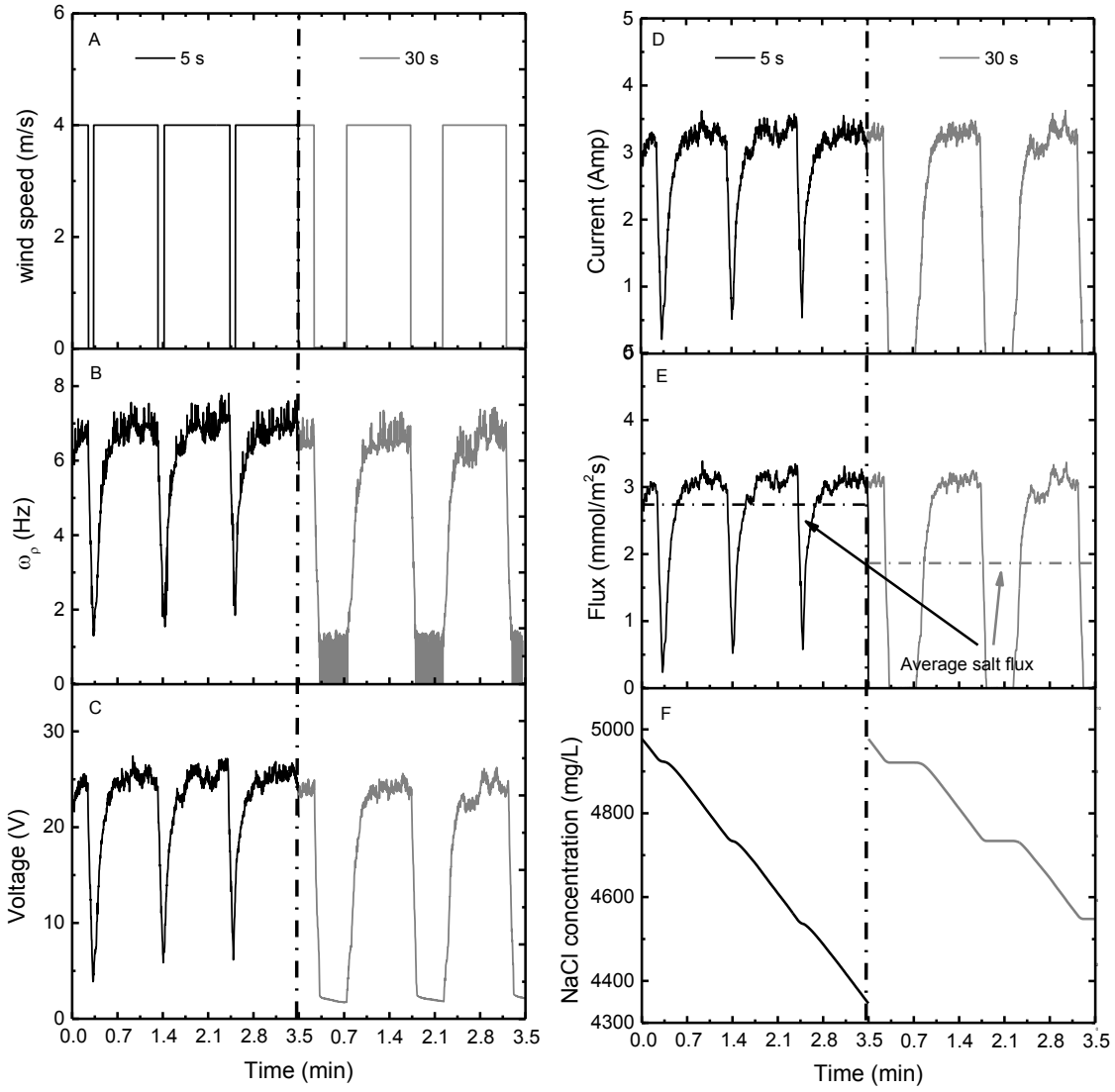

Figure 6.4 Intermittent operation of the wind-membrane system during the first 3.5 minutes of desalination of a feed with a concentration of 5,000 mg/L NaCl, using an ON-period of 60 s and two different off-periods of 5 s and 30 s. (A) = wind speed; (B) = angular velocity of the rotor; (C) = voltage output from the wind turbine; (D) = current driven from the turbine by the ED system; (E) = salt flux through the membranes and (F) = NaCl concentration in the diluate channel; (mode of operation: batch).

The impact of intermittency on the performance of the wind-membrane system was found to be particularly pronounced when the off-wind period of the operation was sufficiently longer than the t_{twd} at the given peak wind speed (*i.e.* the experiment carried out with the off-wind period of 30 s, Figure 6.4). At such a condition, the rotor had enough time to slow down substantially and thus the rotor cycled off

completely (Figure 6.4 A & B). During the shut-down period, the amount of current transferred across the membranes remained negligible, causing the salt flux reaches zero and thus the desalination process to be delayed (Figure 6.4 D - F).

The decline in the desalination performance was less severe when a shorter OFF-wind period of 5 s was applied. With an OFF-wind period shorter than t_{twd} *(i.e.* < 7 s with the peak wind speed of 4 m/s), the angular velocity of the rotor only partially decreased following the sharp decrease in the wind speed; however, the rotor did not stop spinning completely at any time during the process (Figure 6.4 B). As a result, no off cycle was observed during the operation and the desalination process continued with no disruption (Figure 6.4 C-F).

The water production and SEC results obtained from the intermittent experiments carried out over the complete range of OFF-wind periods (0 -90 s) and in three wind speed regimes of low (4 m/s), medium (6 m/s) and rated (8 m/s) are shown in Figure 6.5. In Figure 6.5, 0 s OFF-wind period represents the steady state condition when the wind-membrane system operates under constant wind speeds.

Operating at reduced power levels over every wind speed on/off cycle caused the SEC of the desalination process in the intermittent operations to be slightly lower than the SECs of the tests carried out at constant wind speeds (*i.e.* 0 s OFF-wind period) (Figure 6.5 A). The mechanisms contributing to the operation of the wind-ED system at a reduced power level compared to its steady state optimal conditions were explained in detail in the section 6.3.1 (state II). Operating at averagely lower power levels as well as experiencing delays due to the repetitive cycling on and off of the wind-ED system caused decline in the desalination rate and hence a reduction in the quantity of the water treated per day by the membrane system (Figure 6.5 B). The longer the off-wind period, the longer was the total delay caused in the desalination process and thus the daily water production decreased further.

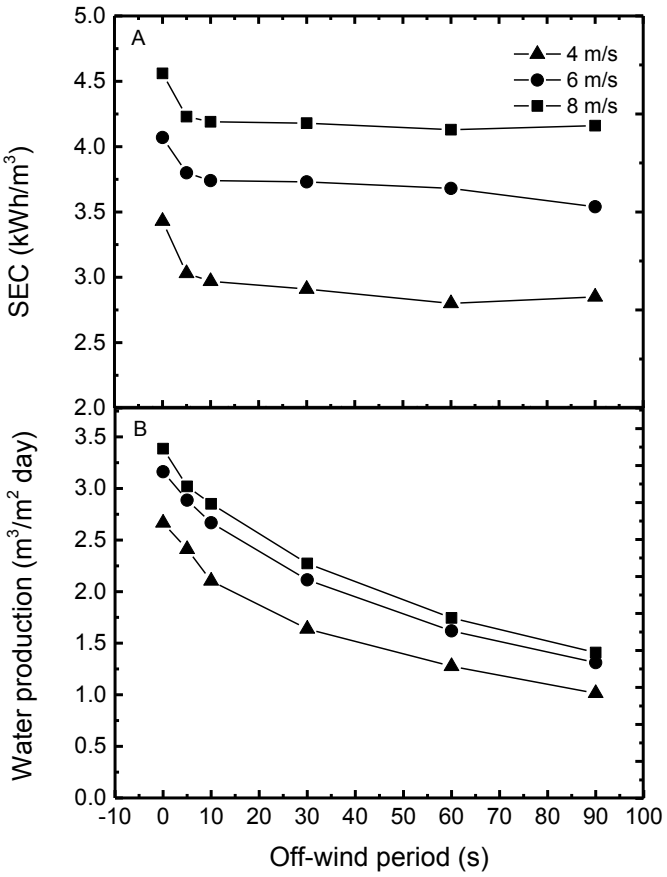

Figure 6.5 SEC (A) and water production (B) when desalinating a feed containing 5,000 mg/L of NaCl at 7L/min at three peak wind speeds of 4, 6 and 8 m/s, using the on-wind period of 60 s and off-wind periods in a range between 0-90 s; (mode of operation: batch).

6.3.3.2 The impacts of wind speed on/off cycling frequency

To study the impact of wind speed on/off cycling on the SEC and the water production of the wind-membrane system, desalination tests were carried out with the peak wind speeds of 4, 6 and 8 m/s and over the wind speed cycling on/off frequency range of 0.003 – 0.1 Hz (Eq. 6.1) (Figure 6.6). All the tests were carried out with the initial feed of 5,000 mg/L NaCl. The desalination process was considered complete when the salt concentration in the diluate channel reached 600 mg/L NaCl. The duty cycle of the wind speed on/off cycling (Eq. 6.2) was set at 50% to make sure that the wind-ED system receives equal total ON-wind period during its operation under all the tested conditions. This helped the focus of the study to be

kept mainly on the impact of rotor's acceleration and deceleration processes, and not the length of ON and OFF-wind periods individually.

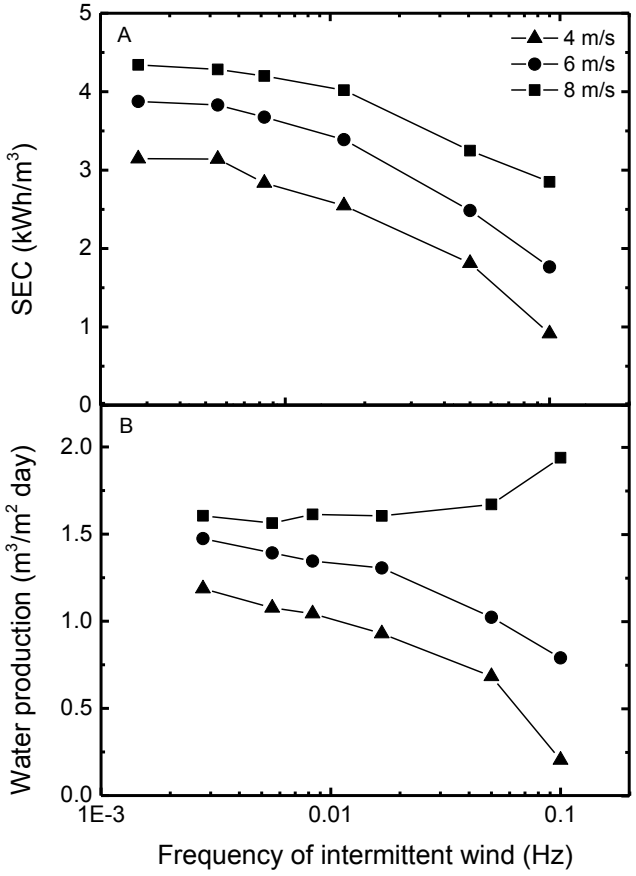

Figure 6.6 SEC (A) and Water production (B) when desalinating a feed of 5,000 mg/L NaCl at 7L/min at three peak wind speeds of 4, 6 and 8 m/s and over a wind speed on/off cycling frequency range of: 0.003 Hz (180 s on/off periods) – 0.1 Hz (5 s on/off period); (mode of operation: batch).

The SEC of the desalination process decreased with increasing frequency of wind speed on/off cycling (Figure 6.6 A). This behaviour can be attributed to the number of t_{twi} transient times experienced by the wind-ED system over the complete course of desalination. As explained in the section 6.3.1 (state II), during t_{twi} the exploitable wind energy is partly consumed for overcoming the counter torque forces applied on the shaft of the wind turbine in order to increase the angular momentum, and thus the angular velocity, of the rotor. As a result, during this period, the system operates at a reduced power level compared to its optimal condition at the steady state and thus has a lower energy level. The larger the frequency of wind intermittency, the more

the number of t_{twi} transient times; hence the energy level and correspondingly with that the SEC of the desalination processes decreases.

The decrease in the SEC at the higher frequencies (> 0.05 Hz) is partially attributed to the length of the ON-wind period being smaller than t_{twi}. Under such wind speed conditions the rotor is not given enough time to fully accelerate during the ON-wind period; therefore, it never reaches its maximum angular velocity at the given peak wind speed. This imposes a limitation on the maximum voltage that can be generated by the wind turbine, causing the wind-ED system to operate at a reduced power level throughout the process and thus SEC to decrease even further. For example when desalinating a feed of 5,000 mg/L NaCl with a constant wind speed of 6 m/s, the angular velocity of the rotor (ω_r) varies between 7.8 and 9.2 Hz, causing the generator to produce voltages in the range of 31-36 V. However, when desalinating the same feed under an intermittent wind regime, with the peak wind speed of 6 m/s and the high wind speed on/off cycling frequency of 0.1 Hz (5 s ON-wind period and 5 s OFF-wind periods) the rotor is not given enough time to fully accelerate at any point during the desalination process. As a result off that, the angular velocity of the rotor remains below 6.3 Hz and thus no voltage larger than 23.9 V is produced by the generator. Operating at an averagely lower voltage level causes the SEC in this test to be 1.7 ± 0.1 kWh/m^3, which is significantly lower than 3.7 ± 0.1 kWh/m^3 SEC obtained for the steady state desalination process conducted at constant 6 m/s.

In all the experiments, except the ones carried out with the peak wind speed of 8 m/s, the water production decreased with an increase in the frequency of the intermittent wind condition (Figure 6.6 B). Having a relatively long t_{twd} transient period of 8.4±0.3 s at 8 m/s prevented the wind-ED system from cycling off when operated at frequencies above 0.03. This facilitated the continuous operation of the desalination process without any significant disruption, causing larger volumes of water to be treated at 8 m/s compared to 4 and 6 m/s. Moreover, the faster acceleration of the rotor with the peak wind speed of 8 m/s (t_{twi} equal to 9±1.2 s) compared to the other two wind speeds, helped the wind system to reach its maximum power level during the ON-wind period at all the frequencies and thus to enhance the water production even further (Figure 6.6 B).

6.3.3.3 The impacts of peak wind speed

The maximum power that can be produced by the wind turbine system (Figure 3.8) as well as the transient times taken for the complete acceleration of the rotor (t_{twi}) and the complete shutdown of the system (t_{twd}) in an intermittent operation (Figure 6.3) are principally dependent on the peak wind speed in the intermittent wind regime. Therefore, any variation in the peak wind speed is expected to influence the total energy consumption and thus the desalination performance of the wind-ED system. To study the impacts of peak wind speed on the SEC and water production of the wind-ED system, a series of desalination tests were carried out over the peak wind speed range of 3 to 8 m/s (Figure 6.7). These wind speeds were chosen to cover the full range between $v_{cut\text{-}in}$ and v_{rated}. The tests were repeated over the following three conditions:

i) Steady state operation, where the desalination is performed at a constant wind speed (equal to that of the peak wind speed) with no intermittency.

ii) Intermittent operation with the OFF-wind period of 5 s; to examine the condition where the system does not have sufficient time to shut down following a sudden decrease in the wind speed (*i.e.* t_{twd} > OFF-wind period)

iii) Intermittent operation with the OFF-wind period of 60 s; to examine the condition where the system has sufficient time to adjust itself to the rapid change in the wind speed and thus to cycle off completely following a sudden decrease in the wind speed (*i.e.* t_{twd} < OFF-wind period)

The ON-wind period of 60 s was chosen for all the intermittent experiments to make sure that the wind-ED system reaches a steady power level following every sudden increase in the wind speed.

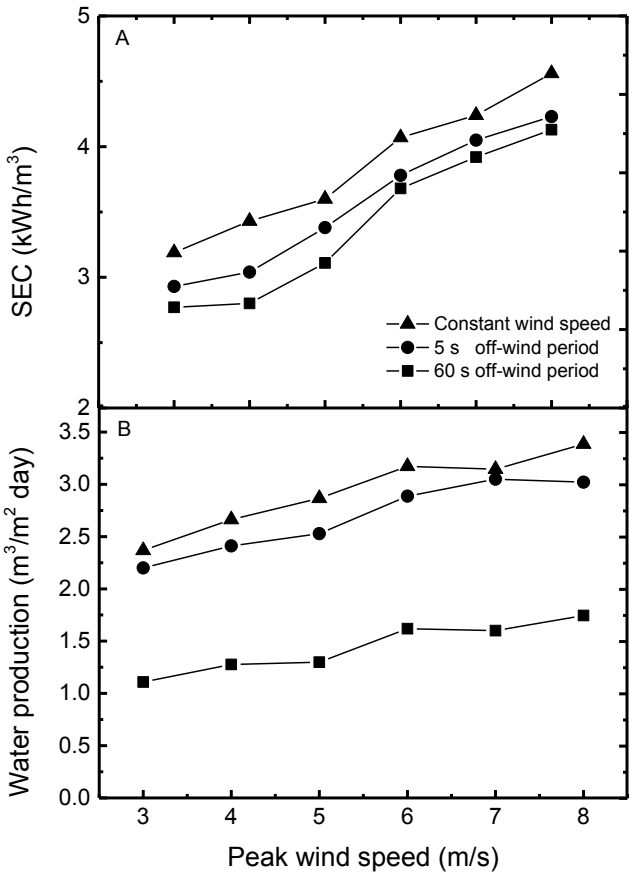

Figure 6.7 SEC (A) and water production (B) when desalinating a feed of 5,000 mg/L NaCl at the wind speeds of 3 -8 m/s and under i) constant wind speed regimes (triangle), ii) intermittent wind regime with 60 s on-wind period and 5 s off-wind period (circle), and iii) intermittent wind regime with 60 s on-wind period and 60 s off-wind period (square); (mode of operation: batch).

The SEC of the desalination process in all the experiments increased with the wind speed (Figure 6.7A). This was independent of the wind regime being steady (*i.e.* constant wind speed) or intermittent. The SEC increase is mainly due to the increase in the voltage output from the wind turbine when operated at higher wind speeds (detailed in sections 5.4.1 and 5.4.2). During intermittent operation, the increase in SEC can be partially attributed to the increased acceleration of the rotor (*i.e.* the shorter t_{twi}) at higher wind speeds; facilitating the wind turbine to reach its maximum voltage level (depending on the given peak wind speed) more quickly and thus operate at this optimal voltage level for a longer period over every intermittent cycle.

With an increase in the wind speed the water production also increase (Figure 6.7B). The significantly low water production observed in the intermittent operation with 60 s OFF-wind period is the result of consecutive delays in the desalination process caused by regular cycling off of the wind turbine. During the desalination experiments carried out under the intermittent wind regimes with OFF-wind periods smaller than t_{twd} (*i.e.* 5 s OFF-wind period), no power shut down occurred during the process and thus the water production remained relatively similar to that produced under constant wind speeds.

6.3.4 Desalination under intermittent conditions: real wind speed data

A desalination test was carried out with real wind speed data to i) determine the impacts of intermittency in a real wind condition on the desalination performance of the wind-ED system, and ii) to verify the results obtained from the intermittent wind-ED experiments conducted with simulated-controlled wind speed data (Figure 6.8).

The general behaviour of the wind-ED system followed the same pattern as those explained for the operation under constant and fluctuating wind speed conditions in section 5.4. Over the course of the desalination process the concentration of NaCl decreased in the diluate stream and proportionally increased in the concentrate channel (Figure 6.8 A). This caused the resistance of the ED stack (R_{stack}) to increase and thus less current to be drawn by the membrane system from the wind turbine (Figure 6.8 B). The decrease in current led to a reduction in the current induction counter torque force applied on the shaft of the wind turbine. This caused the net torque force applied on the shaft of the rotor to increase and thus the rotor to accelerate (angular velocity of the rotor (ω_r) to increase) (Figure 6.8 C). The faster the rotor spun the more was the voltage produced (Figure 6.8 C). This process continued until the angular velocity of the rotor was restricted from any further acceleration by the frequency inverter (max ω_r: 9.7 Hz and max voltage: 36.2 V). The self-protection mechanism, controlled by the frequency inverter in the wind turbine simulator, was explained earlier in section 5.4. The mean power varied within a small range of 83 -96 W prior to the activation of the frequency inverter (minute

21), but it then decreased significantly until it reached the values around 30 W toward the end of the desalination process (Figure 6.8 D).

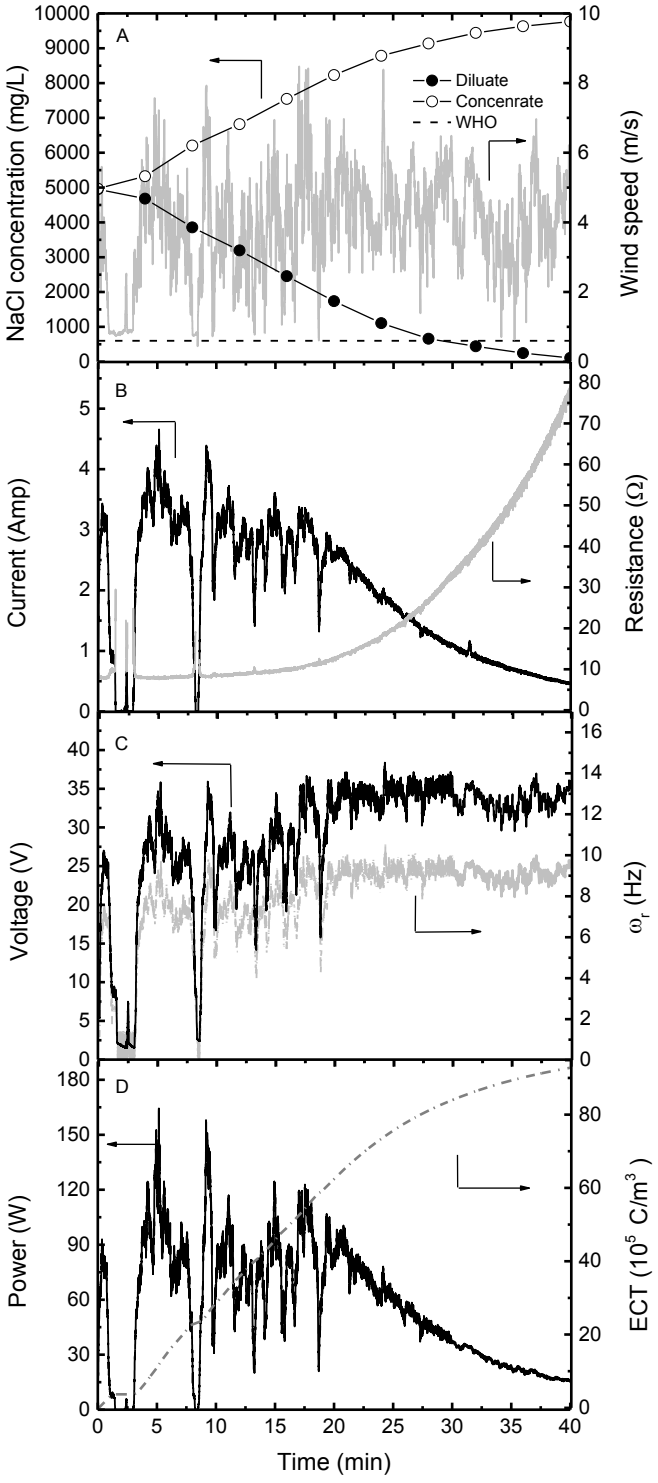

Figure 6.8 Wind-ED system performance under real wind conditions (mean wind speed: 3.11 – 4.56 m/s and TI: 0.11 - 0.55) during desalination of a feed of 5,000 mg/L NaCl at a flow rate of 7 L/min; (mode of operation: batch).

During the desalination process the wind speed fell to levels below $v_{cut\text{-}in}$ of ~2 m/s (severe fluctuations and intermittency in the wind resource) in several occasions; in response to which the wind-ED system exhibited three different behaviours:

i. The slow decrease of the wind speed with the rate of -0.14 m/s at the very beginning of the experiment (minute 0.7), caused the angular velocity of the rotor (ω_r) to decrease from 7.1 to 2.4 Hz over a period of 16 s. Correspondingly with the angular velocity of the rotor the voltage also decreased, from 24 V at 3.2 m/s to 9 V at 0.8 m/s. As a result of the decrease in the voltage output of the wind turbine the power dropped from 77 to 14 W; which led to a drop in the salt flux across the membranes from 2.96 to 0.84 mmol/m^{2}s. The same behaviour was observed in the controlled fluctuating experiments (Chapter 5, section 5.4.4) where applying TI above 0.4, led to reduction in the power produced by the wind system and thus resulted in less water being produced compared to that at the steady state wind condition (up to 18% decrease in the water production when going from TI 0.4 to TI 0.6).

ii. With the rotor continuing to spin at very low angular velocities (< 2.8 Hz) for over 25 s (*i.e.* the continuation of the behaviour (i)) the frictional and inertial forces overcame the angular momentum of the wind turbine, causing the rotor to slow down. This behaviour was also observed at minute 7.9 of the experiment, when an intermittent wind incident was followed by a long period (> 15 s) of very low wind speed (v < $v_{cut\text{-}in}$), causing the wind-ED system to cycle off for a short period. Once the rotor stopped spinning, the system entered a shutdown period during which no power was produced and the salt flux consequently dropped to zero (*i.e.* no desalination took place). Similar behaviours were also observed in the controlled fluctuating tests (*i.e.* with TI of 0.6 and the oscillation periods longer than 40 s) and the intermittent experiments (*i.e.* with the OFF-wind periods longer than 10 s) where the long periods of operating below the cut-in wind speed of 2 m/s resulted in regular cycling off of the wind-membrane system and corresponding reduction in the desalination rate.

iii. The occurrence of intermittency in the wind resource in many other stages of the process did not lead to a significant disruption in the desalination performance (*e.g.* minutes 13 and 18.3 of the process). During these particular short intermittencies of low/OFF-wind periods (< 5 s) inertia and frictional forces did not have time to completely overcome the angular momentum of the turbine and thus the rotor did not halt at any point during the process. As a result the generator kept spinning effectively and produced power regardless of the extreme fluctuations in the wind resource. Similar phenomena were observed in the controlled fluctuating tests, with oscillation periods shorter than 15 s, and during the intermittent tests, with the OFF-wind periods shorter than 10 s.

Operation below the threshold wind speed of 2 m/s led to significant reductions in the power (behaviour i) and in some cases the cycling off of the wind-ED system (behaviour ii). These caused some delay in the desalination process and thus a decrease in water production. The water production in this experiment was 2.41 m^3/m^2day, which was lower than 2.68 m^3/m^2day obtained in operation under semi-steady wind conditions (*i.e.* the test conducted with a similar mean wind speed of 3.04 – 4.16 m/s but with much smaller fluctuations (TI: 0.05 – 0.16) (detailed in Chapter 5, section 5.4.5)).

The impacts of wind speed fluctuations and intermittencies on the energy consumption of the process were negligible. The SECs for both of the above mentioned experiments were in the same range; 3.38 kWh/m^3 for the experiment carried out under severe wind speed fluctuations (Figure 6.8) and 3.36 kWh/m^3 for the experiment carried out under semi-steady conditions (Figure 5.8 A-D). This shows that the wind-ED system is capable of desalinating and producing good quality drinking water (< 600 mg/L NaCl) with no significant drop in its energy performance, even when operating under extreme wind speed fluctuations. These results also reconfirmed the results obtained in Chapter 4, suggesting electrodialysis as an electrically robust system for direct coupling to high frequency power supplies; such as renewable energy sources.

6.4 Conclusions

To determine the impact of wind speed intermittency on the specific energy consumption (SEC) and the water production of the wind-ED system, desalination tests were carried out over a range of wind on-off cycling frequencies (0.003-0.1 Hz), OFF-wind periods (0-180 s) and peak wind speeds (3-8 m/s). Every sudden variation in the wind speed (*i.e.* on/off cycle) was followed by a transient period during which the wind turbine tended to adjust its power production to the available energy in the new wind condition. The transient times t_{twi} and t_{twd} were introduced as the two main characteristic periods in all intermittent operations. The transient time t_{twi} represents the time spent for the rotor to accelerate and reaches a pseudo-steady state following a sudden increase in the wind speed to levels above $v_{cut\text{-}in}$ and t_{twd} represents the time taken for the rotor to slow down completely and thus the wind-ED system to shut down following a sudden decrease in the wind speed to levels below $v_{cut\text{-}in}$.

An increase in the on/off cycling frequency caused a reduction in the average power production by the wind turbine and ultimately led to less water being produced in a given period of time. The water production was more adversely affected by the increase in the off-wind period. With off-wind periods longer than t_{twd}, the rotor slowed down completely ($\omega_r < 1$ Hz); causing the wind-ED system to cycle off. The regular cycling off of the wind-ED system caused the desalination rate, and correspondingly, the water production to decrease significantly. Although both the on/off cycling frequency and the off-wind period influenced the power production by the wind turbine, they did not lead to a considerable change in the SEC of the desalination process.

The rotor acceleration time (t_{twi}) decreased with an increase in the peak wind speed. For instance at maximum wind speed (8 m/s), the decreased acceleration time (t_{twi}) allowed the system to reach its maximum voltage output at peak wind speed more quickly, hence it contributed to the operation of the wind-ED system at higher power levels. The decrease in the acceleration time (t_{twi}) and an increase in the available energy in the wind resource at higher peak wind speeds resulted in both increased SEC and water production.

Having characterised the impact of wind speed fluctuations and intermittencies on the electrodialytic desalination of a single salt (*i.e.* NaCl) solution in Chapters 5 and 6, this work will proceed to look into the impacts of wind speed fluctuations on the competitive removal of some selected common inorganic contaminants (Cl^-, F^-, NO_3^- and SO_4^{2-}) from artificial brackish water using the wind-ED system.

Chapter 7

Impacts of real wind speed fluctuations on the competitive removal of chloride, fluoride, nitrate and sulphate from brackish water using wind-ED

7.1 Introduction

Groundwater sources in parts of Africa and the Middle East contain high concentrations of inorganic salts [6, 7, 114-117, 219], originating from either geological (*e.g.* leaching from surrounding rocks) or anthropogenic (*e.g.* industrial or domestic effluents) sources [6, 17, 18]. Consumption of certain ionic contaminants, such as fluoride (F^-) and nitrate (NO_3^-), at concentrations above their recommended drinking water guideline limits may result in severe short and long-term physical and nervous disorders [19-23]. Other inorganic ions, such as chloride (Cl^-) and sulphate (SO_4^{2-}), are of no significant health concern, but their presence at elevated concentrations can lead to aesthetic problems which negatively affect taste and smell of the water, making it less desirable for consumption [21]. The health and aesthetic issues associated with the above mentioned inorganic contaminants, the concentrations at which these ions exist in brackish groundwater, and the sources from which these contaminants originate were detailed in section 2.2.

During desalination of brackish groundwater using ED, inorganic contaminants are removed at different rates depending on their particular physicochemical properties within the mixture (detailed in section 2.3.4). Zhang *et al.* observed faster transport of monovalent ions (*i.e.* Cl^-, NO_3^- and HCO_3^-) over multivalent ions (*i.e.* SO_4^{2-} and $H_xPO_4^{y-}$) when removing nutrients from RO concentrate using an ED system [101]. They reported even a further increase in the selectivity of the monovalent ions over the multivalent ions when operated at lower current densities. Zhang *et al.* attributed this enhanced selectivity to the ionic flux through the membranes becoming slower at lower current densities, with its impact being more pronounced on the flux of the multivalent ions. Improved selectivity as a result of lowering the current density was also reported by Nikonenko *et al.*, who first associated this to the electric repulsion phenomena [102, 167]. Based on the electric repulsion phenomenon, highly charged multivalent ions migrate at lower rates from the solution-membrane interface into the membrane structure, compared to weakly charged monovalent ions. Using the same theory, Nikonenko *et al.* also showed that with an increase in the electric potential (*i.e.* an increase in the current density) the electric repulsion effects, and correspondingly, the ion selectivity diminished until it became negligible once approached the limiting current density. Similar trends for specific ion selectivity under various operating current/voltage were also observed in the work by many other researchers [61, 220].

The electric field variation impacts on competitive transport of ions through ion-exchange membranes have also been investigated in other studies. Mishchuk *et al.* [61] investigated the selectivity of divalent ions (Ca^{2+}) over monovalent ions (Na^+) in ED and treated a solution of low concentration (1.5×10^{-3} g-equiv/L NaCl-$CaCl_2$) under both conventional (constant 30 V) and pulsed (30 V at 1 and 5 Hz with the duty cycle of 50%) electric field conditions. In the conventional process, the divalent calcium ions were preferentially removed over monovalent sodium ions. This trend changed when the operation was carried out under the pulsed electric field. Using pulsation the resistance imposed by concentration polarisation on the ionic flux through the membranes was eliminated; hence the sodium ions were more effectively removed compared to that in the conventional mode. In a different study, Ortiz *et al.* [70] investigated the removal of multiple ions (K^+, Na^+, Ca^{2+}, Mg^{2+}, Cl^-, NO^{3-},

HCO^{3-}, SO_4^{2-}) from a brackish water of high concentration (*i.e.* TDS concentrations of 2,329 – 5,022 mg/L) using a photovoltaic (PV)-ED system. In contrast to the study by Mishchuk *et al.*, the study by Ortiz *et al.* found no significant variation in the ion selectivity despite fluctuations in the energy resource (solar energy). The discrepancy between these two studies can potentially be attributed to differences in the current density regime at which the experiments were carried out and the differences in the magnitude and frequency of the electric power variation in these studies. However, further investigation on the impacts of energy source fluctuation on competitive removal of ions in ED is needed to fully understand these processes.

This chapter aims to;

i) study the chloride, fluoride, nitrate and sulphate removal from brackish water using the wind-ED system;

ii) determine the impacts of wind speed and its variations (*i.e.* fluctuations and intermittencies inherent to the wind resource) on the competitive transport of the ions within the ED system.

The results in this chapter will further complete the systematic studies carried out on the desalination performance of the wind-ED system in Chapters 5 and 6 and establish whether the wind-ED system can be counted on as a reliable off-grid technology to be used for desalination purposes in remote regions.

7.2 Experimental protocols

Three desalination experiments were carried out using different sets of real wind data as input to the wind turbine simulator. The wind data were chosen carefully from the real wind speed measurements carried out in Emden, Germany (see section 5.2.2) to determine the impacts of wind speed, fluctuations and intermittencies on the competitive removal of inorganic contaminants from water;

Experiment 1: v_{avr}:3.84 m/s & *TI*: 0.05 - 0.22

Experiment 2: v_{avr}:3.84 m/s & *TI*: 0.12 - 0.57

Experiment 3: v_{avr}:6.23 m/s & *TI*: 0.02 - 0.24

An artificial brackish water, containing sodium salts of fluoride, chloride, nitrate, and sulphate, was used in all the experiments. The concentration of the inorganic contaminants of interest were selected carefully to mimic the concentrations encountered in natural brackish groundwater in Africa and the Middle East (9 mg/L F^-, 1,700 mg/L Cl^-, 160 mg/L NO_3^- and 900 mg/L SO_4^{2-}) [6, 7, 114-117, 219]. All the experiments in this section were conducted at the constant flow rate of 7 L/min. The desalination tests continued until the concentration of the total dissolved solids, as well as that of all the individual ions in the diluate stream, decreased to levels below their WHO drinking quality guideline limits (*i.e.* TDS < 600 mg/L, F^- < 1.5 mg/L, Cl^- < 250 mg/L, NO_3^- < 50 mg/L, SO_4^{2-} < 500 mg/L) [21].

A schematic of the wind-ED system used for the experiments was shown in Figure 5.2 (Chapter 5), and the details of its components (*i.e.* the ED system, ion-exchange membranes and the wind turbine simulator) were given in section 3.2 (Chapter 3).

The parameters of interest in this study were specific energy consumption for desalination (SEC, kWh/m^3), water production (WP, m^3/m^2day), current efficiency (η_c, %), electric conductivity (EC, ms/cm), pH, ion concentration (c^i, mg/L), concentration of total dissolved solids (TDS, mg/L), ion removal from the diluate stream (R^i, %), and specific selectivity (S, -).

Among these, SEC, WP and η_c were calculated using Eqs. 3.4, 3.5 and 3.6, respectively. EC and pH were measured using a conductivity meter and a pH meter, respectively (detailed in section 3.4.2). During every experiment 8 to 10 samples, each having an approximate volume of 20 ml, were collected from the diluate and concentrate streams. These samples were then analysed within 24 to 48 hours from their sampling time, using an ion chromatograph system (detailed in section 3.4.3). The IC analysis gave results for the concentration of the anions of interest in the solution (F^-, Cl^-, NO_3^-, SO_4^{2-}), from which the concentration of sodium (Na^+) ions as well as the concentration of total dissolved solids (TDS) in both the diluate and concentrate streams were calculated.

Ion removal from the diluate stream (R_i, *%*) at time (*t, min*) was calculated using the following relationship,

$$R_i(t)\% = \frac{\left(c_{i,0} - c_{i,t}\right)}{c_{i,0}} \times 100 \tag{7.1}$$

where, c represents the concentration of the ion and subscript t represents the time at which the sample was collected.

Specific selectivity (S) was calculated using equation 7.2. This relationship was first introduced by Van der Bruggen *et al.* [162] for studying the competitive transport of ions from the diluate stream to the concentrate channel via ion-exchange membranes;

$$S_j^i(t) = \frac{\left(c_{i,t} \middle/ c_{i,0}\right) - \left(c_{j,t} \middle/ c_{j,0}\right)}{\left(1 - \left(^{i}_{i,t} \middle/ c_{i,0}\right)\right) + \left(1 - \left(c_{j,t} \middle/ c_{j,0}\right)\right)} \tag{7.2}$$

S_j^i has a value between -1 and 1. If the ion i is transported faster than ion j, the S_j^i gains a value between -1 and 0; if ion j is transported faster than i, then S_j^i gains a value between 0 and 1. The closer the S_j^i value to 0, the more similar are the removal rates for the two ions, hence the lower is the specific selectivity between them.

7.3 Results and discussion

7.3.1 Competitive ion removal

Experiments 1, 2 and 3 were conducted with different wind regimes, as described in section 7.2, to study the performance of the wind-ED system in terms of producing good quality drinking water under natural wind energy fluctuations. The results obtained from these experiments are given in Figure 7.1. The global electric performance of the system (*i.e.* the dependence of the voltage output from the wind turbine on the wind speed and R_{stack} during the process) was similar to that of the desalination of single salt (NaCl) solutions using the wind-ED system (section 5.4.1).

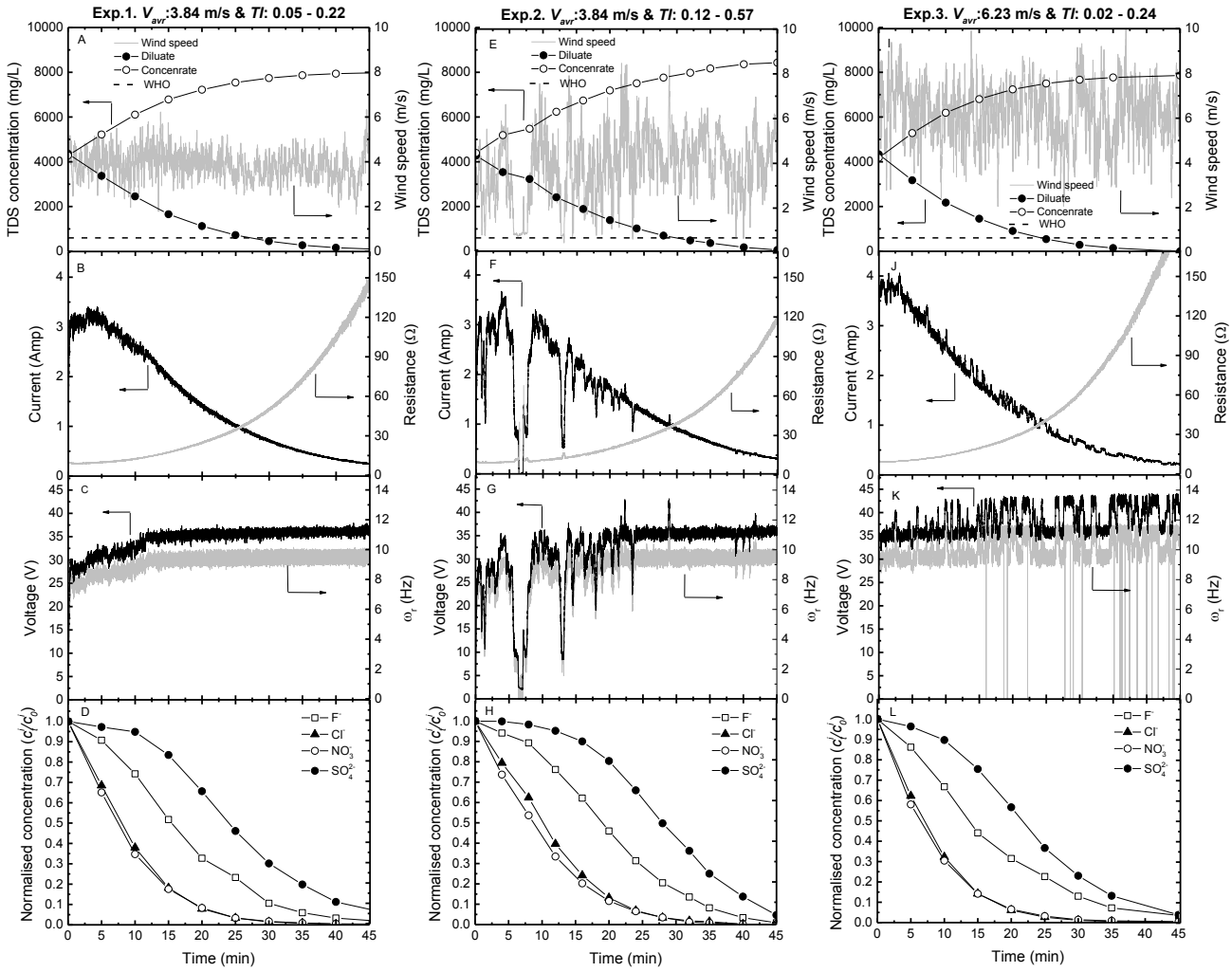

Figure 7.1 Wind-ED performance during desalination of artificial brackish water containing 9 mg/L F^-, 1,700 mg/L Cl^-, 160 mg/L NO_3^- and 900 mg/L SO_4^{2-} at a flow-rate of 7 L/min and under three different wind regimes. Experiment 1 (A-D): v_{avr} = 3.84 m/s & *TI* = 0.05 - 0.22; Experiment 2 (E-H): v_{avr} = 3.84 m/s & *TI* = 0.12 - 0.57; Experiment 3 (I-L): v_{avr} = 6.23 m/s & *TI*= 0.02 - 0.24; (mode of operation: batch).

The results from Experiments 1 and 2 (both conducted at similar average wind speeds but with different turbulence intensities) can be compared to determine the impacts of fluctuations on desalination performance. In Experiment 2, the occurrence of intermittency in the wind resource between minutes 5.6 and 7.9 caused the system to cycle off for a short period of approximately 2 minutes (Figure 7.1 E-G). During the off-period, negligible current and correspondingly negligible ionic mass was transferred across the membranes, resulting in a delay in the desalination process. The intermittency and extreme fluctuations in the wind resource led to a 14% lower

water production in Experiment 2 compared to Experiment 1 (2.64 m^3/m^2day in Exp. 1 vs. 2.27 m^3/m^2day in Exp. 2). However, the increased fluctuations did not have a significant impact on the SEC of the desalination process (3.1 kWh/m^3 in Exp. 1 vs 3.0 kWh/m^3 in Exp. 2). The results of these experiments were in agreement with the results obtained under controlled wind speed fluctuations and intermittencies in Chapters 5 and 6. Comparisons between the results obtained from Experiments 2 and 3 (both conducted at high wind speed fluctuations) showed that with the near doubling in the average wind speed from 3.84 to 6.23 m/s, the voltage output from the wind turbine increased slightly (Figure 7.1K vs. C). The increased voltage facilitated more current transfer across the membranes (Figure 7.1J vs. B) and thereby, an increased desalination rate (Figure 7.1I vs. A). As a result, the water production, calculated using Eq. 3.5, increased by 27% from 2.27 m^3/m^2day in Exp. 2 to 2.90 m^3/m^2day in Exp. 3. The increased wind speed also led to an increase in the SEC of the process from 3.0 kWh/m^3 in Exp.2 to 3.5 kWh/m^3 in Exp. 3.

Normalised concentration is a parameter often used to compare the desalination rate of ions which are present at different concentrations in the initial feed solution [162]. This parameter is calculated by dividing the concentration of an ion at any given time during the process by its initial concentration in the feed solution. In Figure 7.1 D, H and L the variation of the normalised concentration for fluoride, chloride, nitrate and sulphate ions over time in the diluate stream were given for Experiments 1, 2 and 3, respectively. As a general rule, the time taken for the completion of a desalination process is inversely proportional to the available energy [162]. Therefore, the higher and more constant the wind speed, the higher and steadier is the voltage output from the wind turbine, and the faster is the rate of concentration decrease for all the ions in the diluate channel. A comparison between Figure 7.1 D and H reveals that the normalised concentration decreased at a slower rate in the experiment carried out under extreme fluctuations and intermittency (Exp. 2) compared to the one conducted with a relatively steady wind speed (Exp. 1). A comparison between Experiments 2 and 3, both conducted over a similar range of wind speed fluctuations, shows that the increase in the average wind speed results in a faster reduction of the normalised concentration for all the ions in the diluate stream (Figure 7.1 H and L).

Table 7.1 Total electric charge transferred (ECT), pH, TDS and ionic composition of the diluate stream during the Experiments 1- 3.

Time (min)	pH	ECT ($\times 10^6$ C/m^3)	TDS (mg/L)	Ion concentration in the diluate compartment (mg/L)				
				Anion				Cation
				F^-	Cl^-	NO_3^-	SO_4^{2-}	Na^+
Experiment 1								
0	7.23	0	4,357.9	9.3	1,705.1	153.2	900.8	1589.5
5	7.20	1.86	3,371.7	8.5	1,167.5	99.6	875.8	1220.3
10	7.09	3.56	2,454.3	6.9	647.0	53.2	854.3	892.9
15	6.72	5.03	1,657.2	4.8	309.3	26.9	752.1	564.1
20	6.15	6.01	1,125.7	3.0	134.4	12.7	591.2	384.4
25	4.96	6.75	726.6	2.2	56.8	5.1	415.3	247.2
30	4.61	7.25	454.8	1.0	24.3	2.5	271.5	155.5
35	4.53	7.59	271.3	0.5	13.7	1.3	178.6	77.2
40	4.55	7.79	161.8	0.3	5.5	0.7	101.4	53.9
50	4.55	8.00	50.0	0.1	2.4	0.4	36.3	10.8
Experiment 2								
0	7.16	0	4,346.5	9.3	1,700.6	158.0	889.9	1588.7
4	7.15	1.33	3,658.4	8.7	1,351.6	116.5	888.6	1293.0
8	7.13	2.18	3,199.7	8.3	1,061.1	84.8	875.0	1170.5
12	7.05	3.50	2,483.5	7.1	673.7	52.8	847.6	902.3
16	6.83	4.47	1,961.2	5.7	410.9	32.0	801.0	711.6
20	6.59	5.39	1,462.3	4.2	224.0	18.3	715.3	500.5
24	6.00	6.07	1,091.3	2.9	117.2	10.3	587.0	373.9
28	4.85	6.66	772.5	1.9	58.2	5.5	442.9	264.0
32	4.65	7.06	555.2	1.2	31.2	2.0	322.4	198.4
35	4.61	7.28	440.3	0.7	23.8	1.3	222.5	192.0
40	4.57	7.63	250.8	0.3	3.4	0.3	122.3	124.5
45	4.59	7.85	130.1	0.1	2.5	0.2	41.4	85.9
50	4.52	7.97	66.7	0.1	0.6	0.1	22.6	43.3
Experiment 3								
0	7.2	0	4,386.6	9.3	1,732.8	157.0	917.4	1570.1
5	7.17	2.13	3,228.4	7.9	1,079.0	91.2	884.1	1166.2
10	7.03	3.97	2,230.7	6.2	559.1	47.8	823.2	794.4
15	6.64	5.30	1,508.2	4.1	246.3	22.2	692.3	543.3
20	5.62	6.31	961.7	2.9	105.7	10.2	519.9	323.0
25	4.79	6.98	598.2	2.1	46.1	5.0	336.2	208.8
30	4.65	7.45	343.6	1.2	18.9	2.2	211.1	110.2
35	4.59	7.72	198.5	0.6	10.0	1.3	120.7	65.9
45	4.64	7.99	51.2	0.2	2.3	0.8	34.8	13.1

The variations in the TDS concentration, the pH value, total electric charge transferred across the membranes (ECT), and the ionic composition of the diluate stream in all the three experiments are given in Table 7.1. The concentration of the total dissolved solids, as well as that of all the individual ions in the diluate stream, decreased to levels below their WHO drinking quality guideline limits [21] for all the experiments (Table 7.1), proving the wind-ED system to be capable of producing good quality drinking water even under extreme wind speed fluctuations.

Total electric charge transferred across the membranes (ECT) and current efficiency (η_c) were calculated using Eqs. 3.6 and 3.7, respectively. Despite the change in both wind speed and fluctuations from one experiment to another, neither ECT nor current efficiency varied significantly. ECT gained values within a narrow range of 7.97 - 8.00 × 10^6 C/m^3 (Table 7.1), and current efficiency varied in the small range of 83 – 85% in all three experiments (η_c was 83.15% in Exp. 1, 83.5% in Exp. 2 and 84.6% in Exp. 3). The similarity between the current efficiency values obtained in these experiments showed that the wind-ED system is electrically robust and the efficiency of electric charge transfer (*i.e.* ionic mass transfer) across the membranes is not negatively affected by the variations in the wind resource. These findings support the results reported in the Chapter 4 and are also in agreement with the work by Casademont *et al.* [64] where steady current efficiencies for the global desalination process under various pulse regimes was reported. These studies show that only the desalination time is significantly affected by the change in the amplitude and frequency of the power fluctuations. The SEC and current efficiency remain relatively unaffected even under severe energy fluctuations.

Regardless of the wind speed and fluctuations, the pH variations were gradual (from approximately 7.2 to 6) during the early stages of the desalination process (*i.e.* during the first 20-24 minutes) (Table 7.1). Once the TDS concentration in the diluate stream dropped below 1,000 mg/L the pH declined rapidly, from pH 6 to approximately 4.5 during the last 20 minutes of the process. This fast reduction in the pH was attributed to possible dissociation of the water molecules into H^+ and OH^- ions, resulting from operating beyond the limiting current density [131, 137, 204].

To avoid water dissociation the number of ion exchange membranes in the ED stack can be increased; this would split the voltage received from the wind turbine simulator among a greater number of unit cell pairs, thus reducing the operating current. However, increasing the number of ion exchange membranes would result in a reduction of water production per membrane surface area, which would be economically disadvantageous. Another common solution for neutralising the pH is to use buffers, such as bicarbonate salts, in the post-treatment stages of the water purification process in order to neutralise the pH (*i.e.* achieve a pH of 6.5 -8.5) [213-215].

As seen in Table 7.1, as well as Figure 7.1 D, H and L, the rate of transport for the ions F^-, Cl^-, NO_3^- and SO_4^{2-} are different from each other. This difference can be well explained by studying the competitive removal of the ions (Figure 7.2) against their physicochemical properties (Table 7.2).

Table 7.2 Physicochemical properties of the ions of interest F^-, Cl^-, NO_3^- and SO_4^{2-}

Properties	Unit	Fluoride (F^-)	Chloride (Cl^-)	Nitrate (NO_3^-)	Sulphate (SO_4^{2-})	Ref
Ionic radius	**10^{-10} m**	1.3	1.8	3	2.3	[161, 221]
Hydrated radius	**10^{-10} m**	3.4	3.8	5.1	2.73	[161, 221]
Gibbs free energy of hydration	**Kcal/mol**	-119.7	-89.6	-73.1	-257.9	[221-223]
Stokes number	**10^{-10} m**	1.70	1.20	1.29	2.31	[224, 225]
Molar conductivity λ,25 °C	**10^4 Sm^2/mol**	55.4	76.3	71.4	159.6	[225, 226]
Ion mobility in dilute solution, 25 °C	**10^{-8} m^2sV**	5.7	7.9	7.4	8.3	[227]
Bulk diffusion coefficient, 25 °C	**10^{-9} m^2/s**	1.46	2.03	1.9	1.06	[227, 228]
Molecular weight	**g/mol**	19	35.45	62	96.06	
Valence		1	1	1	2	

The order of ion removal (%) from the diluate stream was $NO_3^- \geq Cl^- > F^- > SO_4^{2-}$ (Figure 7.2) for all experiments. A similar sequence of ion removal was reported in a number of other studies, even where the concentration of all the ions were kept the same in the feed solution [23, 101, 152, 154].

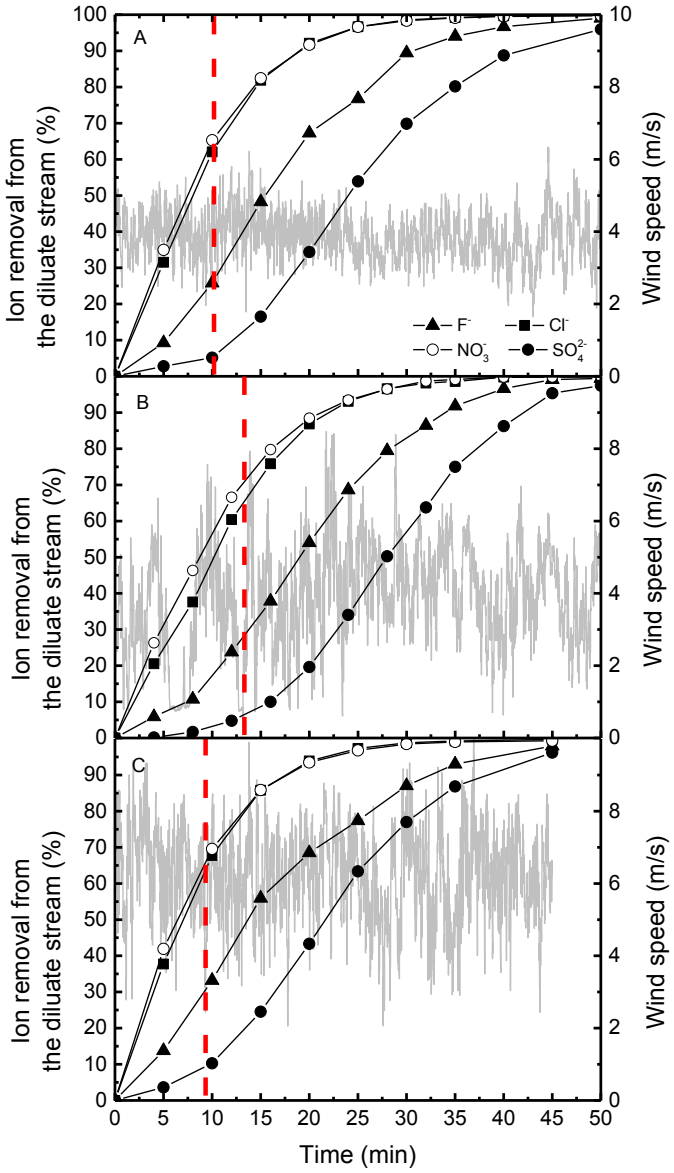

Figure 7.2 Competitive removal of F^-, Cl^-, NO_3^- and SO_4^{2-} from the diluate stream in the Experiments 1 (A), 2 (B) and 3 (C). The dashed red line indicates the time when over 65% Cl^- and NO_3^- were removed.

The results presented in Figure 7.2 show that the competition between the ions for transport across the membranes is independent of the initial concentration of the ions

in the feed solution and governed solely by their physicochemical properties. The key physicochemical properties of the ions of interest in this work (F^-, Cl^-, NO_3^- and SO_4^{2-}) are given in Table 7.2.

The diffusion coefficient and Stokes radius are the two key physiochemical properties used in the Extended Nernst-Plank based models [226, 229, 230], and yet neither of these is able to adequately describe the differences observed between the removals of the monovalent anions in the ED system. Stokes radius is the effective radius of a theoretical dense sphere that diffuses at the same rate as the target ion [231]. The lower the Stokes number, the easier the transport of the ions through the membranes is expected to be. Although this parameter is able to qualitatively explain the lower removal of fluoride compared to the other monovalent ions in the solution, it fails to explain the relatively higher removal of nitrate compared to chloride. A similar case was seen for the ion equivalent conductivity, which is a parameter demonstrating the tendency of an ion, presented in a dilute solution, to transfer electric charge [226, 227]. The lowest transport of F^- among the other existing monovalent ions in the mixture can be partly attributed to its equivalent conductivity being the lowest in the mixture. However, the ion equivalent conductivity was unable to explain the difference observed between removal of Cl^- and NO_3^-. The diffusion coefficient and ion mobility of the ions in the bulk solution are also unable to adequately describe the observed removal behaviours. Having the highest bulk diffusion coefficient and ion mobility compared to other monovalent anions in the mixture, chloride was expected to possess the highest removal among the monovalent anions in the mixture, but this was not the case. The values for Stokes radius, ion equivalent conductivity, bulk diffusion coefficient and ion mobility that are found in the literature are often able to explain transport of the ions within aqueous mixtures but in many cases they fail to fully support the transport behaviours seen through dense membranes (*i.e.* nanofiltration and ion-exchange membranes) [31, 151, 154, 160, 232, 233].

Some recent studies have reported new measurements for the hydrated radius of the monovalent ions (Table 2.1) [161] that discard the inverse relationship between the ionic and the hydrated radius as reported in some literature [152, 234, 235]. It is

suggested that ions with smaller ionic radius maintain stronger molecular bonds with the water molecules in their surroundings and hold to their hydration shells more tightly [155, 236]. As a result, such ions have smaller hydration shells and thus larger Gibbs free energy, that holds the hydration shells to the ion, compared to the ions with bigger ionic radius [235]. In order to pass through the ion-exchange membrane, it has been hypothesised that an ion is required to be dehydrated, either partially or fully, from its hydration shells [151, 160, 161, 233]. Therefore, in order for the separation to take place the energy of transport is required to be larger than the Gibbs free energy of hydration. According to Table 2.1, the difference in the Gibbs free energy of hydration can qualitatively explain the ionic removal sequence existing between the monovalent anions in this work. Fluoride, with the smallest ionic radius (1.3 nm), has the smallest hydration shell (3.4), holds the water molecules more strongly in its hydration shells (Gibbs free energy of hydration: -119.7 kcal/mol) compared to the other monovalent ions in the mixture (*i.e.* Cl^- and NO_3^-) and thus it is more strongly hindered from passing through the membrane.

It was observed that until removal of nitrate and chloride reached 65% (shown by the red dashed line in Figure 7.2) the sulphate removal was not significant (5-10%). However, once significant removal of chloride and nitrate had been achieved, sulphate removal increased steeply and reached > 95%. The initial slow rate of removal observed for sulphate was partly attributed to the higher Gibbs free energy of SO_4^{2-}, making the transport of this ion at the solution-membrane interface more energetically expensive compared to the other ions in the solution. Moreover, SO_4^{2-}, with the molecule weight of 96.06 g/mol and the ionic radius of 0.29 nm, is the largest and heaviest ion in the solution and thus it is naturally expected to exhibit lower mobility [23, 157, 237]. It is important to note that the contribution of the ion's size to its transport through the membrane is strongly dependent on the structure of the ion-exchange membrane. In a study carried out by Amor *et al.* [154] on the competitive removal of Cl^-, NO_3^-, HCO_3^- and SO_4^{2-} through different ion-exchange membranes, SO_4^{2-} showed the slowest removal among all the dissolved anions when a mono-anion perm-selective membrane (ACS) was used; however, the removal rate of SO_4^{2-} was the highest among all the anions when the process was conducted using a diffusion-dialysis membrane (AFN). Unfortunately in the study carried out by

Amor *et al.* the mechanisms of transport were not discussed in detail. The superior removal of SO_4^{2-} through AFN can be linked to the multivalent ion-exchange structure of that particular membrane hindering monovalent ions from freely diffusing through its polymeric matrix; hence it enhanced the relative transport of divalent ions. The lower diffusion coefficient of SO_4^{2-} compared to the other anions in the ionic mixture also plays a role in making the flux to mole fraction ratio of this component lower than the other competing anions in the mixture.

Although electric charge is unable to explain the removal sequence observed between the anions possessing the same valence (*i.e.* for the monovalent charge of F^-, Cl^- and NO_3^-), it can be considered a key parameter describing the significantly slower transport of SO_4^{2-} compared to the other anions in the mixture. Based on Faraday's first law the amount of electric charge required for transport of a charged specie through a system is proportional to the specie's electric charge [226, 229, 230]. Therefore, it is expected that for a unit electric charge transferred across the membranes (*i.e.* defined by the current density of the operation at any given stage of the desalination process) the number of divalent ions travelling across the membrane to be half of that for a monovalent ion in the mixture. It is important to note that the differences between the other physicochemical properties of the ions often cause the transport of divalent ions (*i.e.* SO_4^{2-}) not to be exactly half of that for the monovalent ions (*i.e.* F^-, Cl^- or NO_3^-). These results are in agreement with the findings reported by Zhang *et al.*[157] and El Midaoui *et al.* [23].

It is important to note that although the molar concentration of an ion fails to explain its competition with other ions for transportation across the membranes, it can partially explain the change in the rate of the removal of the ion during the desalination process. The impact of feed concentration on the mole fraction and transport number of the ions, which ultimately determine the rate of removal of each ion during the desalination process, will be discussed in detail in the next chapter (Chapter 8).

This section investigated the performance of the wind-ED system in terms of water production, energy consumption, current efficiency and individual ion (*i.e.* F^-, Cl^- or NO_3^- and SO_4^{2-}) removal in desalination of artificial brackish water under three

different wind regimes. Moreover, the natural competition of the ions in transport from the diluate to the concentrate stream was studied and linked to the differences between the physicochemical properties of the ions. The next section aims to investigate the impact of wind speed fluctuations on the specific selectivity of the ions in relation to each other.

7.3.2 The impacts of wind speed and fluctuations on the specific selectivity of the ions

Specific selectivity (Eq. 7.2) is a valid measure for evaluating the transport of ions relative to each other, and, hence, for determining the impacts of wind speed and fluctuations on the competitive removal of ions from the feed solution. In this research, NO_3^-, as the most preferentially removed ion compared to the other ions (Figure 7.2), was selected as the reference component (ion *j* in Eq. 7.2) relative to which the specific selectivity of the other ions was calculated (Figure 7.3). *S* was calculated until the point that the concentration of the reference ion (*i.e.* NO_3^-) fell below 6% of its initial feed value (*i.e.* $NO_3^- \leq 10$ mg/L). At concentrations below 10 mg/L, the removal of NO_3^- ions from the diluate stream becomes very sluggish (Figure 7.2), causing making accurate selectivity calculations for other ions relative to NO_3^- to be almost impossible.

The combination of low average wind speed and high turbulence intensity in Experiment 2 led to slight improvement in the selectivity of nitrate over both fluoride and sulphate compared to that in Experiments 1 and 3 (Figure 7.3 A and C). The lower the average wind speed, the lower is the current density at which the desalination process takes place. According to Nikonenko *et al.* [102, 167] a decrease in the current density results in the strengthening of electric repulsion (a phenomenon preventing highly charged multivalent ions to migrate as fast as weekly charged monovalent ions from the solution to the membrane structure), causing the specific selectivity of monovalent ions (NO^{3-}) over divalent ions (SO_4^{2-}) to improve slightly. Similar trends, showing improvement in specific selectivity between NO_3^- and SO_4^{2-} due to decrease in the applied current/voltage has been observed in the work of other researchers [61, 220].

As seen in Figure 7.3B the specific selectivity of Cl^- over NO_3^- is close to zero in all the experiments, regardless of the wind regime under which the desalination was carried out. This can be attributed to the very similar physicochemical properties of these ions, causing them to be removed at almost the same rate under all wind conditions (See Figure 7.2).

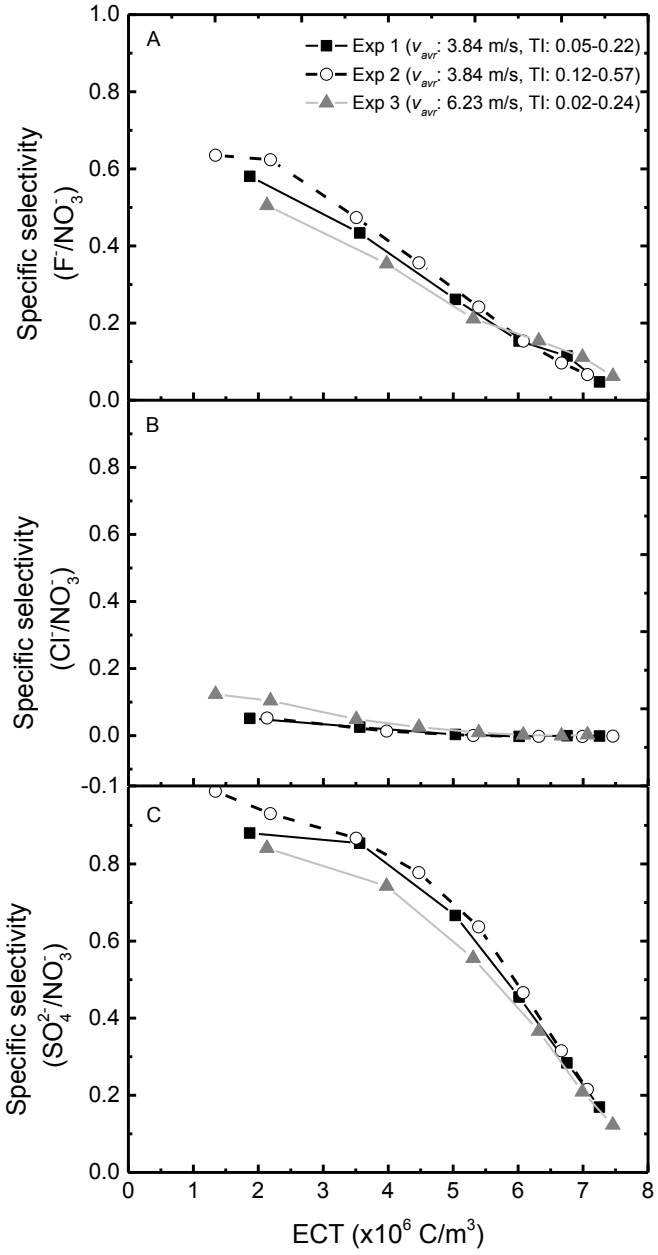

Figure 7.3 Specific selectivity of F^- (A), Cl^- (B), and SO_4^{2-} (C) relative to NO_3^- during the desalination processes conducted under different wind regimes at 7 L/min in the Experiments 1-3.

Large fluctuations and intermittencies in the wind resource were hypothesised to stimulate the partial disruption of concentration polarisation (CP) near the membrane surface. Therefore, the increased selectivity of nitrate over fluoride in the Experiment 2 can be attributed to the higher mobility of NO_3^-, causing this ion to reach the solution-membrane interface faster when the concentration profiles are disrupted by means of fluctuations in the wind source. The same behaviour was reported by Mishchuk *et al.* [61], who observed an increased selectivity for the monovalent ion (*i.e.* Na^+) compared to the divalent ion (*i.e.* Ca^{2+}) when conducting desalination using a pulsed voltage mode (power fluctuations of 1 – 5 Hz). Operating at lower current densities in Experiment 2 also led to less severe CP close to the membrane surface, as a result of which the selectivity of NO_3^- over F^- was enhanced [131, 238].

As seen in Figure 7.3 the impacts of wind speed and fluctuations on the specific selectivity are more pronounced at the beginning of the experiments. However, these effects are diminished as the desalination process progresses. Approaching the limiting current density toward the end of the process in all these experiments caused the electric repulsion effects and correspondingly, the ion selectivity to decrease significantly. The selectivity patterns seen in this section was also observed when repeated Experiments 1-3 at a lower flow rate of 2 L/min (Figure D.3, Appendix D).

7.4 Conclusions

The impacts of real wind speed and energy fluctuations on the removal of the ions of interest (F^-, Cl^-, NO_3^- and SO_4^{2-}) from artificial brackish water were investigated using the wind-ED system. The global desalination performance was similar to that described for the operation under controlled wind speed fluctuations in Chapters 5 and 6. Water production and SEC increased with the wind speed as expected based on the findings from the previous chapters. Extreme fluctuations and intermittency in the wind regime led to some delay in the desalination process; hence it caused lower water production to be obtained. However, the fluctuations did not have a significant impact on the SEC. The current efficiency varied in a small range of 83 – 85% in all the experiments; this together with the sufficient removal of all the inorganic contaminants to levels below their drinking quality guideline limits, suggested the wind-ED system as a reliable and electrically robust off-grid desalination system,

capable of producing good quality drinking water even under extreme wind speed fluctuations.

The ion removal in all the experiments, independent of the difference between the initial concentrations of the ions, followed the order: $NO_3^- \geq Cl^- > F^- > SO_4^{2-}$. The competitive removal of the ions was linked to the differences in their physicochemical properties, primarily Gibbs free energy of hydration. Ions with denser charge distribution, form stronger bonds with the water molecules; hence these ions need more energy to be stripped from their hydration shell before being transported into the membrane structure. The latter causes F^- and SO_4^{2-} ions to be transported less preferentially than the ions with lower Gibbs free energy (*i.e.* Cl^- and NO_3^-). Valence number was also suggested to be a key property, linking the amount of electric charge transferred by a mole of ion to its charge capacity; hence it can explain the lower transport of the divalent ions (*i.e.* SO_4^{2-}) compared to the monovalent ions (*i.e.* F^-, Cl^-, NO_3^-).

Specific selectivity diminished with increasing mean wind speed. This was attributed to the current density of the operation being larger at the higher wind speeds; hence the relative transport of the ions through the membranes is more adversely influenced by concentration polarisation. Increase in the wind speed fluctuations resulted in frequent disruptions of the concentration profiles within the boundary layer, thus it led to some improvement in the relative transport of the monovalent ions compared to the divalent ions from the bulk solution to the solution-membrane interface. The latter resulted in improved selectivity of NO_3^- ions over SO_4^{2-} ions.

So far in this thesis the impacts of wind speed, fluctuations and intermittencies on the inorganic contaminant removal from brackish water have been investigated, and the wind-ED system was proven to be a reliable off-grid desalination technology for the treatment of brackish groundwater containing inorganic impurities. The next chapter aims to study the effects of flow rate and feed concentration on the desalination performance of the wind-ED system.

Chapter 8

Impacts of feed concentration and flow rate on the removal of chloride, fluoride, nitrate and sulphate from brackish water using wind-ED

8.1 Introduction

The focus of this thesis so far has been mainly on investigating the impacts of wind speed fluctuations and intermittencies on the desalination performance of the wind-ED system (Chapters 5-7). However, as discussed in Chapter 5, the power production in a direct drive PMG based wind turbine is dependent not only on the wind speed and the fluctuations in the wind resource, but also on the resistance of the load (*i.e.* the ED stack in this research) that is directly connected to the wind turbine system [95, 96, 188]. Therefore, in addition to the wind speed and fluctuations it is also important to study the impacts of operating parameters which are influencing the resistance of the ED stack (R_{stack}), on the global desalination performance of the wind-ED system.

Feed concentration and flow rate are the two main operating parameters influencing R_{stack} (see section 2.3.5) [31]; hence varying either of these two parameters is expected to trigger a change in the power performance of the wind turbine as well as the desalination performance of the membrane system. Moreover, as suggested by

many studies flow rate, through changing boundary layers' dimensions, and feed concentration, through changing the transport number of ions inside the mixture, can indirectly influence the competitive transport of the salt ions across the membranes (see section 2.3.5) [23, 31, 153, 220, 237]. Therefore, this chapter aims to determine the impact of both flow rate and feed concentration on:

i) the electric behaviour of the wind-ED system (*i.e.* R_{stack}, voltage output from the wind turbine, current efficiency, power and SEC of the desalination process),

ii) the water production by the wind-ED system, and,

iii) the competitive transport of the ions (Cl^-, F^-, NO_3^- and SO_4^{2-}) across the membranes.

8.2 Experimental protocols

8.2.1 Flow rate impacts

Experiments were carried out at 2 and 7 L/min in order to determine the impacts of flow rate on the R_{stack} and ultimately on the energy and desalination performance of the wind-ED system. Both of the experiments were carried out using a moderate real wind speed data regime (v_{avr}: 3.64 – 4.15 m/s and TI: 0.05 – 0.22) as input to the wind turbine simulator. Detailed information regarding the real wind speed data used in this work was given in section 5.2.2. Artificial brackish water, containing the sodium salts of fluoride (9 mg/L F^-), chloride (1,700 mg/L Cl^-), nitrate (160 mg/L NO_3^-) and sulphate (900 mg/L SO_4^{2-}) (the TDS concentration of the brackish water: 4,350 mg/L) were used as the feed to the membrane system in these desalination experiments.

8.2.2 Feed concentration impacts

Experiments were conducted using feed solutions with three different concentrations of Cl^- (500, 1,700 and 2,550 mg/L) and fixed concentrations of F^- (9 mg/L), NO_3^- (160 mg/L) and SO_4^{2-} (900 mg/L). The purpose for keeping the concentration of all the anions, except Cl^-, constant in these experiments was to determine the impact of mole fraction variation for one ion on the transport number of its coexisting ions in

the mixture. These experiments were carried out using highly turbulent wind speed data (v_{avr}: 4.12 m/s and TI: 0.12 – 0.57) in order to observe a wider range of system behaviours (*e.g.* intermittency, larger variations in the operating voltage/current, etc.) as they may occur more significantly under extreme wind speed fluctuations.

A schematic of the wind-ED system used for the experiments was shown in Figure 5.2 (Chapter 5), and the details of the system components of this setup (*i.e.* the ED system, ion-exchange membranes and the wind turbine simulator) were described in section 3.2. The desalination tests in this chapter considered complete once the concentration of the total dissolved solids (TDS), as well as that of all the individual ions in the diluate stream, reached levels below their WHO drinking quality guideline limits (*i.e.*TDS < 600 mg/L, F^- < 1.5 mg/L, Cl^- < 250 mg/L, NO_3^- < 50 mg/L, SO_4^{2-} < 500 mg/L) [21].

The parameters of interest in this study were specific energy consumption for desalination (SEC, kWh/m^3) (Eq.3.4), water production (WP, m^3/m^{2}day) (Eq. 3.5), current efficiency (η_c, %) (Eq. 3.6), ion removal from the diluate stream (R^i, %) (Eq.7.1), and the transport number of the ions in the system. The latter parameter and the expressions used for its calculation will be discussed later in this chapter. Ion concentration (c^i, mg/L) and the concentration of total dissolved solids (TDS, mg/L) were measured using an ion chromatograph (as detailed in section 3.4.3).

8.3 Results and discussion

8.3.1 The effects of flow rate on the desalination performance of the wind-ED system

Experiments were carried out at 2 and 7 L/min to determine the impact of flow rate on the water production, ion removal, and charge transfer using the wind-ED system. Conductivity variation with time, for both the diluate and concentrate streams, at 2 and 7 L/min are reported in Figure 8.1. Over the course of desalination process the conductivity decreased from 7.6 ± 0.1 mS/cm to below 1.1 mS/cm (*i.e.* from 4,000 to < 600 mg/L TDS) in the diluate channel, exhibiting exponential variation with respect to time. Simultaneously, the conductivity in the concentrate channel

increased from 7.6 ± 0.1 mS/cm to over 14 mS/cm in both of the experiments. As seen in Figure 8.1, the desalination process was completed at an earlier stage when the operation was carried out at the higher flow rate (*i.e.* after 27 minutes at 7 L/min vs. 33 minutes at 2 L/min). Using Eq. 3.5. the drinking water production capacity of the wind-ED system was calculated: 2.7 m^3/m^2day at 7 L/min and 2.2 m^3/m^2day at 2 L/min.

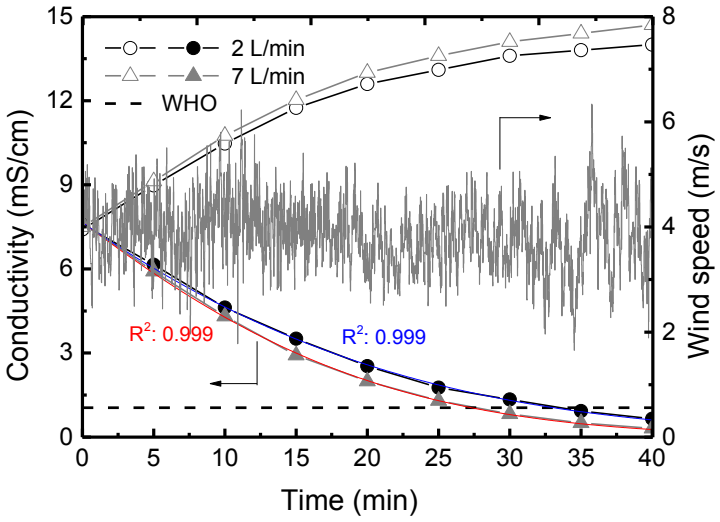

Figure 8.1 Conductivity variations vs time in the diluate (solid symbols) and concentrate (hollow symbols) during desalination. The TDS was 4350 mg/L TDS, the average wind speed 3.64 - 4.15 m/s and the turbulence intensity (TI) 0.05 – 0.22 at two different flow rates: 2 (circles) and 7 L/min (triangles). The coloured lines are the exponential fittings for the diluate conductivity versus time. The dashed line indicates the WHO guideline for acceptable TDS concentration in drinking water (measured by conductivity); (mode of operation: batch).

The higher rate of desalination at 7 L/min compared to that at 2 L/min can be attributed to the thickness of the boundary layer being smaller at the higher flow rate, causing ions to transport with a less resistance from the bulk solution to the surface of the membrane [23, 61]. Boundary layer thickness, calculated using Eq. 2.14 and experimentally obtained limiting current density data (Appendix C), was shown to shrink significantly from 5.52 ± 0.02 × 10^{-5} m at 2 L/min to 2.94 ± 0.03 × 10^{-5} m at 7 L/min.

This is in contrast to results obtained by Sadrzadeh *et al.* [149], Yang *et al.* [165] and Sik Ali *et al.* [51], where the increase in the flow rate was shown to have adverse effects on the ED process. It was argued in these studies that the residence time for the ions passing the ED stack and hence the number of ions available in any time increment to be transferred across the membranes decreased with increasing the flow rate, causing reduction in the rate of desalination. In a study carried out on the removal of nitrate from groundwater by using electrodilysis, Bi *et al.* [159] showed that the possibility of the flow rate having either positive or negative impacts on the desalination process strongly depends on the flow regime at which the operation is carried out. In this study Bi introduced a critical flow rate of 7 L/min, particular to their system, below which an increase in the flow rate improved the desalination rate as it caused reduction in the CP resistance against the transport of the ions. Oppositely, any increase in the flow rate above the critical value of 7 L/min caused the residence time for the ions passing through the ED stack to decrease and thus the desalination rate to diminish. It is important to note that the critical flow rate observed by Bi is particular to the ED setup and the experimental conditions employed in their experiments, and thus it cannot be viewed as a universal optimum flow rate for all ED systems.

The variations in the TDS concentration and ionic composition in the diluate stream and total electric charge transferred across the membranes (ECT) for the experiments carried out at 2 and 7 L/min are given in Table 8.1. As seen in this table, in all the experiments the concentration of the total dissolved solids as well as that of all the individual ions inside the diluate stream decreased to levels below their WHO drinking quality guideline limits [21].

The linear relationship between the conductivity of the diluate stream and electric charge transferred across the membranes (ECT) (Figure 8.2) revealed a relatively steady current efficiency throughout the process. Constant current efficiency in a process is always a desirable factor as it shows that the operation has been carried out below the limiting current density, with no significant current leakage in the system and also with no significant occurrence of fouling or scaling at the surface of the membrane [31, 65, 131, 239].

Table 8.1 Total electric charge transferred (ECT), TDS variation and the ionic composition in the diluate stream in the experiments 1 and 2.

Time (min)	ECT ($\times 10^6$ C/m^3)	TDS (mg/L)	Ionic composition in the diluate stream (mg/L)				
			Anion				Cation
			F^-	Cl^-	NO_3^-	SO_4^{2-}	Na^+
Experiment 1: 2 L/min							
0.0	0.00	4,335.1	9.1	1,701.9	157.4	901.5	1565.2
5.0	1.76	3,509.3	8.2	1,282.0	116.7	879.4	1223.0
10.0	3.31	2,632.1	6.6	808.4	73.5	784.7	958.9
15.0	4.57	1,995.6	4.9	496.1	48.8	707.2	738.6
20.0	5.54	1,433.6	3.6	298.1	31.2	585.0	515.7
25.0	6.29	993.8	2.9	174.5	18.9	455.5	342.0
30.0	6.85	753.0	1.8	103.1	11.9	343.4	292.8
35.0	7.28	516.2	1.4	61.2	7.4	247.6	198.6
40.0	7.61	359.1	0.8	34.8	4.3	178.7	140.5
50.0	8.04	160.7	0.8	13.0	1.6	86.1	59.2
60.0	8.17	63.8	0.2	5.6	0.8	40.0	17.2
Experiment 2: 7 L/min							
0.0	0.00	4,357.9	9.3	1,705.1	153.2	900.8	1589.5
5.0	1.85	3,371.7	8.5	1,167.5	99.6	875.8	1220.3
10.0	3.57	2,454.3	6.9	647.0	53.2	854.3	892.9
15.0	4.97	1,657.2	4.8	309.3	26.9	752.1	564.1
20.0	5.98	1,125.7	3.0	134.4	12.7	591.2	384.4
25.0	6.70	726.6	2.2	56.8	5.1	415.3	247.2
30.0	7.21	454.8	1.0	24.3	2.5	271.5	155.5
35.0	7.57	271.3	0.5	13.7	1.3	178.6	77.2
40.0	7.82	161.8	0.3	5.5	0.7	101.4	53.9
50.0	8.12	50.0	0.1	2.4	0.4	36.3	10.8

Unlike conductivity vs time, which was a function of operating conditions (*i.e.* the flow rate) (Figure 8.1), the conductivity vs ECT exhibited no significant dependence on the operating parameters. This suggested having relatively similar current efficiency values at both 2 and 7 L/min, which was also confirmed with the

calculated current efficiency values at these two flow rates (Eq. 3.6): 88.84 ± 0.7% at 2 L/min and 89.11 ± 0.5% at 7 L/min.

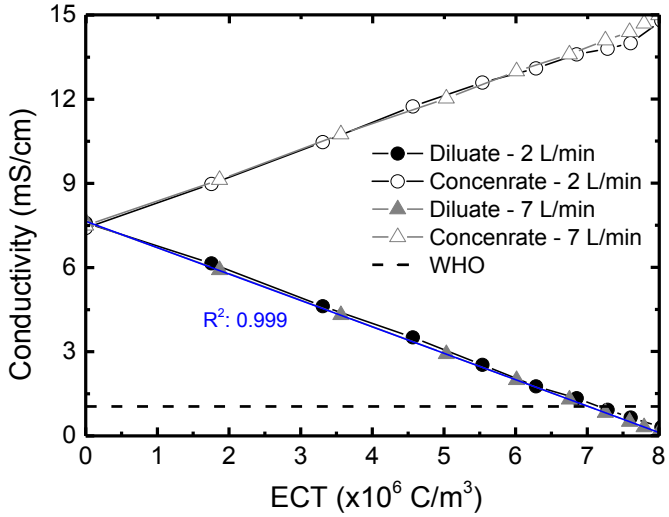

Figure 8.2 Conductivity variations versus cumulative electric charge transferred across the membranes (ECT) for both streams of diluate (solid symbols) and concentrate (hollow symbols) at two different flow rates of 2 (circles) and 7 L/min (triangles). The coloured lines are the exponential fittings for the diluate conductivity versus ECT; (mode of operation: batch).

8.3.2 The impacts of flow rate on the energy consumption of the wind-ED system

From the electrical point of view, the shrinkage of the boundary layer's thickness at the higher flow rate (*i.e.* 7 L/min) caused the R_{stack} to decrease (Figure 8.3 A), hence it allowed the ED stack to drive more electric current from the wind turbine system (Figure 8.3 B). Operating at a higher current density resulted in a larger salt flux across the membranes, and thus the faster completion of the desalination process, at the higher flow rate, as it was previously shown in Figure 8.1.

Moreover, when operating at a higher current, a larger current induction counter torque force is applied on the shaft of the wind turbine. According to the theory given in section 5.3, the higher the current induction counter torque force the smaller is the net torque force applied on the rotor. Therefore, the rotor spins at a lower angular velocity, as a result of which the generator produces less voltage. This can be

evidently seen by comparing both the voltage and the current perfromances of the experiments carried out at 2 and 7 L/min (Figure 8.3 B & C).

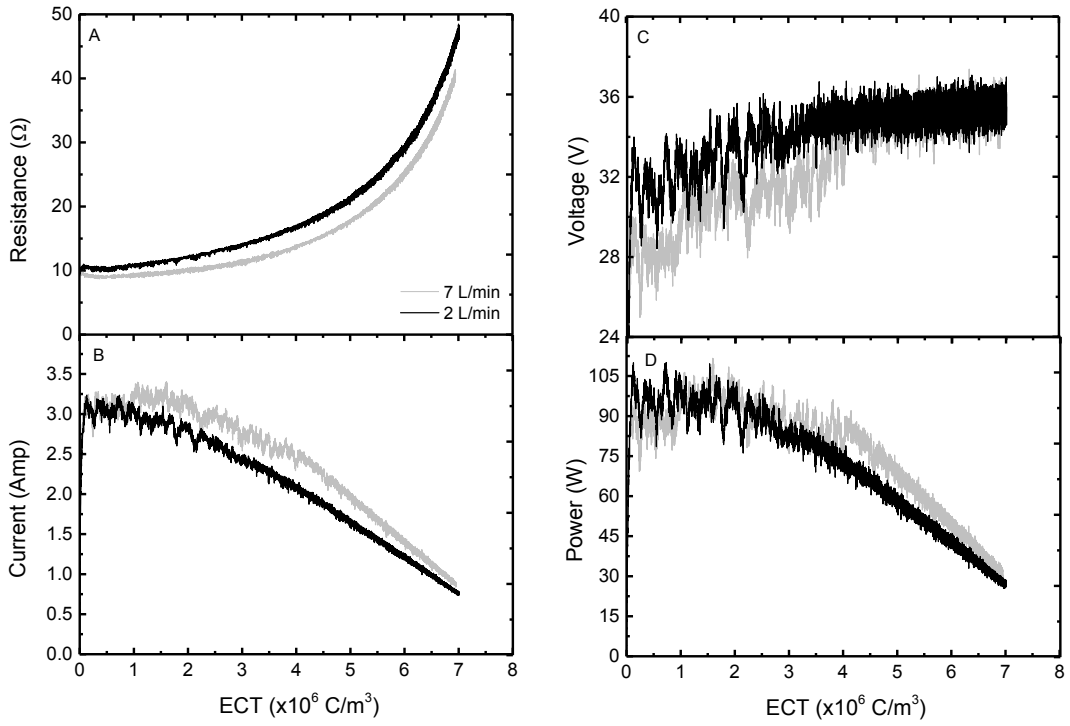

Figure 8.3 Resistance (A), current (B), voltage (C) and power (D) variations vs electric charge in desalinating from synthetic brackish water containing 4350 mg/L TDS using an average wind speed of 3.64 - 4.15 m/s and the turbulence intensity (TI) of 0.05 – 0.22 at two different flow rates of 2 and 7 L/min; (mode of operation: batch).

At a given wind speed, considering that the fluctuations in the wind resource are small (*i.e.* TI ≤ 0.2), the direct drive PMG wind turbine tends to maintain a balance between the voltage and current variations, so the power can oscillate within a narrow range despite variations in the R_{stack} (90 ± 15 W) (Figure 8.3 C). This behaviour of the wind turbine and the mechanisms contributing to it were discussed in detail in Chapter 5. As seen in Figure 8.3 the wind-ED system continues to behave in the aforementioned way until the R_{stack} reached 14.5 ± 0.3 Ω, indicating the resistance at which the self-protecting electronics (*i.e.* the frequency inverter) began to restrict the rotor from any further acceleration. Upon imposing this restriction, the voltage, already near its maximum level (35 ± 1 V in Figure 8.3 C), was stopped increasing any further. As a result of this, the power started to decrease significantly

together with current until it reached very low levels of about 30 W toward the end of the desalination process in both of the experiments.

As seen in Figure 8.3 D, the impact of flow rate on the power production by the wind turbine only became slightly noticeable following the activation of the frequency inverter. However, the overall impact of the flow rate on the power performance of the wind-ED system was so small that it did not result in a significant change in the energy consumption of the process. The SEC of the process, calculated by using Eq. 3.4, was 3.13 kWh/m^3 at 7 L/min and 3.31 kWh/m^3 at 2 L/min. The dependence of SEC on flow rate was also shown to be negligible in the studies carried out by other researchers [36, 170, 171].

8.3.3 The impacts of flow rate on the competitive ion transport

Flow rate is a key operating parameter that not only affects the global desalination rate and SEC of the process, but also directly influences the transport of each ion in competition with its coexisting ions in the mixture [31, 149, 158, 240]. While many researchers so far have investigated the electrodialytic desalination of multi ionic mixtures under different flow regimes [51, 159, 241], no one has yet proposed a comprehensive argument explaining the impact of flow rate on the competitive transport of monovalent and divalent anions in the ED process. This section aims to use the flow rate's effect on the concentration polarisation layer as a basis to elucidate its role in controlling the competition between F^-, Cl^-, NO_3^- and SO_4^{2-}.

Figure 8.4 illustrates the removal of the ions of interest (F^-, Cl^-, NO_3^- and SO_4^{2-}) from the diluate stream against the total electric charge transferred across the membranes (ECT) at the two different flow rates of 2 L/min (Experiment 1) and 7 L/min (Experiment 2). As seen in this figure, the ionic removal in both of the experiments followed the same sequence as observed in Chapter 7 (section 7.3.1): $NO_3^- \geq Cl^- > F^- > SO_4^{2-}$. The difference between the rates of removal of these ions was linked to the difference between their physicochemical properties and discussed in detail in the same chapter.

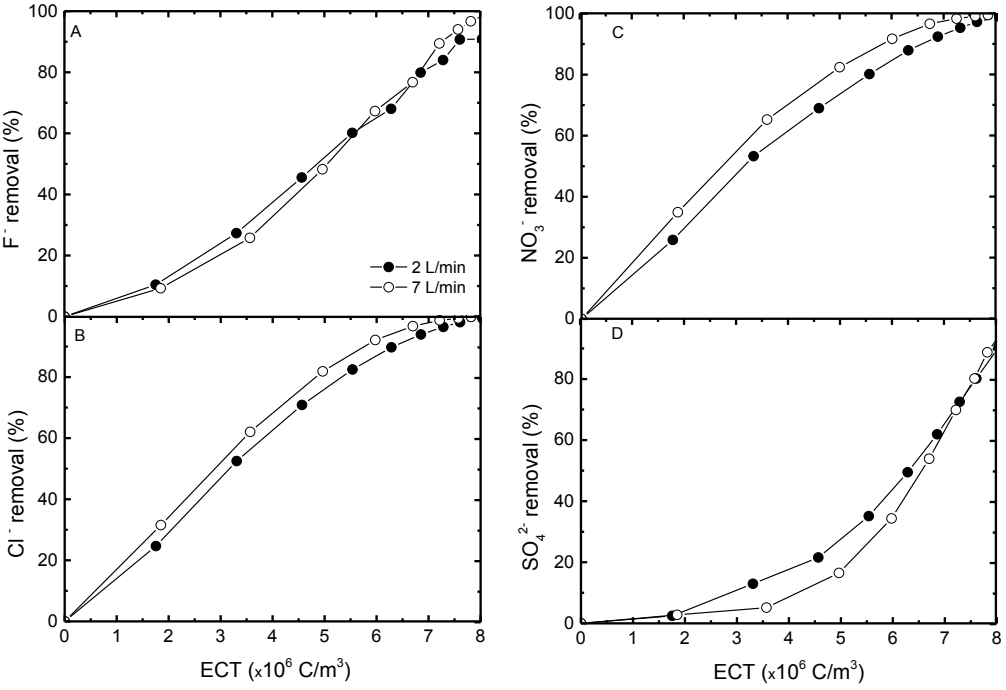

Figure 8.4 F^- (A), Cl^- (B), NO_3^- (C) and SO_4^{2-} (D) removal from the diluate stream vs electric charge transferred across the membranes (ECT) in desalinating from synthetic brackish water containing 4625 mg/L TDS using an average wind speed of 3.64 - 4.15 m/s and the turbulence intensity (TI) of 0.05 – 0.22 at two different flow rates of 2 and 7 L/min; (mode of operation: batch).

Thinning of the boundary layer at the higher flow rate caused the concentration profiles near the membrane surface to become steeper and thus the diffusion process to be enhanced. This resulted in an increase in the share of the diffusion process in transferring the salt ions from the bulk to the solution-membrane interface and ultimately an improvement in the transport of the ions with the highest diffusivity in the mixture. This can explain the enhancement observed in the transport of Cl^- and NO_3^- ions, having the highest diffusivity among the four anions in the mixture (Table 2.1), at 7 L/min compared to their transport at 2 L/min (Figure 8.4). The increase in the removal per unit ECT of Cl^- and NO_3^- at the higher flow rate meant that their share in transferring electric charge across the membranes increased, causing in return the charge transference share of slow removing divalent anions (*i.e.* SO_4^{2-}) to decrease. Having a very small concentration in the mixture, the charge transference share of F^- ions was not significantly affected by the change in the flow rate.

The roles of ion mobility and affinity to the anion-exchange membrane (AEM) in the transport of the ions became more essential at the lower flow rate, where the flux of ions from the bulk solution to the membrane interface was hindered more strongly due to an increase in the thickness of the CP layer. The enhancement of SO_4^{2-} removal per unit ECT at the lower flow rate can be thus attributed to its larger mobility in the solution (Table 2.1) and its higher affinity to AEM compared to the other ions in the mixture. The higher affinity of SO_4^{2-} to AEM is linked to the valence and size of SO_4^{2-} being the largest among all the ions in the mixture [242]. Similar patterns for the impact of flow rate on the competitive transport of ions were observed when conducted desalination on a similar feed solution to that of Experiments 1 and 2 and at two flow rates of 2 and 7 L/min but under different wind regimes (See Figures D.5 and D.6).

It is important to note that the above described effects of flow rate on the competitive transport of ions were mainly detectable until Cl^- and NO_3^- reached 5% of their initial feed concentrations in the diluate stream (*i.e.* ECT $\geq 6\times10^6$ C/m^3). The absence of Cl^- and NO_3^- ions in the mixture toward the end of the experiment caused the competition in the transport of the ions to effectively disappear, allowing the remaining charge to be transferred by the SO_4^{2-} ions.

So far the impact of flow rate on the desalination performance, energy consumption and competitive transport of ions through the membranes were investigated in this chapter. The next section investigates the effects of feed concentration, as another key parameter influencing the R_{stack}, on the performance of the wind-ED system.

8.3.4 The effects of Cl^- concentration on the desalination performance of the wind-ED system

Desalination tests with three different concentrations of Cl^- (500, 1,700 and 2,550 mg/L) and fixed feed concentrations of F^- (9 mg/L), NO_3^- (155 mg/L) and SO_4^{2-} (880 mg/L) were carried out using the wind-ED system (Figure 8.5). The importance of using different Cl^- concentrations in these experiments were to determine how i) the global desalination performance of the wind-ED system and ii) the removal rate of

the other anions present in the mixture are influenced by the increase in the salinity of the brackish groundwater.

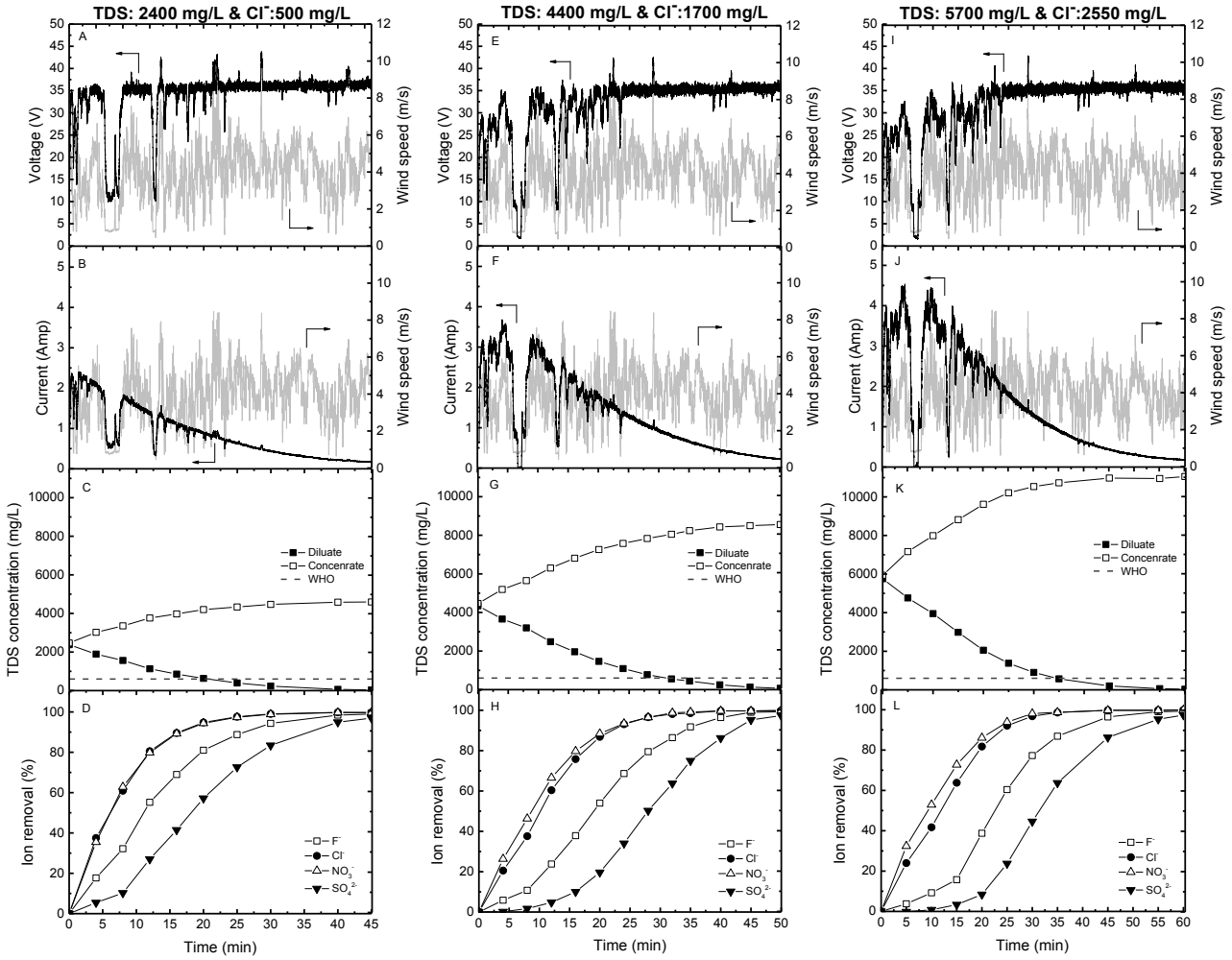

Figure 8.5 Desalination and electric performance of the wind-ED system in demineralising feeds containing different levels of Cl^- (500, 1,700 and 2,550 mg/L) and fixed levels of F^- (9 mg/L), NO_3^- (155 mg/L) and SO_4^{2-} (880 mg/L); (mode of operation: batch).

Increasing the feed concentration caused the electrolyte's conductivity to increase, as a result of which the R_{stack} was lowered; 14.5 ± 0.3 Ω with 2,400 mg/L TDS as feed, 9.6 ± 0.4 Ω with 4,400 mg/L TDS and 7.4 ± 0.3 Ω with 5,700 mg/L TDS. As discussed in Chapter 5, the lower the R_{stack}, the larger the current driven by the membrane system from the wind turbine, correspondingly with which the current induced counter torque force applied on the shaft of the turbine increases. The latter results in lowering of the net torque force applied on the shaft, causing the angular velocity of the rotor and correspondingly with that the voltage output from the

generator to decrease (see the wind-ED operation theory in section 5.3). The impact of feed concentration on the voltage output of the generator was the most evident at the beginning of the test, when the angular velocity of the rotor and with respect to that the angular momentum of the turbine was the lowest. For the experiments carried out with the initial feed concentrations of 2,400, 4,400 and 5,700 mg/L, the voltage output from the wind turbine at the beginning of the desalination test was 34.0 ± 0.4, 26.6 ± 1.1 and 24.8 ± 1.2 V, respectively (Figure 8.5 A, E and I). However, once the angular velocity of the rotor approached its maximum limit, set by the frequency inverter for a given average wind speed (*i.e.* 4 m/s), the voltage output from the generator became relatively steady and thus it stopped varying any further with respect to the feed concentration. Operating with similar wind speed regimes, the maximum voltage reached at the end of the test was similar (35.6 ± 0.51 V) in all the three experiments.

The angular momentum of the wind turbine is directly linked with the rotor's angular velocity [97]. Therefore, increasing the R_{stack} and the resulting decrease in the angular velocity of the rotor directly influences the angular momentum of the wind turbine, consequently causing the wind-ED system to exhibit more sensitivity to wind speed fluctuations when using higher feed concentrations as input to the membrane system. A clear example of such behaviour can be seen at minute 5, when a sharp drop in the wind speed caused the wind-ED system to cycle off in the experiments carried out with the feed TDS concentrations of 4,400 and 5,700 mg/L; however the same wind behaviour for the experiment carried out with the lower TDS feed concentration of 2,400 mg/L only resulted in some reduction in the current (from 1.9 Amp to approximately 0.6 Amp) but no system shut down was observed.

As principally expected, with an increase in the initial feed concentration the total mass of salt required to be removed from the diluate stream and, correspondingly, the specific energy consumption of the desalination process increased. The relationship between the feed concentration and SEC was found to be linear. The SEC of the desalination for the feed TDS concentrations of 2,400, 4,400 and 5,700 mg/L were 1.48, 2.98 and 3.98 kWh/m^3, respectively. Moreover, with an increase in the initial feed concentration the time required for reaching the desalination target (*i.e.* 600

mg/L) in the diluate channel increased, causing the water production of the wind-ED system to diminish. Water production for the feed TDS concentrations of 2,400, 4,400 and 5,700 mg/L were 3.59, 2.33 and 2.12 m^3/m^2day, respectively.

The inorganic contaminants of interest (Cl^-, F^-, NO_3^- and SO_4^{2-}) were all removed effectively (> 95%) from the diluate stream, regardless of the initial feed concentration used. Ion removal in all the experiments followed the same order as observed before (sections 7.3.1 and 8.3.3): $NO_3^- \geq Cl^- > F^- > SO_4^{2-}$; however, the rate of removal for the different ions varied by changing the Cl^- concentration in the feed solution. The impacts of Cl^- concentration on the removal rate of the ions can be explained by studying the variations in the transport number of the ions at each stage of the process in these three experiments.

Ion transport number was first introduced by Johann W. Hittorf [226, 229, 243, 244], as a quantitative measure to determine the contribution of an ion to electric charge transfer inside an electrolyte medium. Ion transport number ranges between zero, indicating no charge being transferred by the ion, and one, indicating that all the electric charge is transferred by the specified ion within the system. Transport number of an ion is a strong function of the ion's mole fraction as well as its physicochemical properties inside a given environment, this being either an electrolyte solution, the ion-exchange membrane or the combination of the both when looking at the overall transport number of an ion in the global process.

Considering that the membrane – electrolyte system behaves ideally, meaning that the anions and cations equally contribute to the electric charge transport across the ion-exchange membranes (*i.e.* the overall transport number for both the total anions and the total cations is the same and equal to 0.5), the overall transport number for an ion in the system can be calculated by using Eq. 8.1, in case of anions, and Eq. 8.2, in case of cations. Eq. 8.1 and 8.2, which are the modified versions of the transport number expression given in [70], consider the electrolyte solution as the reference environment for calculating the overall transport number.

$$t_{i,-} = 0.5\frac{z_{i,-}y_{i,-}x_{i,-}}{\sum_{i,-}^{n} z_{i,-}y_{i,-}x_{i,-}}, \quad (i,\text{-: negatively charged ions in the mixture}) \qquad \text{(Eq. 8.1)}$$

$$t_{i,+} = 0.5\frac{z_{i,+}y_{i,+}x_{i,+}}{\sum_{i,+}^{n} z_{i,+}y_{i,+}x_{i,+}}, \quad (i,+: \text{positively charged ions in the mixture}) \qquad \text{(Eq. 8.1)}$$

In Eqs. 8.1 and 8.2, t_i is the transport number of an ion in the global electrolyte – membrane system, x is the mole fraction; z is the valence number (listed for the ions of interest in Table 2.1) and y is an empirical coefficient related to the overall electrical mobility of an ion in the solution-membrane system; n defines the number of different ions from the same charge that exist inside the mixture; the charge of ions is defined by the subscripts - and +, representing the anions and cations, respectively. Running the measured total charge transfer (ECT) data together with the theoretical estimations for each ion's contribution to the charge transport based on its valence number and concentration in a series of iterating systems, y_i can be calculated phenomenologically for each ion in the mixture (Table 8.2).

Table 8.2 phenomenologically calculated $y_{i,-}$ values for the anions in the experiments carried out with the three different concentrations of Cl^- (500, 1,700 and 2,550 mg/L).

	$y_{i,-}$ value			
	F^-	Cl^-	NO_3^-	SO_4^{2-}
Experiment 1 (2,400 mg/L TDS & 500 mg/L Cl^-)	87.1	207.9	224.6	43.0
Experiment 2 (4,400 mg/L TDS & 1,700 mg/L Cl^-)	59.2	166.2	191.5	27.2
Experiment 3 (5,700 mg/L TDS & 2,350 mg/L Cl^-)	47.8	158.8	197.9	22.1

As seen in Table 8.2, in all the experiments y_i values followed this order $NO_3^- > Cl^- > F^- > SO_4^{2-}$. This was similar to the order of ion's removal seen in the previous chapter (section 7.3), indicating the strong dependence of the electrical mobility of different ions inside the ED system on their physicochemical properties. More details on the relationship between the removal rate and physicochemical properties of the ions can be found in section 7.3.

Figure 8.6 A-D shows the molar concentration variations of the anions in the experiments conducted with different feed concentrations. The gradient of the curves plotted in this figures represent the molar flux of the anions, the variations of which

during the desalination process can be explained based on the transport number of the ions (Figure 8.6 E-H).

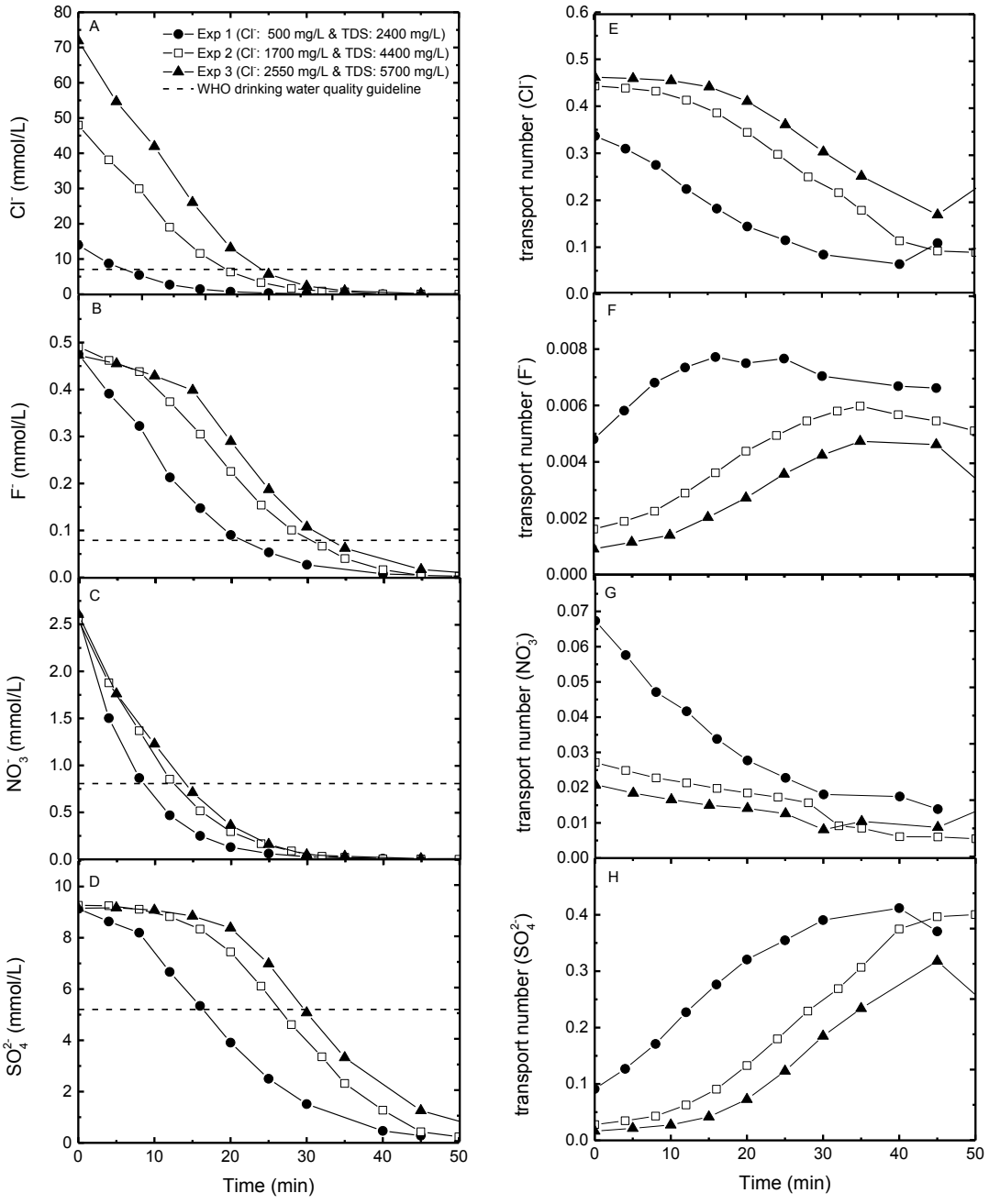

Figure 8.6 Molar concentration and transport number variations for F^-, Cl^-, NO_3^- and SO_4^{2-} in the diluate stream during the desalination of the feeds containing three different initial Cl^- concentrations of 500, 1,700 and 2,550 mg/L; (mode of operation: batch).

The rate of reduction for both Cl^- and NO_3^- at the beginning of the desalination process was significantly higher than those of F^- and SO_4^{2-}. The preferential removal of Cl^- and NO_3^- compared to F^- and SO_4^{2-} can be attributed to their physicochemical properties, as was explained in detail in the previous chapter (section 7.3). The mole fractions and, correspondingly, the transport numbers of Cl^- and NO_3^- decreased substantially as these two ions were removed effectively from the diluate stream. Together with a decrease in the share of Cl^- and NO_3^- in transferring electric charge across the membranes, the transport number of F^- and SO_4^{2-} started to increase, causing the rate of reduction for these two ions in the diluate stream to increase as well (*i.e.* an increase in their flux through the ion-exchange membranes). It is important to note that the sum of the transport numbers for all the anions at every stage of the process is equal to 0.5, considering that the other half of the electric charge in the electrolyte-membrane system is transferred by Na^+ ions (t_{Na} = 0.5). The feed concentration and, correspondingly, the rate of removal (*i.e.* the flux) for all the ions diminished toward the end of the desalination process.

With an increase in the concentration of Cl^- in the initial feed solution, the demineralisation rate of the other anions in the mixture decreased. This was explained to be due to the reduction in the mole fraction leading to a decrease in the transport number of chloride's coexisting anions in the mixture, when increasing the Cl^- concentration in the initial feed solution.

8.4 Conclusions

Flow rate and initial feed concentration, as the two main parameters influencing the resistance of the ED stack (R_{stack}), were varied in a set of desalination experiments using the wind-ED system. The aim was to determine the impacts of the resistance of the directly connecting load (*i.e.* the ED system) on the energy performance of the wind turbine and, thus, ultimately to determine their effects on the desalination performance of the membrane system.

Increased flow rate and resulting decrease in the thickness of the boundary layer caused R_{stack} to decrease. This subsequently led to an enhancement in the current driven by the membrane system and thus an increase in the water production. The

wind turbine automatically adjusted its voltage output corresponding to the current variations, helping with the power to remain relatively unaffected by the flow rate variations when operated at a given wind speed. Having the operating power almost independent of the flow rate resulted in the SEC variations to be negligible; increasing only slightly from 3.13 kWh/m^3 at 7 L/min to 3.31 kWh/m^3 at 2 L/min.

The increased flow rate and the resulting shrinkage of the boundary layer's thickness caused the concentration profiles at the solution-membrane interface to become steeper. This favoured the transport of ions with the highest diffusion coefficients in the mixture (*i.e.* Cl^- and NO_3^-). Decreased flow rate favoured the transport of ions with larger valence numbers and higher electric mobility inside the electrolyte (*i.e.* SO_4^{2-}).

Increasing the feed concentration resulted in a reduced R_{stack}. This inversely influenced the current induction counter torque force applied on the shaft of the wind turbine and caused the rotor to spin at a lower angular velocity. With the decrease in the angular velocity of the rotor the angular momentum of the wind turbine decreased. This led to an increased sensitivity of the wind turbine to wind speed fluctuations. When using the Cl^- concentrations greater than 1,700 mg/L (*i.e.* TDS > 4,400 mg/), the wind-ED system was seen to cycle off due the occurrence of extreme fluctuations and intermittencies in the wind regime, causing the desalination process to be delayed. The SEC of the process changed linearly with regards to the feed salt concentration, increasing from 1.48 kWh/m^3 with the feed of 2,400 mg/L to 3.98 kWh/m^3 for the feed of 5,700 mg/L.

With increasing the Cl^- concentration in the feed solution, the mole fraction of the other anions in the mixture (*i.e.* F^-, NO_3^- and SO_4^{2-}) and correspondingly with that their transport numbers decreased in the global electrolyte-membrane system. Consequently, it caused reduction in the removal rates of F^-, NO_3^- and SO_4^{2-} from the diluate stream when increased the Cl^- concentration.

Chapter 9

Conclusions and future work

"On the one hand, the world needs to provide adequate and sustainable access to the more than 1.3 billion people who still lack electricity and to the more than 700 million people who lack an improved water supply today – which basically means lifting the "bottom billion" out of poverty; and, on the other hand, to keep up with the growing demand for both water and energy associated with population growth, rapid urbanization and economic development in a context of increased scarcity of natural resources, pollution, degraded ecosystems, climate change and regulation of greenhouse gas emissions….. In fact there is an urgent need to address water and energy challenges in an integrated and coordinated manner to ensure the sustainability of both water and energy services." (*Michel Jarraud, the Chair of UN-Water, January 2014)*

Renewable energy powered membrane systems are considered as sustainable, energy efficient and reliable solutions for tackling the emerging issue of drinking water scarcity [10, 26, 28, 79]. Development and implementation of such technologies is of particular importance to remote arid areas of developing countries where people suffer the most from the lack of access to safe potable water. In this research a directly coupled wind – electrodialysis system without energy storage (Wind-ED) was developed for the first time. Modularity, sustainability and above all suitability for the practical use in off-grid locations were the main motivations and design

objectives. The direct coupling of wind energy with membranes was proposed as a solution to reduce the system costs as well as technical drawbacks associated with using intermediate energy storage systems such as acid-lead batteries, super-capacitors and flywheels.

The overall objectives of this research were to:

1. Investigate the impacts of energy fluctuations, in the uniform and well controlled forms of short voltage pulses applied across the membrane system, on ion transport, concentration polarisation (CP), water production and energy consumption aspects.

2. Determine the water production and energy consumption of the wind-membrane system when operated under both controlled and real i) steady state, ii) fluctuating and iii) intermittent wind speed conditions.

3. Study the combined effects of wind speed fluctuations and the ED stack resistance (*i.e.* flow rate and initial feed concentration) on the competitive removal of inorganic contaminants (fluoride, chloride, nitrate and sulphate) from artificial brackish groundwater.

9.1 Conclusions

Pulsed electric field assisted electrodialysis (Pulsed-ED)

The impacts of voltage pulses on ion transport and water dissociation phenomena were investigated over a wide range of voltages (15-50 V DC), frequencies (0.05 - 10 Hz) and duty cycles (20-80%). The desalination tests were carried out under both constant and pulsed voltages, using feed of 5,000 mg/L NaCl. The aims were to i) determine the potential of electric field pulsation on minimising concentration polarisation (CP) in both under and over limiting current density regimes and, ii) to examine the energy performance and desalination behaviour of the membrane system when operated with fluctuating power inputs. The latter was believed to be instrumental to the understanding the impacts of more complex forms of energy fluctuations on the ED behaviour when the membrane system was connected to the renewable energy source in the subsequent stages of the project.

In the sub-limiting regime, CP had a negligible impact on ED performance and thus applying pulsed voltage led to significantly reduced water production. This was attributed to the periodic delays introduced by the off-periods of the pulse regime during the desalination process. However, the energy efficiency of the process was similar to that of the conventional process at constant potential, suggesting that ED is an energetically robust system to be directly coupled with fluctuating energy sources. In the limiting current region, both water dissociation and desalination time decreased noticeably when increasing the frequency. Optimizing the duty cycle helped to prevent from significant water dissociation even when operated in the limiting current density regime. When desalinating a brackish feed salinity of 5,000 mg/L NaCl at 2 L/min and at voltages of 30 and 50 V, experimental findings showed negligible water dissociation at optimum frequency of 5 Hz and duty cycles below 50 and 40%, respectively. Thus, by using an optimally selected pulse regime, it was found to be possible to safely operate above the limiting current density (j_{lim}), obtain higher water production with negligible water splitting, and at only slightly higher energetic cost compared to operating below j_{lim}. The increase in the energy consumption was solely due to operating at higher voltages and was independent of the mode of operation, this being either pulsed or conventional-constant voltage.

Wind-ED: effects of wind speed fluctuations

Experiments were carried out over a wide range of wind speeds (2 – 10 m/s), turbulence intensities (a parameter directly linked to the amplitudes of fluctuations) (TI: 0 – 0.6), and periods of oscillation (0- 180 s). The aim was to determine the impacts of wind speed and its fluctuations on the quality and quantity of water produced as well as the impacts on the energy consumption for the desalination process. SEC and water production were seen to increase with the wind speed, when operated below the rated wind speed (v_{rated} 7.9 – 8.4 m/s). At wind speeds above v_{rated} the power output from the wind turbine levelled off and resulted in both relatively stable SEC and water production.

The impact of wind speed fluctuations on the desalination was found to be insignificant up to a TI of 0.4. Increasing TI to levels above 0.4 led to regular shifting to the rated conditions, causing the power output from the turbine to level off and

thus water production to diminish. The desalination performance declined under high turbulence intensity fluctuations (TIs ≥ 0.5) and long periods of oscillation (> 40 s), as the wind-ED system periodically cycled off in response to operation below the cut-in wind speed of the wind turbine ($v_{cut\text{-}in}$: ~ 2 m/s). The off-cycling of the system caused significant delays in the desalination process, and thus resulted in reduced water production. It was concluded that the main challenge in direct coupling of ED to a wind resource was not the magnitude of the fluctuations but the impact of the power cycling off during long periods of oscillation and lengthy periods of no wind. The interesting fact was that opposite to the water production, the SEC of the process remained relatively unaffected by the fluctuations and intermittencies in the wind resource. This verified the results obtained from the pulsed-ED experiments regarding the energetic solidity of the ED system against extreme energy fluctuations.

Wind-ED: effects of wind speed intermittency

To determine the impacts of wind speed intermittency on the specific energy consumption (SEC) and the water production of the wind-ED system, desalination tests were carried out over a range of wind ON/OFF cycling frequencies (0.003-0.1 Hz), OFF-wind periods (0-180 s) and peak wind speeds (3-8 m/s). An increase in the ON/OFF cycling frequency caused reduction in the average power production by the wind turbine and ultimately led to less water being produced in a given period of time. The water production was more adversely affected by the increase in the OFF-wind period. With OFF-wind periods longer than 10 s the rotor got sufficient time to slow down effectively (ω_r < 1 Hz); hence it caused the wind-ED system to cycle off. The regular cycling off of the wind-ED system caused the desalination rate and correspondingly with that the water production to decrease significantly. Although both the ON/OFF cycling frequency and the OFF-wind period influenced the power production by the wind turbine, their impacts were not significant to cause a considerable change in the SEC of the desalination process.

The transient time required for the rotor to fully accelerate following a sudden increase in the wind speed (t_{twi}) was shown to decrease with an increase in the peak wind speed. This led to an increase in the mean operating power for the system

throughout the process. The decrease in the acceleration time (t_{twi}) and an increase in the available energy in the wind resource at higher peak wind speeds (8 m/s) resulted in both increased SEC and water production.

Wind-ED: operation with real wind conditions using artificial brackish groundwater

The effects of fluctuations on the competitive transport of the ions of interest (F^-, Cl^-, NO_3^- and SO_4^{2-}) from artificial brackish water (approximate TDS: 4350 mg/L) was investigated, using different sets of real wind data as inputs to the wind turbine simulator. The ion removal, independent of the wind regime tested, followed this order: $NO_3^- \geq Cl^- > F^- > SO_4^{2-}$. The competitive removal of the ions was linked to the differences between their physicochemical properties. Ions with smaller Gibbs free energy of hydration (*i.e.* Cl^-, NO_3^-) were shown to remove more preferentially, as they required less energy to be stripped from the water molecules in their surroundings before being transported into the membrane structure. The lower transport of the divalent ions (*i.e.* SO_4^{2-}) compared to the monovalent ions (*i.e.* F^-, Cl^-, NO_3^-) was linked not only to their significantly higher hydration energy but also to their larger valence number, causing their share in transferring electric charge across the membrane to be smaller than the monovalent ions.

Specific selectivity diminished with increasing the mean wind speed. This was attributed to the current density being larger when operated at the higher wind speed; causing the selectivity of the ion-exchange membrane to be further reduced by the growth in the concentration polarisation. Increase in the wind speed fluctuations resulted in frequent disruptions of the concentration profiles within the boundary layer, thus it led to some improvement in the relative transport of the single charged ions (*e.g.* NO_3^-) compared to the double charged ions (*e.g.* SO_4^{2-}).

Wind-ED: effects of flow rate and feed concentration

Power production of the wind turbine was found to be dependent on not only the available wind energy but also the resistance of the load (*i.e.* the ED stack) directly connected to the turbine. Increasing the feed concentration and the flow rate resulted in reduced resistance of the ED stack (R_{stack}), which inversely influenced the current induction counter torque force applied on the shaft of the wind turbine and caused

the rotor to spin at a lower angular velocity. This led to increased sensitivity of the wind-ED system to wind speed fluctuations (*e.g.* system cycled off due to extreme fluctuations and intermittencies with low TDS feed concentration of 2,400mg/L) and hence a reduction of desalination performance.

Increased flow rate and resulting shrinkage of the boundary layer's thickness caused the concentration profiles at the solution-membrane interface to become steeper. This favoured the transport of ions with the highest diffusion coefficients in the mixture (*i.e.* Cl^- and NO_3^-). Decreased flow rate favoured the transport of ions with larger valence numbers and higher electric mobility inside the electrolyte (*i.e.* SO_4^{2-}); as the former property governed the faster migration of SO_4^{2-} ions through the thick boundary layer and the latter property assisted with the improved affinity of the ion-exchange membrane to SO_4^{2-} ions compared to the monovalent anions in the mixture. Increasing the feed concentration of Cl^- led to reduced transport numbers for the other anions in the mixture and significantly reducing their removal rate.

Increasing the feed concentration had a direct influence on the energy consumption of the process. The SEC increased from 1.48 to 3.98 kWh/m^3 when the feed solution increased from 2,400 to 5,700 mg/L TDS. Inversely, the water production decreased 40%, from 3.57 to 2.12 m^3/m^{2}day, when the feed concentration increased from 2,400 to 5,700 mg/L TDS.

Advantages of ED over other common desalination technologies for coupling with RE sources

Based on the findings from this research, certain advantages for ED, in comparison with other common desalination technologies, for direct coupling to renewable energy (RE) sources can be deduced as specified in points 1-4, below:

1- *Flexibility in operation with any amount of available energy*

Common desalination technologies (*i.e.* RO, TVC, MED and MSF) [99, 245-247] often require a minimum level of energy to perform satisfactorily; which limits the employment of such technologies in direct coupling with RE systems for desalination in locations where sufficient RE source may not be available throughout the year. To

address this problem some studies have proposed the use of energy storage systems [81, 83, 208]. However, using energy storage systems increases both the capital and maintenance costs of the operation and also reduces the sustainability of the technology [56, 57]. Therefore, a better approach would be to use an energetically flexible technology, such as ED, that can operate more suitably in direct connection to RE sources with no need for energy storage devices. As shown in this research, in terms of a safe operating window, the wind-membrane system produced good quality drinking water (< 600 mg/L NaCl) over the wide range of wind speeds (2 – 10 m/s) and regardless of the initial feed concentration or the flow rate used for the experiments. Although the rate of the clean water production was significantly influenced by the available energy in the wind resource, the desalination performance by the membrane system did not stop due to having low wind speed unless when the wind turbine itself cycled off.

2- *Robustness with respect to fluctuations and intermittencies in the RE source*

Extreme fluctuations were shown to lead to reduced permeate quality and increased SEC in RO systems [99, 248, 249]. The use of temporary energy storage systems (*e.g.* super capacitors) and energy buffering devices (*e.g.* flywheels) were proposed in some studies, as useful methods for governing uninterrupted operation of the desalination technologies powered from fluctuating energy sources [67, 84, 94, 208]. However, as mentioned before the use of energy storage systems is not favourable, as it leads to increased capital and maintenance costs as well as reduced sustainability. Using ED may again be a solution, as the SEC of this technique when directly powered from a wind resource was found to be relatively unaffected by fluctuations of any size (*i.e.* wind energy exhibits the largest fluctuations among the all REs). Therefore, ED can be introduced as an energetically robust desalination system, suitable for direct coupling with renewable energy sources.

3- *Mechanical Solidity against energy fluctuations*

Energy fluctuations in some studies were suggested to cause reduction in the lifetime and efficiency of the pumps [250, 251] and produce fatigue damage to the membrane polymers [81]. Such problems can be significantly detrimental to the long term

operation of pressure driven technologies such as reverse osmosis. However for ED, since it is not a pressure driven process the ion-exchange membranes are expected to remain relatively unaffected by the fluctuations. Moreover, if the pumps of ED are powered by renewable energies, because they often operate at very low pressures, they are expected to be much less influenced by the fluctuations in the RE resource, compared to the pumps in a RO system. It is important to note that the stated expectations in this section are yet speculative, based on available knowledge of ED systems and their normal operating conditions. therefore, yet further research on the wind-ED system mechanical stability over a long period of operation is required for speculations stated in this section to be either proved or discarded (possible future research).

4- *Specific energy consumption (SEC)*

SEC of the ED process increased with the wind speed, from 2.52 at 2 m/s to 4.15 kWh/m^3 at 10 m/s, when desalinated a feed solution of 5,000 mg/L NaCl. The SEC values obtained were within the range reported in the literature for the ED process (2.64 and 5.5 kWh/m^3) in desalinating brackish waters containing 2,500 – 5,000 mg/L total dissolved solids (TDS) [10, 211]. These SEC values were also very close to the minimum SEC reported by Park *et al.* (2.8 kWh/m^3) for desalinating feeds of 2,500 – 5,500 mg/L TDS, using a directly powered wind-reverse osmosis system (wind-RO) [14]. A comparison between the obtained SEC values in this study and the ones reported in the literature for other common desalination techniques suggests that ED is energetically competitive with RO (1.5-3.0 kWh/m^3) and significantly more efficient than common distillation based desalination systems (*i.e.* MSF: 19.5-27.3 kWh/m^3, MED: 14.5-21.6 kWh/m^3 and VC: 7.0-16.2 kWh/m^3) for treating brackish groundwater containing 5,000 mg/L or lower TDS [10, 11, 191, 192].

The overall conclusion of this research is that the wind-ED system is an energetically robust and technically reliable off-grid desalination method for the use in brackish water desalination applications in water stressed remote regions in both developing and developed countries.

9.2 Future work

Some interesting research questions were raised over the course of this PhD study. Addressing these questions was beyond the scope of this thesis, but they would certainly benefit from further investigation.

In this research only the ED stack was powered by the RE resource, while the pumps in all the tests were operated with constant voltages, using a conventional power supply. This specific configuration was chosen to keep the flow rates steady in both the diluate and concentrate channels during the desalination process and hence to avoid possible complexities associated with flow instabilities inside the ED stack [252]. Now that the full scope of the wind-ED system operation under a wide range of wind speed conditions has been investigated, it would be valuable to take a step forward and use the wind energy to power the pumps as well as the ED stack in order to investigate the impacts of wind speed fluctuations on i) flow mixing and concentration polarisation inside the ED stack, ii) ion transport phenomena with a particular attention to diffusion and conversion processes and iii) mechanical behaviours of the pumps.

Ortiz *et al.* [69, 70, 169] developed a mathematical model using the experimental data obtained from the operation of a solar energy powered electrodialysis system (PV-ED) for brackish water desalination. This model made simulating the behaviour of the PV-ED system under various operating and meteorological conditions possible; hence it was considered as a useful tool for optimising the design and operation of the solar powered membrane system. From the design and operation point of view, it would be valuable to develop a similar mathematical model for the wind-ED system using the experimental data obtained from the tests carried out in this research under various wind conditions, operating parameters (*i.e.* flow rates and feed concentrations) and with different feed mixtures. Such a model will be instrumental to the scaling up of the wind-ED system and optimising the design of the system according to the meteorological conditions, quality and quantity of available brackish water and number of the inhabitants in the remote region for which the off-grid desalination system is meant to be built.

From the practical point of view, it would be also interesting to take the wind-ED system for long term field trials in remote regions of both developed and developing countries to examine the desalination behaviour of the system under real wind speed conditions and with real brackish groundwater mixtures. Such tests can be repeated in different locations and in different seasons to develop a comprehensive database for the use at a later time to optimise the wind-ED system design and to improve any mathematical model that may be developed to simulate the system operation (like the one explained above). Moreover, findings obtained from such field trials can be used to verify the tests carried out under controlled laboratory conditions in this PhD research.

The rapidly increasing concerns regarding the environmental degradation and natural resource depletion caused by desalination technologies necessitates detailed and systematic research of the environmental sustainability of these systems [253-256]. In this sprit, it would be valuable to develop a Life Cycle Assessment (LCA) model for the wind-ED system to evaluate the environmental burden of this technology in comparison with other desalination techniques. Such a LCA model at the minimum must take into account the natural resource consumption and emission discharge (*e.g.* CO2, NOx, SOX and VOC) associated with i) the wind-ED system construction and assembly, ii) membrane fabrication, iii) the wind-ED system operation, iv) maintenance and replacement of the components with limited life time, most importantly the ion-exchange membranes and the electrodes, v) waste management (*e.g.* brine disposal, chemical residuals and used membranes), and vi) transport of the infrastructure to the remote region where the wind-ED system is meant to be sited. Having an up to date financial database available, the LCA model can be combined with a detailed economic input-output (EIO) model that takes into account the cost associated with each of the processes mentioned above.

The possibility of fouling mitigation by the means of applying voltage/current pulses (*i.e.* uniform energy fluctuations) to the ED system was highlighted in some studies [34, 63, 66]. Using current pulses with 1:1 ON to OFF period ratio, total pulse length of 20 s and the peak current density of 40 mA/cm^2 was suggested by Cifuentes-Araya *et al.* [65] as an optimum pulse regime for minimising the formation of

magnesium/calcium based foulants on the surface of cation-exchange membranes. The frequency of the optimum pulse regime suggested in this study is within the range often observed in real wind speed fluctuations [178]. Therefore, it may be valuable to conduct a series of desalination tests using the wind-ED system and feed solutions containing foulants to determine whether or not wind speed fluctuations would be beneficial for controlling the fouling phenomena in ED processes. Indeed, I expect that operating under highly turbulent wind conditions with short oscillation periods (< 15 s) as well as intermittent wind conditions with small OFF-periods (< 10 s) can potentially results in significant reductions of fouling formation on the surface of the ion-exchange membranes!

Appendix A

Pulse amplifier electric circuit

Appendix A includes the electric circuit diagram of the pulse amplifier, designed by Graham Hunter (Heriot-Watt University). The pulse amplifier was employed to couple the outputs from the conventional power supply with the frequencies and duty cycles produced by the pulse generator, in order to create pulse functions with desired peak voltages for each experiment (Chapter 4). The output from the pulse amplifier was then inserted directly as the input to the ED stack.

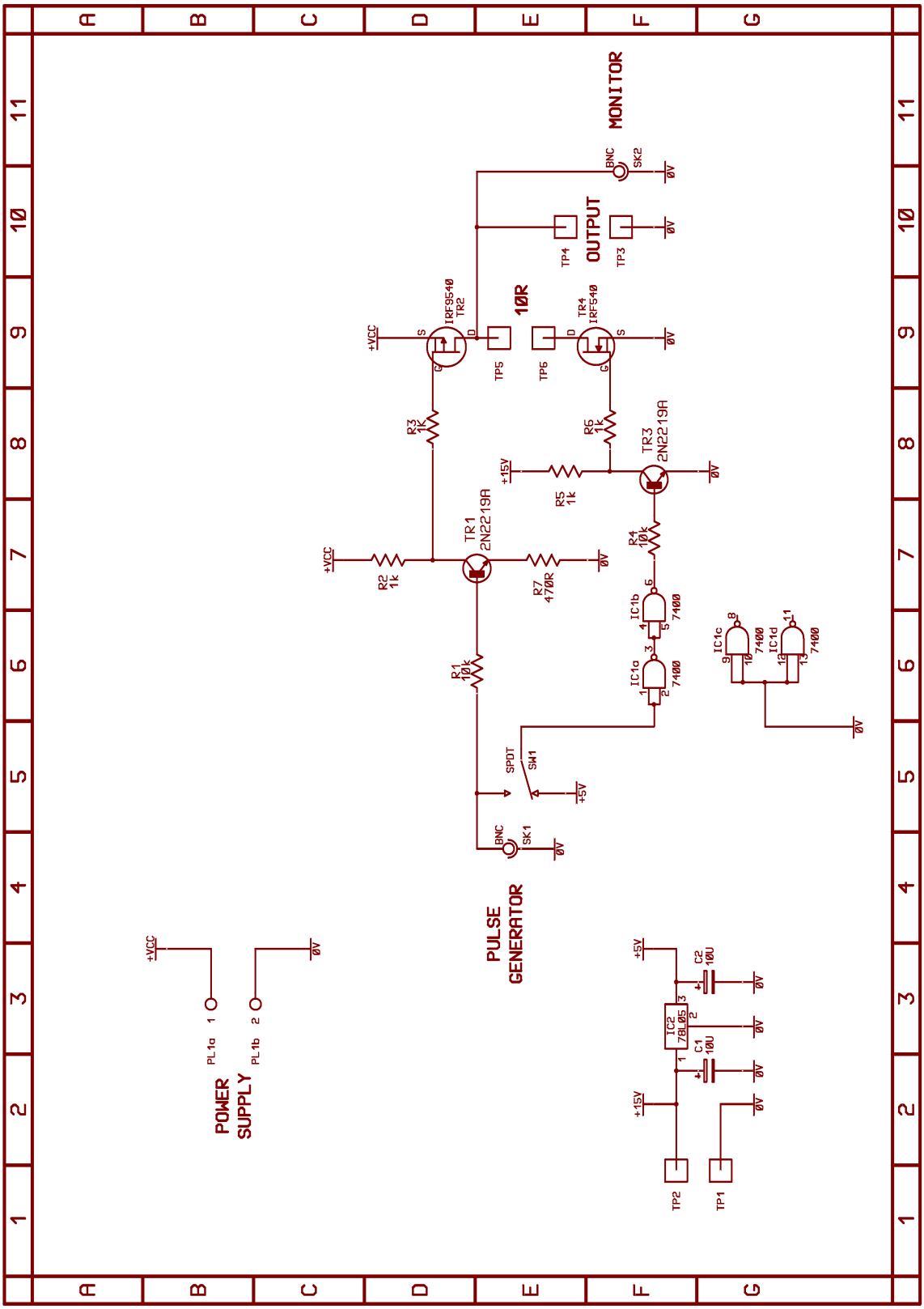

Figure A.1 The pulse amplifier electric circuit diagram.

Appendix B

Calibration curves for analytical instruments

Example calibration curves for the analytical devices used in this research are given in this appendix: electric conductivity (Figure B.1) and ion chromatography (IC) (Figure B.2). These calibration curves can vary slightly with a change in, for example, sample matrices (*e.g.* ionic compositions, pH and the purity of the water), equipment condition (*e.g.* time interval of maintenance/cleaning), preparation of the analytical solutions (*e.g.* eluents and buffers for the IC) and environmental factors (*e.g.* room temperature). Therefore, to ensure the validity of the calibration curves and minimise the impacts of above mentioned factors on the accuracy of the sample analysis the standard calibration solutions were always made fresh on the same day of sample analysis. R-square of the calibration curves used for sample analysis were greater than 0.99.

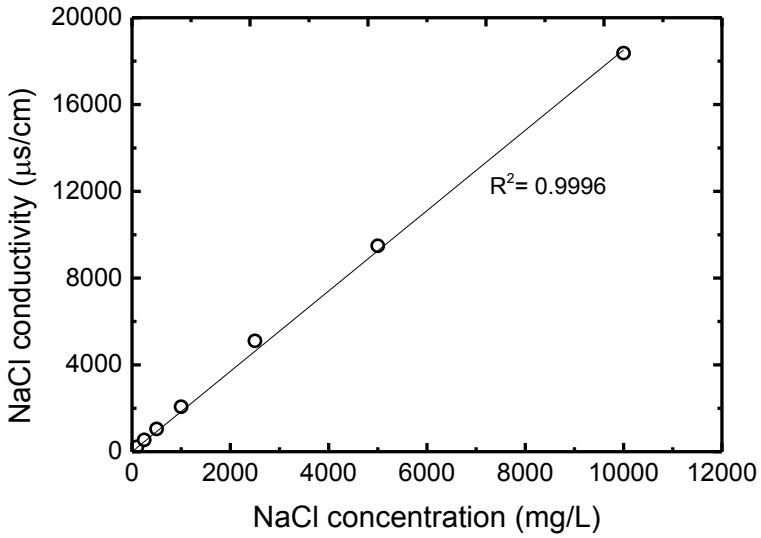

Figure B.1 NaCl calibration curve made using the electric conductivity meter at 19.9 ± 0.4 ºC.

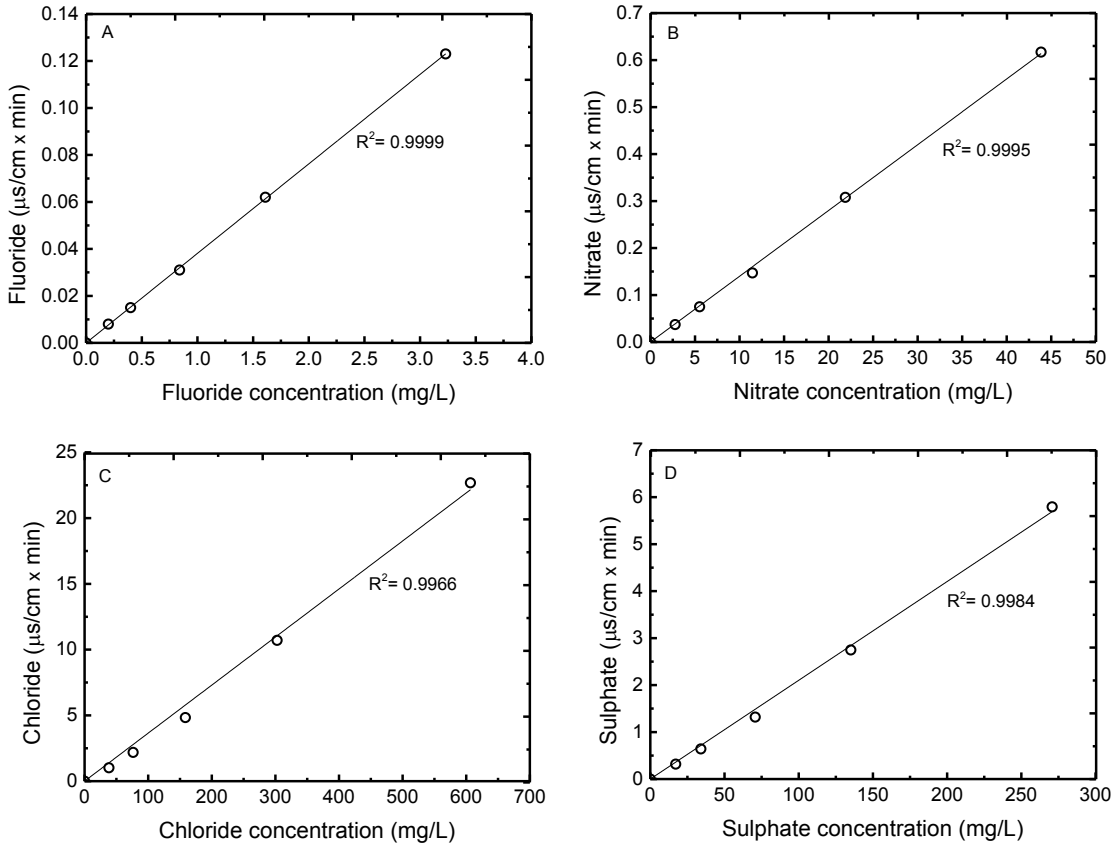

Figure B.2 Calibration curves, generated automatically by the ion chromatograph device, for fluoride (A), nitrate (B), chloride (C) and sulphate (D) at 21.3 ºC.

As explained in Chapter 3, blanks (*i.e.* ultrapure water samples) were analysed at specific intervals during the sample analysis (*i.e.* after every 10 sample) to assess the quality of the background solution as well as to determine the instrument contamination. A series of example results obtained from blank analysis are reported in Table B.1. The detection limit of the IC instrument for each ion can be calculated by multiplying the standard deviation of the results obtained from analysing the blank solutions (n > 10) by 3.

Table B.1 Blank and detection error analysis (N/D: not detected)

Blank	F^-	Cl^-	NO_3^-	SO_4^{2-}
	mg/L			
1	N/D	0.022	0.016	0.07
2	N/D	0.056	0.008	0.042
3	N/D	N/D	0.026	0.016
4	0.009	0.01	N/D	0.008
5	N/D	0.018	0.019	0.074
6	N/D	N/D	0.014	0.006
7	0.007	0.094	0.009	0.132
8	N/D	0.013	N/D	0.083
9	0.004	0.02	N/D	N/D
10	N/D	N/D	N/D	N/D
11	0.178	N/D	N/D	N/D
12	N/D	N/D	N/D	N/D
13	0.005	0.457		0.299
14	N/D	N/D	N/D	N/D
15	N/D	N/D	N/D	N/D
16	0.011	0.579	0.059	N/D
Average Detection	0.01	0.08	0.01	0.05
Standard Deviation (SD)	0.04	0.17	0.02	0.08
Detection limit = SD * 3	**0.1**	**0.5**	**0.1**	**0.2**

Appendix C

Limiting current density

Limiting current density (j_{lim}) values were determined experimentally, using the Cowan and Brown method, for the feeds of 500 and 5,000 mg/L NaCl solution and over a wide range of flow rates (2-11 L/min) [9]. 5,000 and 500 mg/L NaCl correspond to the two extents of concentrations, the start and end points respectively, in the desalination experiments carried out in the Chapter 4-6. The experimentally obtained j_{lim} values, together with the constants listed in Table C.1, were used as inputs to the Eqs. 2.13 and 2.14 to theoretically calculate the boundary layer thickness (δ) and mass transfer coefficient of the process (k_m).

Table C.1 Constants

Parameter	Unit	Value	
NaCl diffusion coefficient (D_i)	$(m^2/s) \cdot 10^{-9}$	1.67	[257]
Chloride transport number in the solution (t_i^b)	-	0.39	[258]
Chloride transport number in AEM (t_i^m)	-	0.98	[259]
Valence (z_i)	-	1	
Faraday constant (F)	C/mol	96,485	

The results for these j_{lim} measurements plus δ and k_m calculations are reported in the Table C.2.

Table C.2 experimentally measured j_{lim} and theoretically clculated δ and k_m for feeds of 500 and 5000 mg/L NaCl over the flow rate range of 2-111 m/s.

	500 mg/L NaCl		
Flow rate	**Limiting current density**	**Mass transfer coefficient**	**Nernst layer thickness**
Q	j_{lim}	$K_m \times 10^{-5}$	$\delta \times 10\text{-}5$
L/min	**A/m²**	**m/s**	**m**
2	42.83	3.00	5.55
5	64	4.49	3.71
7	96	6.74	2.47
9	110	7.72	2.16
11	129	9.06	1.84

	5,000 mg/L NaCl		
Flow rate	**Limiting current density**	**Mass transfer coefficient**	**Nernst layer thickness**
Q	j_{lim}	$K_m \times 10^{-5}$	$\delta \times 10\text{-}5$
L/min	**A/m²**	**m/s**	**m**
2	450	3.16	5.28
5	677	4.75	3.51
7	801	5.62	2.96
9	908	6.38	2.61
11	1,004	7.05	2.36

Appendix D

Supplementary data on the wind-ED system operation with different flow rates and feed concentrations

Appendix D presents supplementary data for Chapters 5, 7 and 8, showing:

i. The impacts of oscillation periods on the wind-ED system operation, with 10,000 mg/L NaCl solution used as feed to the membrane system (Figure D.1),

ii. The impacts of wind speed fluctuations on the water production and SEC of the desalination process using the wind-ED system, with 10,000 mg/L NaCl solution used as feed to the membrane system (Figure D.2).

iii. Specific selectivity of F^- (A), Cl^- (B), and SO_4^{2-} (C) relative to NO_3^- during the desalination processes conducted under different wind regimes at 2 L/min (Figure D.3).

iv. The impacts of flow rate (2-10 L/min) on the SEC and water production of the wind-ED system when operated under real wind speed conditions (v_{avr}: 5.93 – 7.22 m/s, TI: 0.01 – 0.18); feed solutions: 5,000 an 10,000 mg/L NaCl (Figure D.4).

v. The effect of flow rate (2 and 7 L/min) on the competitive removal of ions F^-, Cl^-, SO_4^{2-} and NO_3^- from artificial brackish groundwater under different wind regimes (Figure D.5 and D.6)

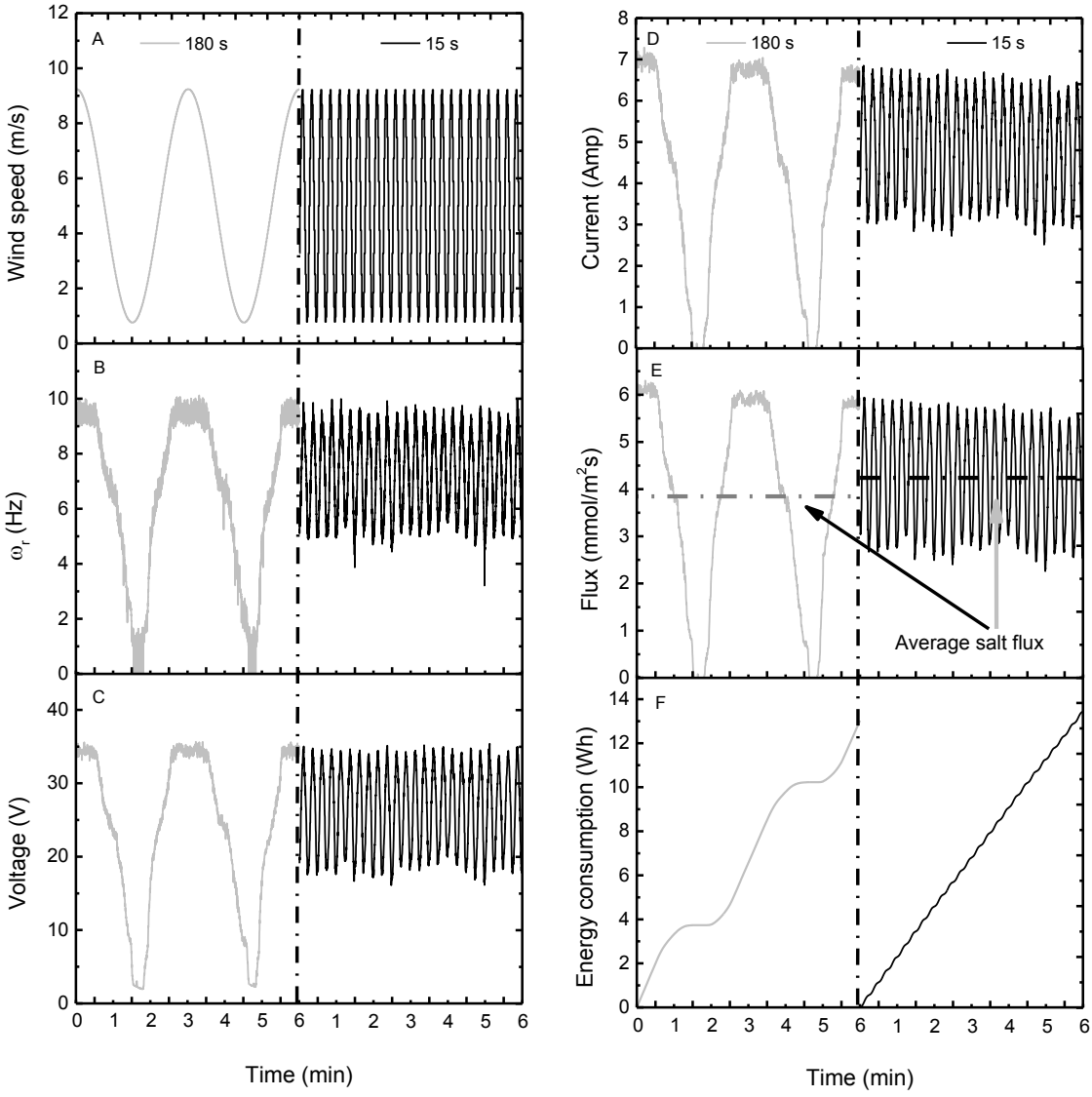

Figure D.1 Wind-ED system performance during the first 6 minutes of the desalination tests using an average wind speed of 5 m/s at TI of 0.6 and oscillation periods of 180 s and 15 s; the initial feed concentration of 10,000 mg/L NaCl and the flow rate of 7 L/min. (supplementary data for section 5.4.3, Chapter 5); (mode of operation: batch).

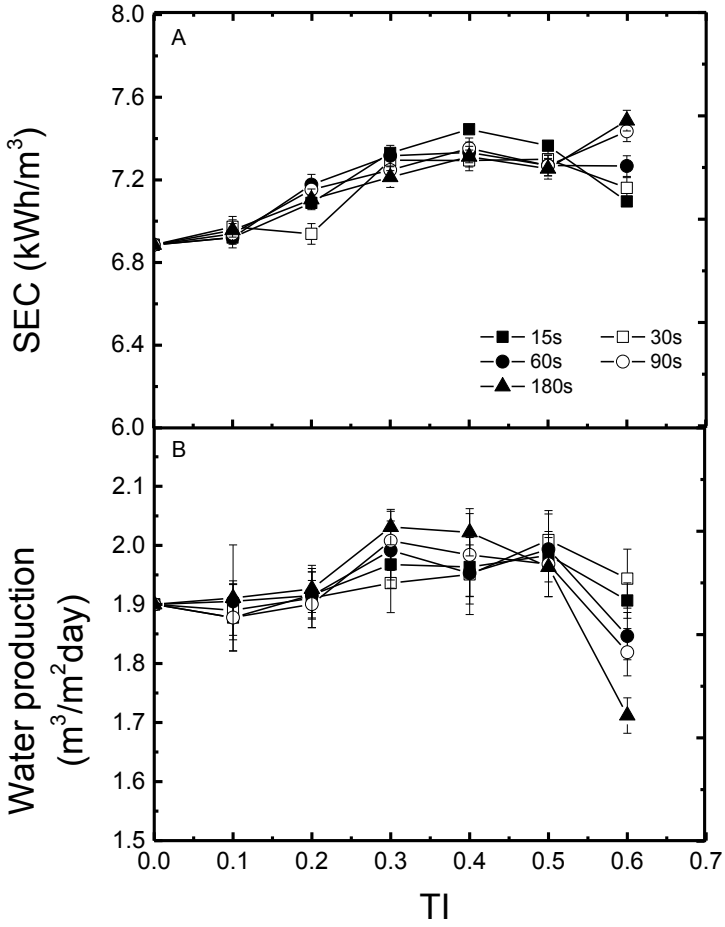

Figure D.2 SEC (A) and water production (B) over a range of wind speed turbulence intensity (TI): 0-0.6 and oscillation periods: 15-180s in desalinating a feed of 10,000 mg/L NaCl at average wind speed of 5 m/s and flow rate of 7 L/min (supplementary data for section 5.4.4, Chapter 5); (mode of operation: batch).

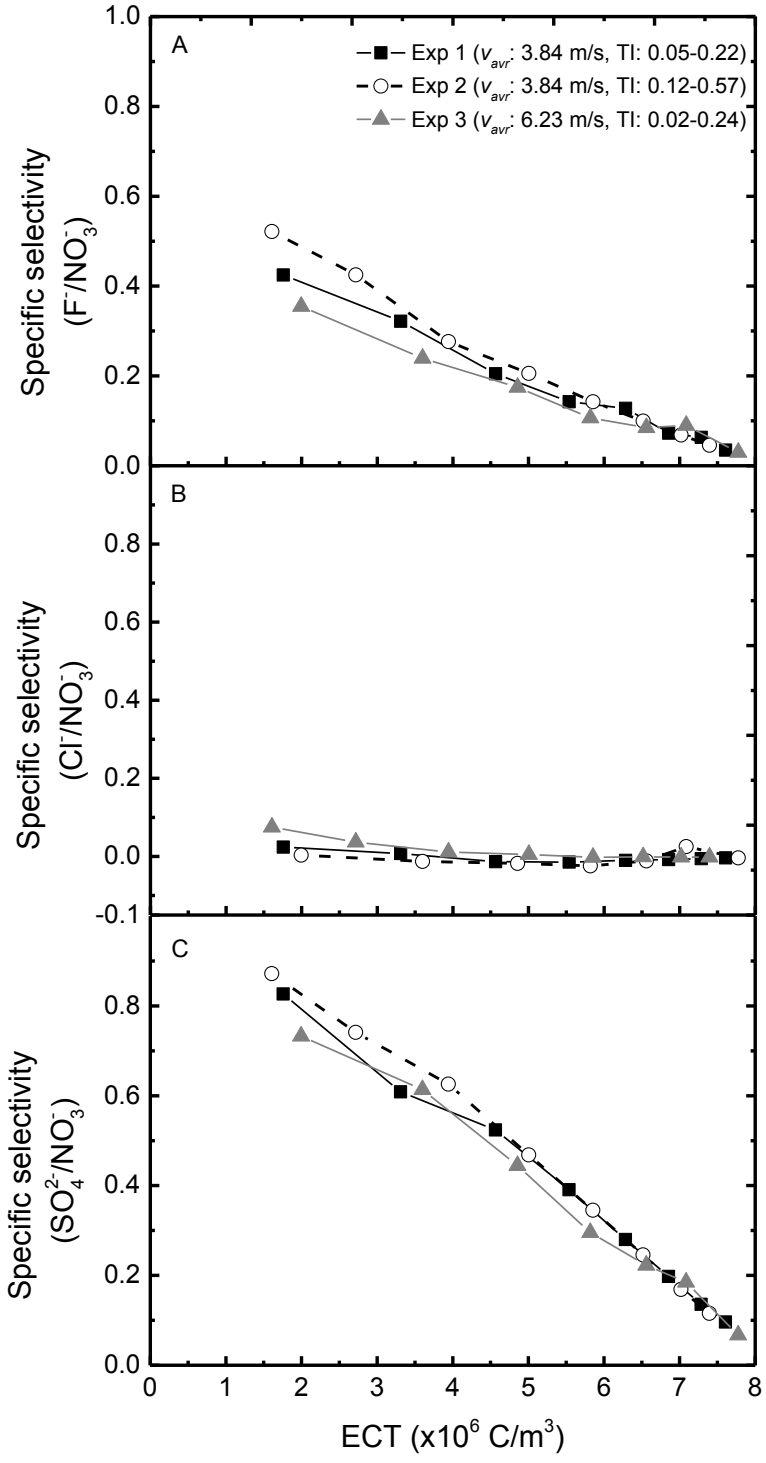

Figure D.3 Specific selectivity of F^- (A), Cl^- (B), and SO_4^{2-} (C) relative to NO_3^- during the desalination processes conducted under different wind regimes at 2 L/min in the Experiments 1-3; (mode of operation: batch).

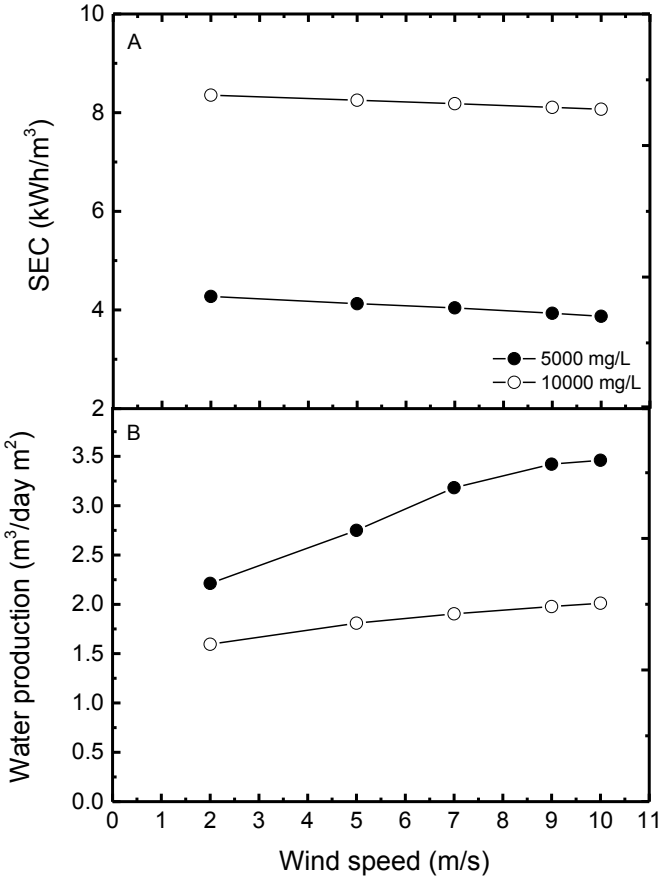

Figure D.4 SEC (A) and water production (B) in desalinating feeds of 5,000 and 10,000 mg/L NaCl with the average wind speed of 5.93 – 7.22 m/s and the turbulence intensity (TI) of 0.01 – 0.18 and at different flow rates: 2-10 m/s (supplementary data for section 8.3.1, Chapter 8); (mode of operation: batch).

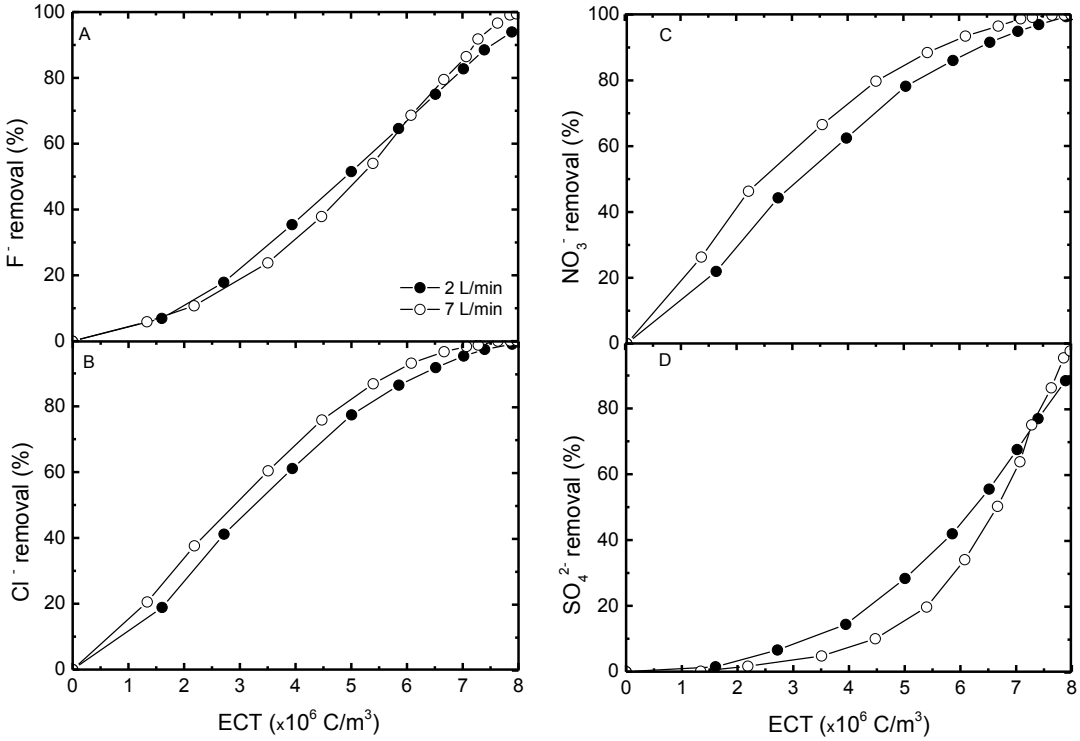

Figure D.5 F^- (A), Cl^- (B), NO_3^- (C) and SO_4^{2-} (D) removal from the diluate stream vs electric charge transferred across the membranes (ECT) in desalinating from synthetic brackish water containing 4625 mg/L TDS using an average wind speed of 3.83 m/s and the turbulence intensity (TI) of 0.12 – 0.57 at two different flow rates of 2 and 7 L/min; (mode of operation: batch).

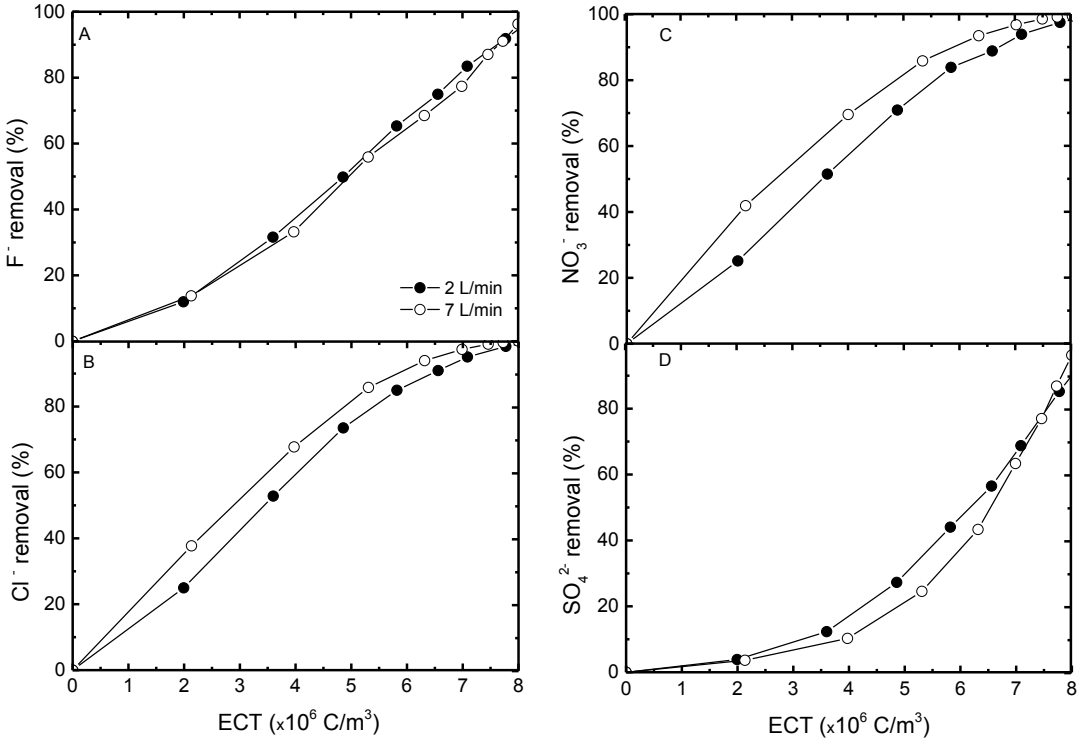

Figure D.6 F^- (A), Cl^- (B), NO_3^- (C) and SO_4^{2-} (D) removal from the diluate stream vs electric charge transferred across the membranes (ECT) in desalinating from synthetic brackish water containing 4625 mg/L TDS using an average wind speed of 6.23 m/s and the turbulence intensity (TI) of 0.02 – 0.24 at two different flow rates of 2 and 7 L/min; (mode of operation: batch).

References

1. Vorosmarty, C.J., et al., *Global threats to human water security and river biodiversity.* Nature, 2010. **467**(7315): p. 555-561.

2. WHO, *Water quality and health strategy 2013-2020*, 2013, World Health Organisation: Geneva.

3. WHO/UNICEF, *Progress on Sanitation and Drinking-Water: 2013 Update*, 2013, WHO/UNICEF Joint Monitoring Programme for Water Supply and Sanitation: WHO, Geneva and UNICEF, New York.

4. IEA, *World Energy Outlook 2011*. 2011, Paris, France: International Energy Agency.

5. Mahmoudi, H., et al., *Assessment of wind energy to power solar brackish water greenhouse desalination units: A case study from Algeria.* Renewable and Sustainable Energy Reviews, 2009. **13**(8): p. 2149-2155.

6. Rossiter, H.M.A., et al., *Chemical drinking water quality in Ghana: Water costs and scope for advanced treatment.* Science of The Total Environment, 2010. **408**(11): p. 2378-2386.

7. Schäfer, A.I., et al., *Physico-chemical water quality in Ghana: Prospects for water supply technology implementation.* Desalination, 2009. **248**(1–3): p. 193-203.

8. Ayoub, J. and R. Alward, *Water requirements and remote arid areas: the need for small-scale desalination.* Desalination, 1996. **107**(2): p. 131-147.

9. Raucher, R., et al., *Guidelines for Implementing Seawater and Brackish Water Desalination Facilities*, 2010, Water Research Foundation and Arsenic Water Technology.

10. Al-Karaghouli, A. and L.L. Kazmerski, *Energy consumption and water production cost of conventional and renewable-energy-powered desalination processes.* Renewable and Sustainable Energy Reviews, 2013. **24**(0): p. 343-356.

11. Al-Karaghouli, A., D. Renne, and L.L. Kazmerski, *Solar and wind opportunities for water desalination in the Arab regions.* Renewable & Sustainable Energy Reviews, 2009. **13**(9): p. 2397-2407.

12. Gude, V.G., N. Nirmalakhandan, and S. Deng, *Renewable and sustainable approaches for desalination.* Renewable and Sustainable Energy Reviews, 2010. **14**(9): p. 2641-2654.

13. Shatat, M., M. Worall, and S. Riffat, *Opportunities for solar water desalination worldwide: Review.* Sustainable Cities and Society, 2013. **9**(0): p. 67-80.

14. Park, G.L., A.I. Schäfer, and B.S. Richards, *Renewable energy powered membrane technology: The effect of wind speed fluctuations on the performance of a wind-powered membrane system for brackish water desalination.* Journal of Membrane Science, 2011. **370**(1–2): p. 34-44.

15. Richards, L.A., B.S. Richards, and A.I. Schäfer, *Renewable energy powered membrane technology: Salt and inorganic contaminant removal by nanofiltration/reverse osmosis.* Journal of Membrane Science, 2011. **369**(1–2): p. 188-195.

16. Schäfer, A. Broeckmann, and Richards, *Renewable Energy Powered Membrane Technology. 1. Development and Characterization of a Photovoltaic Hybrid Membrane System.* Environmental Science & Technology, 2006. **41**(3): p. 998-1003.

17. Bassett, R.L., et al., *Identification of Groundwater Solute Sources Using Boron Isotopic Composition.* Environmental Science & Technology, 1995. **29**(12): p. 2915-2922.

18. Favre-Réguillon, A., et al., *Selective removal of dissolved uranium in drinking water by nanofiltration.* Water Research, 2008. **42**(4–5): p. 1160-1166.

19. Ergun, E., et al., *Electrodialytic removal of fluoride from water: Effects of process parameters and accompanying anions.* Separation and Purification Technology, 2008. **64**(2): p. 147-153.

20. European Union, *Council Directive 98/83/EC of 3 November 1998 on the quality of water intended for human consumption.* Official Journal L 330, 1998: p. 32-54.

21. WHO, *Guidelines for drinking-water quality.* 2011.

22. Tamer, M.N., et al., *Osteosclerosis due to endemic fluorosis.* Science of The Total Environment, 2007. **373**(1): p. 43-48.

23. El Midaoui, A., et al., *Optimization of nitrate removal operation from ground water by electrodialysis.* Separation and Purification Technology, 2002. **29**(3): p. 235-244.

24. Amini, M., et al., *Statistical Modeling of Global Geogenic Fluoride Contamination in Groundwaters.* Environmental Science & Technology, 2008. **42**(10): p. 3662-3668.

25. Al-Karaghouli, A., D. Renne, and L.L. Kazmerski, *Solar and wind opportunities for water desalination in the Arab regions.* Renewable and Sustainable Energy Reviews, 2009. **13**(9): p. 2397-2407.

26. El-Ghonemy, A.M.K., *Water desalination systems powered by renewable energy sources: Review.* Renewable and Sustainable Energy Reviews, 2012. **16**(3): p. 1537-1556.

27. Peñate, B., et al., *Design and testing of an isolated commercial EDR plant driven by solar photovoltaic energy.* Desalination and Water Treatment, 2012. **51**(4-6): p. 1254-1264.

28. Subiela, V.J., et al., *Canary Islands Institute of Technology (ITC) experiences in desalination with renewable energies (1996-2008).* Desalination & Water Treatment, 2009. **7**(1-3): p. 220-235.

29. Xu, T. and C. Huang, *Electrodialysis-based separation technologies: A critical review.* AIChE Journal, 2008. **54**(12): p. 3147-3159.

30. Van der Bruggen, B., et al., *Electrodialysis and nanofiltration of surface water for subsequent use as infiltration water.* Water Research, 2003. **37**(16): p. 3867-3874.

31. Strathmann, H., *Ion-Exchange Membrane Separation Processes*. Membrane Science and Technology. Vol. 9. 2004: Elsevier. 348.

32. Valero, F., A. Barceló, and R. Arbós, *Electrodialysis Technology - Theory and Applications*, in *Desalination, Trends and Technologies*, M. Schorr, Editor 2011: InTech.

33. Karlin, Y.V. and V.N. Kropotov, *Electrodialysis separation of Na^+ and Ca^+ in a pulsed current mode.* Russian Journal of Electrochemistry, 1995. **31**(5): p. 517-521.

34. Ruiz, B., et al., *Application of relaxation periods during electrodialysis of a casein solution: Impact on anion-exchange membrane fouling.* Journal of Membrane Science, 2007. **287**(1): p. 41-50.

35. Lee, H.-J., et al., *Designing of an electrodialysis desalination plant.* Desalination, 2002. **142**(3): p. 267-286.

36. Demircioglu, M., et al., *Demineralization by electrodialysis (ED) — separation performance and cost comparison for monovalent salts.* Desalination, 2003. **153**(1–3): p. 329-333.

37. Tanaka, Y., *Mass transport and energy consumption in ion-exchange membrane electrodialysis of seawater.* Journal of Membrane Science, 2003. **215**(1–2): p. 265-279.

38. Bernardes, A.M., et al., *Electrochemistry as a clean technology for the treatment of effluents: The application of electrodialysis.* Metal Finishing, 2000. **98**(11): p. 52-114.

39. Goodman, N.B., et al., *A feasibility study of municipal wastewater desalination using electrodialysis reversal to provide recycled water for horticultural irrigation.* Desalination, 2013. **317**(0): p. 77-83.

40. Korngold, E., K. Kock, and H. Strathmann, *Electrodialysis in advanced waste water treatment.* Desalination, 1977. **24**(1–3): p. 129-139.

41. Boniardi, N., et al., *Lactic acid production by electrodialysis Part I: Experimental tests.* Journal of Applied Electrochemistry, 1997. **27**(2): p. 125-133.

42. Boniardi, N., et al., *Lactic acid production by electrodialysis Part II: Modelling.* Journal of Applied Electrochemistry, 1997. **27**(2): p. 135-145.

43. Montiel, V., et al., *Recovery by means of electrodialysis of an aromatic amino acid from a solution with a high concentration of sulphates and phosphates.* Journal of Membrane Science, 1998. **140**(2): p. 243-250.

44. Poquis, J.A., et al., *Partial electro-neutralisation of d-α-p-hydroxyphenylglycine in sulphuric acid medium.* Journal of Membrane Science, 2000. **170**(2): p. 225-233.

45. Turek, M., *Dual-purpose desalination-salt production electrodialysis.* Desalination, 2003. **153**(1–3): p. 377-381.

46. Yamamoto, M., et al., *A new electrodialyzer technique for the salt production by ion-exchange membrane*, in *Eighth World Salt Symposium*May 7-11 (2000): The Hague, Netherlands. p. 1647–1652.

47. Takashima, K., et al., *The seawater pretreatment facilities for electrodialysis at Sanuki Salt Manufacturing Co., Ltd.*, in *Eighth World Salt Symposium*May 7-11 (2000): The Hague, Netherlands. p. 1641-1646.

48. Eigenberger, G., H. Strathmann, and A. Grabovskiy, *Membrane assembly, electrodialysis device and method for continuous electrodialytic desalination*, 2005: Germany WO 2005/009596 Int. Cl. A1, B01D 61/44.

49. Strathmann, H., *Electrodialysis, a mature technology with a multitude of new applications.* Desalination, 2010. **264**(3): p. 268-288.

50. Krol, J.J., *Monopolar and bipolar ion-exchange membranes: Mass Transport Limitations*, 1997, University of Twente: Enschede, The Netherlands.

51. Ben Sik Ali, M., B. Hamrouni, and M. Dhahbi, *Electrodialytic Defluoridation of Brackish Water: Effect of Process Parameters and Water Characteristics.* CLEAN – Soil, Air, Water, 2010. **38**(7): p. 623-629.

52. Gnusin, N. and O. Demina, *Modeling of transfer in electrodialysis systems.* Theoretical Foundations of Chemical Engineering, 2006. **40**(1): p. 27-31.

53. Lundstrom, J.E., *Water desalting by solar powered electrodialysis.* Desalination, 1979. **31**(1-3): p. 469-488.

54. Ishimaru, N., *Solar photovoltaic desalination of brackish-water in remote areas by electrodialysis.* Desalination, 1994. **98**(1-3): p. 485-493.

55. Hadjipaschalis, I., A. Poullikkas, and V. Efthimiou, *Overview of current and future energy storage technologies for electric power applications.* Renewable and Sustainable Energy Reviews, 2009. **13**(6–7): p. 1513-1522.

56. Beaudin, M., et al., *Energy storage for mitigating the variability of renewable electricity sources: An updated review.* Energy for Sustainable Development, 2010. **14**(4): p. 302-314.

57. Kousksou, T., et al., *Energy storage: Applications and challenges.* Solar Energy Materials and Solar Cells, 2014. **120, Part A**(0): p. 59-80.

58. Dukhin, S.S. and N.A. Mishchuk, *Intensification of electrodialysis based on electroosmosis of the second kind.* Journal of Membrane Science, 1993. **79**(2-3): p. 199-210.

59. Mishchuk, N.A., *Perspectives of the electrodialysis intensification.* Desalination, 1998. **117**(1-3): p. 283-295.

60. Mishchuk, N.A., L.K. Koopal, and F. Gonzalez-Caballero, *Intensification of electrodialysis by applying a non-stationary electric field.* Colloids and Surfaces A: Physicochemical and Engineering Aspects, 2001. **176**(2-3): p. 195-212.

61. Mishchuk, N.A., S.V. Verbich, and F. Gonzales-Caballero, *Concentration polarization and specific selectivity of membranes in pulse mode.* Colloid Journal, 2001. **63**(5): p. 586-594.

62. Lee, H.-J. and S.-H. Moon, *Enhancement of electrodialysis performances using pulsing electric fields during extended period operation.* Journal of Colloid and Interface Science, 2005. **287**(2): p. 597-603.

63. Lee, H.-J., S.-H. Moon, and S.-P. Tsai, *Effects of pulsed electric fields on membrane fouling in electrodialysis of NaCl solution containing humate.* Separation and Purification Technology, 2002. **27**(2): p. 89-95.

64. Casademont, C., et al., *Electrodialysis of model salt solution containing whey proteins: Enhancement by pulsed electric field and modified cell configuration.* Journal of Membrane Science, 2009. **328**(1-2): p. 238-245.

65. Cifuentes-Araya, N., G. Pourcelly, and L. Bazinet, *Impact of pulsed electric field on electrodialysis process performance and membrane fouling during consecutive demineralization of a model salt solution containing a high magnesium/calcium ratio.* Journal of Colloid and Interface Science, 2011. **361**(1): p. 79-89.

66. Cifuentes-Araya, N., G. Pourcelly, and L. Bazinet, *Multistep mineral fouling growth on a cation-exchange membrane ruled by gradual sieving effects of magnesium and carbonate ions and its delay by pulsed modes of electrodialysis.* Journal of Colloid and Interface Science, 2012. **372**(1): p. 217-230.

67. Subiela, V.J., J.A. Carta, and J. González, *The SDAWES project: lessons learnt from an innovative project.* Desalination, 2004. **168**(0): p. 39-47.

68. AlMadani, H.M.N., *Water desalination by solar powered electrodialysis process.* Renewable Energy, 2003. **28**(12): p. 1915-1924.

69. Ortiz, J.M., et al., *Photovoltaic electrodialysis system for brackish water desalination: Modeling of global process.* Journal of Membrane Science, 2006. **274**(1–2): p. 138-149.

70. Ortiz, J.M., et al., *Desalination of underground brackish waters using an electrodialysis system powered directly by photovoltaic energy.* Solar Energy Materials and Solar Cells, 2008. **92**(12): p. 1677-1688.

71. Uche, J., et al., *On-grid and off-grid batch-ED (electrodialysis) process: Simulation and experimental tests.* Energy, 2013. **57**(0): p. 44-54.

72. Cirez, F., et al., *Batch ED fed by a PV unit: a reliable, flexible, and sustainable integration.* Desalination and Water Treatment, 2013. **51**(4-6): p. 673-685.

73. Maatallah, T., et al., *Wind power assessment and evaluation of electricity generation in the Gulf of Tunis, Tunisia.* Sustainable Cities and Society, 2013. **6**(0): p. 1-10.

74. Chang, T.J. and Y.L. Tu, *Evaluation of monthly capacity factor of WECS using chronological and probabilistic wind speed data: A case study of Taiwan.* Renewable Energy, 2007. **32**(12): p. 1999-2010.

75. Jowder, F.A.L., *Wind power analysis and site matching of wind turbine generators in Kingdom of Bahrain.* Applied Energy, 2009. **86**(4): p. 538-545.

76. de Araujo Lima, L. and C.R. Bezerra Filho, *Wind energy assessment and wind farm simulation in Triunfo – Pernambuco, Brazil.* Renewable Energy, 2010. **35**(12): p. 2705-2713.

77. Ahmed Shata, A.S. and R. Hanitsch, *Electricity generation and wind potential assessment at Hurghada, Egypt.* Renewable Energy, 2008. **33**(1): p. 141-148.

78. Peinke, J., et al., *Turbulence, a challenging problem for wind energy.* Physica A: Statistical Mechanics and its Applications, 2004. **338**(1–2): p. 187-193.

79. Charcosset, C., *A review of membrane processes and renewable energies for desalination.* Desalination, 2009. **245**(1–3): p. 214-231.

80. Dehmas, D.A., et al., *On the use of wind energy to power reverse osmosis desalination plant: A case study from Ténès (Algeria).* Renewable and Sustainable Energy Reviews, 2011. **15**(2): p. 956-963.

81. Infield, D., *Performance analysis of a small wind powered reverse osmosis plant.* Solar Energy, 1997. **61**(6): p. 415-421.

82. Lindemann, J.H., *Wind and solar powered seawater desalination applied solutions for the Mediterranean, the Middle East and the Gulf countries.* Desalination, 2004. **168**(0): p. 73-80.

83. Peñate, B., et al., *Assessment of a stand-alone gradual capacity reverse osmosis desalination plant to adapt to wind power availability: A case study.* Energy, 2011. **36**(7): p. 4372-4384.

84. Veza, J., B. Peñate, and F. Castellano, *Electrodialysis desalination designed for off-grid wind energy.* Desalination, 2004. **160**(3): p. 211-221.

85. Veza, J.M., B. Peñate, and F. Castellano, *Electrodialysis desalination designed for wind energy (on-grid tests).* Desalination, 2001. **141**(1): p. 53-61.

86. Garcia-Rodriquez, L., *Renewable energy applications in desalination: state of the art.* Solar Energy, 2003. **75**(5): p. 381-393.

87. Miranda, M.S. and D. Infield, *A wind-powered seawater reverse-osmosis system without batteries.* Desalination, 2003. **153**(1–3): p. 9-16.

88. Thomson, M. and D. Infield, *A photovoltaic-powered seawater reverse-osmosis system without batteries.* Desalination, 2003. **153**(1–3): p. 1-8.

89. Thomson, M. and D. Infield, *Laboratory demonstration of a photovoltaic-powered seawater reverse-osmosis system without batteries.* Desalination, 2005. **183**(1–3): p. 105-111.

90. Gilau, A.M. and M.J. Small, *Designing cost-effective seawater reverse osmosis system under optimal energy options.* Renewable Energy, 2008. **33**(4): p. 617-630.

91. El-Ghonemy, A.M.K., *Future sustainable water desalination technologies for the Saudi Arabia: A review.* Renewable and Sustainable Energy Reviews, 2012. **16**(9): p. 6566-6597.

92. Souari, L. and M. Hassairi, *Sea water desalination by reverse osmosis: the true needs for energy.* Desalination, 2007. **206**(1–3): p. 465-473.

93. Petersen, G., et al., *Wind and solar powered reverse osmosis desalination units - design, start up, operating experience.* Desalination, 1981. **39**(0): p. 125-135.

94. Carta, J., J. González, and V. Subiela, *The SDAWES project: an ambitious R&D prototype for wind-powered desalination.* Desalination, 2004. **161**(1): p. 33-48.

95. Dubois, M.R.J., *Optimized permanent magnet generator topologies for direct-drive wind turbines*, 2004, Delft University: Les Imprimeries ABC Inc., Lévis, Canada. p. 237.

96. Stander, J.N., G. Venter, and M.J. Kamper, *Review of direct-drive radial flux wind turbine generator mechanical design.* Wind Energy, 2012. **15**(3): p. 459-472.

97. Burton, T., et al., *Wind Energy Handbook*. 2001: John Wiley & Sons Ltd.

98. Manwell, J.F., *Wind Energy Explained: Theory, Design and Application*. 2002: John Wiley & Sons Ltd.

99. Park, G.L., *Wind-powered membrane desalination of brackish water*, in *School of Engineering and Physical Sciences,* 2012, Heriot-Watt University: Edinburgh, UK.

100. Zhang, Y., et al., *Selectrodialysis: Fractionation of divalent ions from monovalent ions in a novel electrodialysis stack.* Separation and Purification Technology, 2012. **88**(0): p. 191-201.

101. Zhang, Y., et al., *Separation of nutrient ions and organic compounds from salts in RO concentrates by standard and monovalent selective ion-exchange membranes used in electrodialysis.* Journal of Membrane Science, 2009. **332**(1-2): p. 104-112.

102. Nikonenko, V.V., et al., *Effect of stationary external electric fields on ion-exchange membrane selectivity.* Soviet electrochemistry, 1980. **16**: p. 472.

103. van Weert, F., J. van der Gun, and J. Reckman, *Global Overview of Saline Groundwater Occurrence and Genesis*, 2009, International Groundwater Resources assessment centre: Utrecht, The Netherlands.

104. NGWA. *Groundwater fact sheets*. 2013 [cited 2014 30 April]; Available from: http://www.ngwa.org/PublishingImages/Fundamentals/NGWA-fact_sheet2a.pdf.

105. Abramson, A., E. Adar, and N. Lazarovitch, *Exploring parameter effects on the economic outcomes of groundwater-based developments in remote, low-resource settings.* Journal of Hydrology, (0).

106. MacDonald, A.M. and R.C. Calow, *Developing groundwater for secure rural water supplies in Africa.* Desalination, 2009. **248**(1–3): p. 546-556.

107. Barnett, C. *Groundwater wake-up*. 2013 [cited 2014 29 April]; Available from: http://ensia.com/features/groundwater-wake-up/.

108. Gleeson, T., et al., *Water balance of global aquifers revealed by groundwater footprint.* Nature, 2012. **488**(7410): p. 197-200.

109. Nriagu, J.O. and J.M. Pacyna, *Quantitative assessment of worldwide contamination of air, water and soils by trace metals.* Nature, 1988. **333**(6169): p. 134-139.

110. Seinfeld, J.H. and S.N. Pandis, *Atmospheric chemistry and physics: From air pollution to climate change*. 2nd ed. Vol. 51. 2006, New York: John Wiley & Sons. 1232.

111. Browne, D., H. Whelton, and D. O'Mullane, *Fluoride metabolism and fluorosis.* Journal of Dentistry, 2005. **33**(3): p. 177-186.

112. Jha, S., et al., *Fluoride in the Environment and Its Metabolism in Humans*, in *Reviews of Environmental Contamination and Toxicology Volume 211*, D.M. Whitacre, Editor. 2011, Springer New York. p. 121-142.

113. Edmunds, W.M. and P. Smedley, *Fluoride in Natural Waters*, in *Essentials of Medical Geology*, O. Selinus, Editor. 2013, Springer Netherlands. p. 311-336.

114. Abu Rukah, Y. and K. Alsokhny, *Geochemical assessment of groundwater contamination with special emphasis on fluoride concentration, North Jordan.* Chemie der Erde - Geochemistry, 2004. **64**(2): p. 171-181.

115. Nair, K.R., F. Manji, and J.N. Gitonga, *The occurrence and distribution of fluoride in groundwaters of Kenya.* Challenges in African Hydrology and Water Resources, Proceedings of the Harare Symposium, IAHS Publ. 144, 75-86., 1984.

116. Tesoriero, A.J., et al., *Linking ground-water age and chemistry data along flow paths: Implications for trends and transformations of nitrate and pesticides.* Journal of Contaminant Hydrology, 2007. **94**(1–2): p. 139-155.

117. Satpathy, K.K., R.K. Padhi, and M.K. Samantara, *Comments on the "Nitrate contamination in ground water of some rural areas of Rajasthan, India" by Suthar et al. [J. Hazard. Mater. 171 (2009)]*. Journal of Hazardous Materials, 2013. **260**(0): p. 192-194.

118. DEFRA, *The government's strategic review of diffuse water pollution from agriculture in England and Wales*, 2002, Department for Environment, Food and Rural Affairs, London.

119. EEA, *Present concentration of nitrate in groundwater bodies in European countries*, 2009, European Environment Agency: Kopenhagen.

120. Brooker, M.P. and P.C. Johnson, *The behaviour of phosphate, nitrate, chloride and hardness in twelve welsh rivers.* Water Research, 1984. **18**(9): p. 1155-1164.

121. Mullaney, J.R., D.L. Lorenz, and A.D. Arntson, *Chloride in Groundwater and Surface Water in Areas Underlain by the Glacial Aquifer System, Northern United States*, 2009.

122. *Department of National Health and Welfare,Guidelines for Canadian drinking water quality (Supporting documentation)*, 1978: Ottawa, Canada.

123. EASAC, *Country report for Greece*, in *Groundwater in the Southern Member States of the European Union: an assessment of current knowledge and future prospects* 2010, European Academies Science Advisory Council.

124. EASAC, *Country report for Portugal*, in *Groundwater in the Southern Member States of the European Union: an assessment of current knowledge and future prospects* 2010, European Academies Science Advisory Council.

125. Sharma, P.K., G.R. Gavalas, and R.C. Flagan, *Calcium pretreatment of coal for sulphur emissions control in combustion.* Fuel, 1987. **66**(2): p. 207-209.

126. Koch, R., *Zoeteman, B. C. J.: Sensory Assessment of Water Quality. Oxford-New York-Toronto-Sydney-Paris-Frankfurt, Pergamon-Press, 1980 148 S., 195 Lit.* Acta hydrochimica et hydrobiologica, 1982. **10**(4): p. 322-322.

127. NAS, *Drinking water and health*, 1977, National Research Council, National Academy of Sciences: Washington, DC.

128. UNEP, *GEMS/Water data summary 1985-1987*, 1990, Centre for Inland Waters; United Nations Environment Programme, Global Environment Monitoring System, GEMS/Water Programme Office: Burlington, Ontario, Canada.

129. Meays, C. and R. Nordin, *Ambient Water Quality Guidelines For Sulphate - Techncal Appendix*, 2013: Water Protection & Sustainability Branch Environmental Sustainability and Strategic Policy Division, BC Ministry of Environment, British Columbia, Canada.

130. Nikonenko, V.V., et al., *Intensive current transfer in membrane systems: Modelling, mechanisms and application in electrodialysis.* Advances in Colloid and Interface Science, 2010. **160**(1-2): p. 101-123.

131. Krol, J.J., M. Wessling, and H. Strathmann, *Concentration polarization with monopolar ion exchange membranes: current–voltage curves and water dissociation.* Journal of Membrane Science, 1999. **162**(1–2): p. 145-154.

132. Larchet, C., B. Auclair, and V. Nikonenko, *Approximate evaluation of water transport number in ion-exchange membranes.* Electrochimica Acta, 2004. **49**(11): p. 1711-1717.

133. Vázquez, L., et al., *Prediction of mass transport profiles in a laboratory filter-press electrolyser by computational fluid dynamics modelling.* Electrochimica Acta, 2010. **55**(10): p. 3446-3453.

134. Koros, W.J., Y.H. Ma, and T. Shimidzu, *Terminology for membranes an membrane processes.* Pure & Appl. Chem., 1996. **68**: p. 1479-1489.

135. Rubinstein, I. and B. Zaltzman, *Electro-osmotically induced convection at a permselective membrane.* Physical Review E, 2000. **62**(2): p. 2238-2251.

136. Rosenberg, N.W. and C.E. Tirrell, *Limiting Currents in Membrane Cells.* Industrial & Engineering Chemistry, 1957. **49**(4): p. 780-784.

137. Strathmann, H., et al., *Limiting current density and water dissociation in bipolar membranes.* Journal of Membrane Science, 1997. **125**(1): p. 123-142.

138. Simons, R., *The origin and elimination of water splitting in ion exchange membranes during water demineralisation by electrodialysis.* Desalination, 1979. **28**(1): p. 41-42.

139. Simons, R., *Electric field effects on proton transfer between ionizable groups and water in ion exchange membranes.* Electrochimica Acta, 1984. **29**(2): p. 151-158.

140. Simons, R., *Water splitting in ion exchange membranes.* Electrochimica Acta, 1985. **30**(3): p. 275-282.

141. Oda, Y. and T. Yawataya, *Neutrality-disturbance phenomenon of membrane-solution systems.* Desalination, 1968. **5**(2): p. 129-138.

142. Lee, H.-J., H. Strathmann, and S.-H. Moon, *Determination of the limiting current density in electrodialysis desalination as an empirical function of linear velocity.* Desalination, 2006. **190**(1–3): p. 43-50.

143. Rubinstein, I. and L. Shtilman, *Voltage against current curves of cation exchange membranes.* Journal of the Chemical Society, Faraday Transactions 2: Molecular and Chemical Physics, 1979. **75**: p. 231-246.

144. Rubinstein, I., *Electroconvection at an electrically inhomogeneous permselective interface.* Physics of Fluids A: Fluid Dynamics, 1991. **3**(10): p. 2301-2309.

145. Cowan, D.A. and J.H. Brown, *Effect of Turbulence on Limiting Current in Electrodialysis Cells.* Industrial & Engineering Chemistry, 1959. **51**(12): p. 1445-1448.

146. Oldani, M., et al., *On the nitrate and monovalent cation selectivity of ion exchange membranes used in drinking water purification.* Journal of Membrane Science, 1992. **75**(3): p. 265-275.

147. Kabay, N., et al., *Effect of feed characteristics on the separation performances of monovalent and divalent salts by electrodialysis.* Desalination, 2003. **158**(1-3): p. 95-100.

148. Firdaous, L., et al., *Transfer of Monovalent and Divalent Cations in Salt Solutions by Electrodialysis.* Separation Science and Technology, 2007. **42**(5): p. 931-948.

149. Sadrzadeh, M., A. Razmi, and T. Mohammadi, *Separation of different ions from wastewater at various operating conditions using electrodialysis.* Separation and Purification Technology, 2007. **54**(2): p. 147-156.

150. Smith, G., *Basic Chemical Thermodynamics*. 2004, London, UK.: Imperial College Press.

151. Li, Y. and T. Xu, *Permselectivities of monovalent anions through pyridine-modified anion-exchange membranes.* Separation and Purification Technology, 2008. **61**(3): p. 430-435.

152. Banasiak, L.J. and A.I. Schaefer, *Removal of boron, fluoride and nitrate by electrodialysis in the presence of organic matter.* Journal of Membrane Science, 2009. **334**(1-2): p. 101-109.

153. Oldani, M., et al., *On the nitrate and monovalent cation selectivity of ion-exchange membranes used in drinking-water purification.* Journal of Membrane Science, 1992. **75**(3): p. 265-275.

154. Amor, Z., et al., *Fluoride removal from brackish water by electrodialysis.* Desalination, 2001. **133**(3): p. 215-223.

155. Tansel, B., et al., *Significance of hydrated radius and hydration shells on ionic permeability during nanofiltration in dead end and cross flow modes.* Separation and Purification Technology, 2006. **51**(1): p. 40-47.

156. Kabay, N., et al., *Effect of salt combination on separation of monovalent and divalent salts by electrodialysis.* Desalination, 2006. **198**(1-3): p. 84-91.

157. Zhang, Y., et al., *Electrodialysis on RO concentrate to improve water recovery in wastewater reclamation.* Journal of Membrane Science, 2011. **378**(1-2): p. 101-110.

158. Zhang, Y., et al., *RO concentrate minimization by electrodialysis: Techno-economic analysis and environmental concerns.* Journal of Environmental Management, 2012. **107**(0): p. 28-36.

159. Bi, J., et al., *Removal of nitrate from groundwater using the technology of electrodialysis and electrodeionization.* Desalination and Water Treatment, 2011. **34**(1-3): p. 394-401.

160. Richards, L.A., et al., *Experimental Energy Barriers to Anions Transporting through Nanofiltration Membranes.* Environmental Science & Technology, 2013. **47**(4): p. 1968-1976.

161. Richards, L.A., et al., *The Importance of Dehydration in Determining Ion Transport in Narrow Pores.* Small, 2012. **8**(11): p. 1701-1709.

162. Van der Bruggen, B., A. Koninckx, and C. Vandecasteele, *Separation of monovalent and divalent ions from aqueous solution by electrodialysis and nanofiltration.* Water Research, 2004. **38**(5): p. 1347-1353.

163. Sata, T., *Studies on anion exchange membranes having permselectivity for specific anions in electrodialysis -- effect of hydrophilicity of anion exchange membranes on permselectivity of anions.* Journal of Membrane Science, 2000. **167**(1): p. 1-31.

164. Sata, T., K. Teshima, and T. Yamaguchi, *Permselectivity between two anions in anion exchange membranes crosslinked with various diamines in electrodialysis.* Journal of Polymer Science Part A: Polymer Chemistry, 1996. **34**(8): p. 1475-1482.

165. Yang, H., X. Zhang, and W. Yuan, *Effect of operating parameters on the condensation of ammonium sulfate by electrodialysis.* Chemical Engineering & Technology, 2008. **31**(9): p. 1261-1264.

166. Banasiak, L.J., T.W. Kruttschnitt, and A.I. Schaefer, *Desalination using electrodialysis as a function of voltage and salt concentration.* Desalination, 2007. **205**(1-3): p. 38-46.

167. Nikonenko, V.V., V.V. Zabolotskii, and K.A. Lebedev, *Model for the competitive transport of Ions through Ion exchange membranes with a modified surface.* Russian Journal of Electrochemistry, 1996. **32**(2): p. 234-236.

168. Zabolotsky, V.I., et al., *Space charge effect on competitive ion transport through ion-exchange membranes.* Desalination, 2002. **147**(1–3): p. 387-392.

169. Ortiz, J.M., et al., *Brackish water desalination by electrodialysis: batch recirculation operation modeling.* Journal of Membrane Science, 2005. **252**(1–2): p. 65-75.

170. Kabay, N., et al., *Separation of monovalent and divalent ions from ternary mixtures by electrodialysis.* Desalination, 2006. **198**(1–3): p. 74-83.

171. Kabay, N., et al., *Separation of fluoride from aqueous solution by electrodialysis: Effect of process parameters and other ionic species.* Journal of Hazardous Materials, 2008. **153**(1–2): p. 107-113.

172. Ortiz, J.M., *Desalinización de aguas mediante sistemas de electrodiálisis alimentados directamente con energía solar fotovoltaica: estudio de viabilidad y modelización*, in *Instituto Universitario de Electroquímica,* 2009, University of Alicante: Alicante, Spain.

173. Johnson, G.L., *Wind Energy Systems*, 2001, Kansas State University: Kansas, USA.

174. Ackermann, T. and L. Söder, *An overview of wind energy-status 2002.* Renewable and Sustainable Energy Reviews, 2002. **6**(1–2): p. 67-127.

175. *IEC 61400-2: Wind Turbine Generator Systems - Part 2: Safety of Small Wind Turbines*, 2006-03, Intrnational Electrotechnical Commission.

176. Farris, A. *Wind*. 2012 [cited 2014 30 April]; Available from: http://www.energybc.ca/profiles/wind.html.

177. Abdel-Karim, N., M. Ilic, and M. Small, *Modeling Wind Speed for Power System Applications*, in *Wind Farm - Impact in Power System and Alternatives to Improve the Integration*, Suvire, Editor 2011: Carnegie Mellon University, USA.

178. Van der Hoven, I., *Power spectrum of horizental wind speed in the frequency rang from 0.0007 to 900 cycles cycles per hour.* Journal of Meteorology, 1957. **14**(2): p. 160-164.

179. Kaya, E., B. BarutÇU, and Ş. Sibel MenteŞ, *A method based on the Van der Hoven spectrum for performance evaluation in prediction of wind speed.* Turkish Journal of Earth Sciences, 2013. **22**(4): p. 681-689.

180. Park, G.L., A.I. Schafer, and B.S. Richards, *The effect of intermittent operation on a wind-powered membrane system for brackish water desalination.* Water Science and Technology, 2012. **65**(5): p. 867-874.

181. Rosen, A. and Y. Sheinman, *The power fluctuations of a wind turbine.* Journal of Wind Engineering and Industrial Aerodynamics, 1996. **59**(1): p. 51-68.

182. Quaschning, V., *Understanding renewable energy systems*. 2005, London, UK: Earthscan.

183. James, P.A.B., et al., *Implications of the UK field trial of building mounted horizontal axis micro-wind turbines.* Energy Policy, 2010. **38**(10): p. 6130-6144.

184. Shariatpanah, H., R. Fadaeinedjad, and M. Rashidinejad, *A New Model for PMSG-Based Wind Turbine With Yaw Control.* Energy Conversion, IEEE Transactions on, 2013. **28**(4): p. 929-937.

185. Polinder, H., et al., *Comparison of direct-drive and geared generator concepts for wind turbines.* Energy Conversion, IEEE Transactions on, 2006. **21**(3): p. 725-733.

186. Jiawei, C., C. Jie, and G. Chunying, *New Overall Power Control Strategy for Variable-Speed Fixed-Pitch Wind Turbines Within the Whole Wind Velocity*

Range. Industrial Electronics, IEEE Transactions on, 2013. **60**(7): p. 2652-2660.

187. Li, H. and Z. Chen, *Overview of different wind generator systems and their comparisons.* Renewable Power Generation, IET, 2008. **2**(2): p. 123-138.

188. Meier, A.v., *Electric power systems [electronic resource] : a conceptual introduction / by Alexandra von Meier*. Wiley survival guides in engineering and science. 2006: Hoboken, N.J. : IEEE Press : Wiley-Interscience, c2006.

189. FutureEnergy. *http://www.futurenergy.co.uk/*. 2010 [cited 2014 01 May]; Available from: http://www.futurenergy.co.uk/.

190. Corbus, D., et al., *Small Wind Turbine Testing and Applications Development*, in *Windpower '99*1999: Burlington, Vermont: NREL/CP-500-27067.

191. Abraham, T. and A. Luthra, *Socio-economic & technical assessment of photovoltaic powered membrane desalination processes for India.* Desalination, 2011. **268**(1–3): p. 238-248.

192. Li, C.N., Y. Goswami, and E. Stefanakos, *Solar assisted sea water desalination: A review.* Renewable & Sustainable Energy Reviews, 2013. **19**: p. 136-163.

193. Lee, H.-J., S.-J. Oh, and S.-H. Moon, *Recovery of ammonium sulfate from fermentation waste by electrodialysis.* Water Research, 2003. **37**(5): p. 1091-1099.

194. Nikonenko, V.V., et al., *Desalination at overlimiting currents: State-of-the-art and perspectives.* Desalination, (0).

195. Tanaka, Y. and M. Seno, *Concentration polarization and water dissociation in ion-exchange membrane electrodialysis. Mechanism of water dissociation.* Journal of the Chemical Society, Faraday Transactions 1: Physical Chemistry in Condensed Phases, 1986. **82**(7): p. 2065-2077.

196. Park, J.-S., et al., *An approach to fouling characterization of an ion-exchange membrane using current–voltage relation and electrical impedance*

spectroscopy. Journal of Colloid and Interface Science, 2006. **294**(1): p. 129-138.

197. Banasiak, L.J., *Removal of inorganic and trace organic contaminants by electrodialysis*, in *School of Engineering, the Institute of Infrastructure and the Environment,* 2010, The University of Edinburgh: Edinburgh, UK.

198. Astom, *Neosepta Ion-Exchange Membranes.* http://www.astom-corp.jp/en/en-main2-neosepta.html, 2013.

199. Carrillo, C., et al., *Review of power curve modelling for wind turbines.* Renewable and Sustainable Energy Reviews, 2013. **21**(0): p. 572-581.

200. Clesceri, L.S., A.E. Greenberg, and A.D. Eaton, *Standard methods for the examination of water and wastewater*. 20th ed. 1998.

201. Park, J.-S., H.-J. Lee, and S.-H. Moon, *Determination of an optimum frequency of square wave power for fouling mitigation in desalting electrodialysis in the presence of humate.* Separation and Purification Technology, 2003. **30**(2): p. 101-112.

202. Cooke, B.A., *Concentration polarization in electrodialysis—I. The electrometric measurement of interfacial concentration.* Electrochimica Acta, 1961. **3**(4): p. 307-317.

203. Spiegler, K.S., *Polarization at ion exchange membrane-solution interfaces.* Desalination, 1971. **9**(4): p. 367-385.

204. Malek, P., et al., *Electrodialytic removal of NaCl from water: Impacts of using pulsed electric potential on ion transport and water dissociation phenomena.* Journal of Membrane Science, 2013. **435**(0): p. 99-109.

205. Ruiz, B., *Procédés électromembranaires sous champs électriques pulses*, 2008, Université de Montpellier II: Montpellier, France.

206. Strathmann, H., *Membrane separation processes.* Journal of Membrane Science, 1981. **9**(1–2): p. 121-189.

207. Justus, C.G., W.R. Hargraves, and A. Yalcin, *Nationwide Assessment of Potential Output from Wind-Powered Generators.* Journal of Applied Meteorology, 1976. **15**(7): p. 673-678.

208. Park, G.L., A.I. Schäfer, and B.S. Richards, *Renewable energy-powered membrane technology: Supercapacitors for buffering resource fluctuations in a wind-powered membrane system for brackish water desalination.* Renewable Energy, 2013. **50**(0): p. 126-135.

209. Tsiakis, P. and L.G. Papageorgiou, *Optimal design of an electrodialysis brackish water desalination plant.* Desalination, 2005. **173**(2): p. 173-186.

210. Kim, M.S., et al., *A robust control of permanent magnet synchronous motor using load torque estimation*. Isie 2001: Ieee International Symposium on Industrial Electronics Proceedings, Vols I-Iii. 2001, New York: Ieee. 1157-1162.

211. Adiga, M.R., et al., *Performance analysis of photovoltaic electrodialysis desalination plant at Tanote in Thar desert.* Desalination, 1987. **67**(0): p. 59-66.

212. Kuroda, O., et al., *An electrodialysis sea water desalination system powered by photovoltaic cells.* Desalination, 1987. **65**(0): p. 161-169.

213. Fritzmann, C., et al., *State-of-the-art of reverse osmosis desalination.* Desalination, 2007. **216**(1–3): p. 1-76.

214. Birnhack, L., N. Voutchkov, and O. Lahav, *Fundamental chemistry and engineering aspects of post-treatment processes for desalinated water—A review.* Desalination, 2011. **273**(1): p. 6-22.

215. Withers, A., *Options for recarbonation, remineralisation and disinfection for desalination plants.* Desalination, 2005. **179**(1–3): p. 11-24.

216. Clark, D. *Are solar, wind and marine power too intermittent to be useful?* 29 May 2012.

217. Rugolo, J. and M.J. Aziz, *Electricity storage for intermittent renewable sources.* Energy & Environmental Science, 2012. **5**(5): p. 7151-7160.

218. Yekini Suberu, M., M. Wazir Mustafa, and N. Bashir, *Energy storage systems for renewable energy power sector integration and mitigation of intermittency.* Renewable and Sustainable Energy Reviews, 2014. **35**(0): p. 499-514.

219. Nair, M. and D. Kumar, *Water desalination and challenges: The Middle East perspective: a review.* Desalination and Water Treatment, 2012. **51**(10-12): p. 2030-2040.

220. Li, H., et al., *Competitive transport of ionic liquids and impurity ions during the electrodialysis process.* Desalination, 2009. **245**(1-3): p. 349-356.

221. Marcus, Y., *Thermodynamics of solvation of ions .5. gibbs free-energy of hydration at 298.15-k.* Journal of the Chemical Society-Faraday Transactions, 1991. **87**(18): p. 2995-2999.

222. Joung, I.S. and T.E. Cheatham, III, *Determination of alkali and halide monovalent ion parameters for use in explicitly solvated biomolecular simulations.* Journal of Physical Chemistry B, 2008. **112**(30): p. 9020-9041.

223. Custelcean, R. and B.A. Moyer, *Anion Separation with Metal–Organic Frameworks.* European Journal of Inorganic Chemistry, 2007. **2007**(10): p. 1321-1340.

224. Sata, T., *Studies on anion exchange membranes having permselectivity for specific anions in electrodialysis — effect of hydrophilicity of anion exchange membranes on permselectivity of anions.* Journal of Membrane Science, 2000. **167**(1): p. 1-31.

225. Choi, J.-H., H.-J. Lee, and S.-H. Moon, *Effects of Electrolytes on the Transport Phenomena in a Cation-Exchange Membrane.* Journal of Colloid and Interface Science, 2001. **238**(1): p. 188-195.

226. Bagotsky, V.S., *Fundamentals of Electrochemistry*. 2nd ed, ed. J.W. Sons. 2005, New York.

227. Atkins, P.P.W. and J. De Paula, *Atkins' Physical Chemistry*. 7th ed. 2002: Oxford University Press, Incorporated.

228. Matsumoto, H., R. Yamamoto, and A. Tanioka, *Membrane potential across low-water-content charged membranes: Effect of ion pairing.* Journal of Physical Chemistry B, 2005. **109**(29): p. 14130-14136.

229. Bard, A.J., *Electrochemical methods : fundamentals and applications / Allen J. Bard, Larry R. Faulkner*, ed. L.R. Faulkner. 1980, New York :: Wiley.

230. Reilly, C.N., *Treatise on Analytical Chemistry*. Fundamentals of electrode processes, ed. I.M. Kolthoff and P.J. Elving. 1963, New York: Wiley.

231. Burgess, J., *Metal ions in solution*, ed. H. Press. 1978, New York.

232. Kesore, K., F. Janowski, and V.A. Shaposhnik, *Highly effective electrodialysis for selective elimination of nitrates from drinking water.* Journal of Membrane Science, 1997. **127**(1): p. 17-24.

233. Van Geluwe, S., et al., *Evaluation of electrodialysis for scaling prevention of nanofiltration membranes at high water recoveries.* Resources, Conservation and Recycling, 2011. **56**(1): p. 34-42.

234. Tansel, B., *Significance of thermodynamic and physical characteristics on permeation of ions during membrane separation: Hydrated radius, hydration free energy and viscous effects.* Separation and Purification Technology, 2012. **86**(0): p. 119-126.

235. Volkov, A.G., S. Paula, and D.W. Deamer, *Two mechanisms of permeation of small neutral molecules and hydrated ions across phospholipid bilayers.* Bioelectrochemistry and Bioenergetics, 1997. **42**(2): p. 153-160.

236. Xue, T., R.B. Longwell, and K. Osseo-Asare, *Mass transfer in Nation membrane systems: Effects of ionic size and charge on selectivity.* Journal of Membrane Science, 1991. **58**(2): p. 175-189.

237. Kim, Y., W.S. Walker, and D.F. Lawler, *Competitive separation of di- vs. mono-valent cations in electrodialysis: Effects of the boundary layer properties.* Water Research, 2012. **46**(7): p. 2042-2056.

238. Bhattacharya, S. and S.-T. Hwang, *Concentration polarization, separation factor, and Peclet number in membrane processes.* Journal of Membrane Science, 1997. **132**(1): p. 73-90.

239. Lee, H.J., et al., *Fouling of an anion exchange membrane in the electrodialysis desalination process in the presence of organic foulants.* Desalination, 2009. **238**(1-3): p. 60-69.

240. Zuo, X., S. Yu, and W. Shi, *Effect of some parameters on the performance of eletrodialysis using new type of PVDF–SiO2 ion-exchange membranes with single salt solution.* Desalination, 2012. **290**(0): p. 83-88.

241. Min, J.-H. and H.-S. Kim, *Effect of operating conditions on the treatment of brackish groundwater by electrodialysis.* Desalination and Water Treatment, 2013. **51**(25-27): p. 5132-5137.

242. Hubicki, Z. and Kołodyńska, *Selective Removal of Heavy Metal Ions from Waters and Waste Waters Using Ion Exchange Methods*. Ion Exchange Technologies. 2012.

243. Goodwin, H.M., et al., *The fundamental laws of electrolytic conduction: Memoirs by Faraday, Hittorf and F. Kohlrausch*. 1899, New York: Harper & brothers.

244. Walton, H.F., *Ion Exchange. F. G. Helfferich. McGraw-Hill, New York, 1962. ix + 624 pp. Illus. $16.* Science, 1962. **138**(3537): p. 133.

245. Peñate, B. and L. García-Rodríguez, *Current trends and future prospects in the design of seawater reverse osmosis desalination technology.* Desalination, 2012. **284**(0): p. 1-8.

246. Likhachev, D.S. and F.-C. Li, *Large-scale water desalination methods: a review and new perspectives.* Desalination and Water Treatment, 2013. **51**(13-15): p. 2836-2849.

247. Alkhudhiri, A., N. Darwish, and N. Hilal, *Membrane distillation: A comprehensive review.* Desalination, 2012. **287**(0): p. 2-18.

248. Tzen, E., et al., *Design and development of a hybrid autonomous system for seawater desalination.* Desalination, 2004. **166**(0): p. 267-274.

249. Tzen, E., D. Theofilloyianakos, and Z. Kologios, *Autonomous reverse osmosis units driven by RE sources experiences and lessons learned.* Desalination, 2008. **221**(1–3): p. 29-36.

250. Vick, B.D. and R.N. Clark, *Experimental investigation of solar powered diaphragm and helical pumps.* Solar Energy, 2011. **85**(5): p. 945-954.

251. Protogeropoulos, C. and S. Pearce, *Laboratory evaluation and system sizing charts for a 'second generation' direct PV-powered, low cost submersible solar pump.* Solar Energy, 2000. **68**(5): p. 453-474.

252. Pérez-Herranz, V., J. García-Antón, and J.L. Guiñón, *Velocity profiles and limiting current in an annular electrodialysis cell in pulsed flow.* Chemical Engineering Science, 1997. **52**(5): p. 843-851.

253. Zhou, J., V.W.C. Chang, and A.G. Fane, *Life Cycle Assessment for desalination: A review on methodology feasibility and reliability.* Water Research, 2014. **61**(0): p. 210-223.

254. Raluy, R.G., L. Serra, and J. Uche, *Life cycle assessment of desalination technologies integrated with renewable energies.* Desalination, 2005. **183**(1–3): p. 81-93.

255. Raluy, R.G., L. Serra, and J. Uche, *Life Cycle Assessment of Water Production Technologies - Part 1: Life Cycle Assessment of Different Commercial Desalination Technologies (MSF, MED, RO) (9 pp).* The International Journal of Life Cycle Assessment, 2005. **10**(4): p. 285-293.

256. Subramani, A., et al., *Energy minimization strategies and renewable energy utilization for desalination: A review.* Water Research, 2011. **45**(5): p. 1907-1920.

257. Nwal Amang, D., S. Alexandrova, and P. Schaetzel, *The determination of diffusion coefficients of counter ion in an ion exchange membrane using electrical conductivity measurement.* Electrochimica Acta, 2003. **48**(18): p. 2563-2569.

258. Robinson, R.A. and R.H. Stokes, *Electrolyte Solutions*. 2nd ed. 1959, London: Butterworths.

259. corporation, A., *Neosepta Ion-Exchange Membranes specification sheet.* 2008.